Optimal Fault-tolerant Flight Control for Aircraft with Actuation Impairments

Saif H. Almutairi

Cranfield University

This dissertation is submitted for the degree of
Doctor of Philosophy

School of Aerospace, Transport
and Manufacturing

January 2016

I would like to dedicate this thesis to my loving family ...

Acknowledgements

All praise is due to Allah, the Lord of the worlds, for all His graces bestowed upon me. Next, I would like to thank my advisor Dr. Nabil Aouf for his continuous support of my PhD study and related research, for his patience, motivation, immense knowledge, and critical reviews. To the memory of my father; I still remember your unlimited support and encouragements. You've been to me a father, friend, and a great example in this life. I would like also to express my sincere gratitude to my mother for her love, care, kindness, and generosity of spirit. "Thank you" is a very small word for the beautiful things you are making for me. I thank my wife Hana for being a great friend and companion during all times. Thanks for her sacrifice and help. My thanks also go to my brothers and sisters for their support and great sharing of joy and entertainment.

Further, thanks to my sponsor KACST for offering me this scholarship to pursue my PhD studies, and the Saudi Embassy in London represented by the Cultural Bureau, for managing my scholarship. In addition, thanks to those who helped to scrutinise my work, give some feedback or help in a resolution of problems, whom I was enjoying to work with, Dr. Hameed and Dr. Mudassir loan. Also, I would like to thank my colleagues in the university Dr. Lounis for his support and motivation and Riyad, Waleed, Tariq, Abdulnoor, Mohammad, Sati, and Ivan for the refreshing discussion and nice times we spent together.

Abstract

Current trends towards greater complexity and automation are leaving modern technological systems increasingly vulnerable to faults. Without proper action, a minor error may lead to devastating consequences. In flight control, where the controllability and dynamic stability of the aircraft primarily rely on the control surfaces and engine thrust, faults in these effectors result in a higher extent of risk for these aspects. Moreover, the operation of automatic flight control would be suddenly disturbed. To address this problem, different methodologies of designing optimal flight controllers are presented in this thesis. For multiple-input multiple-output (MIMO) systems, the feedback optimal control is a prominent technique that solves a multi-objective cost function, which includes, for instance, tracking requirements and control energy minimisation.

The first proposed method is based on a linear quadratic regulator (LQR) control law augmented with a fault-compensation scheme. This fault-tolerant system handles the situation in an adaptive way by solving the optimisation cost function and considering fault information, while assuming an effective fault detection system is available. The developed scheme was tested in a six-degrees-of-freedom nonlinear environment to validate the linear-based controller. Results showed that this fault tolerant control (FTC) strategy managed to handle high magnitudes of the actuator's loss of efficiency faults. Although the rise time of aircraft response became slower, overshoot and settling errors were minimised, and the stability of the aircraft was maintained.

Another FTC approach has been developed utilising the features of controller robustness against the system parametric uncertainties, without the need for reconfiguration or adaptation. Two types of control laws were established under this scheme, the H_∞ and μ-synthesis controllers. Both were tested in a nonlinear environment for three points in the flight envelope: ascending, cruising, and descending. The H_∞ controller maintained the requirements in the intact case; while in fault, it yielded non-robust high-frequency control surface deflections. The μ-synthesis, on the other hand, managed to handle the constraints of the system and accommodate faults reaching 30% loss of efficiency in actuation. The final approach is based on the control

allocation technique. It considers the tracking requirements and the constraints of the actuators in the design process. To accommodate lock-in-place faults, a new control effort redistribution scheme was proposed using the fuzzy logic technique, assuming faults are provided by a fault detection system. The results of simulation testing on a Boeing 747 multi-effector model showed that the system managed to handle these faults and maintain good tracking and stability performance, with some acceptable degradation in particular fault scenarios. The limitations of the controller to handle a high degree of faults were also presented.

Table of contents

List of figures

List of tables

Nomenclature

Greek letters

α	Angle of attack
β	Sideslip angle
Δ	System's uncertainty
δ_a	Aileron angle deflection
δ_e	Elevator angle deflection
δ_f	Flap angle deflection
δ_r	Rudder angle deflection
η	Elevator deflection
γ	Flight path angle
μ	Structured singular value
ω	Frequency
ϕ	Rolling angle
ψ	Heading angle
σ	Upper singular value
Σ	Loss of efficiency factor
τ	Engine thrust
θ	Pitch angle
ξ	Aileron deflection

ζ Rudder deflection

Acronyms

ACE Actuator Control Electronics

AMS Attainable moment set

AoA Angle of attack

ARE Algebraic Riccati Equation

CA Control Allocation

CFIT Controlled Flight Into Terrain

DCA Dynamic control allocation

FBW Fly-by-wire

FDD Fault detection and diagnosis

FTC Fault-tolerant control

FTFC Fault-tolerant flight control

GM Gain margin

LFT Linear fractional transformation

LIP Lock in place

LIP Lock in place

LOC-I Loss of Control in flight

LPV Linear parameter varying

LQR Linear quadratic regulator

MFs Membership Functions

MIMO Multiple-input multiple-output

MPC Model predictive control

MRAC Model-reference adaptive control

PCA Propulsion Controlled Aircraft

PFC Primary Flight Computer

PID Proportional-Integral-Derivative control

PID proportional-integral-derivative

PM Phase margin

RAT Ram Air Turbine

RE Runway Excursion

RP Robust performance

SMC Sliding mode control

STC Self-tuning control

UAV Unmanned Aerial Vehicle

Roman letters

$\dot{u}$ Rate of change of control

$\dot{x}$ States of the system

C_D Drag coefficient

c_i Jammed control deflection for actuator i

C_L Lift coefficient

C_l Rolling moment coefficient

C_m Pitching moment coefficient

C_n Yawing moment coefficient

C_Y Side-force coefficient

D Drag

G_f Gain updating factor

I_x Moment of inertia around x

I_y	Moment of inertia around y
I_z	Moment of inertia around z
I_{xy}	Product of inertia around z
I_{xz}	Product of inertia around y
I_{yz}	Product of inertia around x
K_D	Derivative part for PID
K_I	Integral part for PID
K_p	Proportional gain for PID
L	Lift
Q	Weighting factor for tracking requirements
R	Weighting factor for control energy
T	Sampling time
t	Time
u	Control input of the system
u_A	Adaptive compensation
u_c	Additive faulty control input
U_e	Trimmed linear velocity along x
u_f	faulty control input
u_i	Control input for actuator i
u_s	Steady state control input
u_{max}	Maximum control
u_{min}	Minimum control
v	Virtual control
V_a	Total velocity vector

v_c	Command virtual control
V_e	Trimmed linear velocity along y
W_d	Weighting element for uncertainty
W_e	Trimmed linear velocity along z
W_e	Weighting element for tracking error
W_u	Weighting element for control input
x	An axial length or direction
x_cg	x-coordinate of aircraft centre of gravity
Y	Side-force
y	A lateral length or direction
y	Outputs of the system
z	A normal length or direction
b	Wing span
e	error
h	Altitude
H_∞	Hardy space
L	Total rolling moment around x
M	Total pitching moment around y
N	Total yawing moment around z
p	Rotational angular rates in the x direction
q	Dynamic pressure
q	Rotational angular rates in the y direction
r	Rotational angular rates in the z direction
S	Wing area

X	Total forces in the x direction
Y	Total forces in the y direction
Z	Total forces in the z direction

Chapter 1

Introduction

1.1 Motivation Towards the Fault-tolerant Control

Automated systems have been widely developed and applied to industrial processes to increase precision, productivity, and quality. In the case of flight control of air-vehicles, these systems are built to ensure the stability of the closed-loop system and to achieve a desired performance [1]. In highly automated industrial systems, in which the maintenance or repair cannot always be achieved immediately, systems become more complex and will be more vulnerable against faults [2]. Consequently, a conventional pre-designed feedback controller may result in an inadequate performance in the event of faults in the actuators, sensors, or other components of the system, which may lead to instability, loss of control, or catastrophic failures [3], [4], [5]. It is more convenient and safe to design control methods that ensure the nominal performance in the presence of faults [6], [7]. Loss of control accounts for over 25% of aircraft accidents worldwide [8]. Figure 1 shows the percentage of the total number of accidents since the year 1995 [9], where the categories of the cause of accidents are defined as follows:

- Loss of Control while in flight (**LOC-I**).
- Controlled Flight Into Terrain (**CFIT**): which means in-flight collision with terrain, obstacle, or water without indication of loss of control.
- Runway Excursion (**RE**): an over-run off the runway surface.

All other accident categories representing less than 10% are grouped under the "Other" category. Note that approximately 27% of accidents were due to LOC-I. The time-plot of the average accident rate per million flights due to these accident

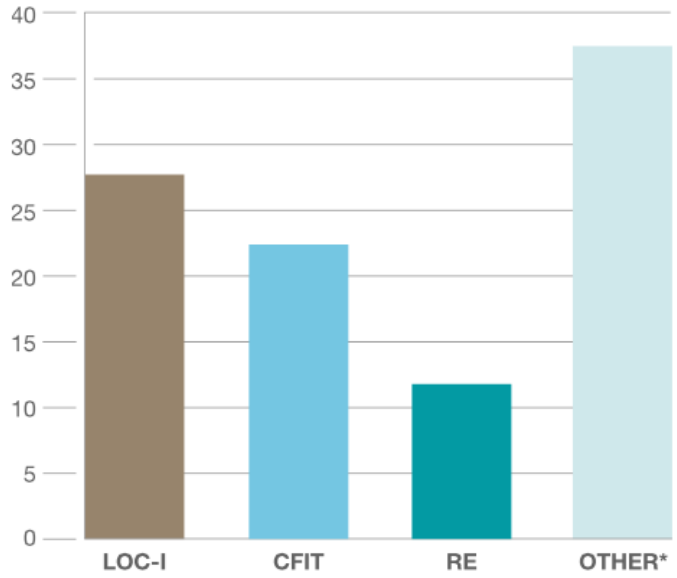

Fig. 1.1 Total number of aircraft accidents since 1995 [9].

categories is shown in Fig. 1.2. As in Fig.1.2, the safety measures taken toward the

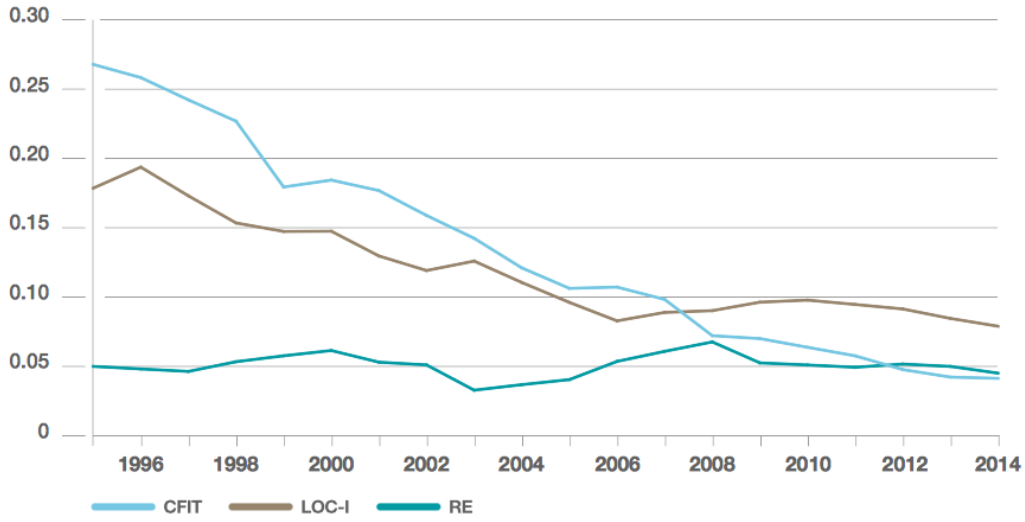

Fig. 1.2 Average accident rate per million flights in the past 10 years [9].

reduction of aircraft accidents resulted in the decrease in accident rates. Yet the LOC-I type of fault only decreased by 50%, while CFIT successfully decreased by 85% between the years 1995 and 2014. In another statistical report produced by Boeing [10], the loss of control in flight type of fault resulted in 1656 fatalities as 41% of the total accident fatalities for the period of 2005-2014. In second place was the CFIT, with 803 fatalities as 20% of total fatalities, followed by RE with 18.8%. Moreover, if we want to consider the probabilities of accidents from the phase of

flight aspect, we can see that in Fig.1.3 48% of aircraft accidents are occurring in the final approach and landing, resulting in 38% of onboard fatalities.

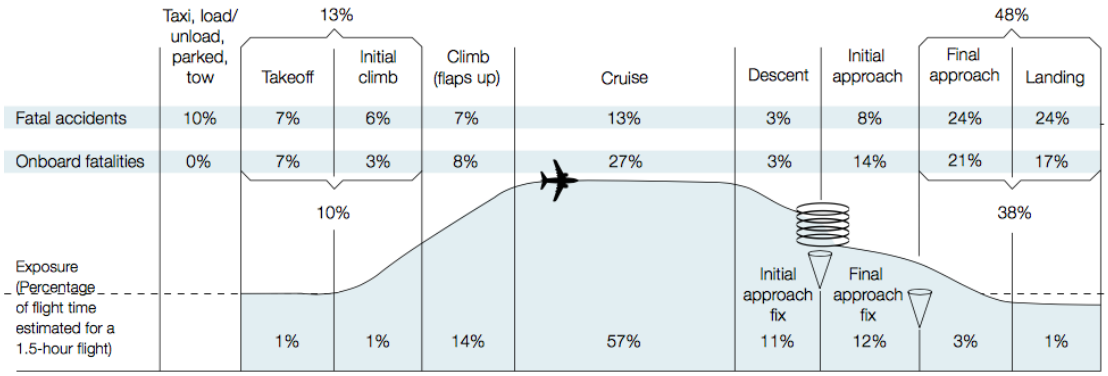

Fig. 1.3 On-board fatalities and fatal accidents by phase of flight [10].

1.2 Safety index and reliability

The reliability of a flight control system is determined by its probability of failure per flight hour. Another alternative description is the mean time between failures, where time is in units of flight hours [11]. Typical reliability requirement figures for some aircraft are presented in Table 1.1.

Table 1.1 Reliability requirements for aircraft automatic flight control system.

System application	Probability of the total system failure
Military combat aircraft with mechanical controls	$< 10^{-5}$ per hour
Military combat aircraft with fly-by-wire control system	$< 10^{-7}$ per hour
Civil transport aircraft with fly-by-wire control system	$< 10^{-9}$per hour

For human and operational safety, these reliability requirements are made very low. To get an idea, a failure probability of a civil aircraft of $< 10^{-9}$ per hour means that a fleet of 1000 aircraft that fly an average of 3000 hours annually will experience a total failure of the fly-by-wire system in 300 years. The current civil transport aircraft reliability figure is approximately $< 10^{-6}$ per hour [12]. The affirmation that a given flight control system meets the reliability requirements is a difficult task

because it is not possible to put the modern flight control system on test for the determined period of time. However, a reliability of the system can be estimated based on the known or estimated failure rates of the components making up the complete system [11].

1.3 System redundancy

In the presence of major actuator failures, it is sometimes impossible to maintain the faulty system at the original levels of performance. It becomes of principal importance to bring the system as close as possible to its best operating condition with respect to the desired performances. Therefore, the primary required feature is to minimize the loss in controllability or/and to sustain the system to operate safely without danger to people or loss of equipment. The system should continue its operation with allowable decrease in performance as long as it remains within particular acceptable limits. The machinery backup tools that are prepared to avoid the cut, or loss of efficiency of any of the system's functions, are called the hardware (physical) redundancy. Thus, it refers to the duplication of critically important systems (i.e. actuators and sensors). This concept, which sometimes also is called direct redundancy, allows for using simple schemes for the alleviation and detection of failures and faults at the price of increased system cost [6]. Hardware redundancy is fundamentally important in systems where the safety of individuals could be affected. In aircraft, for example, multiple flight computers (i.e. five on the A330/A340 and six on the A380) and different power sources are used for the control surface actuation. Three hydraulic sources are used on the A340/A320, while two hydraulic and two electric power sources are used on the A380. Additionally, for the A380 the engine power also pressurizes the hydraulic circuits and supplies the electric network. Moreover, in an emergency situation, a Ram Air Turbine (RAT) is used to provide the energy to pressurize important hydraulic circuits [7]. Likewise, to provide inertial information and air data to other systems, multiple and identical sensors are used. More examples of the hardware redundancy are presented in [7], [12], and [11].

The use of redundant hardware back-up approaches will add cost, volume, and weight penalties to the aircraft [4]. Moreover, redundant architectures can increase the aircraft's maintenance time due to an increase in the number of parts and complexity. Redundant sensors are considerably easier and less expensive to install than actuators.

After the development of fly-by-wire flight control systems in the late 1970s, flight control computers became critical components in automated flight control

systems. This led to the development of analytical redundancy methods, which use signals generated from the mathematical model of the system for the fault accommodation [3]. Analytical redundancy considers the functional relationship between a system's inputs and outputs, rather than the components themselves. For example, measured quantities can often be calculated from other quantities by means of algebraic or, more often, via dynamic relationships. Likewise, outputs strongly influenced by some control input are often also controllable from other inputs, albeit with different gains and time constants. Analytical redundancy is more challenging to use than physical redundancy, but it allows for building more cost-efficient systems [6]. This redundancy approach increases the reliability through software rather than strictly hardware [13]. Nevertheless, attention must be paid to how to effectively and efficiently utilize the analytical redundancy [14]. Challenging issues for FTC design include the integration of hardware and software redundancy [3].

1.4 Thesis outline

In this work, the development of a fault-tolerant control (FTC) system for an aircraft is considered. The FTC exploits both hardware and analytical redundancy, with some specific emphasis on the mitigation of failures to enhance the safety of flight. The thesis is presented as follows: in Chapter 2, fault-tolerant control is described with the classification of FTC application methods. Chapter 3 presents the background theory of aircraft dynamics and control that is essential for the FTC analysis and design. In Chapter 4, a fault-tolerant control system that encompasses optimal linear quadratic regulator control augmented with an adaptive fault-compensation-based scheme is presented. As an optimal multivariable controller, the LQR baseline control law was formulated. It handles the problem of tracking error and control energy minimisation. The FTC system was developed based on a linear dynamic model and then tested initially for performance and stability optimisation. For validation of control viability, a nonlinear 6-degree-of-freedom (dof) simulation was performed. In Chapter 5, the robust features of the H_∞ and μ-synthesis techniques were utilized to design an FTC in which actuator loss of efficiency faults have been modeled as an uncertainty in the system. Robust computation involved the minimisation of a cost function that considers multiple design objectives, which are the tracking error minimisation, control energy minimisation, and the uncertainties handling. Extensive nonlinear simulations were also conducted to validate the developed scheme. Chapter 6 presents the development of a reconfigurable fault-tolerant flight control system for a multi-effector aircraft. The aircraft has redundant ailerons and a rudder,

which act as primary control inputs for the considered lateral motion. The approach includes optimal control allocation development that handles the redundancy of the control surfaces, tracking requirements, and actuator constraints. A new control redistribution process was proposed for the lock-in-place type of faults in the actuators. This approach relies on and assumes an effective onboard fault detection and diagnosis (FDD) system that provides precise fault information of the actuators. To handle the interpolation between the faults and the control redistribution, fuzzy logic was implemented. The system was tested for different fault scenarios. Finally, Chapter 7 concludes with the main outcomes of the experiments and some recommendations for further work.

1.5 Contributions

LQR and Adaptive Compensations:

- An adaptive fault-compensation approach was added to the optimal LQR controller used to control a multiple-input multiple-output (MIMO) aircraft system. The baseline LQR obtains the optimal control solution that maintains the tracking requirements of the aircraft and minimises the control efforts. For a fault-tolerant approach, an adaptive fault-compensation-based technique was developed that can accommodate the loss-of-effectiveness faults.

- To validate the performance of the linear-based FTC control approach, nonlinear simulation testing was performed.

H_∞ and μ-synthesis:

- Robust H_∞ and μ-synthesis techniques have been formulated for a multi-variable aircraft system subjected to actuation faults.

- The nonlinear simulation testing of the scheme was conducted against actuator faults at different operating conditions in the flight envelope (the ascending, cruise, and descending cases were considered).

FTC using reconfigurable CA

- Different than existing methods of fault-tolerant control allocation techniques, the developed approach incorporates a new control redistribution process, which is updated when faults occur.

- Further, fuzzy logic is used to correlate between faults and control redistribution. Existing works assume certain faults in the model and produce the FTC lookup tables accordingly. In contrast, fuzzy logic implementation can handle a wide range of fault magnitudes online, by interpolation.
- Moreover, this method deals with a more severe type of faults, which is the lock-in-place fault. It handles faulty situations and enhances the flying quality with multi-effector controls.

Chapter 2

Fault-Tolerant Control: An Overview

2.1 Definitions of fault-tolerant control

The fault-tolerant control (FTC) system for an aircraft exploits both the hardware and analytical redundancy, with emphasis on failure mitigation to enhance flight safety. Thus, it is suitable to start with a brief definition of some terms and expressions that will be used throughout this thesis. The terminology of faults and failures used in the FTC field was not unique, until the International Federation of Automatic Control (the technical committee) made the relevant definitions related to this subject. The definitions are as follows [15]:

Fault: is a deviation of one or more of the characteristic parameters or properties of the system from an acceptable standard or usual condition.

Failure: is the permanent interruption of a system as it operates or performs certain required functions.

These definitions were given to set a standard in this area to avoid confusion among researchers [16]. The FTC is defined as a physical control system, which not only performs regular control functions but also is capable of maintaining the safety of the system in the event of faults. It has the following features [3]:

- the ability to accommodate faults of the system
- the ability to maintain the overall system's stability and adequate performance in the event of faults

It was also known as a self-repairing, restructurable, reconfigurable, or self-designing control system that survives a major system fault [17]. Consequently, the main objective of this controller is to guarantee the system's stability while the

original performance is restored as much as possible. The unfaulty performance may not be fully achieved; however, the aircraft can be flown in a degraded mode but with sufficiently acceptable handling qualities.

2.2 Fault types and modelling

Faults and failures could be categorized based on their location as follows [18]:
Actuator faults: They represent total or partial loss of control action. Total actuator faults can occur as a result of burned or cut wiring, breakage, short circuits, or due to a foreign body presented in the actuator, etc. Partially failed actuators, which produce only part of the normal actuation, can result from pneumatic or hydraulic leakage, fall in the supply voltage, or increased resistance, etc.
Sensor faults: These faults represent incorrect readings from sensors, and can also be divided into partial and total faults. Total sensor faults give information that is not the real value of the measured physical parameter. Partial sensor faults give readings in such a way that some useful information could be retrieved. To increase fault tolerance, and due to their smaller sizes, sensors can be duplicated in the system.
Component faults: These are faults in components of the plant itself, and represent changes in the system's physical parameters, e.g. mass, aerodynamic coefficients, or damping constants, etc., which are often due to structural damages. They are very diverse and cover an extensive class of unanticipated situations.
The three types of faults are shown in Fig. 2.1 as classified in [18].

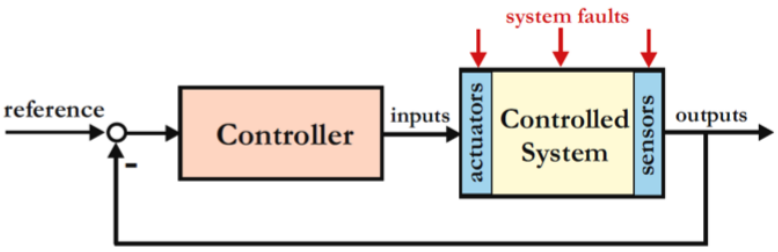

Fig. 2.1 Types of faults affecting the system [18].

In this thesis, only actuator faults are considered. They are classified in the literature as follows [19], [20]:

- **Lock in place**: when an actuator becomes stuck and immovable, because of a mechanical jam, for example, due to lack of lubrication. This type of failure has occurred in incidents such as Flight 1080 (Lockheed L-1011, 1977, San

Diego) where one of the horizontal stabilizers jammed in the full-up position; and Flight 96 (DC-10, 1972, Windsor, Ontario) where the rudder jammed.

- **Float**: where the control surface moves freely and does not provide any moment to the aircraft, which might be due to the loss of hydraulic fluid or the control surface itself. It occurred in incidents including Flight 123 (B-747, 1985, Japan) resulting from a total loss of hydraulics and DHL A300B4 (A300, 2003, Baghdad).

- **Hardover**: a situation in which the control surface moves until it reaches its maximum position limit. Such a failure could be caused by an uncommanded large electric signal sent to the actuators. This type of failure occurred in incidents such as Flight 85 (B-747, 2002, Alaska), which suffered from a lower rudder full left deflection.

- **Loss of effectiveness**: where an actuator's effectiveness reduces. Potential reasons for such a failure are lack of hydraulic fluids or insufficient lubrication.

Fig. 2.2 illustrates these actuation failures.

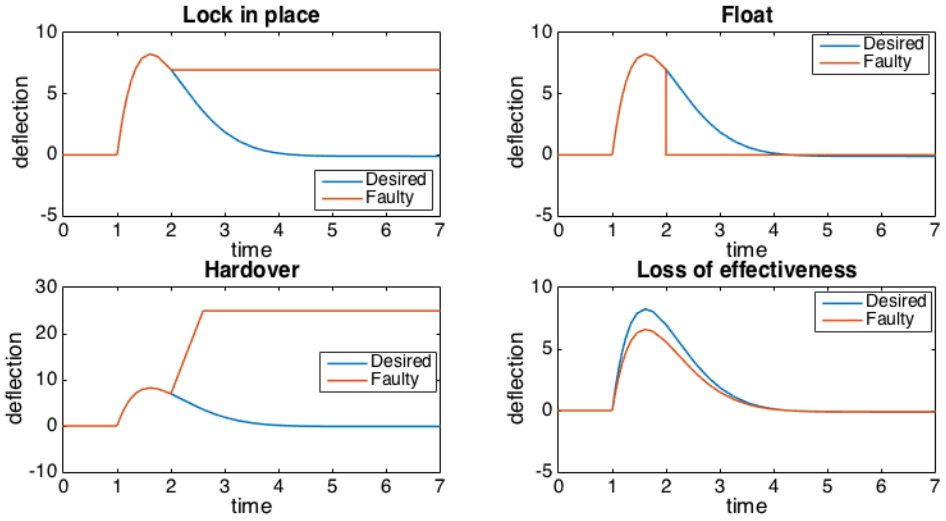

Fig. 2.2 Types of actuator faults

2.2.1 Mathematical description

To formulate a mathematical model for faults, different approaches have been proposed. In general, the modelling depends on the type of the fault (i.e. whether it occurs in the system's actuators or sensors). In this work, faults in the actuators,

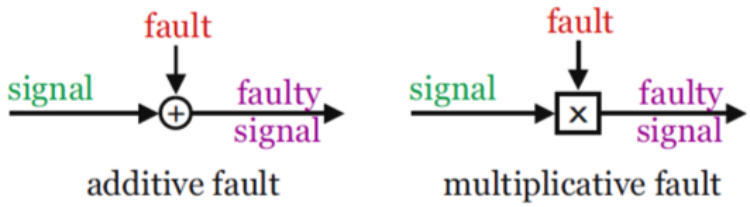

Fig. 2.3 Multiplicative and additive faults to the system input

which are the input of the system, are considered, and they are modelled as additive and/or multiplicative faults, as shown in Fig. 2.2 [18].

The fault is mathematically denoted by a constant that represents the jammed actuator or by a multiplication of a gain to the control input that represent the loss of efficiency. For a number of actuators m, the fault is expressed by:

$$u_i(t) = \begin{cases} u_i(t) & \text{nominal} \\ c_i & \text{lock in place} \\ u_{i,max} & \text{hardover} \\ \rho \times u_i(t), \quad 0 < \rho < 1 & \text{loss of effectiveness} \\ 0 & \text{float} \end{cases}$$

where i=1,. . . .,m, and c_i is a fixed constant angle that represents the jammed deflection of the corresponding actuator. In the work presented in [21], the faults' mathematical integration to the linear system is defined as follows

$$u_f = \sum \times u + u_c$$

where:

- u_f is the faulty control input
- u is the nominal control
- $\sum = diag([\alpha_1, \ \ldots \alpha_m])$ is the loss of efficiency on the nominal control inputs. α varies between 0 and 1
- u_c is the additive faulty input

In this thesis, at each case of the FTC development, a relevant fault modelling method is utilised. In the next section, an overview of fault detection and diagnosis (FDD) systems is given.

2.3 Fault detection and diagnosis

The design of the FDD is beyond the scope of this thesis. However, it is very useful to provide a brief overview of the subject. The definition and classifications of FDD are presented. The FDD scheme has two main tasks that are defined as follows [3], [22], [23]:

- **Detection**: Indicates that something in the system is malfunctioning. It detects the occurrence of a fault and the time of the fault.
- **Diagnosis**: Consists of:
  - Isolation: determines the type and the location of the fault (which component has failed).
  - Identification: determines the magnitude (size) of the fault.

Primarily, two types of FDD approaches exist: the model-based and the data-based approaches [3]. As the predominantly applied technique, the model-based FDD scheme essentially uses a mathematical model to carry out the FDD in real time. The non-model-based approaches utilize artificial intelligence and soft computing to observe the fault [24]. The FDD unit needs to indicate the true status of the entire system as promptly and accurately as possible, while rejecting false alarms resulting from noise or spurious signals [25]. Information provided by the FDD on the system fault has a direct impact on the control reconfiguration. Incorrect reactions will be produced if unfavorable FDD information is supplied, which will affect the safety. Thus, the FDD implementation requires a balance between high rate of fault detection and low rate of false alarms [2]. For more details on FDD, see [2], [3], [20], and [22].

2.4 Real-world FTC operation

In this section, the design philosophy and implementations of fault-tolerant flight control by Airbus and Boeing on selected aircraft are presented.

2.4.1 Airbus philosophy

Dissimilarity: To ensure a fault tolerance, all Airbus aircrafts are fitted with two types of computers, a primary and secondary computer. For example, five multiple FBW computers are used in the A330/A340 aircraft, and six computers on the A380. They are different in their hardware and software, and are developed by different

teams. Figure 7 shows diversities of flight computers for the A340 and A380. To avoid a total loss in the case of any damage, computers are installed at different places on the aircraft [7].

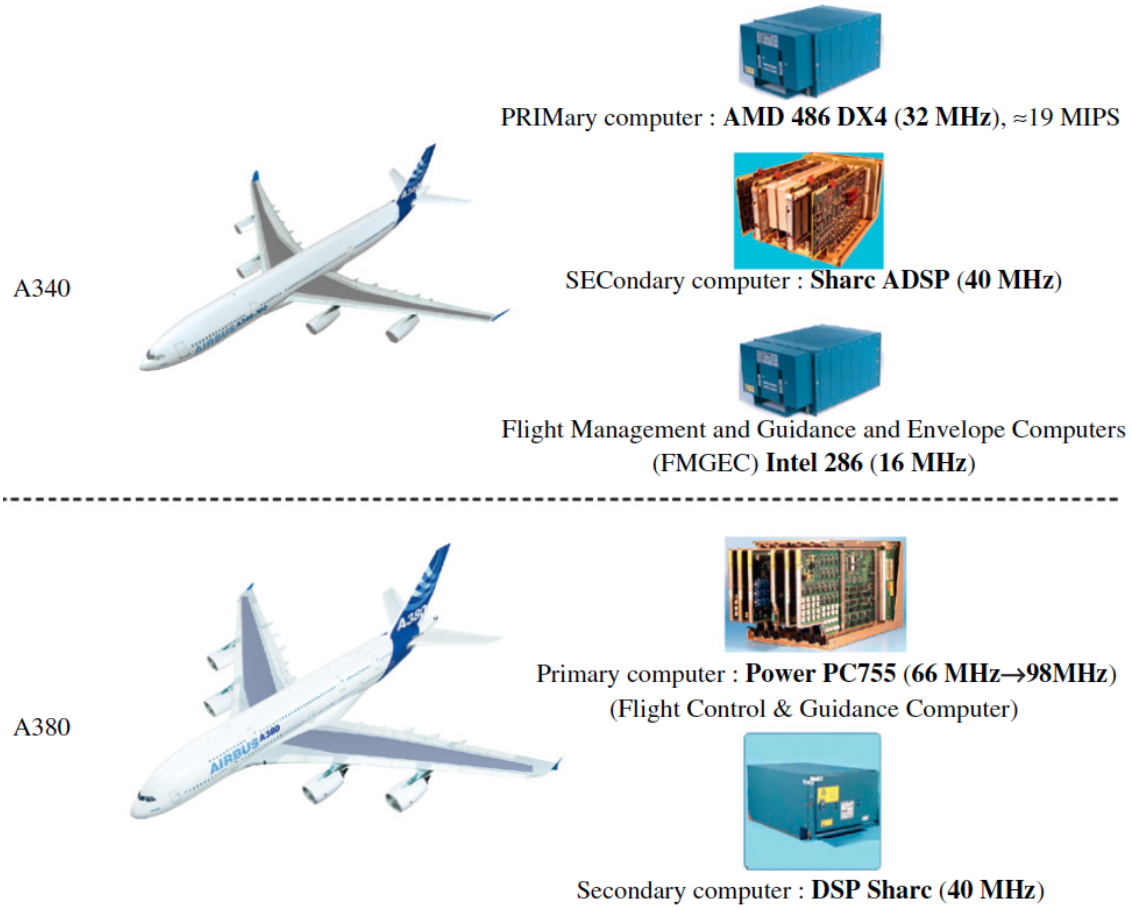

Fig. 2.4 Varieties of flight computers for A340 and A380 [7].

Hardware redundancy: To mitigate the risk of faults or failures, critical systems such as the actuation power sources are duplicated. For instance, three hydraulic sources are used in the A340/A320. The A380 uses two hydraulic and two electric power sources to actuate the control surfaces. Additionally, for the A380, the engine power also pressurizes important hydraulic circuits. Moreover, in an emergency situation, a Ram Air Turbine (RAT) will be used to provide the energy to pressurize important hydraulic circuits [7].

Reconfiguration: This means that automatic management following the system's failure is a central point in the design of the fault-tolerant control. In Airbus aircraft, two levels of reconfiguration are established:

The first type is system reconfiguration, in which the control surface has two actuators, as shown in Figure 8.

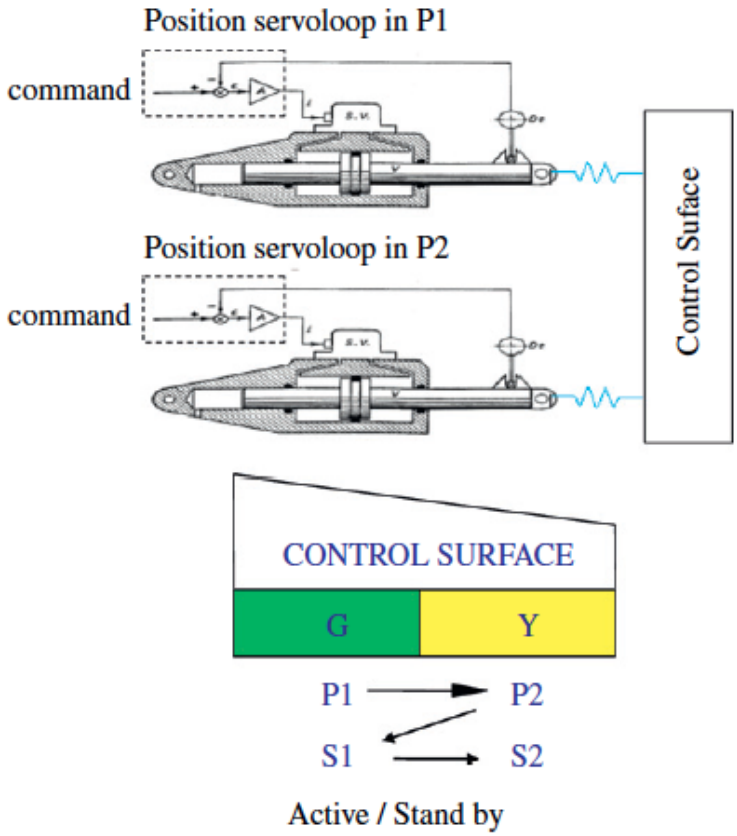

Fig. 2.5 Actuator reconfigurations by Airbus [7].

The first actuator is in active mode and is servo-controlled by a computer P1. The second one is in a standby passive mode and follows the movement of the active actuator. It is connected with a second computer P2. If the active actuator fails, it changes to a passive mode, while the other one become active. Hence, this type of reconfiguration is generally based on the hardware redundancy of systems.
The second type is the flight control law reconfiguration. At the normal conditions, the aircraft is protected against critical events, and the corresponding flight control law is referred to as the "normal law". Operation provides protection against over-speed, excessive load factor, stall, extreme bank angle, etc. Following a failure, i.e. the loss of a control surface, some protection can be lost, and the system begins to enter low-level laws where flight is sill possible but without the full flight envelope protection. The last lower level is the direct law, where no protection is provided and the aircraft is trimmed manually. This type of reconfiguration is due to the loss of hardware redundancy.

2.4.2 Boeing philosophy: the B777 as an example

The first commercial transport manufactured by Boeing that employees the FBW flight control system is the Boeing 777 [26]. In terms of hardware redundancy, hydraulically powered and electrically signaled actuators control the control surfaces on the wing and tail of the B777. Two actuators per surface control the elevators, ailerons, and flaperons, while three control the rudder. The actuation that powers the ailerons, elevators, flaperons, and rudder has several operational modes defined as follows [27]:
Active mode, in which all actuators receive commands from their respective Actuator Control Electronics (ACE) computers, and accordingly position the surface. Actuators will remain in this mode unless commanded by the ACEs.
Bypassed mode, where the actuator does not respond to commands from ACE but instead moves freely while the redundant actuators for a given control surface position the surface.
Damped mode, which is similar to the bypassed mode except the actuators are allowed to move but at a restricted rate sufficient for the airplane control.
Blocked mode in which failed actuators are not allowed to move, providing hydraulic lock in the surface. This mode exists for elevator and aileron actuators.

The Flight Control System of the aircraft has three operating modes: Normal, Secondary, and Direct modes [27], defined as:
Normal mode: in which the PFCs provide actuator position commands to the ACEs with full functionality of envelope protection, enhanced performance, and ride qualities.
Secondary mode: which is similar to the normal mode except the functionality is reduced. An example is that the envelope is no longer protected. When sufficient failures in the system are detected, the system enters this mode automatically.
Finally, the **Direct mode**, in which the ACEs do not take commands from PFCs, but instead decode the pilot's commands directly. Total failure of all the three PFCs, loss of flight control data busses, or internal failures of ACEs will let the system enter this mode.

2.5 Fault tolerance control techniques

In this section, a general overview of the fault-tolerant control methods discussed in literature is presented. Research efforts on Fault-Tolerant Flight Control (FTFC), an area that has gained increased attention in the aerospace community motivated

by several aircraft accidents, were initiated to accommodate in-flight faults and improve the safety and reliability of the systems. FTFC aims to utilize all remaining control effectors of the aircraft after an unanticipated mechanical or structural failure. This is to recover its performance by automatic redesign of the flight control system with sufficiently acceptable handling qualities. An extensive overview of fault-tolerant control approaches is presented in [3]. In general, the fault-tolerant control analysis includes analysis of the system's input to determine the available redundancy. In addition, it includes fault modelling that is to be considered in the control computation. Fault-tolerant control can be classified into two main groups [3], [28], [29]:

- Passive fault-tolerant control systems
- Active fault-tolerant control systems

Passive fault-tolerant control relies on the robustness of the control design paradigm against faults and uncertainties. Therefore, in the event of a fault, the controller should be able to maintain the system's stability with an acceptable degradation in the performance. This control system does not require a fault detection system nor controller reconfiguration or adaptation. Conversely, active fault-tolerant control systems respond to failures in an active way by control reconfiguration or adaptation so that the stability of the entire system can be maintained. This reconfiguration requires a fault detection scheme to provide fault information [15]. Figure 2.4 shows classifications of fault-tolerant control systems and provides examples of control techniques.

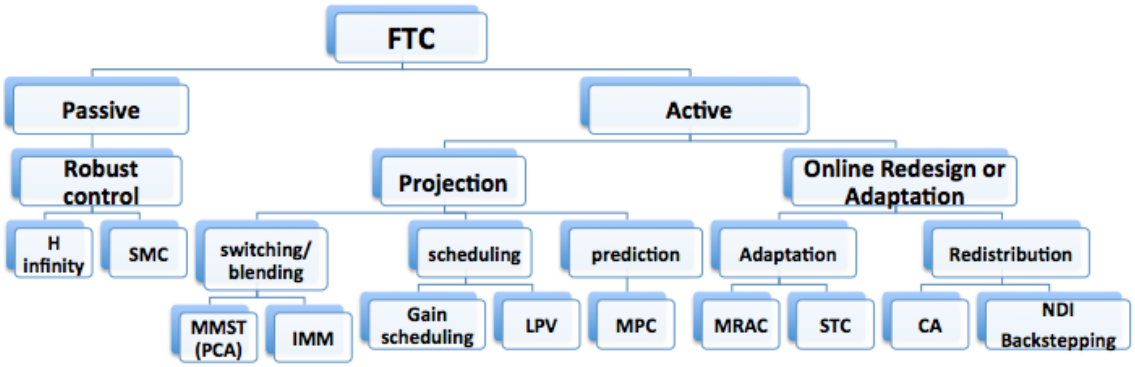

Fig. 2.6 Classifications of FTC methods [3, 28, 29].

A limited amount of time available for recovery is available for the safety-critical systems when they are experiencing malfunctions in operation. In the active fault-tolerant control system where fault detection and diagnosis is needed, the time of

recovery will play an important role in the stability of the system, as illustrated in Figure 2.7. The time available for recovery depends on the magnitude of the fault, its occurrence time, and the states of the system. The time needed by the FTC to cope with the problem is closely tied with control efficiency, FDD efficiency, fault type, and the degree of severity of faults [2].

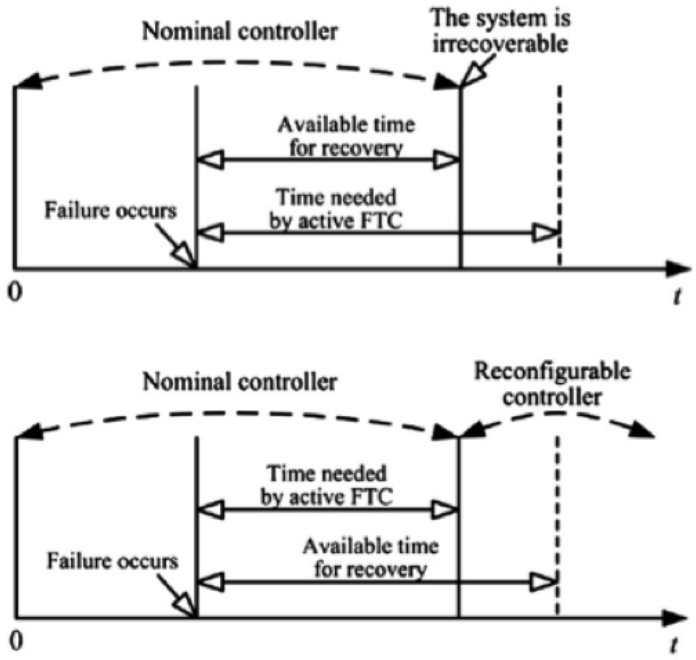

Fig. 2.7 Time for recovery vs. time needed by FTC [2].

When the time needed by FTC to recover the system exceeds the available time for recovery, then the system becomes unstable or unrecoverable. A work presented by [30] includes a comparative study between passive and active faults. Although different types of faults are introduced to various controllers, the study presents the advantages and disadvantages of each method. In the next section, the two main categories of FTC methods are presented.

2.5.1 Passive fault-tolerant control

In the absence of fault information, several methods have been proposed to achieve robust performance and/or stability in the presence of a bounded uncertainty. The passive approach neither has a reconfiguration mechanism nor an FDD unit; hence, it is relatively simple to implement compared to the active methods. Moreover, the controller is always engaged, no time delay issue exists, and there are no additional actions to be taken in any passive FTC scheme. As a result, switching is no longer a concern [2]. However, its fault-tolerant capabilities will shrink as the number or

magnitudes of fault increase. If too many faults are to be considered at the design process, one may not be able to find a passive FTCS altogether [30]. Considering these advantages and disadvantages, different passive control methods can be employed. The main techniques are briefly presented.

Robust Control (H_∞ Control)
One of the most common robust control methodologies established in the 1990s is the H_∞ control technique, which was proposed by Duncan McFarlane and Keith Glover [31]. It was one of the most developed methods for multivariable control, and had a variety of applications (i.e. industrial process control and aircraft control problems) [32]. One shortcoming of the H_∞ technique is that in some cases the controller is conservative in the nominal conditions, and the performance is sometimes sacrificed for robustness. Moreover, the designed controller is typically of a higher order than the system. In the field of FTC, papers such as [33] and a chapter in [32] describe some of the research applied in the area of flight control.

Sliding Mode Control (SMC)
The primary advantage of the SMC is its robustness against model uncertainties, external disturbances, and variations in system parameters [34]. The benefits of this controller for reconfigurable systems are that it can handle structural failures that modify the dynamics of the plant within the assumed uncertainty, and the online adaptation can handle partial loss of actuator. Although this technique improves the aircraft control system, the use of SMC has limitations if presented with the full reconfigurable problem. For every controlled variable, there must be one control surface to handle uncertainties resulting from faults. Extensive tuning of the controllers that include all possible failure cases is required [18].

2.5.2 Active fault-tolerant control

The active FTC approaches are more flexible for dealing with different types of faults. Failure scenarios beyond the design-based faults are possibly considered. However, the quality of the active FTCS depends profoundly on the FDD scheme to provide accurate and timely fault information. Any time delay or uncertainties in the FDD can reduce the effectiveness of the active FTCS. Some reconfigurable flight control systems have been flight tested, but currently no reconfigurable fault-tolerant flight controls have been certified or applied in any commercial or military aircraft [18]. In the following paragraphs, the main procedures used in the active fault-tolerant

approach are presented.

Switching or blending / multiple model

Using multiple models for control reconfiguration was introduced in the early 1990s [35]. In real systems, linear controllers are adapted to changes in operating conditions. Therefore, using multiple model schemes is a proposed way to ensure that the controller is designed to guarantee stability and performance for a wide flight envelope. A devoted model describes the dynamics at each fault scenario. The models are then paired with their corresponding controllers. The control system is reconfigured by choosing the model/controller pair that is the most appropriate at each time step. Different controllers for different possible faults and failure modes are designed, and related controllers are only activated when faults occur. Limitations of this approach appear when unmodelled faults are encountered. Moreover, the method cannot handle multiple failures/faults simultaneously. Additionally, the number of individual pairs of models to be designed may at times become remarkably large if the system is to successfully operate with a wide range of failure scenarios [36]. The application of multiple model ideas as an FTC for aircraft systems can be found in [37] and recently in [38].

Propulsion Controlled Aircraft (PCA)

After the possibility of controlling the aircraft using only the engine throttles had been demonstrated by the Sioux City accident, and following a recommendation from the NTSB of America, the PCA problem was investigated by the NASA Dryden Flight Research Centre [39], [40]. The aim was to provide a backup in the case of total hydraulic failure. PCA is a multi-model approach in which the fault model is similar to the nominal one, but the control surfaces are assumed to be free floating. In 1995, demonstrations were made where an MD-11 and an F-15 had been recovered from complete hydraulic failures and landed successfully under propulsion-only control [41]. PCA is a useful and essential idea and solves very practical problems. However, it is not appropriate to solve general reconfigurable control problems [15].

Scheduling

Gain scheduling deals with decomposing the nonlinear system into a set of linear systems and designing a linear controller for each case [42]. The computed linear models and their associated controllers are then scheduled. Models vary based on some parameters of the system, i.e. the states. In the case of a non-normal operation, no changes are made to the structure of the controller, but instead the controller

gains are changed accordingly, where pre-defined gains are chosen for certain flight conditions. The switching between two gains is made by a simple logic switch or through the use of look-up tables or curve fitting [43]. The gain scheduling is easily understood and implemented; however, in some fault cases, the structure of the nominal controller cannot cope sufficiently. Thus, the control adaptation or reconfiguration could be a prominent solution. Information on gain scheduling can be found in [42].
The linear parameter varying (LPV) control method is another type of scheduling. It was developed due to the lack of stability and performance of classical gain scheduling [44]. Moreover, it was needed for the problem of designing multiple controllers for different models for a large flight envelope [24]. The idea behind an LPV is to obtain linear models that vary with parameters such as altitude or speed. Different methods for obtaining the LPV models are presented in [43]. After obtaining the LPV models, the controller can be designed. Methods such as the Lyapunov [45] or the small gain theorem can be used to obtain the controllers. Compared to the classical gain scheduling technique in which the gains are interpolated from pre-computed values, the LPV controllers are dependent on the parametric changes in the system. For the FTC problem, works that are based on the LPV technique with actuator faults/failures are presented in [44], [46], and [47].

Prediction

Initially, model predictive control (MPC) was developed in the process industry because the concept and the mathematical description are easy to understand by most control engineers. Therefore, it is not surprising that, other than classical PID control, MPC is the most broadly implemented method in the process control industry [48]. The original idea for MPC was to allow the production process to run very close to the process limits to maximize production and therefore profit. Model predictive control has been applied for flight control reconfiguration due to its ability of handling constraints and changing model dynamics systematically [18]. An example of MPC in the field of fault-tolerant flight control can be found in [32]. During faults/failures, the remaining working control surfaces will be driven to their limits [49]. As a result of the boost in computational power in modern control systems, MPC had been used for real-time control of a small hovercraft [50]. Another example is discussed in [51], in which MPC had been implemented for real-time control of an unmanned aerial vehicle. MPC in its most powerful form requires an on-line solution to the constrained optimization problem [48], which is still hard to achieve for systems that require fast responses—such as aircraft. Moreover, tuning

the flight control system requires trial and error experience [29].

Adaptation

Adaptive control was proposed to deal with a wide range of flight conditions [52]. The proposal was followed by the need to design autopilots for high-performance aircraft. It is used to automatically adjust the parameters of the controller to achieve the desired performance. In adaptive control, two approaches can be taken: direct and indirect adaptation [53]. In indirect adaptation, the system parameters that changed due to operating conditions changes (i.e. faults) are estimated; these estimations are used to design the controller. A common example of this adaptation is self-tuning control (STC).

In contrast, the direct adaptation approach does not require estimating the system parameters to design the controller. A practical example of this adaptation is the model-reference adaptive control (MRAC), in which the unknown parameters are not estimated; rather, they are tuned and adjusted for the output of the plant to follow the desired trajectory [15].

Control Signal Redistribution

The idea of redistributing control signals to the remaining healthy actuators is also called "restructuring" [28]. It was not explored in the 90s but re-emerged in recent years as control allocation. This was because of the development of high-performance, highly redundant aircraft and the improvements in computational power. Control allocation (CA) has the ability of redistributing the control command signals to actuators, especially during faults/failures. The controller is designed based on "virtual control" signals by mapping them for the actual control demand to the actuators. The controller design is independent of the control allocation unit; therefore, it can be used in combination with any other controller design paradigm. Another advantage is that the actuator limitations are handled by including the actuator constraint in the optimization process [29]. The challenge of CA is that, for linear systems, the pure factorization of the input distribution matrix is strongly required, and therefore some approximations have to be made [54].

2.6 Conclusion

In this chapter, an overview of fault-tolerant control for fixed wing aircraft is given. The individual definitions of faults and failures of system components are presented, followed by types of actuator faults and how they are represented mathematically in

the system. Further, a brief presentation of the developments of FTC systems in aircraft by Airbus and Boeing is given. Finally, the fault-tolerant control techniques in the literature are presented. The next chapter discusses the essentials of aircraft flight dynamics and control.

Chapter 3

Aircraft Dynamics and Automatic Control

Flight dynamics deals primarily with the response of an aerial-vehicle to the control inputs and to perturbations from the flight environments. In this response realisation, it is necessary to characterize the propulsive and aerodynamic forces and moments acting on the vehicle, which depend on the flight variables, including airspeed and the vehicle's geometry and orientation [55]. Systems can be described by mathematical equations, which provide the means of systems analysis, control, and other applications. They are represented by different types of models, based on how their parameters are correlated. Table 3.1 lists some basic definitions for different system models [56].

This chapter will present the basic principles of aircraft dynamics and control required for the realisation of aerodynamic notations, stability, equations of motion, and flight control.

3.1 Basic aerodynamics

To implement a suitable mathematical model for the aircraft motion, the basic definitions and characteristics are studied. The aircraft's standard notations for translational and rotational motions are shown in Fig. 3.1 and described below:

- The variables x, y, z represent the aircraft's axes. The x-axis starts from the origin and points toward the nose of the aircraft. The z–axis, which is perpendicular to the x-axis, is pointing down; while the y-axis is perpendicular to the x and z axes and pointing out toward the right wing.

Table 3.1 Basic definitions of systems' models [56]

Type of model	Definition criterion	Type of model equation
Nonlinear	Superposition does not apply	Nonlinear differential equations
Linear	Superposition applies	Linear differential equation
Time-varying	Model parameters vary in time	Differential equations with time-varying coefficients
Continuous	Dependent variables defined over continuous range of independent variables	Differential equations
Discrete	Dependent variables defined only for distinct values of independent variables	Time-difference equation

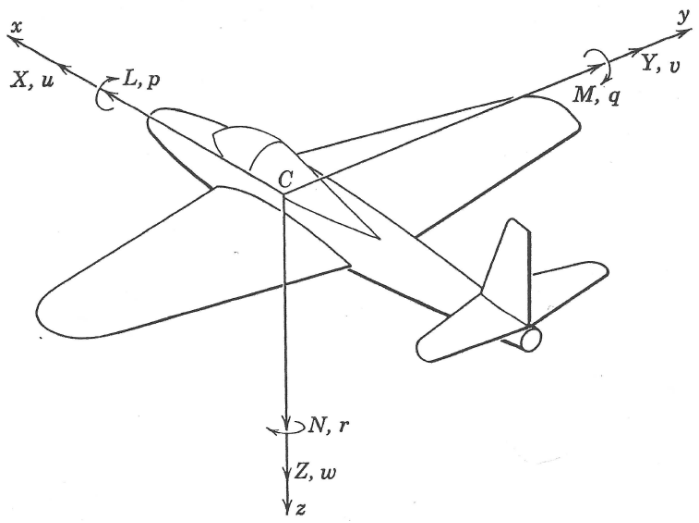

Fig. 3.1 Aircraft motion variables [55].

- The variables u, v, w represent the components of the linear velocities along the x, y, and z directions, respectively.

- The variables X, Y, Z represent the components of the total forces in the directions of x, y, and z.

- The variables p, q, r represent the rotational angular rates around the x, y, and z axes.
- The variables L, M, N represent the components of the total moments about the x, y, and z axes.

3.1.1 Forces and moments

The forces and moments acting on the aircraft's body are defined in terms of the aerodynamic coefficients as follows:

Forces	Drag	$D = qSC_D$
	Lift	$L = qSC_L$
	Side force	$Y = qSC_Y$
Moments	Rolling moment	$L = qSbC_l$
	Pitching moment	$M = qScC_m$
	Yawing moment	$N = qSbC_n$

where q is the free stream dynamic pressure, S is the reference wing area, b is the wing span, and c is the wing's mean aerodynamic chord.
Forces and moments are expressed in terms of their coefficients. The coefficients have some changing terms with time, while some terms, related to aircraft specifications, are constant. Changing terms are those that depend on angle of attack (α), sideslip angle (β), Mach number, and the actuation deflections, as presented in the following equations.

Force coefficients

$$C_L = C_{L0} + C_L^{\alpha} \cdot \alpha + C_L^{\delta_f} \cdot \delta_f + C_L^{\delta_e} \cdot \delta_e + \frac{c}{2V_a}(C_L^{\dot{\alpha}} \cdot \dot{\alpha} + C_L^{q} \cdot q) + C_L^{M} \cdot M \tag{3.1}$$

$$C_D = C_{D0} + \frac{(C_L - C_{L0})^2}{\pi e AR} + C_D^{\delta_f} \cdot \delta_f + C_D^{\delta_e} \cdot \delta_e + C_D^{\delta_a} \cdot \delta_a + C_D^{\delta_r} \cdot \delta_r + C_L^{M} \cdot M \tag{3.2}$$

$$C_Y = C_Y^{\beta} \cdot \beta + C_Y^{\delta_a} \cdot \delta_a + C_Y^{\delta_r} \cdot \delta_r + \frac{b}{2V_a}(C_Y^{p} \cdot p + C_Y^{r} \cdot r) \tag{3.3}$$

Moment coefficients:

$$C_m = C_{m0} + C_m^{\alpha} \cdot \alpha + C_m^{\delta_f} \cdot \delta_f + C_m^{\delta_e} \cdot \delta_e + \frac{c}{2V_a}(C_m^{\dot{\alpha}} \cdot \dot{\alpha} + C_m^{q} \cdot q) + C_m^{M} \cdot M \tag{3.4}$$

$$C_l = C_l^{\beta} \cdot \beta + C_l^{\delta_a} \cdot \delta_a + C_l^{\delta_r} \cdot \delta_r + \frac{b}{2V_a}(C_l^{p} \cdot p + C_l^{r} \cdot r) \tag{3.5}$$

$$C_n = C_n^{\beta} \cdot \beta + C_n^{\delta_a} \cdot \delta_a + C_n^{\delta_r} \cdot \delta_r + \frac{b}{2V_a}(C_n^{p} \cdot p + C_n^{r} \cdot r) \tag{3.6}$$

Detailed description of the above-mentioned parameters are found in [55, 57, 58].

The angle of attack (α), as shown in Fig. 3.2, is the angle of the body x-axis of the aircraft relative to the stream of the moving air, while pitch angle (θ) is the angle relative to the horizon. Flight path angle (γ) is the angle between the direction of flight path and the horizon.

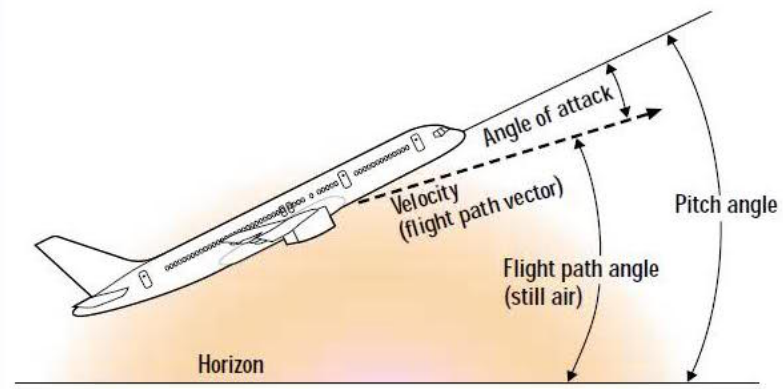

Fig. 3.2 Definitions of angle of attack, pitch angle, and flight path angle.

The analyses of stability and control are concerned with the motion of the aircraft and the rotation around the centre of gravity. The CG location of the aircraft is given with respect to the vehicle's nose and defined in terms of x,y,z coordinates. For example, for all the aircraft's elements, the x coordinate is given by

$$x_{cg} = \frac{\sum_i W_i x_i}{\sum_i W_i}$$

where W_i is the weight of the element and x_i is the distance from the nose to the element of the x-axis. Similarly, for y_{cg} and z_{cg}, they are determined from the reference point (the nose of the aircraft). However, due the symmetry on the Oxz plane, the y_{cg} equals 0. This assumption may not be valid if stores loading and fuel will deter the mass and change the CG, which then have to be taken into account.

3.1.2 Axes of orientation

The formation of equations of motion, which describe the aircraft dynamics using forces and moments, can be made using any axis of orientation [59] as long as the variables are defined consistently. The variables can be transformed from one axis to another using the transformation equation. However, here are the main axes of aircraft orientation, used in the literature, for the aircraft's nomenclature and notations [60], [59]:

Body axis

This right-handed axis of orientation is fixed to the aircraft body, and it is regularly used for deriving equations of motion. The axis is chosen, as shown in Fig. 3.3, where the origin is at the centre of gravity, the x-axis directs toward the nose, the y-axis directs toward the starboard wing, and the z-axis directs downward. Angular

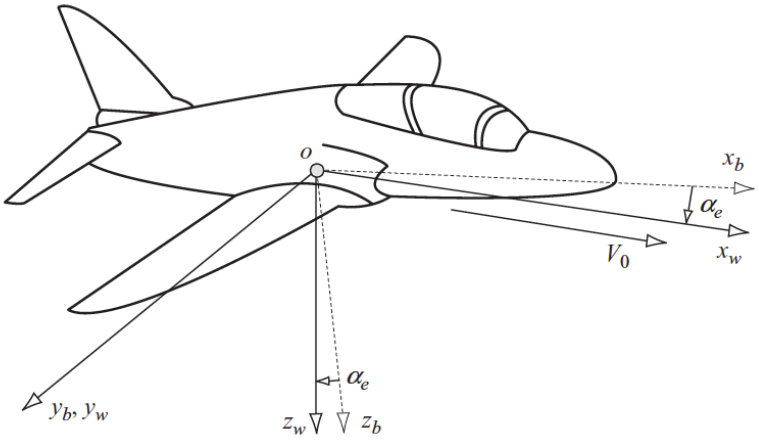

Fig. 3.3 Aircraft body-axis.

velocities and moments are prescribed to be positive when the direction of rotation is clockwise looking toward the axis from the origin.

Earth axis

For the normal atmospheric flight consideration, it is usual to measure the aircraft's motion with reference to an Earth fixed axis, as shown in Fig. 3.4. The horizontal plane defined by ($o_E x_E y_E$) is assumed to be parallel to the plane ($o_0 x_0 y_0$) at the surface of Earth. The flight is described by its coordinates, assuming a flat Earth surface, and the vertical z-axis is aligned with the gravity vector.

3.1.3 Euler angles

The attitude of the aircraft is described as the angular orientation of the body-fixed axis with respect to the Earth axis. The position of an aircraft in the space can be specified by orientation change between an axis fixed to the centre of gravity of the aircraft and the aircraft's attitude. These right-handed rotations are called the Euler angles and defined by the yaw angle ψ, the pitch angle θ, and the bank angle ϕ, as shown in Fig. 3.5 [60].

To determine these angles, the following sequence of plane orientations (yaw, pitch roll) is followed:

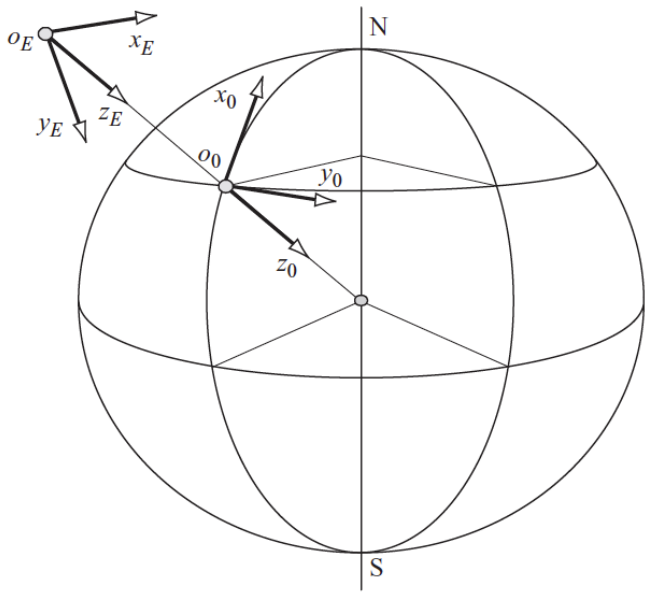

Fig. 3.4 Conventional Earth axis

- First, rotate about oz0 through the yaw angle ψ to ($Ox_1y_1z_1$)
- Second, rotate about oy1 through the pitch angle θ to ($ox_2y_2z_2$)
- Third, rotate about ox2 through the roll angle φ to ($ox_3y_3z_3$).

The transformation of the linear velocity components from aircraft's wind axis to body axis might be a typical example.

3.2 Aircraft stability

The tendency of an aircraft to converge to its initial equilibrium conditions following a small disturbance from a trim is referred as the static stability. Conversely, the dynamic stability of an aircraft describes the convergence of a transient motion involved in the process of recovering equilibrium after a disturbance. Fig. 3.6 describes these definitions.

3.2.1 Longitudinal static stability

When an aircraft is in a longitudinal equilibrium condition and flying steadily, and then exposed to a small disturbance, the equilibrium condition changes as some parameters such as angle of attack change. Thus, the stability will be classified as follows [57] [60]:

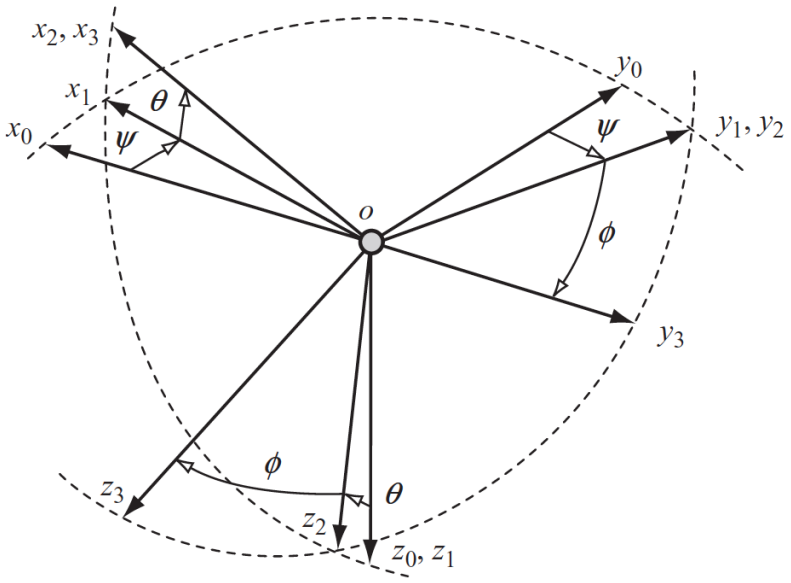

Fig. 3.5 Axes transformation using Euler angles [60]

- If the change in pitching moment coefficient $dC_m$with respect to the change in angle of attack $\alpha$is with a negative slope, i.e. $\frac{dC_m}{d\alpha} < 0$, then the aircraft is statically stable. The nose-up disturbance will increase α and take the aircraft to the point p, which is out of trim. The pitching moment coefficient becomes negative and therefore restores the equilibrium.
- If $\frac{dC_m}{d\alpha} > 0$, then the aircraft is unstable because of the opposite pattern compared to the first condition.
- If $dC_m = 0$, and $\frac{dC_m}{d\alpha} = 0$, then the aircraft is neutrally stable.

This is illustrated in Fig. 3.7 for a statically stable aircraft for which the slope is negative.

Static lateral-directional stability analysis involves the yawing moment coefficient C_n, the rolling moment coefficient C_l, and the side force coefficient C_y. These quantities are expressed in terms of the Mach number M, the rolling angle ϕ, the sideslip angle β, the aileron deflection δ_A, and the rudder deflection δ_R. The rolling motion is controlled primarily by the ailerons, while yawing motion is controlled by the rudder [61].

3.2.2 Lateral static stability

Lateral static stability is expressed as the ability of the aircraft to maintain the wing-level equilibrium condition in the roll sense. Wing dihedral, for instance, is the most noticeable parameter that increases the lateral static stability of the aircraft.

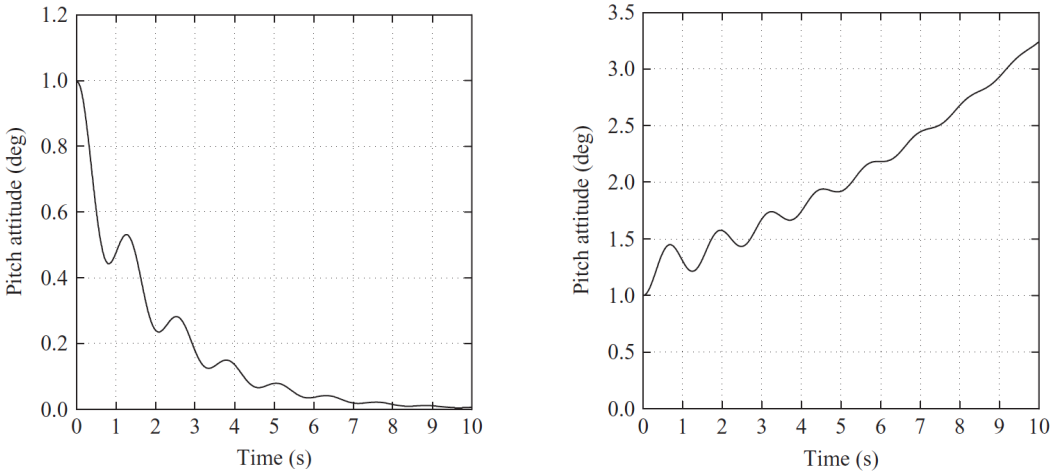

(a) Statically and dynamically stable (b) Statically unstable and dynamically stable

Fig. 3.6 Static and dynamic stability [60]

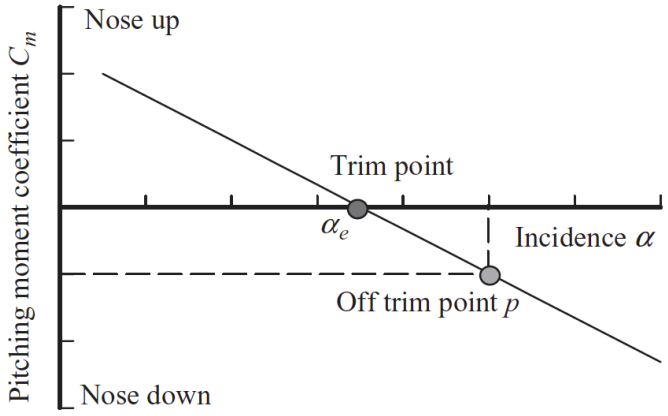

Fig. 3.7 Variation of pitching moment coefficient with respect to angle of attack [60]

It is worth mentioning that too much lateral static stability will make the aircraft reluctant to manoeuvre laterally. For the lateral static stability, it is required that the change in rolling moment coefficient C_l with respect to the rolling angle ϕ is less than 0 (i.e. $\frac{dC_l}{d\phi} < 0$).

3.2.3 Directional static stability

It is expressed as the ability of the aircraft to yaw to maintain directional equilibrium and fly with zero sideslip in the yaw sense. The aircraft's vertical tail, i.e. the fin, is the most perceptible contributor to directional static stability. For the directional stability, it is required that the slope of C_n versus β is greater than 0 (i.e. $\frac{dC_n}{d\beta} < 0$) [57].

3.3 Aircraft equations of motion

3.3.1 Generalised forces and moments equations

For the equations of motion of the flight vehicle, it is usually preferred to use the body-fixed coordinate system, with the right-handed orientation and centre of mass as the origin of the system [55]. Assuming a rigid body aircraft, the equations of motion are obtained from Newton's Second Law [57], [60], [55], [62], which states:

- The summation of all external forces acting on the aircraft is equal to the time rate of change of the momentum of the body. That is

$$\sum F = \frac{d}{dt}(mV) \tag{3.7}$$

- The summation of the external moments acting on the aircraft is equal to the time rate of change of angular momentum:

$$\sum M = \frac{d}{dt} H \tag{3.8}$$

From Eq. 3.7, the vector equations consisting of the three force components can be written as

$$\begin{aligned} F_x = X &= \tfrac{d}{dt}(mu) \\ F_y = Y &= \tfrac{d}{dt}(mv) \\ F_z = Z &= \tfrac{d}{dt}(mw) \end{aligned} \tag{3.9}$$

Assuming a constant mass of the aircraft m, the rate of change of velocities results in the acceleration components along each axis. When working out the acceleration, the contributions to its velocity from both linear velocities (U, V, W) of the aircraft's centre of gravity, as well as the rotational rate (p, q, r) contributions about the axes are considered.

Thus,

$$\begin{aligned} a_x &= \dot{U} - rV + qW \\ a_y &= \dot{V} + rU - pW \\ a_z &= \dot{W} + pV - qU \end{aligned} \tag{3.10}$$

Hence, the total forces along the x,y,z axes, respectively, are represented by

$$\begin{aligned} X &= m(\dot{U} - rV + qW) \\ Y &= m(\dot{V} + rU - pW) \\ Z &= m(\dot{W} + pV - qU) \end{aligned} \tag{3.11}$$

The moment of momentum can be written in terms of the angular velocities $\omega$and position vector r as follows:

$$H = \sum [r \times (\omega \times r)]\delta m$$

For the rotary motion, the mass and acceleration are represented as the moment of inertia and angular acceleration; hence,

$$\begin{aligned} H_x &= pI_x - qI_{xy} - rI_{xz} \\ H_y &= -pI_{xy} + qI_y - rI_{yz} \\ H_z &= -pI_{xz} - qI_{yz} + rI_z \end{aligned} \tag{3.12}$$

where (I_x, I_y , I_z) are the moments of inertia and (I_{xy}, I_{xz}, I_{yz}) are the products of the inertia, and they are given by:

$$\begin{aligned} I_x &= \iiint (y^2 + z^2)\delta m \\ I_y &= \iiint (x^2 + z^2)\delta m \\ I_z &= \iiint (x^2 + y^2)\delta m \\ I_{xy} &= \iiint xy\ \delta m \\ I_{xz} &= \iiint xz\ \delta m \\ I_{yz} &= \iiint yz\ \delta m \end{aligned} \tag{3.13}$$

The total moments about the rotational body frame are expressed as follows

$$\begin{aligned} L &= \dot{H}_x + qH_z - rH_y \\ M &= \dot{H}_y + rH_x - pH_z \\ N &= \dot{H}_z + pH_y - qH_x \end{aligned} \tag{3.14}$$

By substituting for the derivatives of moments of momentum equations with Equation 3.12 into Equation 3.14 and assuming a symmetric aircraft about the *oxz* axis (i.e. $I_{xy} = I_{yz} = 0$) yields

$$\begin{aligned} L &= I_x\dot{p} - (I_y - I_z)\, qr - I_{xz}(pq + \dot{r}) \\ M &= I_y\dot{q} + (I_x - I_z)\, pr + I_{xz}(p^2 - r^2) \\ N &= I_z\dot{r} - (I_x - I_y)\, pq + I_{xz}(qr - \dot{p}) \end{aligned} \tag{3.15}$$

The equations (Equation 3.11 and Equation 3.15) represent the aircraft forces and moments equations. The total forces (X, Y, Z) and moments (L, M, N) of the aircraft result from the aerodynamic, gravitational, controls, and power contributions. The resulting equations are nonlinear, and their solution using the analytical methods is not generally practicable. They must be linearised so they can be used for further analysis and control design processes. The linearisation process is accomplished by

constraining the motion of the aircraft to small perturbations about its trimming point.

3.3.2 The aircraft's linear dynamic model

Small perturbation theory

When the aircraft is assumed to be flying in a steady trimmed condition with zero roll, sideslip, and yaw angles, the components of the linear velocity are (U_e,V_e,W_e) and the angular velocity components are zero. If the aircraft experiences small perturbations about the trim, then the total velocity components about the cg are:

$$\begin{aligned} U &= U_e + u \\ V &= V_e + v \\ W &= W_e + w \end{aligned} \tag{3.16}$$

where (u, v, w) are the linear disturbance velocities and (p, q, r) are the components of the angular disturbance velocities. By substituting (last equation) into Equation 3.11 and Equation 3.15, and neglecting the insignificantly small terms, the linearised equations of motion can be obtained:

$$\begin{aligned} m(\dot{u} + qW_e) &= X_a + X_g + X_c + X_p \\ m(\dot{v} - pW_e + eU_e) &= Y_a + Y_g + Y_c + Y_p \\ m(\dot{w} - qU_e) &= Z_a + Z_g + Z_c + Z_p \end{aligned} \tag{3.17}$$

and

$$\begin{aligned} I_x\dot{p} - I_{xz}\dot{r} &= L_a + L_g + L_c + L_p \\ I_y\dot{q} &= M_a + M_g + M_c + M_p \\ I_z\dot{r} - I_{xz}\dot{p} &= N_a + N_g + N_c + N_p \end{aligned} \tag{3.18}$$

where a, g, c, p are the aerodynamic, gravity, control, and power contributions.

Main contributors of aircraft forces and moments:

The gravitational, control, and power contributions are illustrated in literature, see [55]. The aerodynamic contributions during a disturbance are computed by assuming that the aerodynamic terms depend on the disturbed variables and their derivatives. It is conveniently expressed as a sum of a number of Taylor's series expansion [60]. For example, the axial force aerodynamic term X_a is expressed by:

$$X_a = X_{a_e} + \mathring{X}_u u + \mathring{X}_v v + \mathring{X}_w w + \mathring{X}_p p + \mathring{X}_q q + \mathring{X}_r r + \mathring{X}_{\dot{w}} \dot{w}$$

where X_{a_e} is a constant term, and the terms $\mathring{X}_u u + \mathring{X}_v v + \mathring{X}_w w + ...$ etc, are called aerodynamic stability derivatives. The dressing $\mathring{()}$ denotes dimensional derivatives. By substituting the appropriate expressions for the aerodynamic, gravitational, control, and thrust into Equations 3.17-3.18, the complete linearised equations of motion are obtained as follows:

$$\begin{aligned}
m(\dot{u} + qW_e) &= X_{a_e} + \mathring{X}_u u + \mathring{X}_v v + \mathring{X}_w w \mathring{X}_p p + \mathring{X}_q q + \mathring{X}_r r + \mathring{X}_{\dot{w}} \dot{w} \\
&\quad -mgsin\theta_e - mg\theta cos\theta_e + \mathring{X}_\xi \xi + \mathring{X}_\eta \eta + \mathring{X}_\zeta \zeta + \mathring{X}_\tau \tau \\
m(\dot{v} - pW_e + eU_e) &= Y_{a_e} + \mathring{Y}_u u + \mathring{Y}_v v + \mathring{Y}_w w \mathring{Y}_p p + \mathring{Y}_q q + \mathring{Y}_r r + \mathring{Y}_{\dot{w}} \dot{w} \\
&\quad +mg\psi sing\theta_e + mg\phi cos\theta_e + \mathring{Y}_\xi \xi + \mathring{Y}_\eta \eta + \mathring{Y}_\zeta \zeta + \mathring{Y}_\tau \tau \\
m(\dot{w} - qU_e) &= Z_{a_e} + \mathring{Z}_u u + \mathring{Z}_v v + \mathring{Z}_w w \mathring{Z}_p p + \mathring{Z}_q q + \mathring{Z}_r r + \mathring{Z}_{\dot{w}} \dot{w} \\
&\quad +mgcos\theta_e - mg\theta_e + \mathring{Z}_\xi \xi + \mathring{Z}_\eta \eta + \mathring{Z}_\zeta \zeta + \mathring{Z}_\tau \tau
\end{aligned} \tag{3.19}$$

$$\begin{aligned}
I_x \dot{p} - I_{xz} \dot{r} &= L_{a_e} + \mathring{L}_u u + \mathring{L}_v v + \mathring{L}_w w \mathring{L}_p p + \mathring{L}_q q + \mathring{L}_r r + \mathring{L}_{\dot{w}} \dot{w} \\
&\quad +\mathring{L}_\xi \xi + \mathring{L}_\eta \eta + \mathring{L}_\zeta \zeta + \mathring{L}_\tau \tau \\
I_y \dot{q} &= M_{a_e} + \mathring{M}_u u + \mathring{M}_v v + \mathring{M}_w w \mathring{M}_p p + \mathring{M}_q q + \mathring{M}_r r + \mathring{M}_{\dot{w}} \dot{w} \\
&\quad +\mathring{M}_\xi \xi + \mathring{M}_\eta \eta + \mathring{M}_\zeta \zeta + \mathring{M}_\tau \tau \\
I_z \dot{r} - I_{xz} \dot{p} &= N_{a_e} + \mathring{N}_u u + \mathring{N}_v v + \mathring{N}_w w \mathring{N}_p p + \mathring{N}_q q + \mathring{N}_r r + \mathring{N}_{\dot{w}} \dot{w} \\
&\quad +\mathring{N}_\xi \xi + \mathring{N}_\eta \eta + \mathring{N}_\zeta \zeta + \mathring{N}_\tau \tau
\end{aligned} \tag{3.20}$$

3.3.3 The decoupled equations of motion

When the small perturbation transient motion is considered, the longitudinal and lateral coupling is usually negligible. Hence, the decoupled longitudinal motion is constrained to the longitudinal plane of symmetry only, which is the oxz plane. Therefore, the motion is described by the axial force X, the normal force Z, and the pitching moment M equations only. Since no lateral-directional motion is involved, the lateral motion variables, aileron and rudder controls, and their derivatives are all zero. By further simplification due to the symmetry of the referred plane, the decoupled equations of longitudinal motion become

$$\begin{aligned}
m\dot{u} - \mathring{X}_{\dot{w}} \dot{w} &= \mathring{X}_u u + \mathring{X}_w w + (\mathring{X}_q - mW_e) q - mg\theta cos\theta_e + \mathring{X}_\eta \eta + \mathring{X}_\tau \tau \\
m\dot{w} - \mathring{Z}_{\dot{w}} \dot{w} &= \mathring{Z}_u u + \mathring{Z}_w w + (\mathring{Z}_q + mU_e) q - mg\theta sin\theta_e + \mathring{Z}_\eta \eta + \mathring{Z}_\tau \tau \\
I_y \dot{q} - \mathring{M}_{\dot{w}} \dot{w} &= \mathring{M}_u u + \mathring{M}_w w + \mathring{M}_q q + \mathring{M}_\eta \eta + \mathring{M}_\tau \tau
\end{aligned} \tag{3.21}$$

Additionally, the auxiliary equation relating the pitch rate to attitude rate is

$$\dot{\theta} = q$$

Similarly, for the lateral-directional motion, as no longitudinal motion is involved, the motion is described by the rolling moment L, the yawing moment N, and the side force Y. The equations become

$$\begin{aligned} m\dot{v} - \mathring{Y}_v v - p\mathring{Y}_p - (\mathring{Y}_r - mU_e)r - mg\phi &= \mathring{Y}_\xi \xi + \mathring{Y}_\zeta \zeta \\ -\mathring{L}_v v + I_x \dot{p} - \mathring{L}_p p + I_{zx}\dot{r} - \mathring{L}_r r &= \mathring{L}_\xi \xi + \mathring{L}_\zeta \zeta \\ -\mathring{N}_v v - I_{xz}\dot{p} - \mathring{N}_p p + I_z \dot{r} - \mathring{N}_r r &= \mathring{N}_\xi \xi + \mathring{N}_\zeta \zeta \end{aligned} \tag{3.22}$$

3.3.4 Linear EoM in a state space form

Powerful computational tools, i.e. computers, are very good in handling the numerical matrix calculations. Thus, the use of matrix methods for solving linear dynamic systems became an essential topic in modern applied mathematics. The matrix format gives a compact expression of equations that could be solved using matrix algebra. Thus, the equation of motion of the linear time-invariant system is written as:

$$\dot{x}(t) = Ax(t) + Bu(t)$$

where x(t) is the state column vector of n variables, u(t) is the input column vector of m variables, A is the (n x n) state matrix, and B is the (n x m) input matrix. For systems in which some of the state variables may not be accessible or measurable, an equation that determines some particular output variables is required, as follows:

$$y(t) = Cx(t) + Du(t)$$

where y(t) is the column vector of r output variables, C and D are (r x n) and (r x m) constant matrices, respectively.

Now, the aircraft's decoupled equations of motions (Equation 3.21 and Equation 3.22) may be written in matrix form as

$$M\dot{x}(t) = \grave{A}x(t) + \grave{B}u(t) \tag{3.23}$$

Finally, the state equations are obtained by multiplying Equation 3.23 by the inverse of the matrix M, which yields for the longitudinal motion

$$\begin{bmatrix} \dot{u} \\ \dot{w} \\ \dot{q} \\ \dot{\theta} \end{bmatrix} = \begin{bmatrix} x_u & x_w & x_q & x_\theta \\ z_u & z_w & z_q & z_\theta \\ m_u & m_w & m_q & m_\theta \\ 0 & 0 & 1 & 0 \end{bmatrix} \begin{bmatrix} u \\ w \\ q \\ \theta \end{bmatrix} + \begin{bmatrix} x_\eta & x_\tau \\ z_\eta & z_\tau \\ m_\eta & m_\tau \\ 0 & 0 \end{bmatrix} \begin{bmatrix} \eta \\ \tau \end{bmatrix} \tag{3.24}$$

In a similar manner, the lateral-directional equation is

$$\begin{bmatrix} \dot{v} \\ \dot{p} \\ \dot{r} \\ \dot{\phi} \\ \dot{\psi} \end{bmatrix} = \begin{bmatrix} y_v & y_p & y_r & y_\phi & y_\psi \\ l_v & l_p & l_r & l_\phi & l_\psi \\ n_v & n_p & n_r & n_\phi & n_\psi \\ 0 & 1 & 0 & 0 & 0 \\ 0 & 0 & 1 & 0 & 0 \end{bmatrix} \begin{bmatrix} v \\ p \\ r \\ \phi \\ \psi \end{bmatrix} + \begin{bmatrix} y_\xi & y_\zeta \\ l_\xi & l_\zeta \\ n_\xi & n_\zeta \\ 0 & 0 \\ 0 & 0 \end{bmatrix} \begin{bmatrix} \xi \\ \zeta \end{bmatrix}$$

For both equations, the coefficients of the state matrix A represent the aerodynamic stability derivatives, while the coefficients of the input matrix B represent the control derivatives. Detailed expressions for them are available in [60].

3.4 Dynamic stability

Static stability treats primarily the situation when the controls are fixed. However, dynamic stability describes the response of the system against controls or disturbances. System asymptotic stability describes the ability of the system variables to return to their desired states after a disturbance. The excitation of aircraft dynamics resulted in dynamic modes in the longitudinal and lateral motions, which will be presented next.

3.4.1 Longitudinal dynamic stability modes

When the aircraft is disturbed from its equilibrium trim state initiated by, for example, a change in power setting, pilot control inputs, and external atmospheric influences, this will excite the dynamics for certain modes. Longitudinally, there are two modes, the short period mode, and the phugoid mode [57]. The short period mode is highly damped high-frequency pitching oscillation, as shown in Fig. 3.8. The lower frequency mode is called the phugoid. The damping ratio of both modes must be positive for the aircraft to be completely longitudinally stable.

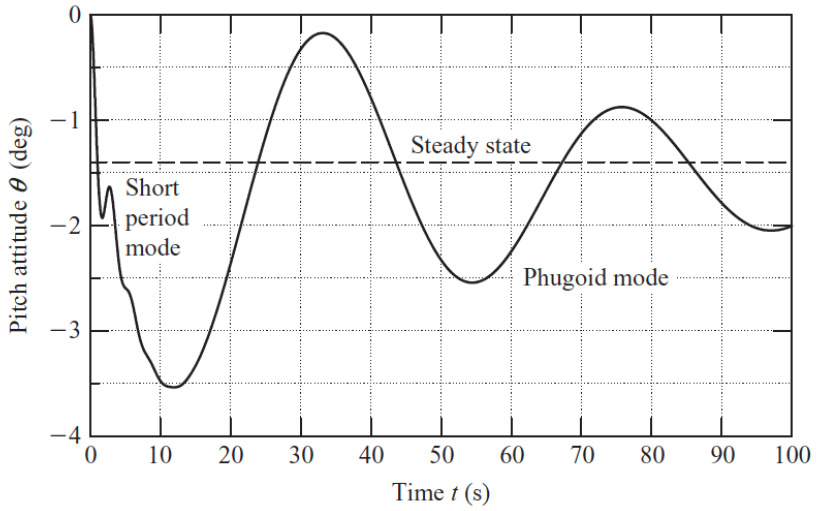

Fig. 3.8 Longitudinal short period and phugoid modes

The phugoid is classical damped motion that results in the aircraft flying along a converging sinusoidal flight trajectory, where the angle of attack (α) remains constant.

3.4.2 Lateral dynamic stability modes

Generally, lateral motion has three modes: the roll, spiral, and dutch roll modes [61]. The roll subsidence mode is a stable and non-oscillatory mode, while the spiral mode is a non-oscillatory mode resulting from slow recovery of bank angle disturbance. It involves a coupled motion in roll, sideslip, and yaw. The dutch-roll mode is a stable and short-period oscillatory mode [63]. Typically, from the characteristic equation, a real root describes the spiral mode with high time constant, another real root describes the roll subsidence mode with small time constant, and two complex roots describe the oscillatory dutch-roll mode.

3.5 Aircraft nonlinear simulation

With a variety of formulations, aircraft nonlinear simulations attempt to provide an imitation of the real world's system operation. It is desirable to create a dynamic representation of the behaviour of the aircraft's motion in a manner that allows the human to interact with it. These engineering simulations will allow designers to explore different configurations and operations of the flying vehicle without having to encounter the expenses and delays arising from building and testing ranges of prototypes [64]. Thus, they provide a great means to model and repeatedly test the system responses to challenges similar to those in real life.

The mathematical modelling of the equations of motion is central to the analysis of air-vehicle motion and dynamics. The nonlinear six-degree-of-freedom dynamic model provides a comprehensive description of the aircraft response to control malfunctions and external disturbances. Generally, they are represented in terms of displacement, velocity, and acceleration variables in the translational and rotational axes. These complex equations are solved using numerical methods by linearizing the model about selected trim conditions using the Small Perturbation theory. The linearised models describe the system at these selected operating points within the flying envelope, and thus, a linear-based control system is developed. Among the modelling and analysis software packages used widely in research institutions as well as industrial enterprises is the Matlab/Simulink software environment. It was developed by Mathworks for system's dynamics simulations and analysis. Matlab is technical computing software that provides core mathematical tools for data analysis, visualisation, and algorithm design. While Simulink is the graphical block-diagramming tool integrated with Matlab that provides modelling, simulation, and analysis of dynamic systems. It includes block sets that implement aerospace mathematical representations.

3.5.1 Modelling procedure

The nonlinear six-degree-of-freedom aircraft dynamic model is implemented using blocks-based modelling in the body-axis. Figure 3.9 summarizes the nonlinear equation of motion (EoM) modelling procedure. Control inputs are provided from the pilot (i.e. joystick) for manual flight, or from the autopilot for autonomous flight.

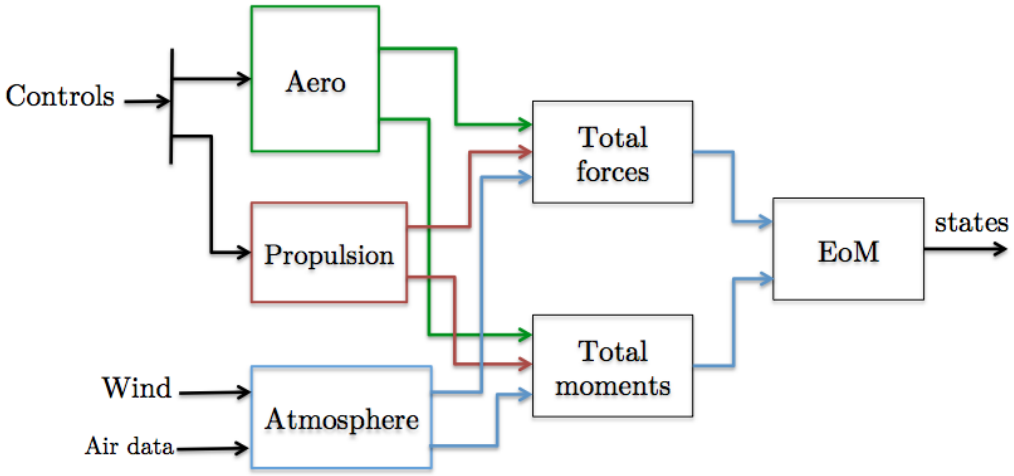

Fig. 3.9 Nonlinear modelling layout

Aerodynamic forces and moments coefficients are computed using linear combinations of aerodynamic derivatives, as mentioned before.

3.5.2 Trimming and linearisation

We may examine the dynamic motion of the aircraft near a singular point by slightly perturbing some of the motion variables. This singular point is where all of the forces and moment components exerted on the body of the aircraft are constant or zero, and this case is typically called a steady-state condition [65]. This is provided by a certain configuration of control surface deflections and engine throttle settings, which constitutes trim values of flight mode. Hence, the aircraft motion is to be trimmed around this point and then the linearisation process is applied to have a linear mathematical representation of the system. The linear equations, composed of longitudinal and lateral dynamics, needed for the control design, will mostly be derived by numerical methods from the nonlinear computer model using the Runge-Kutta method for linearisation [40].

3.6 Aircraft flight control

For automatic control of aircraft states, feedback control laws are used as shown in Fig. 3.10. In this process, the parameter to be controlled is compared to a desired reference signal, and the difference is used to compute corrective control action [66].

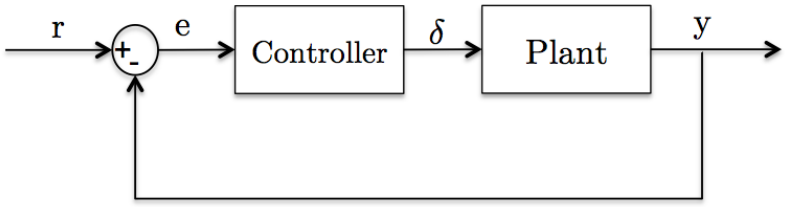

Fig. 3.10 Feedback control

3.6.1 PID controllers

For a control system to track an input command, one widely used control technique for single-input single-output (SISO) systems is the proportional-integral-derivative PID controller. The general form of PID controller C(s) is given by [67]:

$$C(s) = K_p + \frac{K_I}{s} + K_D s$$

Figure 3.11 shows the structure of a PID controller in which s is the Laplace operator, and the design of the controller involves the adjustment of K_P, K_I, and K_D coefficients. The proportional term makes the response faster in reaching the

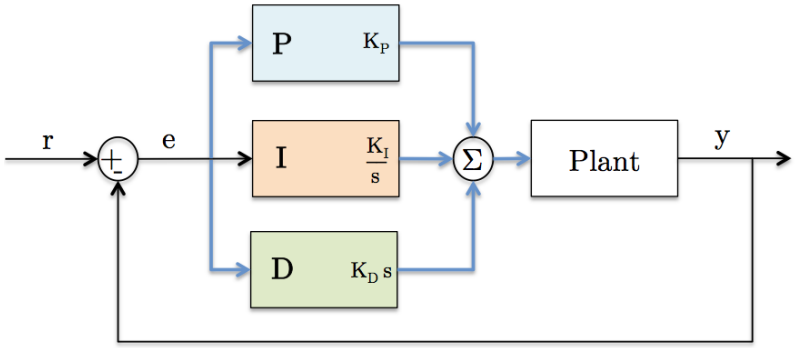

Fig. 3.11 Structure of the PID controller

steady state; however, error and overshoot may be introduced. Thus, the integral part is used to eliminate the steady-state error, while the derivative part is used to decrease the overshoot and settling time [57].

3.6.2 Aircraft control surfaces

Flight control surfaces are classified based on their roles in primary (such as elevator, aileron, rudder, and spoiler) and secondary (such as trailing-edge flaps, leading-edge slats, and airbrake) control surfaces. Control surfaces for fixed wing aircraft are shown in Fig. 3.12.

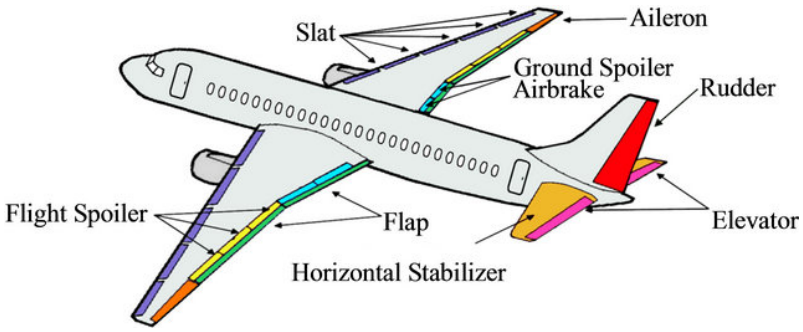

Fig. 3.12 Aircraft control surfaces

For most recent aircraft transporters, the actuation systems of the control surfaces are electronically signalled and hydraulically powered. Functions of the primary flight control surfaces are critical to safety and controllability of the aircraft [58]. Figure 3.13 shows the thrust and primary control surfaces for the longitudinal and lateral dynamics of the aircraft.

Generally, a positive control action by the pilot gives rise to a positive aircraft response, whereas a positive control surface displacement gives rise to a negative aircraft response [60]. Thus:

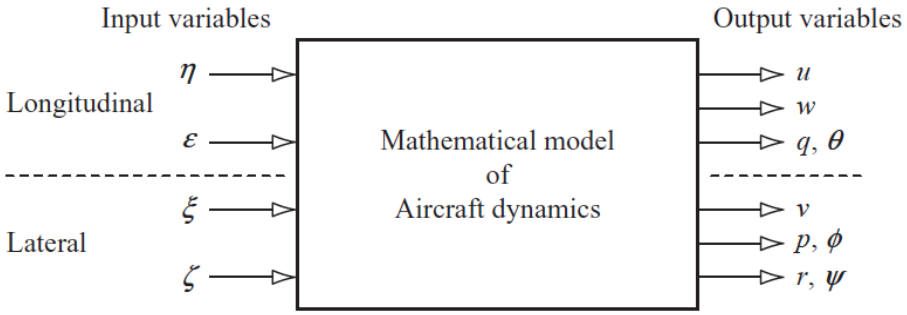

Fig. 3.13 Inputs and outputs to the aircraft dynamics [60]

- In roll: positive right push force on the stick ⇒ positive stick displacement ⇒ right aileron up and left aileron down (negative) ⇒ right wing down roll response (positive).

- In pitch: positive pull force on the stick ⇒ positive aft stick displacement ⇒ elevator trailing edge up (negative) ⇒ nose up pitch response (positive).

- In yaw: positive push force on the right rudder pedal ⇒ positive rudder bar displacement ⇒ rudder trailing edge displaced to the right (negative) ⇒ nose to the right yaw response (positive).

By introducing incremental lift forces on control surfaces, the control of the aircraft can be achieved. In the following paragraphs, the contributions from primary control surfaces are presented [57].

Elevator

The change in the aircraft's pitching moment can be written as

$$\Delta C_m = C_{m\delta_e}\delta_e$$

where δ_e is the elevator deflections and $C_{m\delta_e}$ is the elevator control power which can be expressed as:

$$C_{m\delta_e} = -V_H \eta \left(\frac{d\, C_{Lt}}{d\, \delta_e} \right)$$

$$V_H = \frac{l_t\, S_t}{S\, \bar{c}}$$

is the horizontal tail volume ratio, where l_t is the tail moment arm.

$$\eta = \frac{Q_t}{Q_w}$$

is the dynamic pressure ratio. The elevator effectiveness can be expressed as:

$$\frac{d\ C_{Lt}}{d\ \delta_e} = \left(\frac{d\ C_{Lt}}{d\ \alpha_t}\right)\ \left(\frac{d\ \alpha_t}{d\ \delta_e}\right) = C_{L\alpha_t}\ \tau$$

$$C_{L\alpha_t}$$

is the lift curve slope of the tail, and $\tau$is the value of the change between $\alpha$and the deflections for the specific control surface area.

Aileron

Considering the lift coefficient C_l of the segment containing the aileron, it can be expressed as a function of aileron deflections and properties as follows:

$$C_l = C_{l\alpha}\left(\frac{d\alpha}{d\delta_a}\right)\delta_a = C_{l\alpha}\tau\delta_a$$

where $C_{l\alpha}$ is the lift curve slope at the section, $\tau$is the parameter relating change in $\alpha$to the changes in deflections for the corresponding control surface area, and δ_a is the aileron deflections.

Rudder

For the realization of rudder contribution, the yawing moment is considered:

$$C_n = C_{n\delta_r}\delta_r$$

where δ_r is the rudder deflection, and $C_{n\delta_r}$is the rudder control power expressed by

$$C_{n\delta_r} = -\frac{Q_v}{Q_w}\ \left(\frac{l_v S_v}{S\ b}\right)\left(\frac{dC_{Lv}}{d\delta_r}\right)$$

where Q_v is the dynamic pressure of the vertical tail, $l_v$is the moment arm of the vertical tail, and $\frac{dC_{Lv}}{d\delta_r}$ is the rudder effectiveness expressed by

$$\frac{dC_{Lv}}{d\delta_r} = \frac{dC_{Lv}}{d\alpha_v}\ \frac{d\alpha_v}{d\delta_r} = C_{L\alpha_v}\tau$$

where $\tau$is the parameter of change in alpha due to the change in rudder for the specific area of the rudder, and $C_{L\alpha_v}$is the lift curve slope of the vertical tail (the rudder).

3.7 Conclusion

In this chapter, basic aerodynamics notations are illustrated, and forces and moments that generate the motion are prescribed. A complete generation of equations of motion is presented. For control law development, linear dynamics are used followed by a linearisation process that is described in the chapter. Finally, functions of the control surfaces and measures of their effectiveness are explained. In the following chapter, a development of FTC for aircraft is presented.

Chapter 4

Optimal FTC using LQR and Adaptive Fault Compensation

4.1 Introduction

One widely used feedback-based technique in flight control problems is based on the consecutive loop closure of certain selected parameters [62]. Well-known tools such as the root locus, Bode plot, and Nyquist plot enable the designer to visualize how the system dynamic is changing for this one-loop at a time design approach. As more loops are needed, this control design approach becomes increasingly difficult and the control law solution, in this case, requires continuous adjustment in order to maintain good stability and handling qualities [60]. On the other hand, solving a matrix of mathematical equations containing the tracking requirements and the control law gains will allow all of the gains to be computed simultaneously. This yields that the loops are closed at the same time, which is considered to be a significant advancement for the control design of multi-input multi-output systems [62]. Non-inclusive techniques among this approach are Eigen-structure assignment [68], model following [69], dynamic inversion [70], and the Linear Quadratic Regulator LQR approach [71]. The linear quadratic regulator (LQR) is applied to control linear systems, where the regulation's main role is to maintain the states close to zero and obtain desirable closed-loop response features. The problem is posed as a quadratic cost function with additional constraints to be minimised such as the efforts of the control inputs. This technique is considered to be a modern control technique suitable for MIMO systems. It had been utilised in tracking desired trajectories by a stable regulation of the system. Some applications of LQR in the fault tolerant control domain are as follows. A technique presented in [72] includes a reformulated Algebraic Riccati equation. Additionally, for a fault-tolerant control,

the weighting matrices Q and R were adjusted. The method does not take into account the constraints induced by actuator saturation. A synthesis of a robust and optimal controller was proposed by [73] for unstable systems. It comprises a linear quadratic state feedback regulator to maintain stability in the presence of certain actuator faults. Another work encompasses LQR and a Kalman filter to control a discrete-time system subject to faults [74]. A feedback linearisation method was exploited in conjunction with LQR for hypersonic flight vehicles subjected to uncertainties [75]. In [76] (B. Yu, Zhang, Minchala, & Qu, 2013), a comparison was made between the LQR and the model predictive controller (MPC) techniques, to control a quadrotor helicopter UAV subjected to partial loss of effectiveness actuator faults. As stated, both methods led to acceptable performance and control. Robust fault tolerant LQ control based on model matching was presented in [77]. In the case of the fault, the work aimed to match the model to a pre-specified set of admissible models, rather than to search for an optimal approximation online. This allowed for some performance degradation, which yielded a set of solutions for the fault accommodation problem. Nevertheless, the selection of one solution among the set was still an open problem. These techniques are considered to be robust fault tolerant methods.

In this work, the LQR-based approach controls a MIMO system subjected to actuator faults in an adaptive way by taking information about the fault into account. The baseline optimal controller is augmented with an adaptive fault compensation framework to cope with actuator loss of effectiveness, where the fault's information are assumed to be known. In this work, the contribution is as follows:

- First, the integration of an adaptive fault compensation approach to the optimal LQR controller used to control a MIMO aircraft system. The baseline LQR obtains the optimal control solution that maintains the tracking requirements of the aircraft, and minimises the control efforts by the actuators. For the fault tolerant approach, an adaptive fault-compensation-based technique was developed that can accommodate loss of effectiveness faults.

- The system was designed based on a linear model. In order to validate the performance of the fault tolerant control scheme, a full 6-dof nonlinear simulation testing was performed.

4.2 Concept of Linear Quadratic Regulator control

4.2.1 The Linear Quadratic Regulator problem

The linear quadratic regulator relies on the feedback of the system's outputs or states that are presented as a quadratic cost function minimisation problem. The state feedback is a special case of output feedback with C=I, assuming that the aircraft's states are measurable [62].

Consider the system

$$\dot{x} = Ax + Bu$$

with $x \in R^n$,$u \in R^m$, and the pair (A,B) are assumed to be stabilizable. The control law for state feedback having the following form is to be examined

$$u = -Kx \tag{4.1}$$

where K is the control gain to be computed. Thus, the closed loop system has the form

$$\dot{x} = (A - BK)\, x = A_c x \tag{4.2}$$

Now, the problem becomes one of finding a controller gain K that drives any initial condition error to zero. For optimal control, the performance of the system and the complexity of the optimal control problem are determined by the performance index. The most popular cost function is the quadratic function of the state variables and the control input [78]. It is of the form:

$$J = \frac{1}{2}\int_0^\infty \left(x^T Q x + u^T R u\right) dt \tag{4.3}$$

where x(t) represents the states, u(t) are the controls, and $Q,\ R > 0$are weighting matrices which are typically chosen to be diagonal. Properties of the system, such as the performance and the control input, depend on the selection of the weighting matrices Q and R. With appropriate selection, the trade-off between those two properties is handled. As mentioned previously, the performance index J, that has to be minimized, encompasses both the state x(t) vector and control input u(t). If J is minimized, then it certainly will become finite and x(t) goes to zero as time goes to infinity, which guarantees the stability of the closed-loop system. The performance index is expressed in terms of the gain K by substituting Equation 4.1 into Equation 4.3, which yields,

$$J = \frac{1}{2}\int_0^\infty x^T Q x + (-Kx)^T R(-Kx)\ dt$$

$$J = \frac{1}{2}\int_0^\infty (x^T Q x + K^T x^T\ R\ Kx)\ dt$$

$$J = \frac{1}{2}\int_0^\infty x^T (Q + K^T\ R\ K)x\ dt$$

The optimisation problem could be converted to an equivalent static problem as follows. Assume that there is a solution for P that makes

$$\frac{d}{dt}\left(x^T P\ x\right) = -x^T (Q + K^T RK)\ x \tag{4.4}$$

Then, J may be written as,

$$J = \frac{1}{2}x^T\,(0)\ \ Px\,(0) - \frac{1}{2}\lim_{1\to\infty} x^T(t)Px(t)$$

Assuming that the closed-loop system is stable, and the regulation will make x(t) become 0 as time $\to \infty$, then

$$J = \frac{1}{2}x^T\,(0)\ \ Px\,(0)$$

Using Equation 4.4 and substituting for Equation 4.2, then

$$-x^T\left(Q + K^T RK\right)x = \frac{d}{dt}\left(x^T Px\right) = \dot{x}^T Px + x^T P\dot{x}$$

$$= (A_c x)^T Px + x^T P(A_c x)$$

$$= x^T\left(A_c^T P + PA_c\right)x$$

Accordingly, for a fixed K, there is a solution of Algebraic Riccati Equation (ARE):

$$PA + A^T P + Q - PBR^{-1}B^T P = 0 \tag{4.5}$$

that makes the optimal stabilising solution of the form

$$K = R^{-1}B^T P$$

where R is the chosen weighing matrix and B is the control input matrix. The solution of the controller K will preserve the trade-off between the transient response and the control efforts.

4.2.2 The LQR tracking problem

In many practical applications, the system is designed to follow some required varying states of the aircraft. The design of the controller, to achieve this goal, is known as the tracking problem. The basic mathematical formula of LQR is exploited to track a non-zero constant reference input. The idea is to extend the model with an error equation that reflects the difference between the desired and the actual states [78]. For tracking design, the error equation is introduced as follows [79]:

$$\dot{x}_I(t) = e(t) = r(t) - y(t)$$

$$= r(t) - Cx(t)$$

So, the dynamical equations are modified to be:

$$\begin{bmatrix} \dot{x}(t) \\ \dot{x}_I(t) \end{bmatrix} = \begin{bmatrix} A & 0 \\ -C_y & 0 \end{bmatrix} \begin{bmatrix} x(t) \\ x_I(t) \end{bmatrix} + \begin{bmatrix} B_u \\ 0 \end{bmatrix} \begin{bmatrix} u(t) \end{bmatrix} + \begin{bmatrix} 0 \\ 1 \end{bmatrix} \begin{bmatrix} r(t) \end{bmatrix}$$

Figure 4.1 shows the linear quadratic tracking structure with the state feedback (x) for tracking the reference input (r), which represents one variable or more.

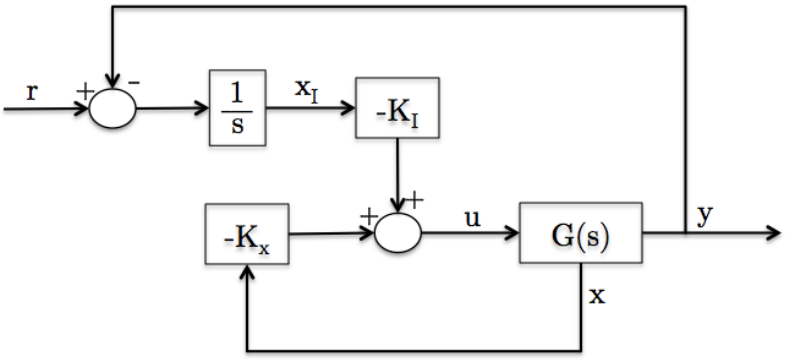

Fig. 4.1 LQR structure incorporating the tracking error

The change in the state space system imposes changes in the Q, R, and K matrices. The controller gains K to be computed are in the form

$$K = [K_x \quad K_I]$$

Accordingly, the control input u(t) becomes a formula of the states and error functions as follows

$$u\left(t\right) = -[K_x \;\; K_I] \begin{bmatrix} x(t) \\ x_I(t) \end{bmatrix}$$

and the system is written as:

$$\begin{aligned} \dot{x} &= Ax + B(-K_1 x - K_2 z) \\ &= \left(A - BK_1\right) x - BK_2 z \end{aligned} \tag{4.6}$$

4.3 LQR optimal control for a linear aircraft model

In this section, an optimal controller is implemented for a MIMO aircraft dynamical model. The optimal performance of LQR control is tested against a classical approach using a proportional-integral-derivative (PID) control.

4.3.1 Aircraft model

Consider a dynamical system having the following state space properties:

$$\dot{x}(t) = Ax(t) + Bu(t)$$

$$y(t) = Cx(t) + Du(t)$$

where u , x , $y$are inputs, states, and outputs respectively. In most aircraft flight control designs, this linearised form is used to represent the longitudinal or lateral dynamics. In this design problem, the following state space form that represents the lateral dynamics of DC-8 aircraft will be used [60],

$$\begin{bmatrix} \dot{v} \\ \dot{p} \\ \dot{r} \\ \dot{\phi} \end{bmatrix} = \begin{bmatrix} -0.1 & 0 & -468.2 & 32.2 \\ -0.006 & -1.2 & -0.397 & 0 \\ -0.003 & -0.035 & -0.257 & 0 \\ 0 & 1 & 0 & 0 \end{bmatrix} \begin{bmatrix} v \\ p \\ r \\ \phi \end{bmatrix} + \begin{bmatrix} 0 & 13.48 \\ -1.62 & 0.392 \\ -0.01875 & -0.864 \\ 0 & 0 \end{bmatrix} \begin{bmatrix} \xi \\ \zeta \end{bmatrix}$$

$$\begin{bmatrix} v \\ p \\ r \\ \phi \\ \beta \end{bmatrix} = \begin{bmatrix} 1 & 0 & 0 & 0 \\ 0 & 1 & 0 & 0 \\ 0 & 0 & 1 & 0 \\ 0 & 0 & 0 & 1 \\ 0.00214 & 0 & 0 & 0 \end{bmatrix} \begin{bmatrix} v \\ p \\ r \\ \phi \end{bmatrix} \tag{4.7}$$

where [v, p, r, ϕ] are sideslip velocity, roll rate, yaw rate, and bank angle, respectively. The control inputs for the system are the aileron and rudder deflections (ξ, ζ), respectively.

4.3.2 Classical proportional-integral-derivative (PID) Controller

As a gain-tuning method, the PID controller was developed to control the bank angle of the aircraft (ϕ), as shown in the block diagram in Fig. 4.2. The proportional term aims to produce an output value that is correspondingly proportional to the current error value, thus increasing the rise time. The integral part, on the other hand, considers both the magnitude and the duration of the error, which is helpful to eliminate the residual steady-state error. Lastly, the derivative term is used to decrease the overshoot and settling time.

As in Fig. 4.2, the inner loop roll rate feedback is an augmented stability element used to provide rate damping for the system. A rate gyroscope of 0.1 was modelled as a motion sensor. Feedback of the deviation signal of the bank angle of the system (the outer loop) can then be used to control the roll angle of the aircraft. This will enhance the flying performance and stability. To simulate the actuator dynamics, a linear second-order model was used with 0.5 natural frequency ω_n and 0.9 damping ratio ζ. The PID gains were tuned to improve the tracking performance in the time domain.

Then, the control deflections signal sent to actuators δ is calculated by

$$\delta = \left[0.018 + \frac{7.6}{s} + 0.05s\right] \times \ e_{roll}$$

where

$$e_{roll} = p_{command} - p_{actual}$$

$$p_{actual} = C1 * rate\ gyro * p$$

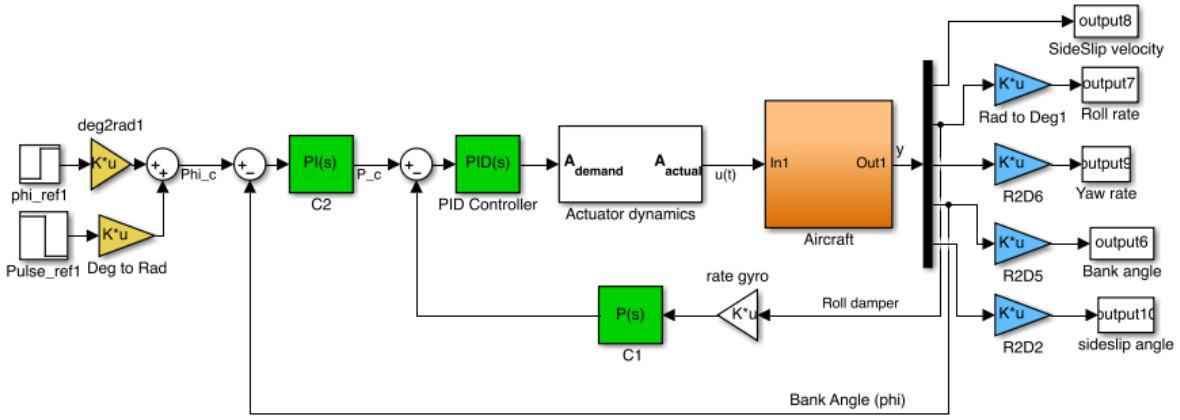

Fig. 4.2 Bank angle PID control with roll rate damper

$$= -209 \times 0.1 \times p$$

while $p_{command}$ is

$$p_{command} = \left[-24.6 - \frac{0.21}{s}\right] \times \ e_{\phi}$$

A plot of the bank angle controlled by the classical control system is shown in Fig. 4.3, where the dotted line is the required bank angle with step input. The plot shows the response with a 3.2 s rise time (the time needed for the response to jump from 10% to 90% of the required manoeuvre), and zero steady state error. The damping pattern yields to a 12 seconds settling time.

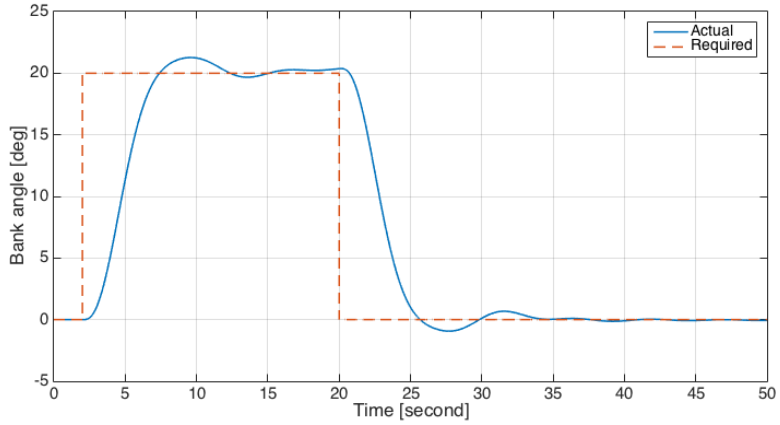

Fig. 4.3 Aircraft bank angle response using PID controller

The designed single-input multi-output control system resulted in changes in the aircraft's outputs, as shown in Fig. 4.4. As anticipated, there was a change in both the roll rate and yaw rate due to the coupling effects in the lateral-directional motion. All aircraft states show a smooth transient response.

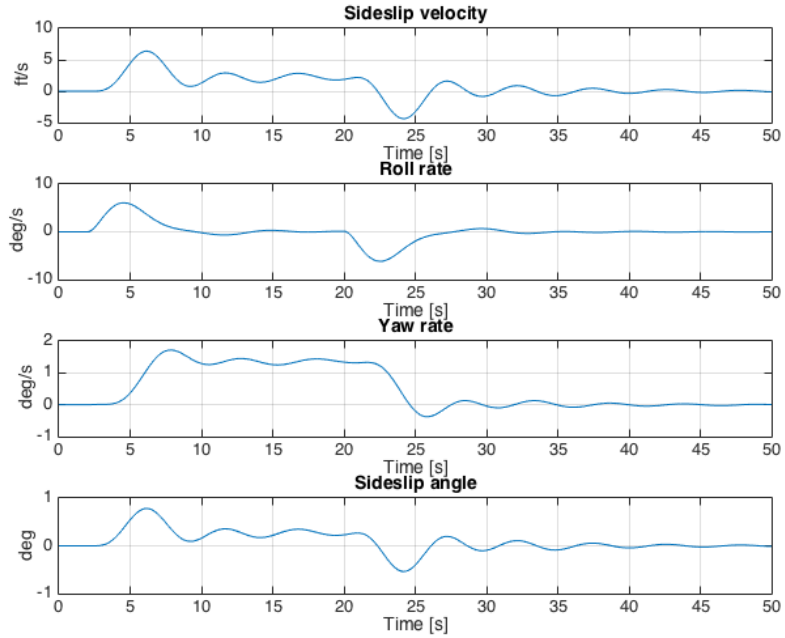

Fig. 4.4 Responses of other outputs using the PID

The required control input, the aileron deflection, to perform this manoeuvre is shown in Fig. 4.5. It shows the deflections with acceptable rate of change and smooth transient behaviour. The dynamical model of the actuator takes into account those control input constraints.

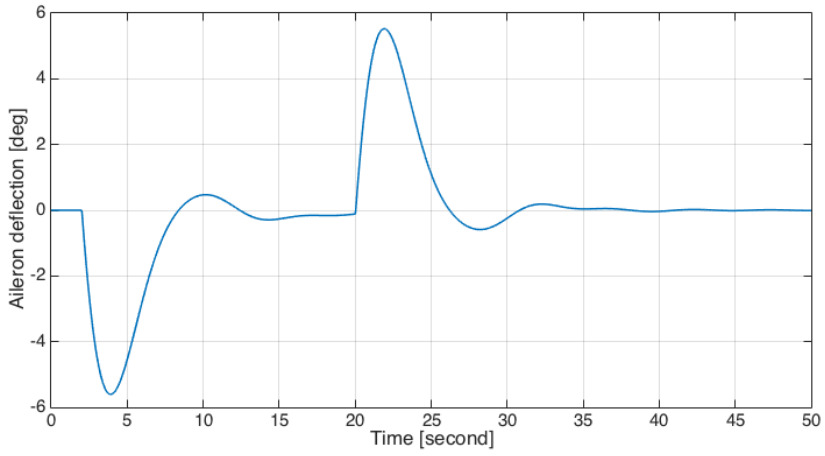

Fig. 4.5 Aileron deflections using the PID controller

Furthermore, the control system for the afore-mentioned aircraft model is developed using the LQR optimal control in order to study the responses and features compared to the classical approach.

4.3.3 Optimal LQR tracking control

Here, the optimal LQR tracking controller is implemented to demonstrate the differences compared to the nominal classical PID method. Once the structure of LQR reference tracker is set, the control gains K includes K_x and K_I are computed. The tracking state space form of the model is as follows:

$$\begin{bmatrix} \dot{v} \\ \dot{p} \\ \dot{r} \\ \dot{\phi} \\ v \\ p \\ r \\ \phi \\ \beta \end{bmatrix} = \begin{bmatrix} -0.101 & 0 & -468.2 & 32.2 \\ -0.006 & -1.2 & -0.397 & 0 \\ -0.003 & -0.035 & -0.257 & 0 \\ 0 & 1 & 0 & 0 \\ -1 & 0 & 0 & 0 \\ 0 & -1 & 0 & 0 \\ 0 & 0 & -1 & 0 \\ 0 & 0 & 0 & -1 \\ -0.002 & 0 & 0 & 0 \end{bmatrix} \begin{bmatrix} v \\ p \\ r \\ \phi \end{bmatrix} + \begin{bmatrix} 0 & 13.48 \\ -1.62 & 0.392 \\ -0.01875 & -0.864 \\ 0 & 0 \\ 0 & 0 \\ 0 & 0 \\ 0 & 0 \\ 0 & 0 \\ 0 & 0 \end{bmatrix} \begin{bmatrix} \xi \\ \zeta \end{bmatrix} + \begin{bmatrix} 0 \\ 0 \\ 0 \\ 0 \\ 1 \\ 1 \\ 1 \\ 1 \\ 1 \end{bmatrix} r(t)$$

The weighting functions Q and R are as follows

$$Q = diag([1\ 1\ 1\ 10\ 1\ 1\ 1\ 10\ 1])$$

$$R = diag([2\ 4])$$

The tracking weighting function, Q, gives more emphasis to certain reference inputs. Here, for a lateral manoeuvre, the term corresponding to the bank angle is 10 times larger than the other variables. The control input weighting function R has two terms representing the aileron and rudder actuators. As the corresponding number increases, this will limit the use of that control input. The Algebraic Riccati Equation 4.5 can be solved for controller gains [K_x K_I] towards this tracking problem. By defining the Q and R matrices, the program code shown in Appendix C solves for the optimal state-feedback control gain K. The results are

$$K_x = \begin{bmatrix} -1.96 & -1.3 & 0.036 & -4.46 \\ 0.1 & -13.2 & 0.27 & 0.98 \end{bmatrix}$$

$$K_I = \begin{bmatrix} 0 & 0.03 & -0.03 & 2.45 & 0 \\ 0 & 0 & -0.24 & -0.03 & 0 \end{bmatrix}$$

Figure 4.6 shows the multi-input multi-output controlled system using LQR, where the aileron and rudder deflections are the inputs to the system u(t), while v,

p, r, ϕ, β are the outputs. The tracking problem incorporates all the outputs of the system, where only a bank angle manoeuvre is conducted, while other variables are driven to zero.

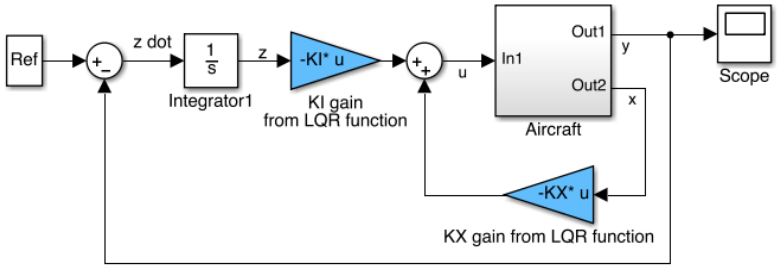

Fig. 4.6 LQR tracking model

The aircraft's dynamical system represented by the A,B,C matrices is shown in the block diagram in Fig. 4.7.

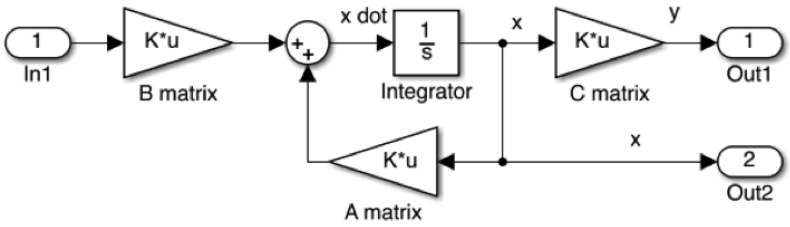

Fig. 4.7 Modelling of the system's dynamics

The controlled bank angle plot is shown in Fig. 4.8 where the solid line represents the actual controlled bank angle response. The plot shows a critically damped response with a 2.5 second rise time, and zero steady state error. The response settled quickly after 7 seconds using the tracking optimal control.

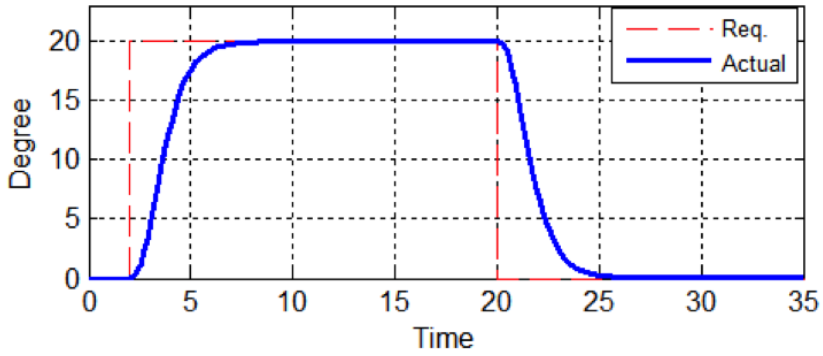

Fig. 4.8 Bank angle controller using LQR

In terms of minimizing other output variables, the LQR controller maintained their regulation, as shown in Fig. 4.9. It worth's mentioning that the yaw rate

was changing with the trajectory requirements of bank angle. This was due to the coupling between these parameters, where the rudder is regulating this rate.

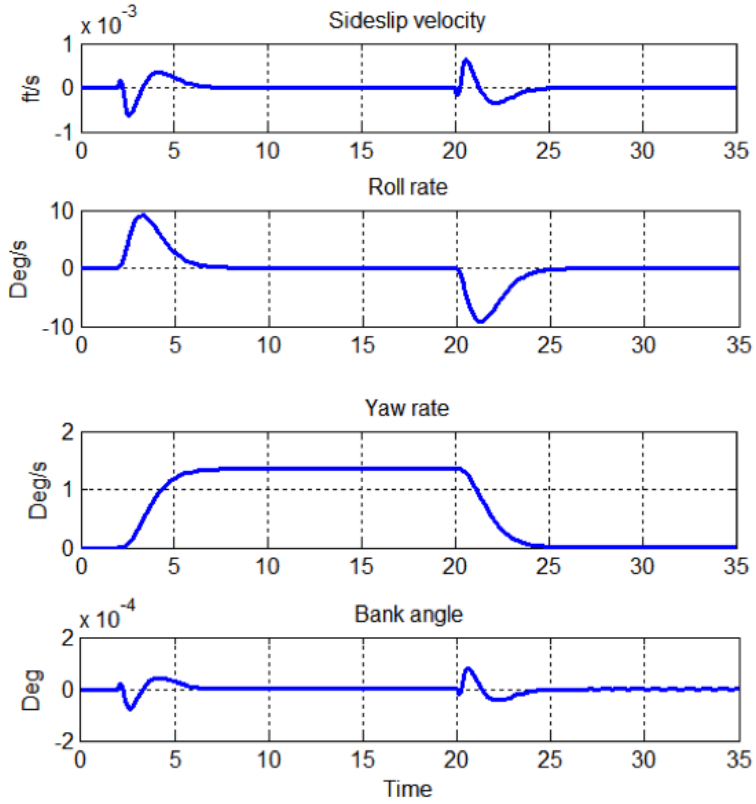

Fig. 4.9 Aircraft other variable responses using LQR.

The implemented LQR optimally utilized the aircraft actuators to produce the required manoeuvre. Together, the aileron and rudder were used as shown in Fig. 4.10.

As shown in the figure, the aileron has a magnitude higher than the rudder deflection since it is the main bank angle controlling effector. Rudder deflections were needed to counteract any yaw rate and sideslip variation incidents. A maximum deflection of ± 10, and a rate of change of deflections of 20 deg/s are satisfactory. For the classical and optimal controllers, both responses and control surface deflections were acceptable. However, the optimal controller was implemented for the MIMO system compared to the PID where only single input was considered. Moreover, the optimal controller took the model's constraints into account in the optimisation. Therefore, there was no need to model the actuator dynamics. This will certainly guarantee optimal control to meet the actuator constraints if implemented in real applications. Consequently, these results demonstrate the advantages of using an optimal control method to control the multivariable aircraft system compared to the classical PID control.

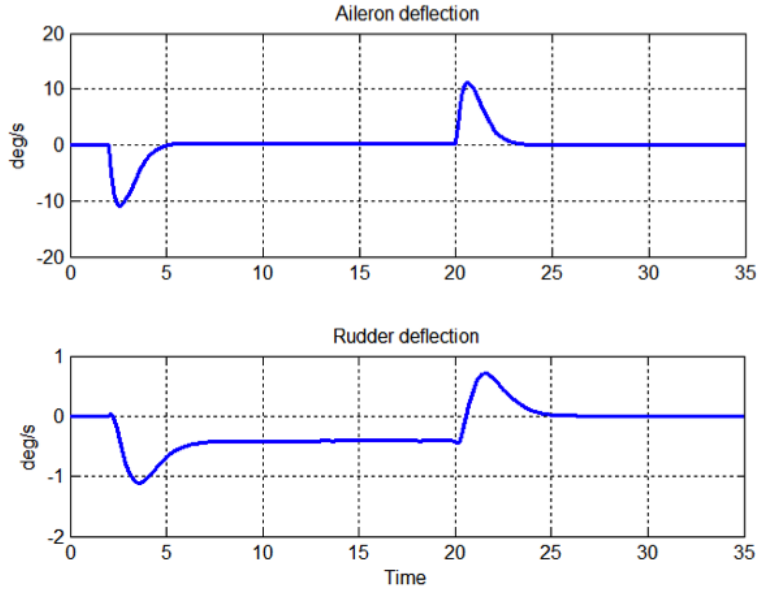

Fig. 4.10 Actuators deflections to control the system using LQR.

4.4 Fault-Tolerant Adaptive Control

When designing the optimal controller, the tracking performance was presumably achieved when using the full readiness of the actuators. With actuators subjected to loss of efficiency faults, the manipulation of weighing functions will reduce the tracking requirements (using the Q matrix) or adjust the relationship between the contributions of different actuators (with R). However, due to the large effect of ailerons to the rolling motion, when this actuator is faulty, the maximum rudder contribution will not be sufficient. Thus, there is a need to handle these control impairment cases with adaptive control laws. The next section addresses this problem.

4.4.1 Adaptive fault compensation

The adaptive fault-compensation-based strategy towards a fault-tolerant control system is primarily based on estimated faults. These faults in the linearised system are represented mathematically using the multiplicative and/or additive terms [18]. In the work presented in [21], the fault's mathematical integration to a linear discrete system was defined. This approach is utilised here, but for a continuous time system with the appropriate modifications. Suppose that the faulty actuator input is represented by the multiplicative and additive terms as follows

$$U_f = \alpha \times U + U_{f0}$$

where:

- U_f is the total faulty control input
- U is the total nominal control
- $\alpha = [\alpha_1, \ \ldots \alpha_m]$ is the loss of efficiency on the nominal control inputs
- U_{f0} is the total additive faulty input

To represent the faults within the state space model, let us consider $u_f = U_f - U_0$, where u_f is the faulty control input around the operating point and U_0 is the initial total control input. Hence,

$$\begin{aligned} \dot{x} &= Ax + Bu_f \\ \dot{x} &= Ax + B(\alpha \times U + U_{f0} - U_0) \end{aligned}$$

However, $u = U - U_0$, then

$$\begin{aligned} \dot{x} &= Ax + B(\alpha \times U + U_{f0} - U + u) \\ &= Ax + Bu + B(\alpha \times U + U_{f0} - U) \\ &= Ax + Bu + B((\alpha - I)U + U_{f0}) \end{aligned}$$

which can be written as,

$$\dot{x} = Ax + Bu + F_a f_a \tag{4.8}$$

where F_a corresponds to the faulty elements in the matrix B, and the fault magnitude $f_a = (\alpha - I)U + U_{f0}$.

For feedback control, the tracking control law, as described in the LQR tracking problem, can be written as

$$u\,(t) = -\,KX\,(t) = -[K_1 \ K_2] \begin{bmatrix} x(t) \\ z(t) \end{bmatrix} \tag{4.9}$$

Then, Equation 4.8 becomes

$$\begin{aligned} \dot{x} &= Ax + B(-K_1 x - K_2 z) + Fa \ fa \\ &= (A - BK_1)\,x - BK_2 z + Fa \ fa \end{aligned} \tag{4.10}$$

To compensate for the fault effects on the system, a new control term u_A is added to the nominal control law as follows:

$$u = -K_1 x - K_2 z + u_A$$

Hence, the closed loop equation of the system with faulty actuators will become:

$$\dot{x} = (A - BK_1)\, x - BK_2 z + Fa\ fa + Bu_A \tag{4.11}$$

The adaptation term u_A can be calculated by equating Equation 4.11 to the ordinary closed-loop equation that represent the system without fault terms, as follows:

$$(A - BK_1)\, x - BK_2 z = (A - BK_1)\, x - BK_2 z + Fa\ fa + Bu_A$$

then,

$$F_a\ f_a + B\ u_A\ =\ 0$$

Thus,

$$u_A = -B^{-1} F_a\ f_a$$

In the case that B is not a square matrix, where the number of system inputs is less than the number of states, as in the considered problem, then the states have to be subdivided into primary and secondary variables as follows:

$$\begin{bmatrix} \dot{x}_p \\ \dot{x}_s \end{bmatrix} = \begin{bmatrix} A_{pp} & A_{ps} \\ A_{sp} & A_{ss} \end{bmatrix} \begin{bmatrix} x_p \\ x_s \end{bmatrix} + \begin{bmatrix} B_p \\ B_s \end{bmatrix} u + \begin{bmatrix} F_{ap} \\ F_{as} \end{bmatrix} f_a \tag{4.12}$$

We can choose the primary variables such that the matrix Bp becomes a non-singular square matrix. For the adaptive FTC tracking problem, the control input in Equation 4.9 is written as,

$$u\,(t) = \ -[K_p\ K_s\ K_z] \begin{bmatrix} x_p \\ x_s \\ z \end{bmatrix}$$

Substituting into Equation 4.12 leads to,

$$\dot{x}_p = (A_{pp} - B_p K_p) x_p - B_p K_2 z + (A_{ps} - B_p K_s) x_s + F_{ap} f_a + B_p u_A \tag{4.13}$$

$$\dot{x}_s = (A_{ss} - B_S K_s)x_s - B_S K_2 z + (A_{sp} - B_s K_p)x_p + F_{as} f_a + B_s u_{Add} \tag{4.14}$$

Now, as the fault effects are to be eliminated from the primary state model, the additive control law can be calculated by

$$(A_{ps} - B_p\ K_s\ )\, x_s\ (t) + \ F_{ap}\ f_a\,(t) + \ B_p\ u_A\ (t)\ =\ 0$$

and then u_A can be calculated by:

$$u_A\ (t) = -{B_p}^{-1}\ [(A_{ps} - B_p\ K_s\ )\, x_s\ (t) + \ F_{ap}\ f_a\,(t)] \tag{4.15}$$

It is worth mentioning that, due to the splitting of states to primary and secondary variables in order to obtain a square B matrix, the adaptation term u_{add} becomes a function of the secondary state variables, their corresponding control gains, and the fault information. The development of a FTC based on this strategy utilizing the LQR control is presented next.

4.4.2 Development of the Adaptive FTC for linear aircraft dynamics

By selecting the primary state variables and formulating the state space model as in Equation 4.12, the adaptation control part u_{Add} is calculated. Due to the coupling between the roll rate motion and the yaw rate, and their influence on lateral-directional angles and velocities, they have been selected as the primary variables. Sideslip velocity and bank angle were considered to be secondary variables. This led to the rearrangement of the state space model to be in the following form:

$$\begin{bmatrix} \dot{p} \\ \dot{r} \\ \dot{v} \\ \dot{\phi} \end{bmatrix} = \begin{bmatrix} -1.2 & 0.397 & -0.0058 & 0 \\ -0.035 & -0.257 & 0.0028 & 0 \\ 0 & -468 & -0.1008 & 32.2 \\ 1 & 0 & 0 & 0 \end{bmatrix} \begin{bmatrix} p \\ r \\ v \\ \phi \end{bmatrix} + \begin{bmatrix} -1.62 & 0.392 \\ -0.019 & -0.864 \\ 0 & 13.48 \\ 0 & 0 \end{bmatrix} \begin{bmatrix} \xi \\ \zeta \end{bmatrix} + \begin{bmatrix} F_{ap} \\ F_{as} \end{bmatrix} f_a \tag{4.16}$$

The fault's magnitudes, $\alpha = [\alpha_1 \ \alpha_2]^T$ for aileron and rudder, was assumed to be known. Since the loss of effectiveness actuation fault was only considered, the faulty control input was modelled by a multiplicative equation while the additive fault term U_{f0} was omitted. Fault scenarios were assumed to be 50% and 90% loss of effectiveness in actuation performance. Required bank angle (ϕ) for the manoeuvre was applied to the system by a ramp input with a slope of 5 deg/s, as shown in Fig. 4.11, to test the effects of the fault. Other remaining outputs [p,r, v, β] were driven to zero.

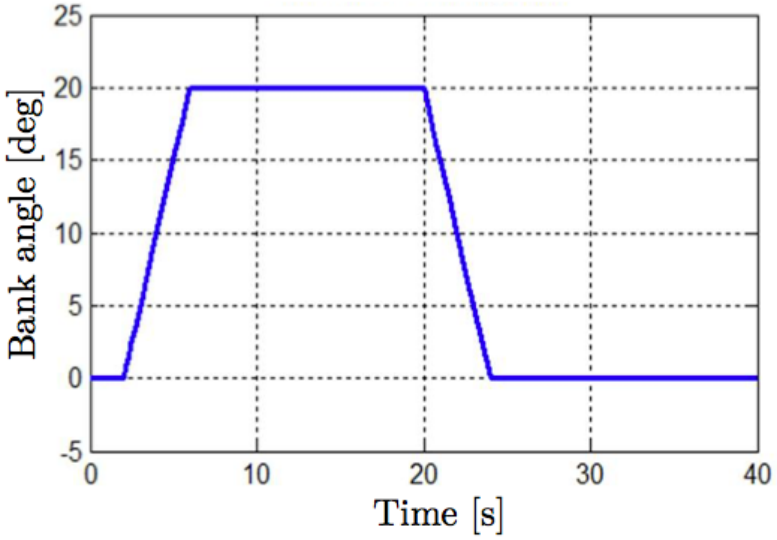

Fig. 4.11 Reference bank angle (ϕ)

As presented in the mathematical formula, the fault tolerant control strategy encompasses the optimal control and a fault compensation term that is added to the control input. Referring to Equation 4.16, the sideslip velocity and bank angle were considered to be secondary variables x_s, where B_p and A_{ps} are

$$B_p = \begin{bmatrix} -1.62 & 0.392 \\ -0.019 & -0.864 \end{bmatrix}$$

$$A_{ps} = \begin{bmatrix} -0.0058 & 0 \\ 0.0028 & 0 \end{bmatrix}$$

The term k_s is related to the elements in the computed control gain K corresponding to the secondary states, $F_{ap} = B_p$, and f_a is the measured magnitude of the faulty input. The linear-based scheme was constructed as in Fig. 4.12.

The inner loop contains the states feedback multiplied by the relevant LQR gain; the feedback-loop of the output (y) simulates the measurement of the system's output

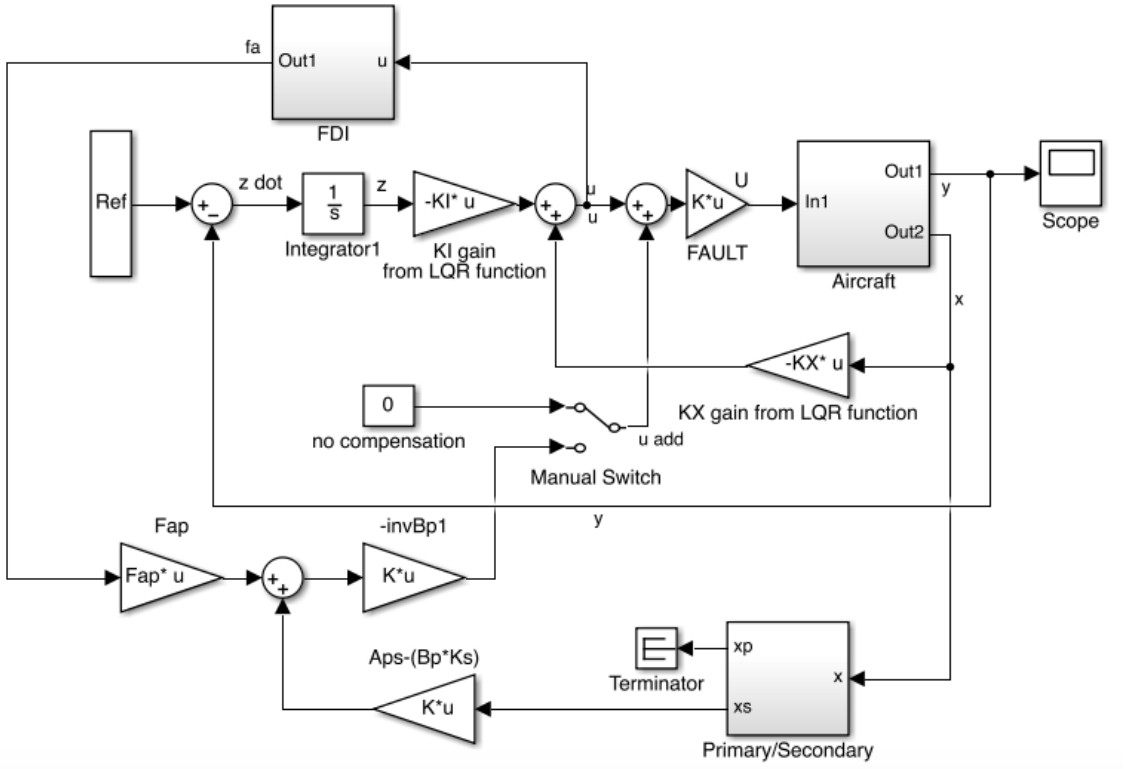

Fig. 4.12 FTC using LQR tracking control and fault compensation

to keep tracking the output reference values. Fault compensation was calculated based on Equation 14 and then added to the total control input (u).

4.4.3 Results of the adaptive Fault Tolerant Control

Fault scenario 1: 50% Loss of effectiveness fault:
In this case, the optimal LQR control dealt with the fault scenario very efficiently, and provided an acceptable response, as in Fig. 4.13, due to the optimality features resulting from the tuning of the weighting matrices and minimisation of the cost function.

The FTC improved the response of the bank angle and reduced the effects of the 50% loss of effectiveness fault further. The control deflections required by those different cases are depicted in Fig. 4.14.

Fault Scenario 2: 90% Loss of effectiveness fault:
As shown in Fig. 4.15, in the case of a 90% fault, the LQR-based response had an enormous overshoot (50%), long delay in the response (of about 10 seconds), and highly undamped oscillatory behaviour. Due to the optimality feature, the LQR still maintained a stable system as the bank angle converged around the required reference value. On the other hand, the FTC with the fault compensation mechanism

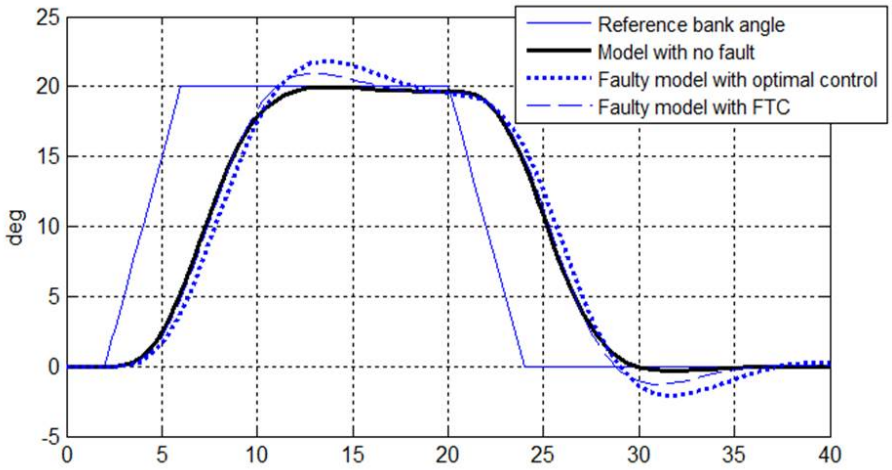

Fig. 4.13 Bank angle (ϕ) response with 50% faulty actuators

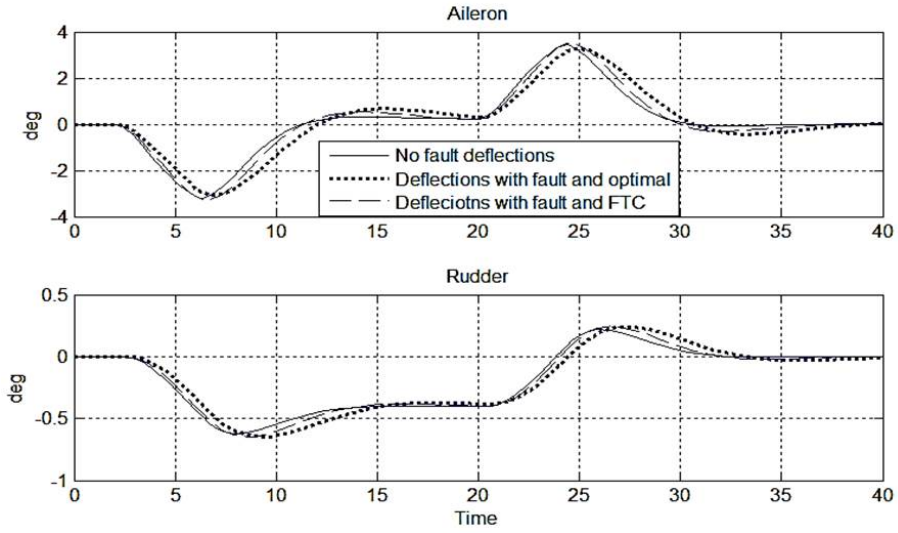

Fig. 4.14 Deflections with 50% faults.

yielded better results when acting against the 90% actuation fault, with relatively acceptable overshoot and settling time, which were both halved compared to the case when only the LQR was applied. The fault compensation added an extra required term to the control input in order to overcome this fault, and the results in terms of bank angle response were improved.

As depicted in Fig. 4.16, the deflections of control surfaces were severely affected by the faults that resulted in undesirable aircraft response. However, the compensation of FTC led to actuation having a reasonably similar pattern to the required control input, although it is faulty.

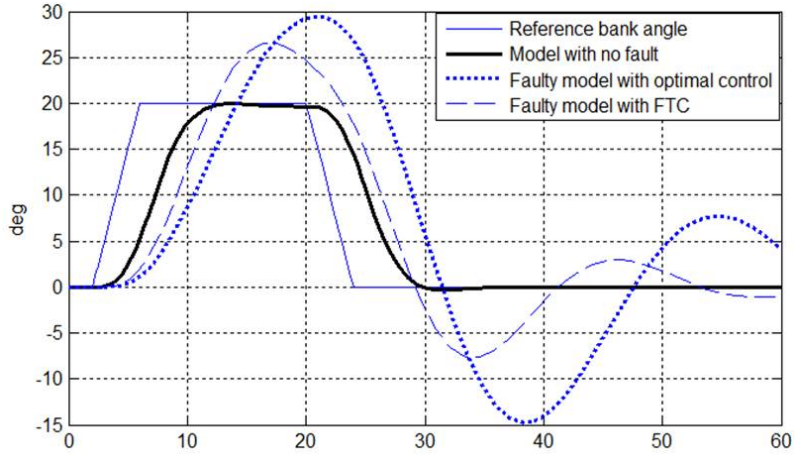

Fig. 4.15 Bank angle response with 90% loss of effectiveness faults

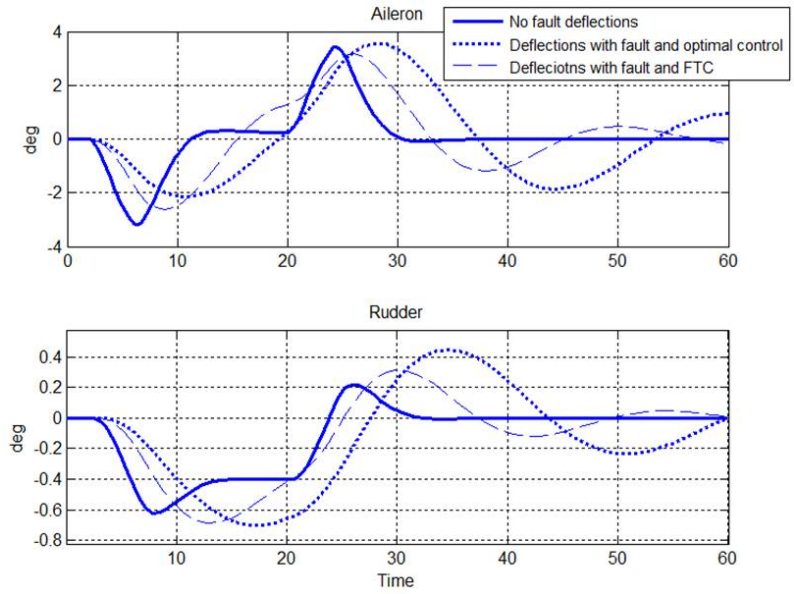

Fig. 4.16 Control surface deflections with 90% loss of effectiveness faults.

4.5 Nonlinear simulations and testing

Combining the developed adaptive LQR controller based on the approximated linear system into the 6-dof modelling of the nonlinear equations of motion of the aircraft will test its practicality and limitations.

4.5.1 Aircraft business jet model

In this work, a business jet aircraft nonlinear 6-dof dynamical model, built to conduct control-related research, was utilised. The aircraft has rear twin jet engines and a T-shape tail, as shown in Fig. 4.17, and has a mass of 6100 kg and a 14.7 m wingspan.

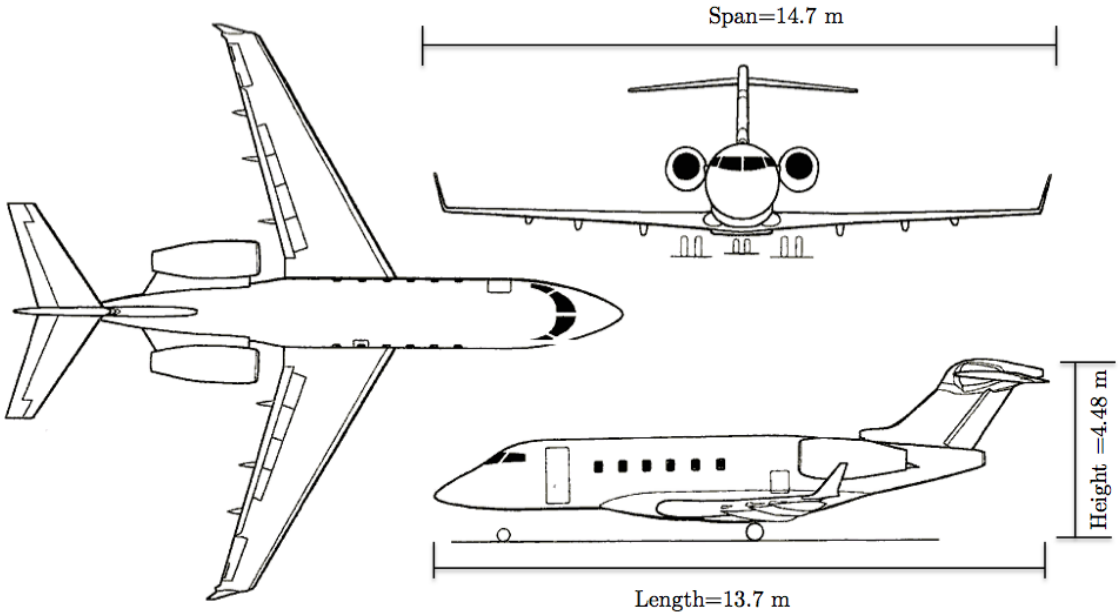

Fig. 4.17 Aircraft's dimensions and configuration layout

Basic aircraft specifications are listed in Table 4.1.

Table 4.1 Specifications of the business jet aircraft.

Mass	$m = 6100$	kg
Moment of inertia	$I_{xx} = 25418$	kg m^2
	$I_{yy} = 68684$	kg m^2
	$I_{zz} = 78324$	kg m^2
	$I_{xz} = 4286$	kg m^2
Span	$b = 14.7$	m
Wing area	$S = 25.7$	m^2
m.a.c.	$\bar{c} = 1.904$	m
CG location	$CG_{x,y,z} = [-0.017,0,-0.269]$	m

4.5.2 Trimming and linearisation

In this work, the aircraft was trimmed at steady-state wing-level flight around Mach 0.3 and altitude 4000 m. The trimming states and controls x_e and u_e were computed from the nonlinear equations $\dot{x} = f(x, u)$, such that $f(x_e, u_e) = 0$ for definite x_i. This steady state condition, which requires no changes in the angular rates or airspeed, yields,

$$\dot{P}, \dot{Q}, \dot{R} = \quad \dot{V}_T, \ \dot{\beta}, \ \dot{\alpha} \ \equiv 0$$

The aim is to design a controller for the linear model that will operate in the region defined by the trimming conditions mentioned above. The trimming and linearisation process yielded an elevator deflection equal to 2.8 deg., and engine throttle of 20.33%; while aileron and rudder deflections are both zero. Aircraft flying states of motion were computed and listed in Table 4.2.

Table 4.2 Basic states of the trimmed aircraft.

V_T	Airspeed [m/s]	97.37
α	Angle of attack [deg]	3.4
θ	Pitch angle [deg]	3.4
h	Altitude [m]	4000

Numerical linearisation resulted in the decoupled linear lateral motion of the aircraft in a state space form $\dot{x} = Ax(t) + Bu(t)$ as follows:

$$\begin{bmatrix} \dot{p} \\ \dot{r} \\ \dot{\psi} \\ \dot{\phi} \\ \dot{\beta} \end{bmatrix} = \begin{bmatrix} -2.6 & 0.87 & 0 & 0 & -6.5 \\ -0.31 & -0.178 & 0 & 0 & 2.2 \\ 0 & 1 & 0 & 0 & 0 \\ 1 & 0.064 & 0 & 0 & 0 \\ 0.062 & -0.1 & 0 & 0.1 & -0.246 \end{bmatrix} \begin{bmatrix} p \\ r \\ \psi \\ \phi \\ \beta \end{bmatrix} + \begin{bmatrix} -0.13 & 0.036 \\ -0.012 & -0.025 \\ 0 & 0 \\ 0 & 0 \\ 0.002 & 0.0008 \end{bmatrix} \begin{bmatrix} \xi \\ \zeta \end{bmatrix}$$

Where ϕ and ψ are the bank and heading angles; and ξ, ζ are the aileron and rudder deflections, respectively. Based on the linear form of the lateral dynamics, the aircraft control law was designed. The variables to be controlled were the heading angle $\psi$and the rolling angle ϕ.

To test the linearisation fidelity of the open-loop system, the linear model at cruise was verified against the nonlinear model for a pulse input from the control surfaces, as shown in Figures 4.18 and 4.19. These show a complete match between them for different variables, which validates the linearisation approximation.

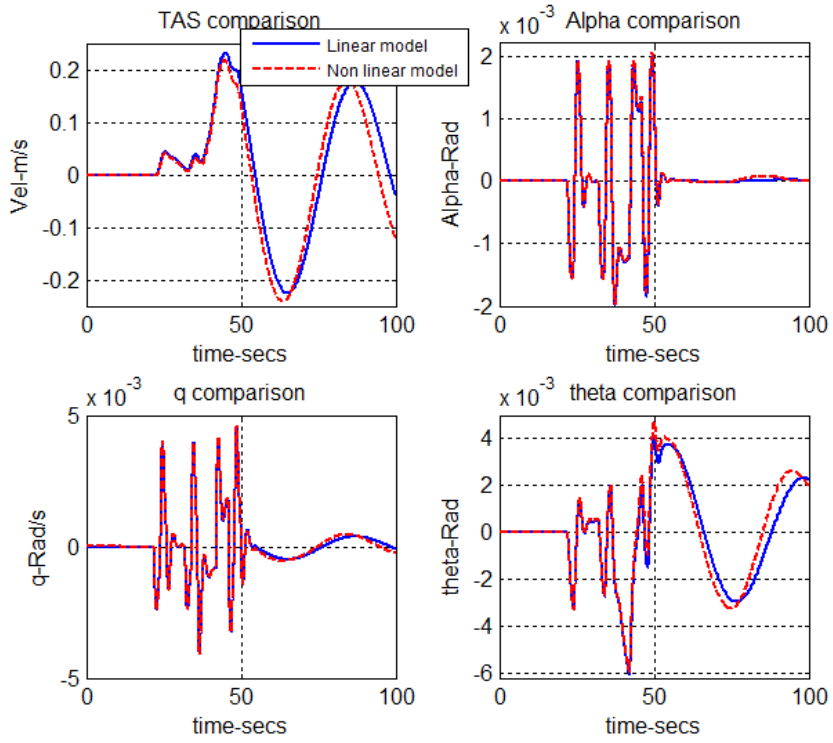

Fig. 4.18 Elevator pulse input effects on the longitudinal dynamics.

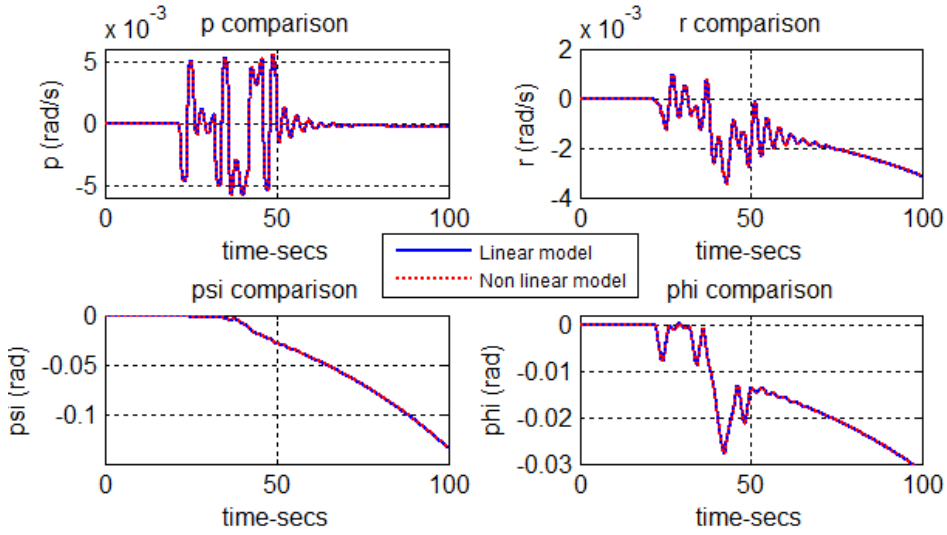

Fig. 4.19 Aileron pulse input effects on the open-loop lateral dynamics.

4.5.3 The FTC Controller development

The LQR tracking control law was formulated by the error equation augmented in the linear model, shown in the second row in the following equation, as follows:

$$\begin{bmatrix} \dot{x}(t) \\ \dot{z}(t) \end{bmatrix} = \begin{bmatrix} A & 0 \\ -C & 0 \end{bmatrix} \begin{bmatrix} x(t) \\ z(t) \end{bmatrix} + \begin{bmatrix} B \\ 0 \end{bmatrix} [u(t)] + \begin{bmatrix} 0 \\ 1 \end{bmatrix} r(t) \tag{4.17}$$

Where

$$\dot{z}\,(t) = reference_{singal} - actual_{singal}$$

and C is a diagonal matrix for the corresponding tracked states. Accordingly, the system input $u\,(t)$ is in the form:

$$u\,(t) = -[K_x \;\; K_z] \begin{bmatrix} x(t) \\ z(t) \end{bmatrix} \tag{4.18}$$

From Equation 4.18, in order to achieve the required response, the system input $u(t)$ is to be designed by finding the best controller gain $K = [K_x \;\; K_z]$ that maintains closed-loop stability and provides the required tracking responses. Using the linear quadratic tracker strategy that is based on the minimization of the cost function, the Q and R tuning for best performance resulted in

$$Q = diag([0.2 \;\; 0.2 \;\; 0.2 \;\; 1.2 \;\; 0.2 \;\; 0.05 \;\; 0.05])$$

$$R = diag([0.21 \;\; 0.51])$$

Thus, the controller gains were calculated to be:

$$K_x = \begin{bmatrix} -1.8 & -6.13 & -4.76 & -6.76 & -4.6 \\ -0.19 & -0.762 & -0.57 & -0.725 & -0.553 \end{bmatrix}$$

$$K_z = \begin{bmatrix} -0.48 & -0.479 \\ -0.06 & -0.06 \end{bmatrix}$$

The compensation term of fault u_A was computed using Equation 4.15, where the primary variables selected are $[p \;\; r]^T$ and the secondary variables are $[\psi \;\; \phi \;\; \beta]^T$, thus:

$$u_A\;(t) = -{B_p}^{-1}\;[(A_{ps} \;-\; B_p\;K_s\;)\,x_s\;(t) + \;F_{ap}\;f_a\,(t)]$$

where:

$$B_p = \begin{bmatrix} -0.1335 & 0.036 \\ -0.0124 & -0.0252 \end{bmatrix}$$

$$A_{ps} = \begin{bmatrix} 0 & 0.0008 & -6.524 \\ 0 & 0.0021 & 2.2343 \end{bmatrix}$$

$$K_s = \begin{bmatrix} -4.76 & -6.76 & -4.595 \\ -0.567 & -0.7246 & -0.553 \end{bmatrix}$$

$$F_{ap} = \begin{bmatrix} -0.1335 & 0.036 \\ -0.0124 & -0.0252 \end{bmatrix}$$

and f_a is the measured faulty input.

4.6 Simulation Testing and Results

Effects of faults on the aircraft lateral motion were analysed in the nonlinear simulations. Figure 4.20 shows the closed loop system that includes the developed controller.

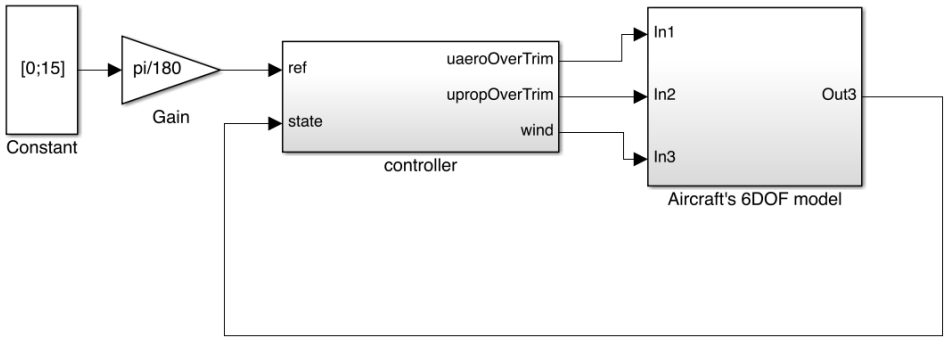

Fig. 4.20 Top-level view of the closed-loop system.

Modelling of the adaptive LQR fault-tolerant control system in the nonlinear environment is presented in Fig. 4.21, while the baseline LQR computed gains integrated in the control system are shown in Fig. 4.22.

Faults were introduced to the system by certain assumed gains starting with a small magnitude of fault, and then followed by increasing the severity of the fault. This enabled the author to test the controller limitations. High fault scenarios are presented.

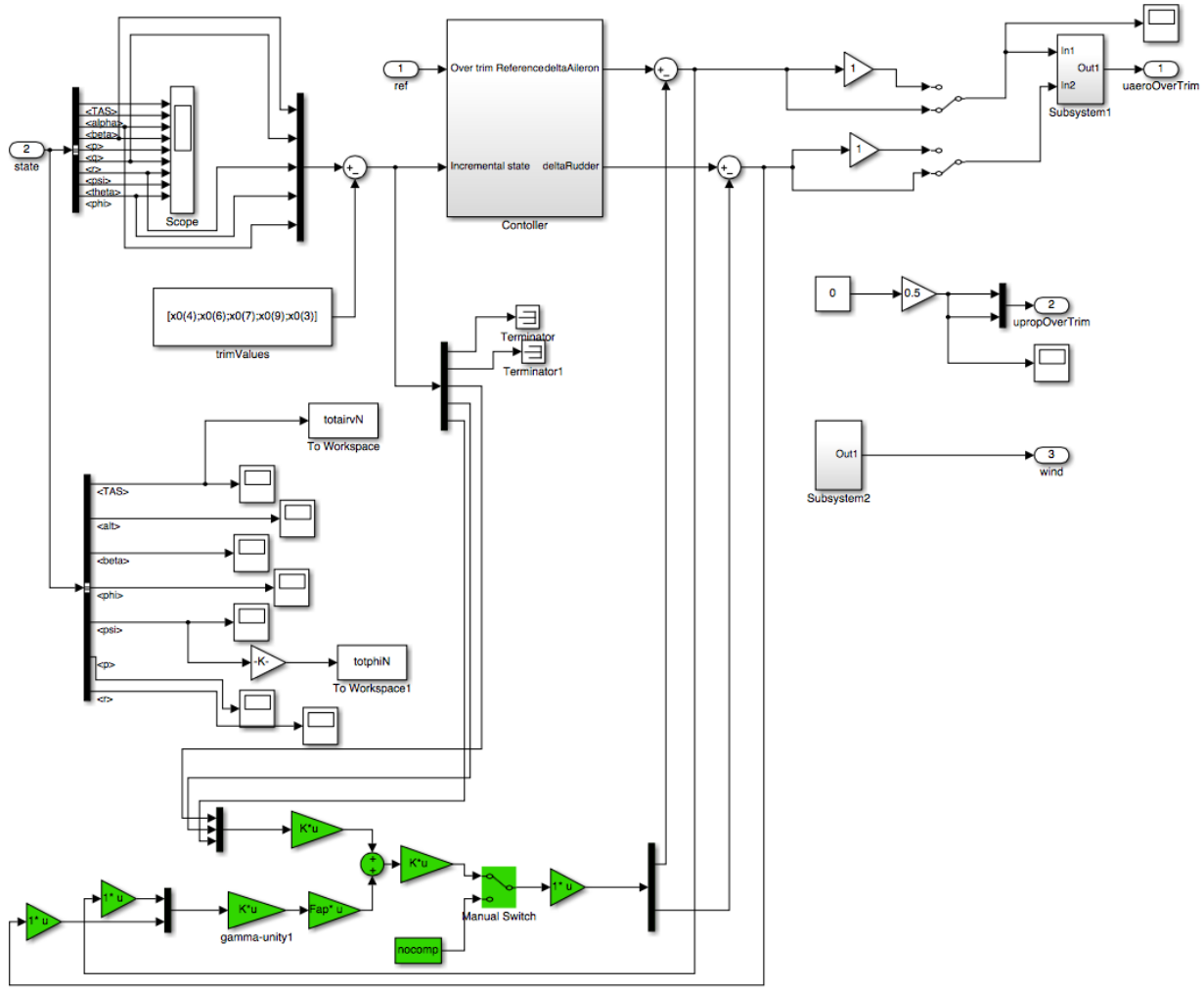

Fig. 4.21 Adaptive FTC layout in the nonlinear simulations.

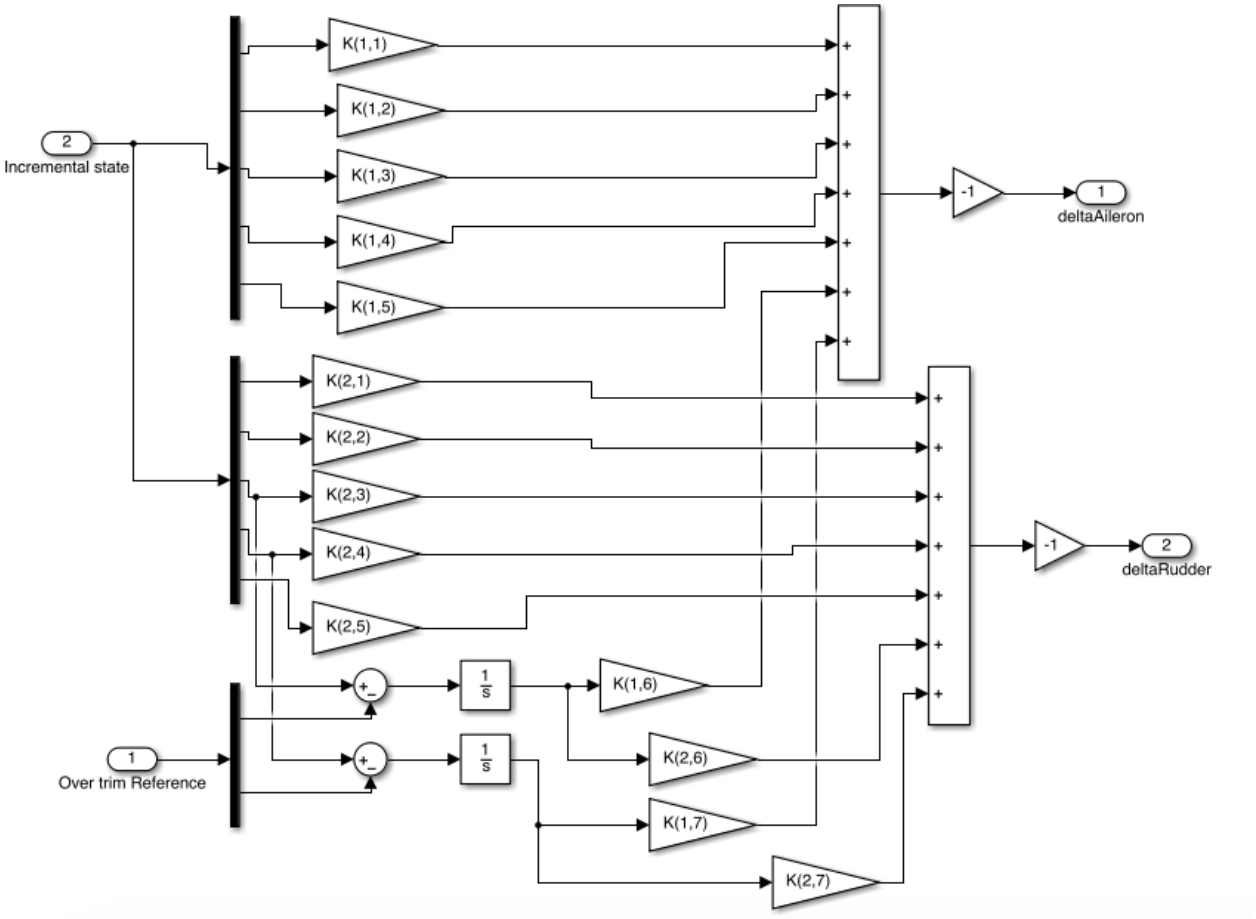

Fig. 4.22 LQR control model for the computed gains

4.6.1 Fault Scenario 1: 70% loss of effectiveness fault

When applying a 70% fault, the bank angle response for the faulty system (with only the LQR controller) had an overshoot and was poorly damped, resulting in a high settling time, as depicted in Fig. 4.23. This affected the tracking performance. The LQR-based response had a 19.5 second rise time compared to the FTC based response, which was 25 seconds, yet, the FTC strategy greatly damped the oscillation of the bank angle, which minimized the bank angle settling error and time.

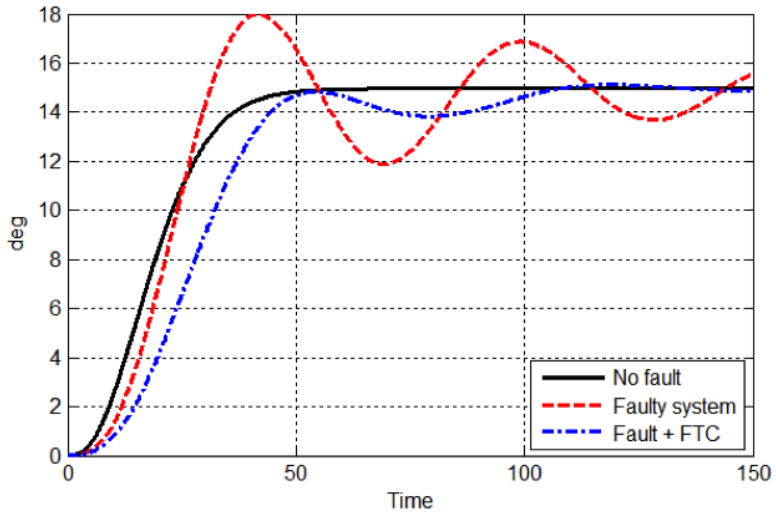

Fig. 4.23 Nonlinear bank angle response with 70% faulty actuator.

To observe how the control surfaces will respond, Fig. 4.24 the required deflections, where both surfaces had acceptable rates of changes in the two controller cases (the LQR and FTC). Yet, the oscillation was minimized when using the FTC, resulting in faster convergence and settling of actuator deflections.

4.6.2 Fault Scenario 2: 80% loss of effectiveness.

When applying 80% actuation faults, the LQR-controlled system became dynamically unstable and the required bank angle could not be maintained, as shown in Fig. 4.25. Noticeably, the FTC strategy had a slower response by 5 seconds but managed to maintain the stability with a slight degradation in the tracking performance. This clearly showed the advantages of this fault tolerant technique, which brought the faulty system back to stability compared to the LQR only control, where stability was lost.

As in Fig. 4.26, the faulty system had high overshoot and oscillatory non-stable behaviour in both control surfaces. This was minimized when applying the FTC technique as the deflections were damped and quickly settled to a certain deflection

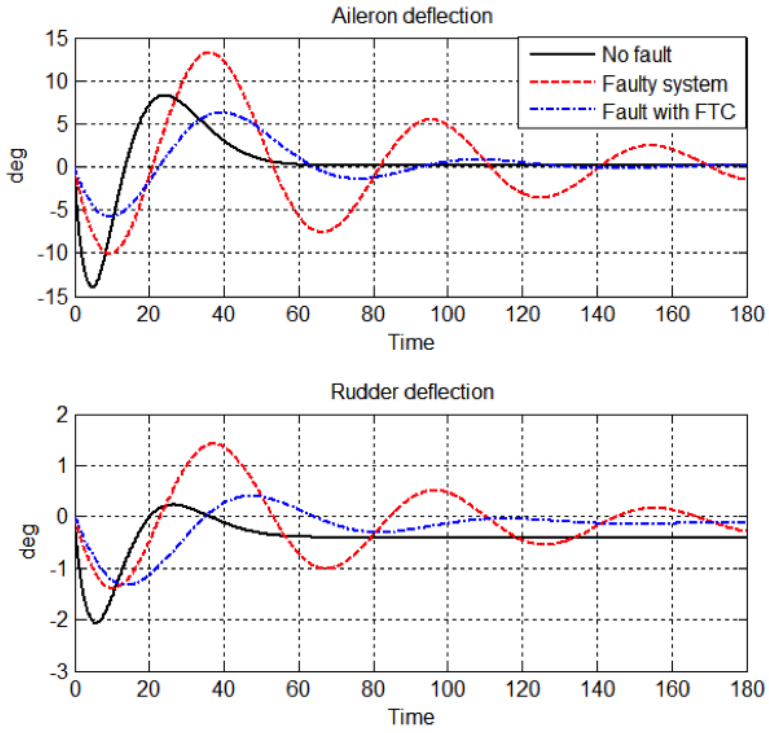

Fig. 4.24 Control surface deflections with 70% actuator faults.

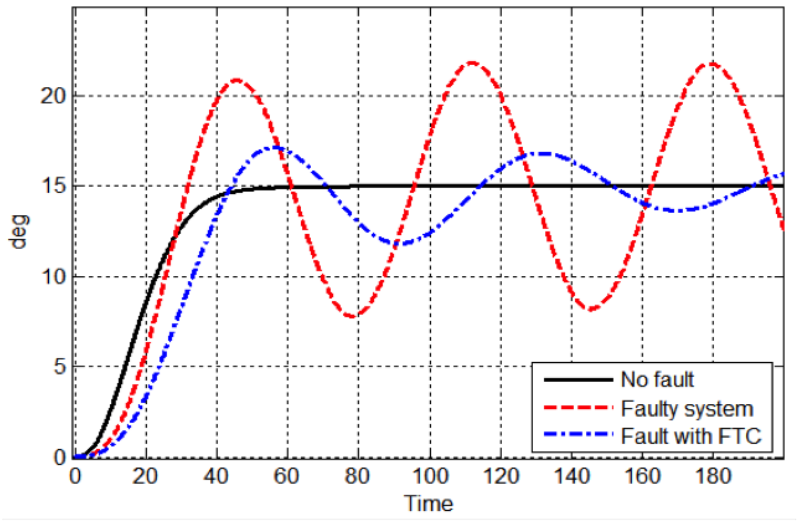

Fig. 4.25 Nonlinear bank angle response with 80% faulty actuator.

angle. The FTC approach has culminated in the enhancement of the tracking performance of the controller and has maintained the stability of the system when it encountered actuation faults.

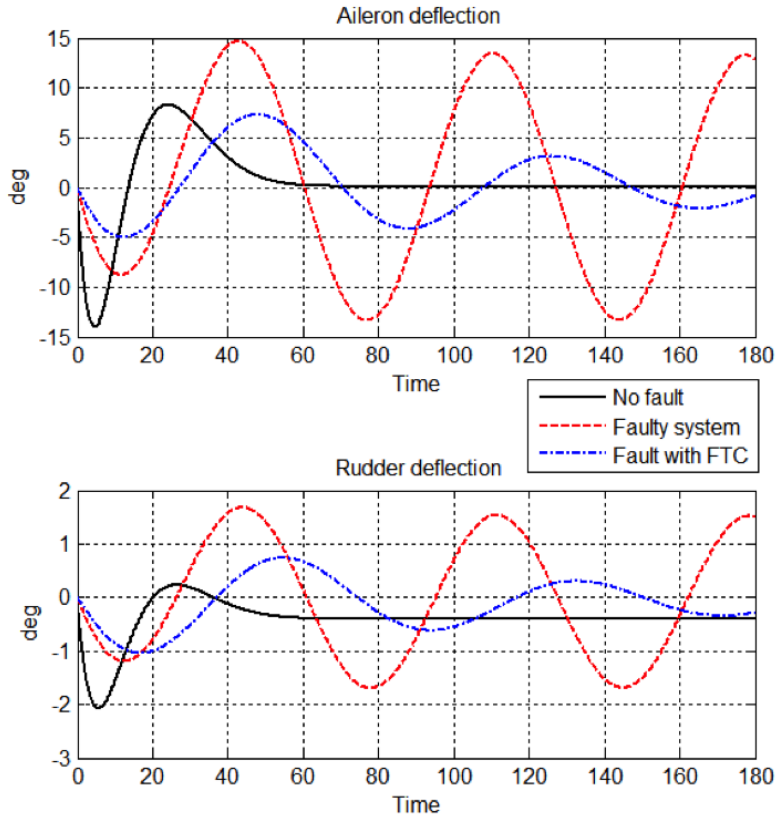

Fig. 4.26 Control surface deflections with 80% faulty actuator.

4.7 Conclusion

In this work, a fault tolerant control system was developed for an aircraft subjected to actuator faults. The system encompasses an optimal linear quadratic regulator control augmented with an adaptive fault-compensation-based scheme. The aircraft's lateral motion was considered, with the aileron and rudder as the main effectors. As an optimal multivariable controller, the LQR baseline control law was formulated. It handles the problem of tracking error and control energy minimisation. By an appropriate adjustment of the control weighting matrices, an optimal baseline control solution was obtained. In the analysis, loss of efficiency type faults were assumed.

The adaptive scheme was developed in order to accommodate the faults and prevent the degradation of the stability or deterioration of the tracking performance. It includes fault representation and adaptive compensation terms that are added to the model. The compensation term was computed by generating a faulty model as it was equal to the free-fault one, then solving for the adaptation term. The scheme relies on the availability of a fault detection system, which was assumed to be providing fault information to the FTC system. The FTC system was developed based on a linear dynamical model and then tested initially for performance and

stability optimisation. For validation of control viability, a nonlinear 6-dof simulation was performed. The LQR based controller was able to handle faults with magnitudes up to 70%, with large induced overshoot and oscillations. Yet, the rise time of the aircraft response was acceptable. When the fault increased, the system became unstable using the LQR only control. Tracking performance deteriorated as well, and the control surface deflections became unsettled. On the other hand, the FTC strategy control managed to handle high magnitudes of loss of efficiency faults in actuators. The aircraft response was slightly slower in rise time but overshoot was greatly minimised, to assure the stability of the system and eliminate the settling error. While accommodating the effect of faults on the stability, the approach also yielded a faster settling response and converged control surface deflections. Further improvements of the work may include studying of the effects of the delay of fault information delivery on the FTC performance, and how to avoid any shortcomings. Moreover, to cover the whole problem, the design of the fault detection and diagnosis (FDD) scheme is also suggested. Additionally, the investigations of the lock in place fault effects and accommodation will enrich the study to deal with different kinds of fault scenarios, where a redundant-effector aircraft model could be utilised. Another important investigation is to introduce the wind effects to the system, with a further step of testing and validation processes.

Chapter 5

Robust Optimal FTC using H_∞ and μ-synthesis Techniques

5.1 Introduction

In the absence of abrupt changes in the system, the pre-designed controller gains programmed in the autopilot usually work adequately well to generate the required manoeuvres automatically. However, this may not be the case when the aircraft confronts an actuation fault that reduces the effectiveness of the control surfaces and may lead to a degradation in the stability or tracking performance. It is important to enhance the automatic operation of the closed-loop system to tolerate some failures. As mentioned in the literature, in recent decades, designers have proposed different ways of dealing with the fault-tolerant control (FTC) problems. They have followed two main approaches: active or passive design methods [3, 18, 28]. Passive methods are basically robust control techniques that are suitable for certain types of perturbation that can be modelled as an uncertainty region around the nominal model. Robust control is designed to operate under the assumption of worst-case conditions. The computation is based on matrix singular value decomposition, which is a good measure of gains, especially for multivariable control [80]. Moreover, faults in actuators can be represented as an input multiplicative uncertainty. On the other hand, active FTC methods do not assume a static nominal model but instead take fault information explicitly into account. They require a fault detection and diagnosis scheme to obtain fault information [29]. Examples appear in [81–83]. Progressive complexities in the active technique may arise owing to the need for the development of fault diagnosis schemes, and this may result in adverse consequences that cause errors and inevitable delays. Moreover, the success of the FTC system is strongly based on the reliability of the fault information [21]. Thus, in this study, the robust

optimal control technique is considered to solve the stability and tracking problems for aircraft working with faulty actuators. Skogestad and Postlethwaite [84] defined robust stability analysis as determining, for a given controller K, whether the system will remain stable for an uncertainty set. In contrast, robust performance (RP) means that the performance objectives are satisfied for all the possible plants in the set of uncertainty. Thus, the robust control problem can be summarised as in [85] for a given a nominal process with acceptable values for perturbations: a robust controller should provide satisfactory performance in a closed-loop system for all the processes despite uncertainties in the model. Various types of uncertainties are grouped into two main categories: parametric uncertainties, where some of the parameters of the system are not certain, and unmodelled dynamics uncertainties, which are due to missing dynamics or lack of understanding of a physical process [80], [84]. Research on robust control of uncertain dynamic systems is based mainly on the frequency-domain transfer function analysis or the time-domain state space representation [85]. In this paper, a frequency-domain analysis is performed to design an optimal robust controller. Examples of robust methods include H_∞ control [86], [87], μ-synthesis [88–90], or a combination of the two, such as [91]; linear-quadratic Gaussian control, either alone [92] or in combination with linear-quadratic regulator control [93]; linear matrix inequality control [94]; and robust linear parameter-varying control [95]. In this work, the H_∞ and μ-synthesis robust techniques will be used. H_∞ control is a frequency-domain framework for fulfilling standard control design requirements such as speed of response, disturbance rejection, bandwidth, and robust stability, which are expressed in terms of H_∞ gain constraints [87]. On the other hand, robust stability and performance could be achieved using design methods that are based on the structured singular value (σ), such as the μ-synthesis robust technique [84].

Robust controllers are considered as optimal techniques, but they are different to the others, i.e. LQR, by the involvement of uncertainty in the framework. The analysis and design of H_∞-based control laws for linear systems with uncertainties ensure a worst-case performance, in which, for example, the faults bounds could be encompassed. Thus, when an optimal solution for specific uncertainty magnitude is found, this will increase the inherent capabilities of the controller to self−accommodating the faults.

Application of the H_∞ control design technique to the marine dynamic positioning (DP) control problem was presented in [96] where effective wave filtering can be obtained with guaranteed stability robustness. The reduction of the high control order is discussed in [97]. Automatic weight tuning is presented in [98], while an automatic

weight selection algorithm for the robust controller design for an active magnetic bearing system is proposed in [99]. An electric vehicle cruise control is researched based on an H2/H_∞ robust control approach [100]. Similar techniques are used for the braking system of electric vehicles (EV), to guarantee system performance, robust stability, and to attenuate the parameter perturbation and nonlinear uncertainties [101]. For time-varying uncertainties, a state-feedback control strategy that stabilizes the system and guarantees the H-norm bound constraint for disturbance attenuation is presented in [102].

For a fault tolerant application, a robust H_∞ control against actuator and sensor faults for satellite attitude control is presented in [103]. In the study, faults were represented by parametric uncertainty and uncertainty in the FDD. Simulation results validate the effectiveness of the scheme. A mix of H_2 and H_∞ infinity fault tolerant control methods for aircraft subjected to loss of efficiency faults was proposed by [104]. The conditions of closed-loop stability and mix of H_2/H_∞ infinity constraints were derived for both nominal and faulty cases. Simulations were also presented to show the advantages of the method.

In contrast to the work in [98, 99, 105–109], this paper studies the fault-tolerant flight control design for an aircraft subjected to actuator faults, where optimal H_∞ and μ-synthesis techniques have been investigated towards the robustness of the system in faulty cases. Moreover, the work encompasses the nonlinear simulation testing of the scheme against actuator faults at different operating conditions in the flight envelope (namely, the ascending, cruising, and descending cases).

In this work, the main goal is to achieve closed-loop stability and tracking performance while providing adequate stability margins for an actuator-faulty flying vehicle. The work encompasses no adaptation in the control law during faults, but instead assumes particular uncertainties in the control design process to take faults into account. The limits of robust control methods to handle actuation faults in a flying aircraft and the possible levels of degradation of the stability and tracking performance are also investigated. First, the closed-loop structure, including a linear dynamical model of the aircraft and fault-tolerant optimal control elements, is constructed. Second, stability, tracking performance requirements, and fault constraints are formulated within the cost function. By appropriate selection and tuning of the weighting elements, a robust stabilising solution is obtained. To cover major parts of the flight envelope, three main flying conditions were investigated: the ascending, cruising, and descending cases. For all of these cases, robust fault-tolerant controllers were computed, and the closed loop system was tested in a nonlinear simulation environment against loss of effectiveness faults.

5.2 Robust Fault-tolerant Control

5.2.1 Problem Formulation

Consider a linear time-invariant aircraft dynamical model described by:

$$\dot{x}(t) = Ax(t) + Bu(t), \qquad y(t) = Cx(t) + Du(t) \tag{5.1}$$

where $x(t) \in R^n$ is the state vector, $u(t) \in R^m$ is the control input, and $y(t) \in R^p$ is the measured output. A, B, C, and D and are known constant matrices of appropriate dimensions. The initial states $x(0)$ are the initial trimming conditions of the aircraft. As mentioned above, the aim of this work is to develop an actuation fault-tolerant tracking control, exploiting the inherent stability criteria in the robust control technique. To formulate the fault-tolerant tracking control problem, a fault model must first be established. Consider a loss-of-effectiveness fault in the aircraft actuators, assuming that there are no redundant systems such as multiple ailerons or rudders. The input multiplicative uncertainty, as shown in Figure 5.1, has the relation:

$$u_\Delta = u + (u * \Delta) \Rightarrow u_\Delta = u(I + \Delta) \tag{5.2}$$

where $\Delta = diag[\rho_1, \rho_2, ..., \rho_m]$ represents the loss-of-efficiency actuator faults for m actuators. Now, for any actuator i, the loss-of-effectiveness fault was set as:

$$\rho_i = \begin{cases} -1 & \text{complete loss} \\ -1 < \rho < 1, \text{except } 0 & \text{partial loss} \\ 0 & \text{no loss} \end{cases}$$

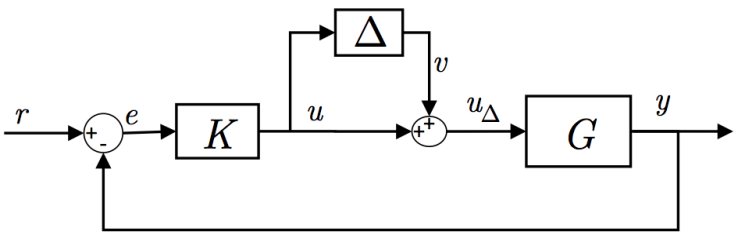

Fig. 5.1 System with input multiplicative uncertainty.

Hence, the aircraft dynamics with the actuator fault are described by:

$$\begin{aligned} \dot{x}(t) &= Ax(t) + Bu(t)(I + \Delta) \\ y(t) &= Cx(t) + Du(t)(I + \Delta) \end{aligned} \tag{5.3}$$

From Figure 5.1, the transfer function from signal v to u, as illustrated in [80], is

$$T_{uv} = -KG(I + KG)^{-1} \tag{5.4}$$

hence, from the small-gain theorem, we conclude that:

For a stable $\Delta(s)$, the closed-loop system is robustly stable if the controller $K(s)$ stabilises the nominal system and the following hold:

$$\begin{aligned} &\left\|\Delta KG(I + KG)^{-1}\right\|_\infty < 1 \\ &\textit{and} \\ &\left\|KG(I + KG)^{-1}\Delta\right\|_\infty < 1 \end{aligned} \tag{5.5}$$

which could be written in another form as:

$$\left\|KG(I + KG)^{-1}\right\|_\infty < \frac{1}{\|\Delta\|_\infty} \tag{5.6}$$

thus, for the largest possible perturbation, we need to solve the minimisation problem

$$\underset{K stabilizing}{min} \left\|KG(I + KG)^{-1}\right\|_\infty \tag{5.7}$$

Typically, we want to guarantee the stability of a system having uncertainty and also maintain good tracking performance, robust stabilisation, and less control energy with respect to the input multiplicative uncertainty. This is formulated as a multiple cost function minimisation problem. From Figure 5.2, we immediately have the relationships:

$$\begin{aligned} y &= GK(I + GK)^{-1}r \\ u &= K(I + GK)^{-1}r \\ e &= (I + GK)^{-1}r \end{aligned}$$

The design problem is now represented by finding the optimal stabilising controller K that minimises the following [84]:

to obtain good tracking

$$\left\|(I + GK)^{-1}\right\|_\infty \tag{5.8}$$

to reduce the control energy

$$\left\|K(I + GK)^{-1}\right\|_\infty \tag{5.9}$$

For shaping the output z_1 and z_2 for error and control input minimisation, it is very

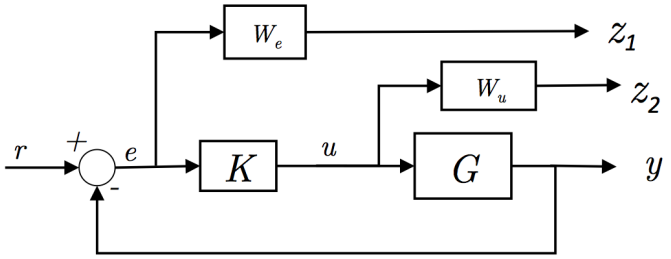

Fig. 5.2 Optimisation structure for tracking error and actuator input.

useful to use W_e and W_u as weighting functions, where $z_1 = W_e\, e$ and $z_2 = W_u\, u$; this yields the overall cost function

$$\min_{K stabilizing} \left\| \begin{array}{l} W_e(I+GK)^{-1} \\ W_uK(I+GK)^{-1} \end{array} \right\|_\infty \tag{5.10}$$

5.2.2 Robust Stability H_∞ Control

To adopt a unified solution process, the system structure in Figure 5.2, including the cost functions in equation (5.10), can be recast into a standard H_∞ configuration, as shown in Figure 5.3. Where the external exogenous inputs are denoted by w,

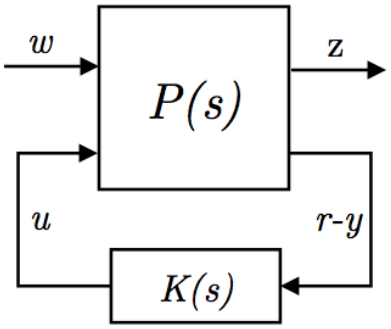

Fig. 5.3 System layout for H_∞ control computation.

including the reference r. While z, which includes both performance and robustness measures, denotes the output signals to be minimised. The vector $(r-y)$ represents the error measurements available to the controller K, and finally, u is the vector of the control input. $P(s)$ is called the interconnected system or generalised plant. Now, the objective is to find a stabilising controller (K) that minimises the output z. this will represent a minimisation of the H_∞ norm of the transfer function from w to z [80]. The solution can be obtained using the lower linear fractional transformation

technique [84]. First, the interconnected system P is partitioned as:

$$P(s) = \begin{bmatrix} P_{11}(s) & P_{12}(s) \\ P_{21}(s) & P_{22}(s) \end{bmatrix}$$

Then

$$z = [P_{11} + P_{12}K(I - P_{22}K)^{-1}P_{21}]w \tag{5.11}$$

Referring to our problem, the interconnected system $P(s)$ can be written from Figure 2, including the weighting functions, as:

$$\begin{bmatrix} z_1 \\ z_2 \\ r - y \end{bmatrix} = \begin{bmatrix} W_e & -W_eG \\ 0 & W_u \\ I & -G \end{bmatrix} \begin{bmatrix} w \\ u \end{bmatrix}$$

where $z = \begin{bmatrix} z_1 \\ z_2 \end{bmatrix} = \begin{bmatrix} W_e\, e \\ W_u\, u \end{bmatrix}$, $w = r$, $P_{11} = \begin{bmatrix} W_e \\ 0 \end{bmatrix}$, $P_{12} = \begin{bmatrix} -W_e\, G \\ W_u \end{bmatrix}$, $P_{21} = I$, and $P_{22} = -G$. The H_∞ controller is computed by solving the minimisation problem in the sense of energy; the controller will be robust if the cost function:

$$\gamma = \|T_{zw}\| = \left\| \begin{array}{l} W_e(I + GK)^{-1} \\ W_uK(I + GK)^{-1} \end{array} \right\|_\infty \tag{5.12}$$

is less than 1 [80], [84].

5.2.3 Robust Performance μ-synthesis Control

Let N be a closed system that includes the interconnected system P(s) and the controller K. Then, the structured singular value μ of N with respect to (Δ) is the number defined such that $\mu_\Delta^{-1}(N)$ is equal to the smallest $\bar{\sigma}(\Delta)$ that is needed to make $(I - N\Delta)$ singular [84]. That is:

$$\mu_\Delta^{-1}(N) = min\,\{\bar{\sigma}(\Delta) : det(I - N\Delta) = 0\}$$

Theorem: *Let the feedback plant (N) be a stable system and let $\beta > 0$ is the uncertainty bound where $\|\Delta\|_\infty < \beta$. Therefore, the perturbed system shown in Figure 5.4 is robustly stable with respect to Δ if and only if [80]*

$$\mu_\Delta(N) \leq \frac{1}{\beta} \Rightarrow \|N\|_\mu < 1$$

$$\Rightarrow \mu_\Delta(N(j\omega)) < 1, \forall\omega$$

Robust performance requires that the H_∞ norm of the upper linear fractional transformation transfer function $F = F_u(N, \Delta)$ in Figure 5.4 remains less than 1 for all Δ [84], as follows.
Assume N is stable; then:

$$\begin{aligned} RP &\overset{def}{\Leftrightarrow} \|F\|_\infty = \|F_u(N,\Delta)\|_\infty < 1, \forall \|\Delta\|_\infty \leq 1 \\ &\Leftrightarrow \|N\|_\mu < 1 \end{aligned} \tag{5.13}$$

for the structured uncertainty Δ.

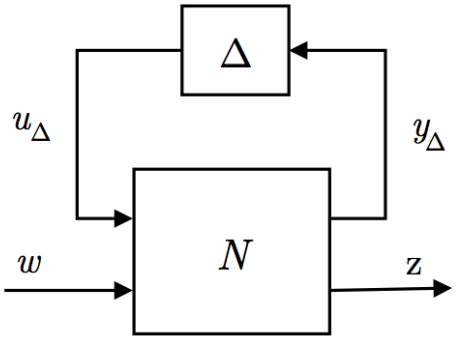

Fig. 5.4 NΔ structure for robust performance.

There is no direct method of synthesising a μ-optimal controller. However, for complex perturbations Δ, the $D-K$ iteration technique can be used to find a controller that maintains the robust performance criteria Eq.(5.13) [84]. First, for $\bar{\sigma}(\Delta) \leq 1$

$$\mu(N) = max_\Delta \rho(N\Delta)$$

μ is bounded by the spectral radius and singular value (spectral norm) as:

$$\rho(N) \leq \mu(N) \leq \bar{\sigma}(N)$$

Consider $\mathcal{D}$ to be set of matrices D that alter with Δ (i.e. $D\Delta = \Delta D$); then the upper bound of μ is:

$$\mu(N) \leq^{min}_{D\in\mathcal{D}} \bar{\sigma}(DND^{-1}) \tag{5.14}$$

The $D-K$ iteration method combines both H_∞ control and μ-synthesis. Because the upper bound condition in the inequality (5.14) is used, the problem now is to find a controller that minimises the peak value over the frequency of the upper bound by

alternating between minimising K or D while keeping the other variable fixed, as in the formula

$$\overset{min}{K}(\overset{min}{D \in \mathcal{D}} \left\| DN(K)D^{-1} \right\|_{\infty}) \tag{5.15}$$

The iteration process finishes when satisfactory robust performance, i.e. $\|DND^{-1}\|_{\infty} < 1$, is achieved.

5.3 Implementation of the Robust FTC

Consider a lateral-dynamical model $G(s)$ of a DC-8 aircraft having a weight of 190,000 lb and flying at a speed of 0.44 Mach at an altitude (h) of 15,000 ft, with the following state space matrices [60]:

$$A = \begin{bmatrix} -0.1008 & 0 & -468.2 & 32.2 \\ -0.0058 & -1.232 & 0.397 & 0 \\ 0.003 & -0.035 & -0.257 & 0 \\ 0 & 1 & 0 & 0 \end{bmatrix},$$

$$B = \begin{bmatrix} 0 & 13.48 \\ -1.62 & 0.392 \\ -0.019 & -0.864 \\ 0 & 0 \end{bmatrix}, C = \begin{bmatrix} 0 & 0 & 0 & 1 \end{bmatrix},$$

and $D = \begin{bmatrix} 0 & 0 \end{bmatrix}$.

Where the states of the model are side-slip velocity (v) (ft/s), roll rate (p) (rad/s), yaw rate (r) (rad/s), and the bank angle (ϕ) (rad), respectively. The inputs to the system are aileron and rudder deflections ξ, ζ (rad) respectively. The closed loop system, including $G(s)$, the controller $K(s)$, and the weighting functions W_e, W_d, and W_u, is shown in Fig. 5.5.

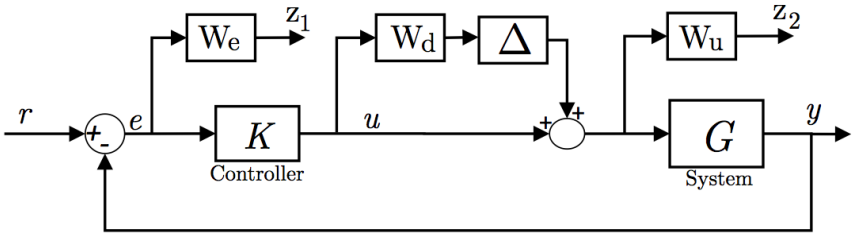

Fig. 5.5 Closed loop System including the weighting functions.

To shape the output $z = \begin{bmatrix} z_1 \\ z_2 \end{bmatrix}$ in Fig. 5.5 based on the tracking and actuation requirements, the system includes the following weighting functions:

First, $W_e(j\omega)$ for minimizing the tracking error of the bank angle was chosen to be a low-pass filter with the following transfer function:

$$W = \frac{f\ s + m_0}{(\frac{f}{m_\infty})\ s + 1} \tag{5.16}$$

where f is the frequency when magnitude of the weight reaches or drops from 100%, m_0 is the magnitude at low frequency, and m_∞ is the magnitude at high frequency. In tuning W_e for best performance, the parameters were determined to be f= 0.01 rad/s, m_0= 0 dB, and m_∞=-36 dB. This resulted in W_e being as depicted in Fig. 5.6.

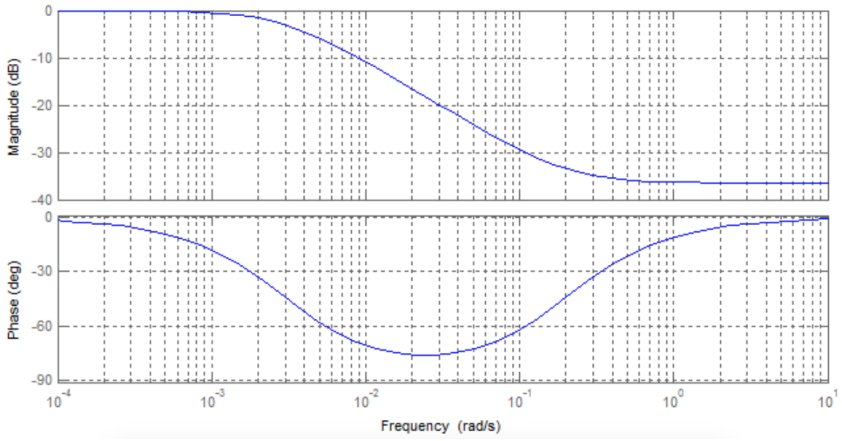

Fig. 5.6 Bode diagram of the tracking weighting function W_e.

Second, W_d for shaping the variation of the nominal value of fault (Δ) over different frequencies was determined. This weighing function could be frequency-dependent weight or merely a constant. In this work, it was assumed to be a 2x2 unity matrix for fault magnitude that doesn't vary with different frequencies.

Finally, $W_u(j\omega)$ to shape the control efforts and capture the actuators limitations is required. Moreover, it is a trade-off between robustness and deflection. As this weight is decreased, the system becomes more robust, but the deflection increases, and vice versa. In this study, aileron and rudder actuators inputs are available, and both of them have a specific weight W_u in a transfer function with high-pass filter form (Eq.5.16). The aileron, as the primary rolling control surface, has a smaller weight by a ratio of 4 compared to the rudder. This will give it more freedom to actuate. Fig.5.7 shows the Bode diagram of the aileron weighting function W_u.

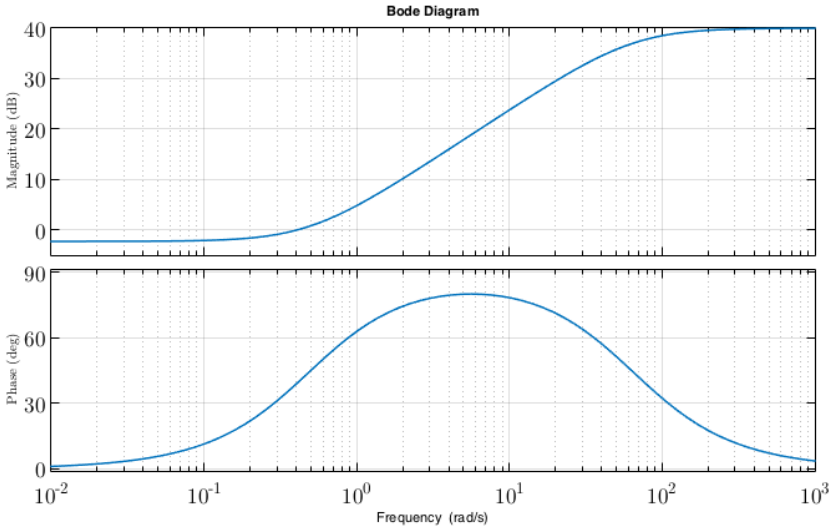

Fig. 5.7 Bode diagram of the aileron weighting function W_u.

5.3.1 H_∞ Control Design for System without Fault

The closed loop system depicted in Fig. 5.14 is put in the generalized plant P form (as in Fig. 5.3) with the following relationship:

$$\begin{bmatrix} z_1 \\ z_2 \\ r-y \end{bmatrix} = \begin{bmatrix} W_e & -W_e\, G \\ 0 & W_u \\ I & -G \end{bmatrix} \begin{bmatrix} w \\ u \end{bmatrix}$$

The H_∞ controller is computed under the assumption that the uncertainty is neglected. It is required to find the nominal stabilizing solution that fulfils the following condition:

$$\|T_{zr}\|_\infty = \left\| \begin{matrix} W_e(I+GK)^{-1} \\ W_u K(I+GK)^{-1} \end{matrix} \right\|_\infty < 1$$

$\gamma = \|T_{zr}\|_\infty$ that fulfils the robust controller requirements was found by adjusting the weighting functions (W_e, W_u) and using a MATLAB function *hinfsyn*. This process yielded to a stabilising solution where:

$$\gamma = 0.955$$

Time-domain Testing:

To test the H_∞ nominal controller, the following reference input of bank angle was used:

$$\phi(t) = \begin{cases} 15 \text{ deg/s} & 2<t<20 \\ 0 & otherwise \end{cases}$$

Figure 5.8 shows the bank angle response using H_∞ controller with good rise time response (2.5 seconds), relatively small overshoot, and acceptable steady state error. This indicates that this robust controller had maintained the aircraft's stability and yielded to a good tracking performance.

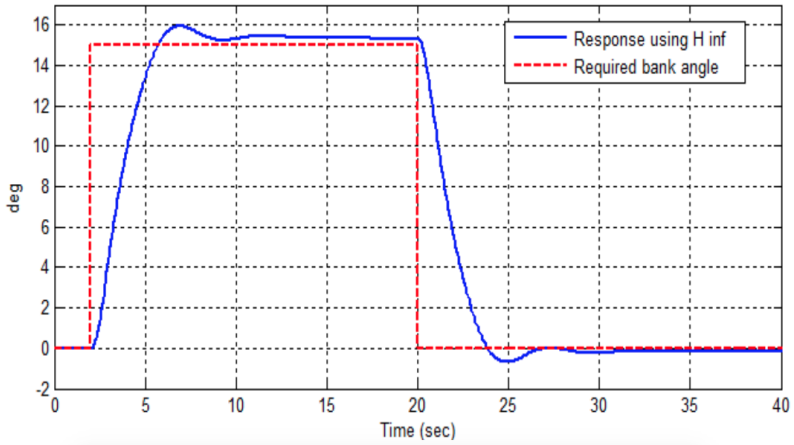

Fig. 5.8 Bank angle response using H_∞ controller.

Deflections of control surfaces resulted from using the H_∞ controller were also scrutinized as depicted in Fig. 5.9. Actuator dynamics were taken into account. Apparently, in order to perform the required manoeuvre, the aileron actuates to higher positions with higher rates compared to the rudder. Both of them have acceptable limits.

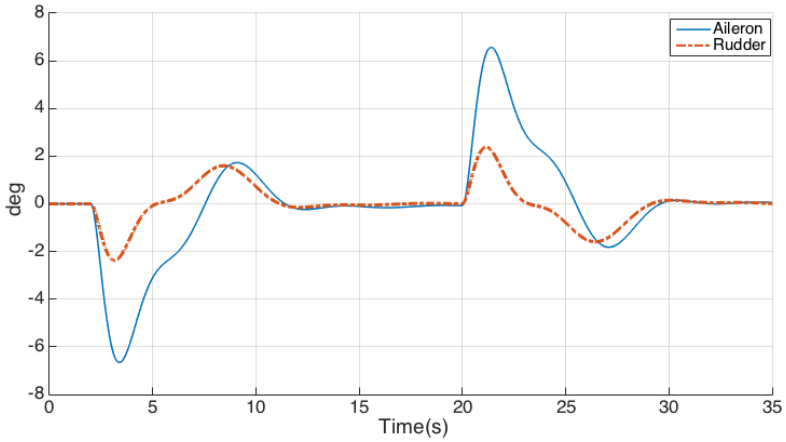

Fig. 5.9 Aileron and rudder deflections for the required manoeuvre using H_∞ controller.

This emphasizes the durability of using H_∞ in this robust stability multi-variable control system design. The robust performance controller design against actuator faults will be investigated next.

5.3.2 Robust Stability and Performance against Faults

In robust control computation, it was assumed that the uncertainty represents an actuator loss of effectiveness fault, with the following bounds:

$$-1 \leq \Delta \leq 1$$

Both H_∞ and μ-synthesis controllers have been computed for the faulty system. The generalized plant P, as in the figure shown in Appendix B.0.1, has the following relationship

$$\begin{bmatrix} W_d \\ z_1 \\ z_2 \\ r-y \end{bmatrix} = \begin{bmatrix} 0 & 0 & I \\ 0 & W_e & -W_e\, G \\ W_u & 0 & W_u \\ -G & I & -G \end{bmatrix} \begin{bmatrix} u_d \\ w \\ u \end{bmatrix}$$

The robustness condition of the μ-synthesis controller is expressed in terms of the upper bound of (μ). Results of robustness conditions for both controllers are as follows: Results in Table 5.1 clearly indicate that the condition of robustness has

Table 5.1 Results of the robust computation.

Controller	Condition of robustness	Result
H_∞	$\gamma < 1$	3.932
μ-synthesis	$\mu < 1$	0.99

not been achieved when using the H_∞ controller. However, μ-synthesis solution has maintained the robustness condition.

Time-domain Testing:

To test the closed-loop system with these computed controllers, faults were introduced to the actuators by a gain that represents the magnitude of the fault. Fault scenarios of $\Delta = 10\%, 30\%$, and 50% were assumed at the beginning of the simulation (i.e t=0). First, the H_∞ controller was tested. Fig. 5.10 shows the bank angle response and actuator deflections to make the required manoeuvre. When a 30% loss of effectiveness fault was introduced to aircraft actuators, the system

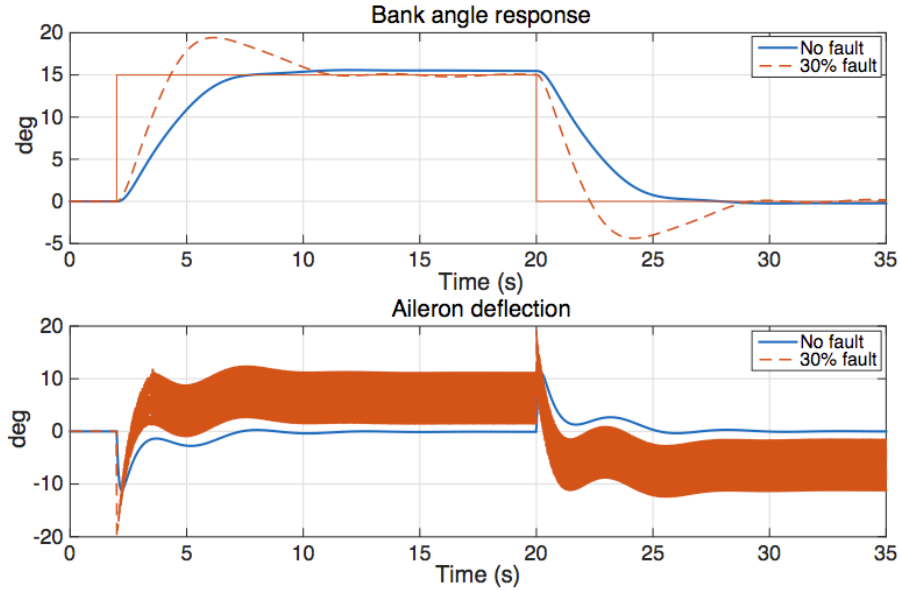

Fig. 5.10 Bank angle response and aileron deflections using H_∞ controller.

had a 25% overshoot in the bank response. Moreover, aileron deflections, as in Fig. 5.10, change very rapidly from 0 to 10 degrees. This enormously exceeds the actuators' deflection rates. On the other hand, by controlling the system using the μ-synthesis controller with fault magnitude reaching 50%, the system remains stable with acceptable degradation in the tracking performance, as shown in Fig. 5.11.

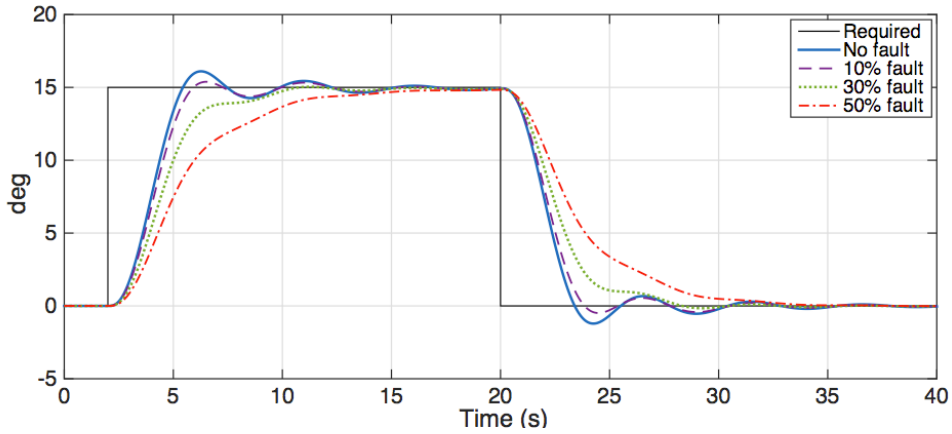

Fig. 5.11 Bank angle response using μ-synthesis controller.

Tracking features of rise time (2 seconds), overshoot ($< 5\%$), and steady-state error (0%) are very satisfactory. Aircraft control deflections, shown in Fig. 5.12, reach very standard positions (max ± 6 deg) at normal rates (max ± 6 deg/s) when using the μ-synthesis controller.

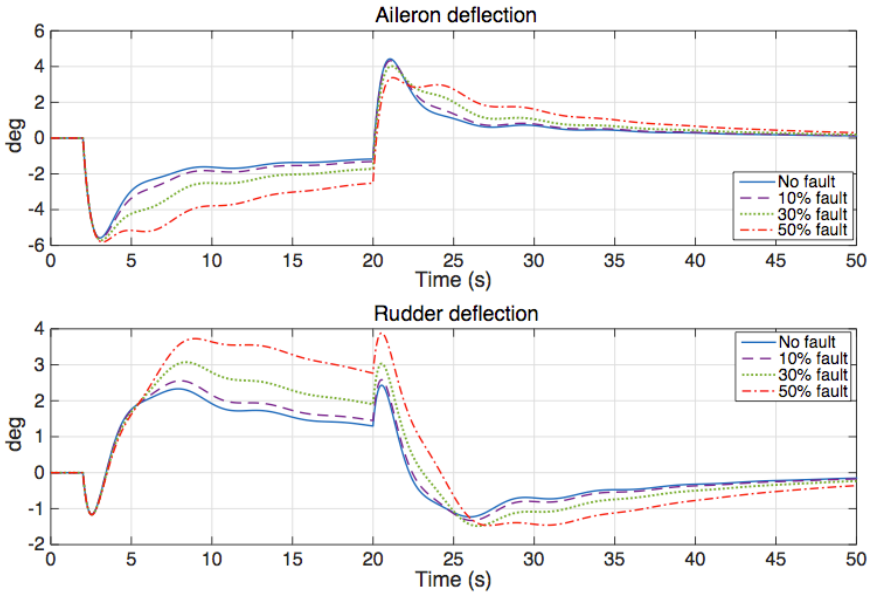

Fig. 5.12 Aircraft control deflections using the μ-synthesis controller.

The results noticeably demonstrate the ability of the μ-synthesis controller to automatically preserve stability and performance criteria against actuator faults for multi-variable aircraft dynamics.

5.4 Non-linear Testing and Validation

5.4.1 Aircraft Mission Profile

The Business Jet aircraft nonlinear model, expressed in section 4.5.1, is used in this analysis. The flight control law of the aircraft is designed using linear mathematical representations of aircraft dynamics at specific flying points. Figure 5.13 shows

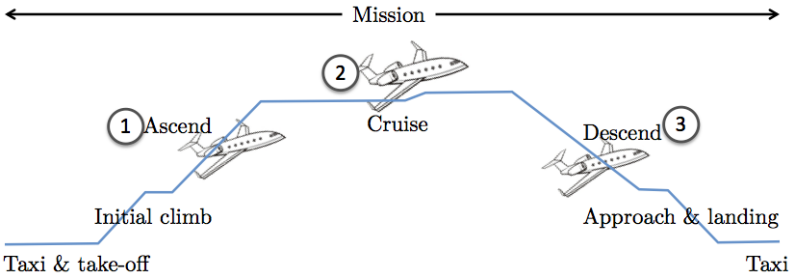

Fig. 5.13 Selected trimming points within the mission profile.

three points within the flight envelope that have been selected for this robust control design and testing. At these particular points, in order to get the linear models that represent the aircraft motion, the forces and moment exerted on the body of the aircraft are assumed to be constant or zero. The aircraft is trimmed around equilibrium points, typically called steady-state conditions [60], and a linearisation process is applied. The trimming states and controls x_e and u_e were computed from the nonlinear equations by solving for $f(x_e, u_e) = 0$ for definite x_i. This steady-state condition requires no changes in the angular rates or airspeed yields; $\dot{P}, \dot{Q}, \dot{R} \equiv 0$; $\dot{V}_T, \dot{\beta}, \dot{\alpha} = 0$; and flight path angle is constant.
The aim, now, is to design robust controllers for the derived linear models that will operate in the region around their trimming conditions.

5.4.2 Linear Models

In this work, the aircraft was trimmed at three flight conditions at certain Mach numbers, heights, and flight path angles, as listed in Table 5.2.

The trimming and numerical linearisation process yielded linear models (Equations (5.17) and basic states, as listed in Table A.1 For this FTC study, it was assumed that faults occur in the lateral motion effectors, namely, the aileron and rudder. Thus, the dynamics of the lateral motion only are investigated. The linear lateral model of the aircraft in the cruise flying condition is

Table 5.2 Aircraft basic trimming conditions.

Symbol	Condition	Ascending	Cruise	Descending
M	Mach number	0.2	0.3	0.2
h	Altitude, m	600	4000	300
γ	Flight path angle, deg	15	0	−10

$$\begin{bmatrix} \dot{p} \\ \dot{r} \\ \dot{\psi} \\ \dot{\phi} \\ \dot{\beta} \end{bmatrix} = \begin{bmatrix} -2.6 & 0.87 & 0 & 0 & -6.5 \\ -0.31 & -0.178 & 0 & 0 & 2.23 \\ 0 & 1 & 0 & 0 & 0 \\ 1 & 0.064 & 0 & 0 & 0 \\ 0.062 & -0.1 & 0 & 0.1 & -0.246 \end{bmatrix} \begin{bmatrix} p \\ r \\ \psi \\ \phi \\ \beta \end{bmatrix} + \begin{bmatrix} -0.13 & 0.036 \\ -0.012 & -0.025 \\ 0 & 0 \\ 0 & 0 \\ 0.002 & 0.001 \end{bmatrix} \begin{bmatrix} \xi \\ \zeta \end{bmatrix} \quad (5.17)$$

where p, r are the roll and yaw rates, and ψ, ϕ, β are the heading, bank, and sideslip angles, respectively. ξ and ζ are the aileron and rudder deflections, respectively. The aircraft dynamics for the ascending and descending cases in state-space forms are given in Appendix A.1.

5.4.3 Fault-tolerant Flight Control

Control Configuration and Performance Consideration

For each trimming condition case, the optimal fault-tolerant controller is computed. The generic closed-loop structure of the system $G(s)$ with a controller $K(s)$, including the weighting functions W_e, W_d, and W_u, is shown in Figure 5.14.

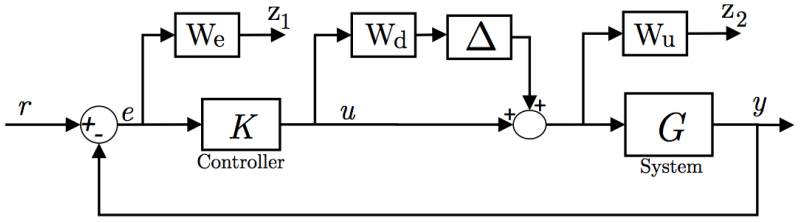

Fig. 5.14 Closed-loop system, including weighting functions.

To shape the output $z = \begin{bmatrix} z_1 \\ z_2 \end{bmatrix}$ according to the robustness and performance requirements, the system includes the following weighting functions:
First, W_e, for minimising the tracking error was designed to track the heading and bank angles; where the performance requirements of the sensitivity function S are

captured by the upper bound:

$$|S(j\omega)| < \frac{1}{W_e}, \forall\omega$$

W_e was chosen to be a low-pass filter, as shown in Figure 5.15, and tuned for the required manoeuvres in each trimming case. Table 5.3 lists parameters of W_e for heading angle ψ at different flying conditions.

Table 5.3 W_e parameters for tracking requirements of the heading angle (ψ).

W_e parameters	Ascending	Cruise	Descending
Low-frequency gain, dB	6	13	14.9
Crossover frequency, rad/s	0.04	0.11	0.085
High-frequency gain, dB	-40	-40	-20

To reduce the tracking efforts for a more robust stabilising solution, the heading (ψ) and bank (ϕ) angles tracking requirements in W_e are identical in shape, however, their magnitudes are different. Figure 5.15 shows the illustration of Bode diagram for W_e for bank angle.

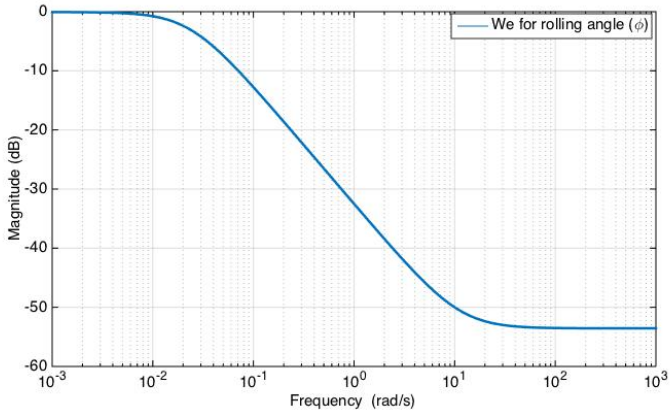

Fig. 5.15 Bode diagram of tracking weighting functions W_e for bank angle (at cruise).

Second, we consider W_d for shaping the variation of the nominal value of the fault (Δ) over different frequencies. This weighting function could be frequency-dependent or just a constant. In this work, a 2×2 constant matrix was assumed with values of ± 1.

Finally, W_u is needed for shaping the control efforts and capturing the actuator limitations. This weight represents a trade-off between robustness and deflection. As

Table 5.4 W_u parameters for control efforts.

W_u	Ascending	Cruise	Descending
Aileron	0.1226	0.09	0.075
Rudder	0.16	0.135	0.0975

this weight is decreased, γ (the robustness condition) decreases, but the deflection increases, and vice versa. In addition, to use the aileron actuator more than the rudder for a rolling motion, W_u for the rudder exceeds the weight of the aileron. Table 5.4 lists the W_u parameters.

Robust Control Computation

The closed-loop system in Figure 5.14 is given in the generalised plant P form (Figure 5.3) with the following relationship:

$$\begin{bmatrix} z_1 \\ z_2 \\ r-y \end{bmatrix} = \begin{bmatrix} W_e & -W_e\, G \\ 0 & W_u \\ I & -G \end{bmatrix} \begin{bmatrix} w \\ u \end{bmatrix}$$

The H_∞ controller is computed assuming that uncertainty is neglected. It is necessary to find the nominal stabilising solution that fulfils the condition:

$$\|T_{zr}\|_\infty = \left\| \begin{matrix} W_e(I+GK)^{-1} \\ W_u K(I+GK)^{-1} \end{matrix} \right\|_\infty < 1$$

The value of $\gamma = \|T_{zr}\|_\infty$ that fulfils the robust controller requirements was found by adjusting the weighting functions and using the MATLAB function *hinfsyn* for computation. For robust control design against uncertainty, that represents an actuator loss-of-effectiveness fault, the faults are modelled as follows:

$$\Delta = \begin{bmatrix} 30\% & 0 \\ 0 & 1\% \end{bmatrix}$$

for 30% fault in the aileron and 1% fault in the rudder. The generalised plant P, depicted in Figure **??** in Appendix B.0.1, has the relationship

$$\begin{bmatrix} W_d \\ z_1 \\ z_2 \\ r-y \end{bmatrix} = \begin{bmatrix} 0 & 0 & I \\ 0 & W_e & -W_e\, G \\ W_u & 0 & W_u \\ -G & I & -G \end{bmatrix} \begin{bmatrix} u_d \\ w \\ u \end{bmatrix}$$

The μ-synthesis controller based on $D-K$ iteration was computed in terms of the upper bound of (μ), whereas H_∞ was analysed in terms of the (γ) bounds, as mentioned before. Computational optimisation and iterations yielded the best possible results for the robustness conditions of the controllers, as listed in Table 5.5.

Table 5.5 Robustness condition results for nonlinear model.

Controller	The condition	Ascending	Cruise	Descending
H_∞	$\gamma < 1$	1.153	1.151	1.154
μ-synthesis	$\mu < 1$	0.994	0.998	0.999

The results indicate that the conditions of stability and performance robustness were guaranteed when the μ-synthesis control technique was used, but could not be achieved when the H_∞ controller was used for the aircraft under different operating conditions. Aircraft motion was examined for those two controllers with the 30% loss of effectiveness aileron fault. Aircraft response, when using the μ-synthesis, is damped with shorter settling time compared to the H_∞ based response as shown in Figure 5.16. Moreover, the response when using the μ-synthesis had neither an overshoot nor a steady state error.

Aileron deflections when using the H_∞ controller fluctuate very rapidly as shown in Figure 5.17. It also saturated swiftly reaching the maximum deflection limit. On the other hand, the aileron deflections when using the μ-synthesis controller had a very acceptable rate of changes and position limits, which assures the actuator dynamics. These results emphasise the robustness and viability of the μ-synthesis controller against loss of effectiveness faults, which eventually enhance the aircraft's stability and performance.

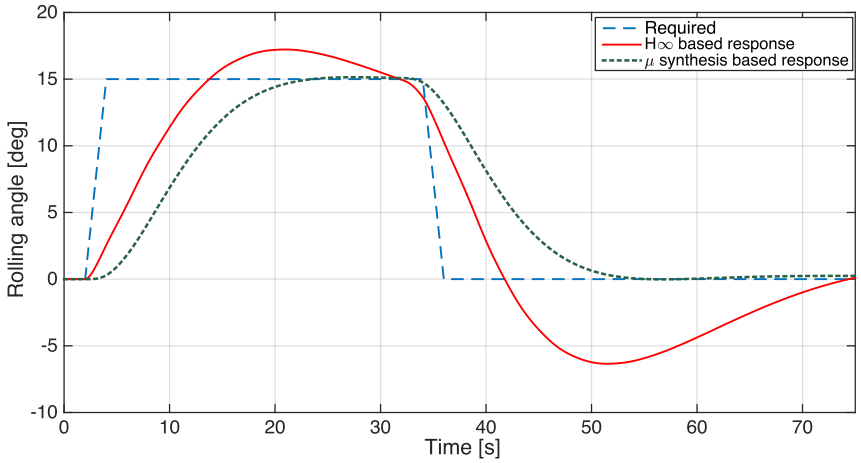

Fig. 5.16 Bank angle response using the two controllers with 30% faulty actuators.

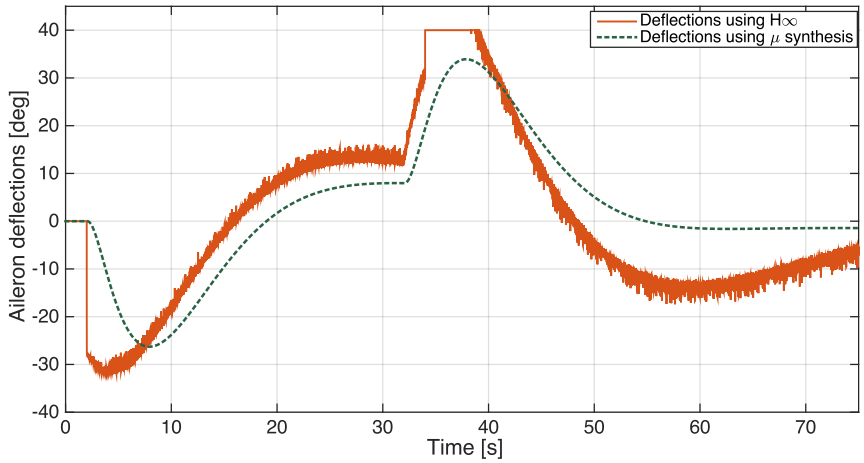

Fig. 5.17 Aileron deflections with 30% loss of effectiveness faults.

5.4.4 Simulation and Results for μ controller

The robust computation for a stabilising controller shows that μ-synthesis, but not H_∞ control, can guarantee the stability and performance robustness; therefore, μ-synthesis is now further tested in a nonlinear environment. In this study, a steady atmosphere is assumed, and the effect of wind is neglected. The strength of the controller is tested against a wider region around the trimming equilibrium point in order to cover a major part of the flight envelope.

Cruising Case

Because it is the largest segment of flight, the cruise case is analysed first. To test the performance of the controller in the time domain, the bank angle signal reference

input was assumed to be:

$$\phi(t) = \begin{cases} 7.5 \ \ deg/s & 2<t<4 \\ 15 \ \ deg & 4<t<34 \\ -7.5 \ \ deg/s & 34<t<36 \\ 0 & otherwise \end{cases}$$

Table 5.6 lists the testing conditions around the trimming point. The results of

Table 5.6 Trim and testing operating conditions.

Condition	Altitude, m	Mach	Speed, km/h
Trimming point	4000	0.3	367
Test condition 1	3475	0.26	318
Test condition 2	3750	0.28	342
Test condition 3	4266	0.32	392

nonlinear testing are shown in Figure 5.18. With a 30% faulty aileron, the nonlinear

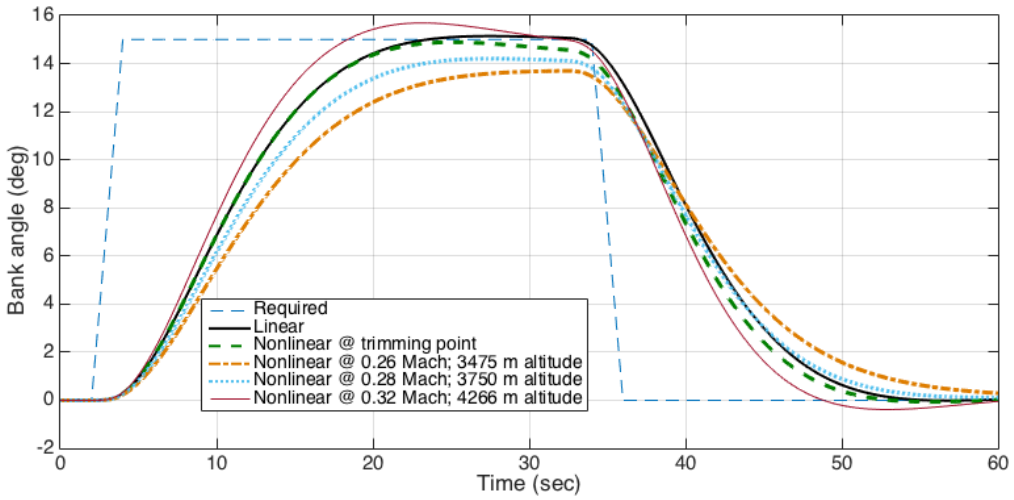

Fig. 5.18 Nonlinear simulation of bank (rolling) angle ϕ at cruise.

test of the entire system showed good consistency between the linear and nonlinear controlled closed-loop models. Moreover, from a control design viewpoint, the robust μ-synthesis controller led to a good tracking response of the bank (rolling) angle ϕ, where the steady-state error was very small. The aircraft response was slightly sluggish (rise time, 11 s) owing to the effects of the fault. However, the robust controller maintained good performance under different operating conditions.

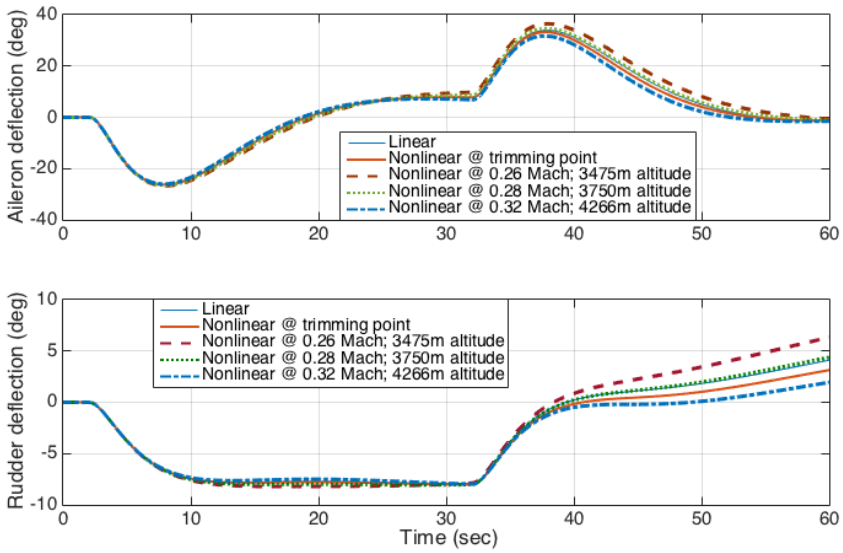

Fig. 5.19 Aileron (ξ) and rudder (ζ) deflections to generate the required response.

For control surfaces deflections shown in Figure 5.19, the aileron actuates smoothly at a maximum rate of 5 deg/s and a deflection of 32 deg. However, the deflection was high when testing at low speed (0.26 Mach).

The phase and gain margins indicate that there is still a safety margin before instability. The feedback closed loop system between ϕ_{ref} and ϕ_{actual} is expressed by:

$$\frac{\phi_{ref}}{\phi_{actual}} = L = \frac{GK}{1+GK}$$

where G is the aircraft lateral dynamical model and K is the μ-controller. Results as shown in Figure 5.20 are: the gain margin GM= 17.7 dB @ 0.582 rad/s and the phase margin PM= 117 deg. @ 0.129 rad/s. This is also confirmed by the Nyquist

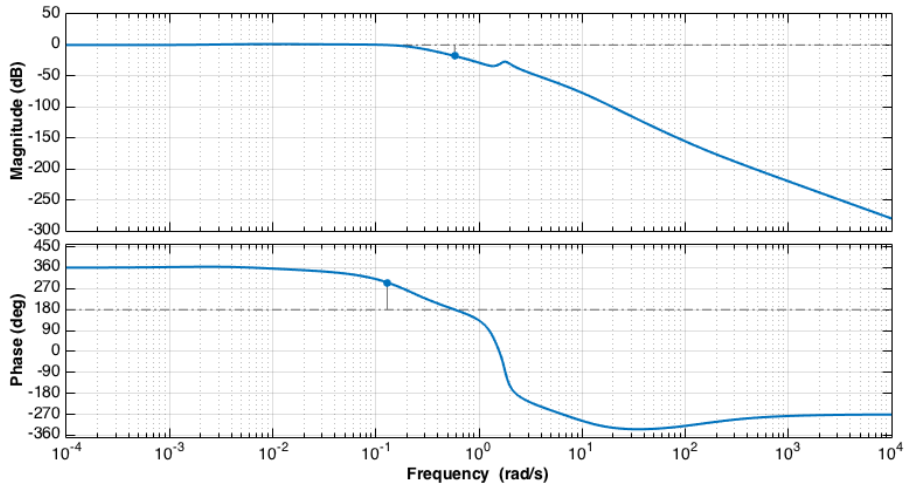

Fig. 5.20 Bode plot for the closed loop system with μ-controller.

plot as in Figure 5.21, where the gain margin is determined by the expressions below. From the Nyquist plot, $L(j\omega_p)$ is found as shown in Figure 5.22. Then the gain

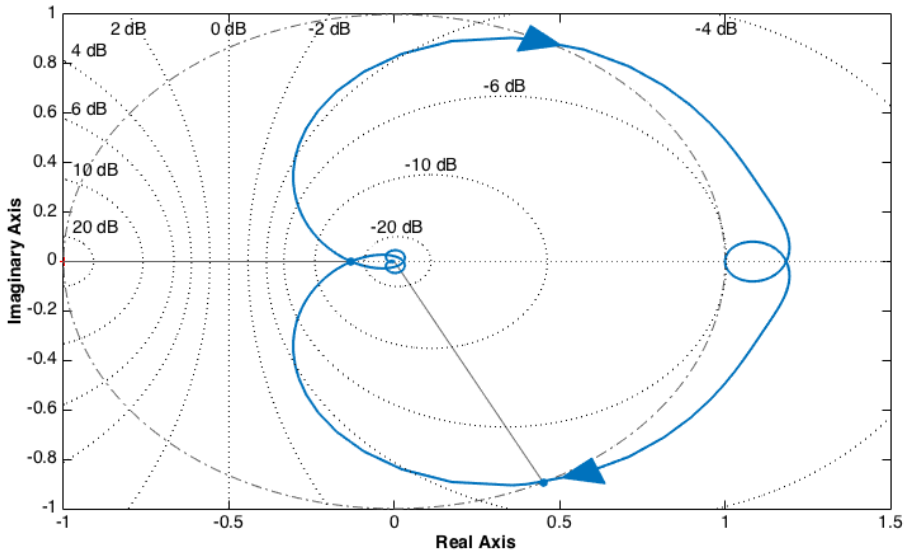

Fig. 5.21 Nyquist plot for stability.

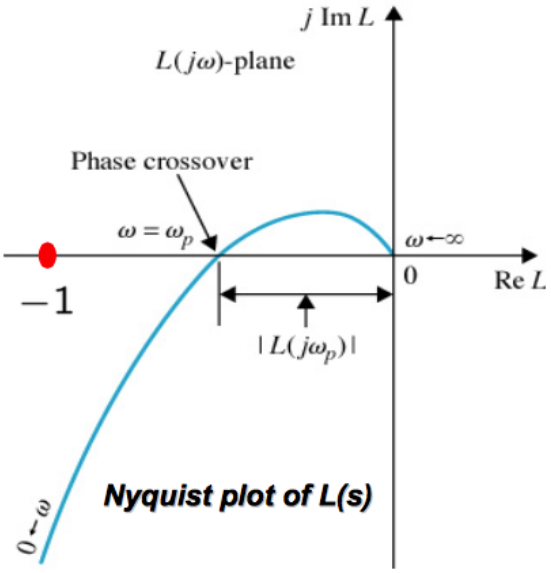

Fig. 5.22 Computing GM using Nyquist plot.

margin is:

$$GM = 20log_{10}\frac{1}{|L(j\omega_p)|}$$

$L(j\omega_p)$= 0.13, thus, GM=17.7 dB. Phase margin is angle between 0 and where the plot crosses the unity circle in the counter clockwise direction, which is equal to PM= 117 deg.

Ascending Case

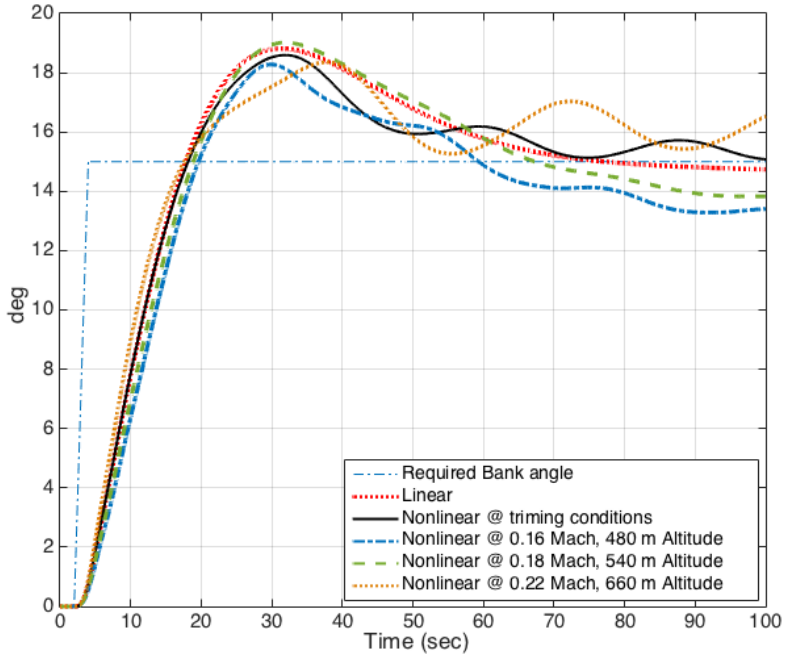

Fig. 5.23 Nonlinear simulation of bank angle ϕ under ascent operating conditions.

For the ascending scenario, the bank angle reference signal was requested, and the aircraft response was analysed accordingly. Figure 5.23 shows the testing results for

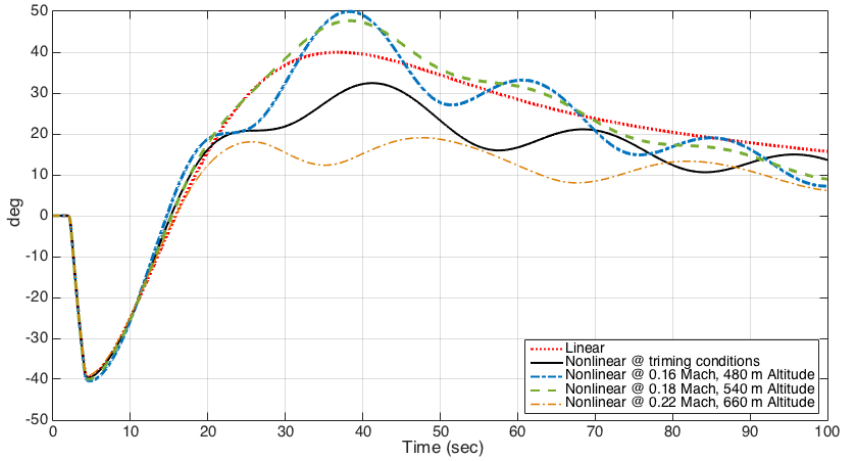

Fig. 5.24 Nonlinear simulation of aileron deflection angle ξ under ascent operating conditions.

the bank angle response at different operating points around the trimming condition. First, the slow response and overshoot were due to the 30% fault in the aileron, which limited the control power. However, the response was stable and converging, and the controller maintained stability under different ascending trimming conditions. In

Figure 5.24, the aileron deflection is analysed. At very low speeds (0.16 and 0.18 Mach), the deflection was high. This was because the moments generated by the actuators depend on the aircraft's speed squared; so at low speed, high deflection of the actuators was required. In addition, the test showed that the linear model has no actuator dynamics, resulting in a non-oscillatory deflection pattern compared to the nonlinear response.

Descending Case

Finally, the last testing case is the aircraft descent. The response of the bank angle ϕ (Figure 5.25) shows an acceptable response for the linear and nonlinear cases in terms of the overshoot, stability, and settling error. For the aileron deflections

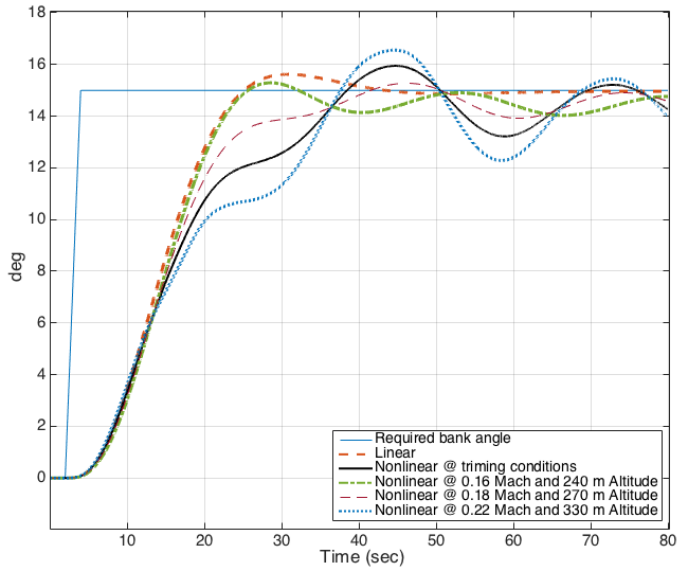

Fig. 5.25 Nonlinear simulation of bank angle ϕ under descent operating conditions.

(Figure 5.26), the maximum limit and rate of change were acceptable. Moreover, the controller asymptotically stabilised the system under different operating conditions even with a 30% actuator loss-of-efficiency fault.

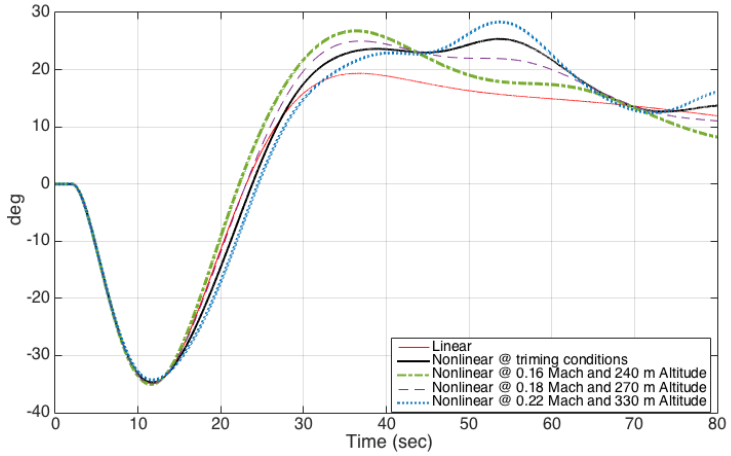

Fig. 5.26 Nonlinear simulation of aileron deflection angle ξ under descent operating conditions.

5.5 Conclusion

In this chapter, an optimal fault tolerant controller was developed for a flying vehicle where the robust features of the H_∞ and μ-synthesis techniques were utilised. The work contained modelling of actuator loss of efficiency faults as an uncertainty in the system, which can be handled inherently with these control techniques. Thus, this type of method does not rely on any fault detection schemes. Robust computation involved the minimisation of a cost function that takes into account multiple design objectives. These objectives are the tracking error minimisation, control energy minimisation, and uncertainties. The modelling of faults as an uncertainty in the system enabled the author to exploit the robustness of the controllers and test the control law for aircraft subjected to actuator faults. The weighting functions for optimisation objectives are selected and designed to shape the corresponding relevant requirements. When the linear-based optimised solutions were found, the system was tested in the nonlinear environment for more practical validation. Three design points were chosen within the flight envelope, which are the ascending, cruising, and descending operating cases. At these selected flying scenarios, the robust optimal fault-tolerant controllers were tested.

Results showed that the H_∞ baseline controller managed to give good tracking and control input performance for the multi-variable system. However, it could not withstand against actuator faults. The system's deflection performance was deteriorated by very high-frequency, rapid fluctuations, and sharp deflections as well. On the other hand, in all flying cases, when testing the μ-synthesis-based controller, the system maintained great tracking performance and smooth rate of change control deflections with 30% fault magnitudes.

Moreover, the system was tested at operating points near to the trimming points to test the region around them, which can be covered by one controller. Results showed that when the testing point is at lower speed, the robust μ-synthesis controller maintained the tracking performance, but led to higher aileron deflections. The gain and phase margins for the system were computed in the cruising case and results showed that the system has acceptable margins with the robust controller before it becomes unstable.

Further work may include further optimisation of the μ-synthesis-based controller that may lead to the increase in the fault-tolerance degree. This could be by the tuning of control or tracking weighting functions or the way the optimisation problem is solved. Another extension is the lock in place fault accommodation problem, which may need a considerably reconfigured control law.

Chapter 6

Reconfigurable Dynamic Control Allocation against Lock in Place Faults

6.1 Introduction

The primary means of control surfaces used to control the rolling, pitching, and yawing motion of the aircraft are the ailerons, elevators, and rudder, respectively. When one of the actuators incurs a loss of effectiveness fault, the adaptation or robustness of the controller could enhance the controllability and handle the situation by maintaining minimum stability requirements, as discussed in the previous chapters. Now, a more sophisticated problem, when one actuator experiences a lock in place fault, is investigated. This type of fault usually occurs due to, for instance, a structural jam that prevents the actuator from moving, or hydraulic oil leakage. etc. [110]. The lock in place faults will certainly introduce undesirable adverse moments that divert the aircraft out of its trajectory. In the passive fault-tolerant control techniques, discussed in Chapter 5, deviations of the plant parameters or the actuators from their expected position were accommodated by a fixed robust feedback controller that accounts for uncertainties up to a certain limit. However, if these deviations became excessively large and exceed the robustness properties, other actions need to be taken. Therefore, an active fault-tolerant control approach is proposed here. The problem includes the exploitation of the other available control effectors, which needs a thorough investigation to resolve this critical problem automatically. For these jam actuator effects, functional redundancy is considered. Typically, it will be assumed that the redundant hardware that powers the faulty actuator are unusable, thus, it is the role of the other healthy actuators to cope with this situation. In

flight control real applications, the redundancy is extended to cover the aerodynamic control effectors. For example, the Boeing 747 has a three-segment rudder, where the redundant control system's channels independently power each segment [11]. In this work, the utilisation of healthy effectors to handle lock in place faults is considered for automatic closed loop operation. An advanced optimal multivariable approach is exploited for this fault tolerant control problem, which is the control allocation.
In recent years, flight control design techniques that compute the moments to be produced in pitch, roll, and yaw orientations, rather than the control surface deflections, have gained increased attention. These methods generate the virtual, or generalized, control commands v(t), as shown in Fig. 6.1, that are transferred and allocated to the aircraft's control surfaces. The problem of transforming these virtual control commands is commonly known as the control allocation problem [111].

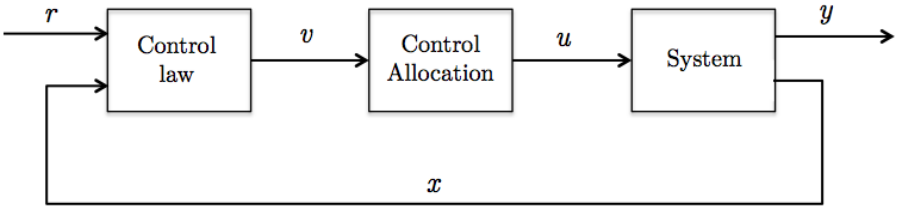

Fig. 6.1 Control allocation generic scheme

Thus, the main objective of control allocation is to compute a control input u(t) that ensures that the commanded virtual control v(t) is cooperatively produced by all effectors [112]. The control allocation (CA) approach has the following features [113], [110]:

1. It handles the redundancy of the control surfaces for certain optimized objectives, such as trajectory following and surface deflection prioritization, etc.

2. Actuator constraints, such as rate and position limits, are taken into account in the optimisation solution. When one actuator is saturated, the other control surfaces can produce the required control efforts.

3. The allocation problems, which are based on optimization techniques, are emphasized since their computational requirements are within the capabilities of current embedded computer technology.

The principles of control allocation, in general, are not restricted to motion control systems. Therefore, virtual control command $v(t)$ is not limited to representing the generalised forces or moments, but could also represent quantities such as mass and

energy [112]. In this work, a fault-tolerant constrained control allocation system is developed to cope with an aircraft's lock-in-place faulty actuators. The next section will present the techniques and formula used in the control allocation problems.

6.2 Related work

Consider a linear system represented by

$$\dot{x}(t) = Ax(t) + B_u u(t)$$

$$y = Cx(t) + Du(t)$$

Assume that B_u can be factorised as

$$B_u = B_v B$$

where the matrix $B_v \in R^{n\times k}$, $B \in R^{k\times m}$, and $k = rank(B_u)$. Thus, the system, alternatively, can be written as:

$$\dot{x} = Ax + B_v v$$

$$v = Bu$$

$$y = Cx$$

where $v \in R^n$is the total required control efforts and will be referred to as the virtual control vector [114]. The computation of the control law that leads to the required virtual control can be performed via different multivariable control techniques. Allocation is the next step of the approach. Control allocation techniques vary based on the inclusion of the actuator constraints and computational method. They are classified into two categories, unconstrained and constrained control allocation methods [115], [116], as shown in Fig. 6.2. A comparison study between the constrained and unconstrained methods is available in [117].

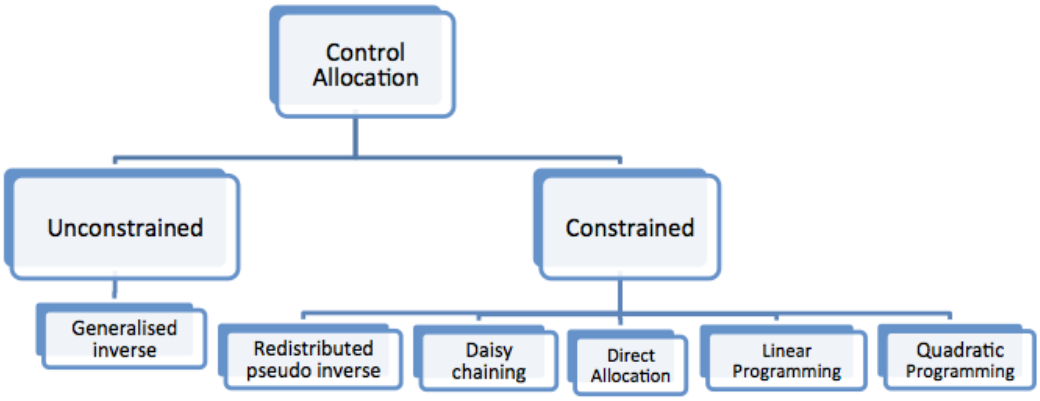

Fig. 6.2 Control allocation techniques (Based on [112])

6.2.1 Unconstrained Control methods

In the unconstrained control allocation methods, the saturation and rate constraints on the input u(t) are neglected. The challenging problem of inverting the model

$$v(t) = Bu(t) \tag{6.1}$$

is that B is not a square matrix. Normally, for a multi-effector system, B has full row rank, which result in an infinite number of control inputs u(t) that satisfy Equation 6.1 for any given v(t). In this case, the generalized inverse method is used to deal with this extra freedom, as in [118] and [119]. The unconstrained control approach is presented in the context of minimizing a least-square cost function. Assuming the saturation and rate constraints of input u are neglected, the control allocation cost function is formulated as a quadratic cost function as follows

$$\min_{u \in R^p} \frac{1}{2}(u - u_p)^T W (u - u_p) \tag{6.2}$$

subject to $v = Bu$, where $W \in R^{p \times p}$ is a positive definite weighting matrix, and u_p is the preferred value of u. Subsequently, when B has a full rank, this weighted least-square problem has the following solution [115]:

$$u = (I - CB)u_p + C\ v(t)$$

where

$$C = W^{-1}B^T(BW^{-1}B^T)^{-1}$$

is a generalised inverse derived from Equation 18 using the Lagrange multipliers, see [120].

6.2.2 Constrained Control methods

Methods based on the generalized inverse do not consider the constraints on the input u(t). When the unconstrained solution is exposed to a simple saturation process, this will not guarantee that the allocated virtual control will be equal to the required virtual command. Moreover, minimisation of the error between them is not guaranteed [115]. Hence, some constrained control allocation methods have been proposed to solve these problems.

Redistributed pseudo-inverse and Daisy Chaining

The first step of the redistributed pseudo-inverse technique is to solve the unconstrained control allocation problem (Equation 6.2). If a solution that doesn't exceed the position and rate limits is found, no further steps are needed. However, if one or more effector saturate, the problem is solved again, taking out the saturated elements in the B matrix [121]. In order to reduce the gap between the allocated and the desired generalized forces, the unsaturated elements of the control vector $u(t)$ are re-computed by solving a reduced problem using a reduced pseudo-inverse. This method includes firstly, the decomposition of the control input $u(t)$ and control matrix B into two set of elements, the saturated and the unsaturated elements. If one element is saturated, the requirements are redistributed among the unsaturated elements. The redistribution process is repeated until a feasible solution is found or no further improvement can be made. This method neither guarantees the feasible solution nor the minimization of the allocation error [112]. Examples of the redistributed pseudo-inverse CA methods are found in [122] , [123], [124].

The Daisy Chaining technique assumes a hierarchy of control effectors [125]. They are grouped into two or more groups and prioritized based on their contribution to the required command. The first allocation problem is solved for the group with the highest priority. If the first group saturates, the second is utilized and so on. In some cases, this technique may lead to a solution where some effectors are not utilized. Examples of the daisy chaining technique are found in [126], [127].

Direct allocation

This method of direct control allocation was proposed by [128]. In this approach, the moment vectors achievable within the predefined actuator constraints are generated

offline as an attainable moment set (AMS), denoted as A, and then stored in lookup tables [129]. When the desired moment is requested, the on-board computer finds the corresponding command for each actuator to follow using the lookup tables [130]. The approach starts with the unconstrained control allocation problem using the pseudo-inverse. If the control input satisfies the input constraints, then no further steps are required. Otherwise, another solution within the boundary of A that maintains the direction of $v(t)$ and meets the constraints, has to be computed as follows

$$\max_{\alpha \leq 1} \alpha$$

such that $Bu = \alpha\ v$, where $\alpha\ v\ \in A$, and $\alpha\ \in\ [0,\ 1]$.

Error minimisation using linear programming

As stated earlier, the primary objectives of a control allocation technique is to compute a control input that fulfils the control constraints and ensures that the commanded virtual control $v\ =\ h(u,\ x,\ t)$ is produced by the control surfaces. For error minimization, if a feasible u(t) cannot be found, the control allocation algorithm degrades the performance objectives and searches for a control input u(t) $\in$ U that minimizes the following allocation error [124, 131, 132]:

$$v_c - v\ =\ v_c - h(u,\ x,\ t)$$

The objectives then can be expressed as an optimisation problem, as follows

$$\min_{u \in \mathbb{R}^p, s \in \mathbb{R}^m} \|Qs\| \tag{6.3}$$

subject to $v_c - h(u, x, t) = s,\ u \in U$.

where s represent a minimization variable, $\|.\|$ is some selected norm, and Q is a weighting matrix. With the linear effector relations, the problem in Eq. 6.3 will be subjected to $v_c - B\,(x,t)\,u = s,\ u \in U$

The solution to Equation 6.3 is not unique, which gives more opportunity to introduce another cost function that reflects on actuator constraints or any other criteria [115]. Hence, the optimization framework becomes

$$\min_{u \in \mathbb{R}^p, s \in \mathbb{R}^m} (\|Qs\| + J(x, u, t))$$

subject to $v_c - h(u, x, t) = s, \qquad u \in U$.

With the cost function defined using the 1-norm, the resulting problem becomes a linear programming one (LP), with the form

$$\min_{u,s} \left(\sum_{i=1}^{m} q_i \left| s_i \right| + \sum_{j=1}^{p} w_j \left| u_j \right| \right)$$

subject to $Bu = v_c + s, \qquad u_{min} \leq u \leq u_{max}.$

The simplex, active set, and interior point methods are the most common numerical methods for linear programming [133].

Sequential Quadratic programming for error minimisation

The control allocation problem, with the 2-norm formulation, yield a quadratic problem that can be solved using numerical quadratic programming methods [116], such that

$$\min_{u,s} \left(\sum_{i=1}^{m} q_i s_i^2 + \sum_{j=1}^{p} w_j u^2 \right) \tag{6.4}$$

subject to $Bu = v_c + s, \qquad u_{min} \leq u \leq u_{max}.$

The technique to solve this problem is to find a solution vector that minimizes the quadratic problem subject to particular constraints. An approach proposed by [111] involves a two-step minimization problem. First, find a set of all feasible solutions of u(t) that minimize the virtual control error, and call it Ω. Then, the second problem includes the selection of the minimum solution resulting from the first step that fulfils the control input constraints and steady state control distribution. The two-step optimisation is as follows:

$$\Omega = \underset{u_{min} \leq u \leq u_{max}}{arg\ min} \left\| W_v (B\ u - v) \right\|_2$$

$$u = \underset{u \in \Omega}{arg\ min} \left\| W_u (u - u_d) \right\|_2$$

The first includes minimizing the virtual control error weighted by W_v. This will allow prioritisation of certain elements of v. The second problem includes the selection of the minimum solution resulting from the first step. Therefore, the problem is summarized as follows; from Ω,the set of feasible control inputs that minimize the virtual control error $Bu - v$, pick the control input u that minimizes the cost function $(u - u_d)$ weighted by W_u, where u_d is the desired control input. The weighting matrices W_u and W_v are square diagonal matrices of proper dimensions.

Contribution highlights

In this chapter, the contribution is summarised in the following points:

- Different from the methods of Fault Tolerant Control Allocation techniques such as those described in [134–138], this approach incorporates a new control redistribution process, which is updated by the occurrence of a fault. This approach relies on and assumes an effective on-board FDD system to provide precise fault information of the control surfaces.
- Further, it uses fuzzy logic to implement the correlation between fault and control redistribution. Existing works assume certain faults in the model and produce the FTC lookup tables accordingly, i.e. [130] (Naskar et al., 2015). Here, the implementation of fuzzy logic can handle a wide range of fault magnitudes online by interpolation.
- Moreover, unlike the works of FT control allocation techniques described in [117, 136, 139, 140], [138, 141], that only consider loss of efficiency faults; this method deals with the more severe lock in place fault. It handles the faulty situation and enhances the flying quality with multi-effector controls.

6.3 Dynamic Control Allocation using the Quadratic Programming approach

Several existing control allocation methods, such as daisy chaining, direct control allocation, and methods based on constrained linear or quadratic programming, have been investigated, see [112] for a survey. These methods are static in the sense that the control surface deflection commands, computed at any time t, only depend on the virtual control commands

$$u = f(v)$$

To allow different actuators to produce control efforts at different frequency ranges, a dynamic mapping of the following form is needed [111]:

$$u(t) = f(v(t), u(t-T), v(t-T), u(t-2T), v(t-2T), ..)$$

where T is the sampling period. The formula requires the mapping of the previous values of v and u, to capture the saturation in the actuators and penalize the actuator rates as proposed by [142]. Now, consider a linear dynamical model of an aircraft given by:

$$\dot{x} = f(x, u)$$

subject to the following position and rate constraints:

$$u_{min} \leq u \leq u_{max},\ |\dot{u}| \leq u_{rate} \tag{6.5}$$

In modern aircraft, where digital control systems are implemented, the rate constraint in Equation 6.5 can be transformed into position limits [143]. Accordingly, the actuator rate and position limits can be written as

$$\underline{u}(t) \leq u \leq \overline{u}(t) \tag{6.6}$$

where,

$$\overline{u}(t) = max[u_{min},\ u(t-T) - u_{rate}T]$$

$$\underline{u}(t) = min[u_{max},\ u(t-T) + u_{rate}T]$$

The dynamic control allocation task can be posed as a sequential quadratic programming problem using the Euclidean 2-norm [111]:

$$\Omega = \underset{u_{min} \leq u \leq u_{max}}{arg\ min} \|W_v(B\ u(t) - v(t))\| \tag{6.7}$$

$$u = \underset{u \in \Omega}{arg\,\min} \left(\|W_1(u(t) - u_s(t))\|^2 + \|W_2(u(t) - u(t-T))\|^2 \right)$$

where $B \in R^{k \times m}$ is the control effectiveness matrix, u(t) $\in R^m$ is the commanded control input, $v \in R^k$ is the virtual control, $u_s \in R^m$ is the desired steady state control input, and W_v, W_1, and W_2 are square diagonal weighting matrices of proper dimensions. The optimization problem works as follows; pick from the feasible set of control input Ω that minimize the virtual control error, a control input u(t) that fulfils the control input constraints. When Ω is calculated, the optimization for u(t) is made by keeping u as close as possible to the steady state value (u_s), and minimizing the change between the control input u(t) and the previous sampling instant $u(t-T)$. The steady state control input is calculated by $u_s(t) = Sv(t)$ where $BS = I$, and S is the control distribution matrix. In order to design a closed loop system that fulfils the tracking requirements and control deflection constraints, the problem is then split into two main tasks. Firstly, the virtual control command is represented in terms of the total moments generated by the actuators, subtracting

the effects of the general states, as follows: The roll, pitch, and yaw moments (L, M, N) are represented by their coefficients, which are functions of the deflections and the states as follows:

$$C_m = C_{m0} + C_m^{\alpha} \cdot \alpha + C_m^{\delta_f} \cdot \delta_f + C_m^{\delta_e} \cdot \delta_e + \frac{c}{2V_a}(C_m^{\dot{\alpha}} \cdot \dot{\alpha} + C_m^{q} \cdot q) + C_m^{M} \cdot M \tag{6.8}$$

$$C_l = C_l^{\beta} \cdot \beta + C_l^{\delta_a} \cdot \delta_a + C_l^{\delta_r} \cdot \delta_r + \frac{b}{2V_a}(C_l^{p} \cdot p + C_l^{r} \cdot r) \tag{6.9}$$

$$C_n = C_n^{\beta} \cdot \beta + C_n^{\delta_a} \cdot \delta_a + C_n^{\delta_r} \cdot \delta_r + \frac{b}{2V_a}(C_n^{p} \cdot p + C_n^{r} \cdot r) \tag{6.10}$$

Assuming $C_m^{\dot{\alpha}} = C_{m0} = C_m^{\delta_f} = 0$, then, the coefficients in Eq. 6.8-6.10 are equivalently written as:

$$\begin{bmatrix} C_l \\ C_m \\ C_n \end{bmatrix} = \begin{bmatrix} C_l^{\delta_{A-ir}} & C_l^{\delta_{A-il}} & C_l^{\delta_{A-or}} & C_l^{\delta_{A-ol}} & C_l^{\delta_r} \\ C_m^{\delta_{A-ir}} & C_m^{\delta_{A-il}} & C_m^{\delta_{A-or}} & C_m^{\delta_{A-ol}} & C_m^{\delta_r} \\ C_n^{\delta_{A-ir}} & C_n^{\delta_{A-il}} & C_n^{\delta_{A-or}} & C_n^{\delta_{A-ol}} & C_n^{\delta_r} \end{bmatrix} \begin{bmatrix} \delta_{A-ir} \\ \delta_{A-il} \\ \delta_{A-or} \\ \delta_{A-ol} \\ \delta_r \end{bmatrix} + \begin{bmatrix} C_l^{\alpha} & C_l^{\beta} & \frac{b}{2V_a}C_l^{p} & C_l^{q} & \frac{b}{2V_a}C_l^{r} & C_l^{M} \\ C_m^{\alpha} & C_m^{\beta} & C_m^{p} & \frac{b}{2V_a}C_m^{q} & C_m^{r} & C_m^{M} \\ C_n^{\alpha} & C_n^{\beta} & \frac{b}{2V_a}C_n^{p} & C_n^{q} & \frac{b}{2V_a}C_n^{r} & C_n^{M} \end{bmatrix} \begin{bmatrix} \alpha \\ \beta \\ p \\ q \\ r \\ M \end{bmatrix} \tag{6.11}$$

Thus, the virtual control will be

$$v\,(t) = C_{\delta} \times \delta - C_x x \tag{6.12}$$

where C_{δ} are the of variation of moment coefficients with respect to the deflections, and δ are the actuator deflections computed by $\delta = e(r, y) \times K$, where e is the reference error and K is a control law computed using any multivariable design approach.

Secondly, distribute the virtual control command over the available effectors, which is known as the control allocation task. In this problem, the control command u(t), that is feasible with the constraints of the actuator and satisfies $v(t) = Bu(t)$,

is determined at each sampling time. The S matrix is the control distribution matrix with parameters that relate to the effects of each control surface on the corresponding rotational motion. It also prioritizes the roles of the control surfaces.

$$
\mathbf{S}=\begin{bmatrix}
(S_{\xi_{ir}})_{roll} & (S_{\xi_{ir}})_{pitch} & (S_{\xi_{ir}})_{yaw} \\
(S_{\xi_{il}})_{roll} & (S_{\xi_{il}})_{pitch} & (S_{\xi_{il}})_{yaw} \\
(S_{\xi_{or}})_{roll} & (S_{\xi_{or}})_{pitch} & (S_{\xi_{or}})_{yaw} \\
(S_{\xi_{ol}})_{roll} & (S_{\xi_{ol}})_{pitch} & (S_{\xi_{ol}})_{yaw} \\
(S_{\zeta})_{roll} & (S_{\zeta})_{pitch} & (S_{\zeta})_{yaw}
\end{bmatrix}
\begin{matrix}
\leftarrow \text{Inner right aileron} \\
\leftarrow \text{Inner left aileron} \\
\leftarrow \text{Outer right aileron} \\
\leftarrow \text{Outer left aileron} \\
\leftarrow \text{Rudder}
\end{matrix}
$$

In order to solve the sequential least square problem in Equation 6.7, it is reformulated into another form where the two cost functions are merged together, making the weighted least square problem as follows:

$$\arg \min_{\underline{u} \leq u \leq \bar{u}} \|W_u(u - u_p)\|^2 + \gamma \|W_v(Bu - v)\|^2 \tag{6.13}$$

to emphasise the minimisation of $Bu - v$, then the weighting factor γ has a large value in the computation. Now, rearranging Equation 6.13,

$$\|W_u(u - u_p)\|^2 + \gamma \|W_v(Bu - v)\|^2 = \left\| \underbrace{\begin{pmatrix} \gamma W_v B \\ W_u \end{pmatrix}}_{A} u - \underbrace{\begin{pmatrix} \gamma W_v v \\ W_u u_p \end{pmatrix}}_{b} \right\|^2 \tag{6.14}$$

and solve for

$$\arg \min_{u} \|Au - b\| \tag{6.15}$$

subject to $\underline{u} \leq u \leq \bar{u}$.
To solve Equation 6.15, consider

$$\min_{u} \|Au - b\| \tag{6.16}$$

$$Bu = v \tag{6.17}$$

$$Cu \geq U \tag{6.18}$$

where Equation 6.18 is equal to $\underline{u}(t) \leq u \leq \overline{u}(t)$ when $C = \begin{bmatrix} I \\ -I \end{bmatrix}$ and $U = \begin{bmatrix} \underline{u} \\ \overline{u} \end{bmatrix}$.

Given u^k for the number of iterations k, find p (the optimal perturbation) such that:

$$\min_p \left\| A(u^k + p) - b \right\|$$

if $u^k + p$ is a feasible solution, set $u^{k+1} = u^k + p$ and compute $\begin{bmatrix} \mu \\ \lambda \end{bmatrix}$ for which μ is associated with $Bu - v$and λ is associated with Equation 6.18. Otherwise, remove the constraints for negative λ.

The Lagrange multipliers $\begin{bmatrix} \mu \\ \lambda \end{bmatrix}$ are computed from:

$$A^T(Au - b) = \begin{bmatrix} B^T \\ C_0^T \end{bmatrix} \begin{bmatrix} \mu \\ \lambda \end{bmatrix}$$

where C_0 is the row of C corresponding to the constraints. This method of solving the weighted least square problem is referred to as the active set algorithm (see [144]).

Dynamic control allocation without saturation: a special case

Under the assumption that the actuators do not reach saturation, the actuator position constraints can be ignored and the optimisation problem is reduced to

$$\underset{u(t)}{min} \left(\| W_1(u\,(t) - u_s(t)) \|^{\,2} + \| W_2(u\,(t) - u(t-T)) \|^{\,2} \right) \tag{6.19}$$

$$\text{Subject to } B\ u\,(t) = v(t).$$

The solution of this optimisation problem is computed with the following conditions. First, the matrices W_1 and W_2 are symmetric matrices, i.e. each matrix is equal to its transpose. Second, W is non-singular and represented by

$$W = \sqrt{W_1^2 + W_2^2}$$

When these assumptions hold, the control allocation problem in Equation 6.19 has the solution

$$u\,(t) = Eu_s\,(t) + Fu\,(t-T) + Gv(t) \tag{6.20}$$

Where,

$$E = (I - GB)W^{-2}W_1^2$$

$$F = (I - GB)W^{-2}W_2^2$$

$$G = W^{-1}(BW^{-1})^{\dagger}$$

The symbol † denotes the pseudo-inverse of the function which is defined as $B^{\dagger} = B^T(BB^T)^{-1}$ for a $(k \times m)$ matrix B with a full row rank. Proof of this formula is shown in [111] and [142]. This illustrates that the optimal solution for control input $u(t)$ to the unconstrained control allocation problem, is given by the linear filer (Equation 6.20).

6.4 Flight Control Allocation System for multi-aileron aircraft

An optimal control allocation is developed using a twin-engine, multi-effector Boeing 747 aircraft lateral dynamical model. The aircraft has two ailerons per wing (inboard and outboard) and a rudder as control surfaces, as shown in Figure 6.3.

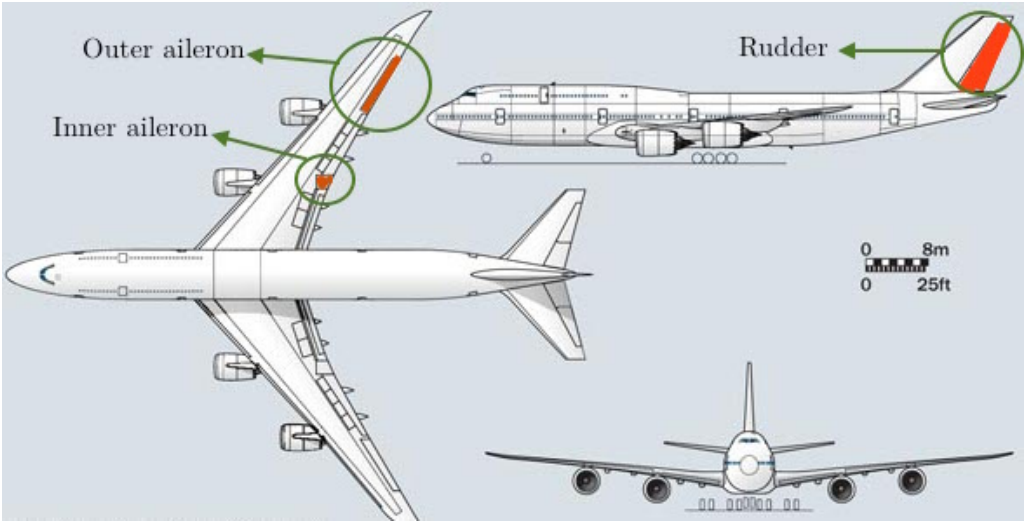

Fig. 6.3 Boeing 747 lateral control configuration

The twofold aileron control surfaces may introduce an additional workload in the control redundancy management; however, this will give an extra freedom to control the rolling motion of the aircraft, particularly in faulty situations.

6.4.1 Aircraft Dynamic Model

At trimmed conditions of 0.8 Mach and 2500 m altitude, the linearised aircraft dynamics [145] is given by:

$$\dot{x}(t) = Ax(t) + Bu(t)$$

$$y(t) = Cx(t) + Du(t)$$

where

$$A = \begin{bmatrix} -1.06 & 0.172 & -1.65 & 0.0004 \\ -0.12 & -0.21 & 0.28 & -0.002 \\ 0.1014 & -0.989 & -0.1 & 0.106 \\ 1 & 0.09 & 0 & 0 \end{bmatrix}$$

$$B = \begin{bmatrix} -0.083 & 0.083 & -0.2285 & 0.2285 & 0.1187 \\ -0.0154 & 0.0154 & -0.0123 & 0.0123 & -0.2478 \\ 0 & 0 & 0 & 0 & 0.0174 \\ 0 & 0 & 0 & 0 & 0 \end{bmatrix}$$

$$C = \begin{bmatrix} 0 & 0 & 1 & 0 \\ 0 & 0 & 0 & 1 \end{bmatrix}$$

and D is a (2×5) zero matrix. The states $x = [p\ r\ \beta\ \phi]^T$ are the roll rate (rad/s), the yaw rate (rad/s), the sideslip angle (rad), and the roll angle (rad). The control input $u = [\xi_{ir}\ \xi_{il}\ \xi_{or}\ \xi_{ol}\ \zeta]^T$ consists of the inboard right and left ailerons, outboard right and left ailerons, and the rudder, respectively. Measured outputs y(t) represent the sideslip angle β and the roll angle ϕ.

The aircraft's main effectors for lateral dynamics are shown in Fig. 6.3. The maximum deflection for the actuators is ±30 degree, and the maximum rate of change is ±50 degree per second. A positive aileron deflection is defined when the right aileron is up and the left aileron is down. A positive rudder deflection is defined with the trailing edge to the right, as viewed from above.

Table 6.1 Control surfaces deflections and primary effects

Control surface	Deflection	Sign	Primary effects
Inboard right aileron	Trailing edge up	+	Positive roll moment
Outboard right aileron	Trailing edge up	+	Positive roll moment
Rudder	Trailing edge right	+	Positive yaw moment

The flight control law

The control law, that yields the virtual control command v(t) based on Equation 23, is designed first in the control allocation problem. An H_∞ controller is developed to utilize the optimizing features of minimising the tracking error and total control energy. For a closed loop system, the control law problem is represented by finding an optimal stabilizing solution that minimises the following cost function:

$$\left\| \begin{array}{c} W_e(I+GK)^{-1} \\ W_uK(I+GK)^{-1} \end{array} \right\|_\infty \tag{6.21}$$

for the feedback control law shown in Fig. 6.4.

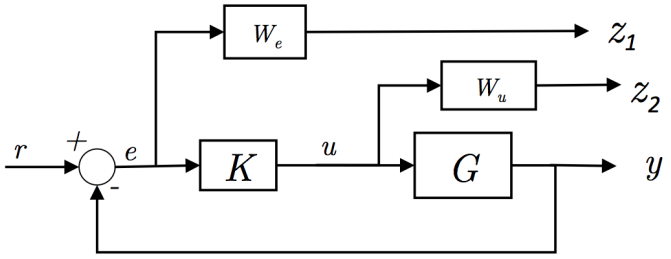

Fig. 6.4 Closed loop system with the weight minimisation functions.

The weighting functions W_e and W_u are used to shape the output $[z_1 \;\; z_2]^T$, for the tracking error and control input minimisation. This would lead to the generic structure of the H_∞ control system as shown in Fig. 6.5, where w represents the external exogenous input, i.e. the reference input, noise, etc. In this work, w denotes the reference-required command.

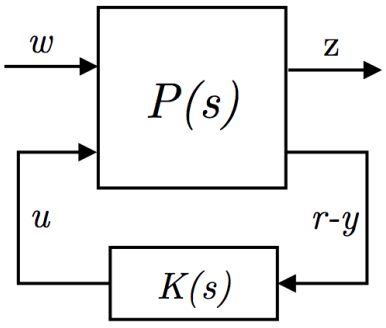

Fig. 6.5 General layout of the system for H infinity computation.

The system has the following interconnected matrix (P), partitioned as follows:

$$P(s) = \left[\begin{array}{cc} P_{11}(s) & P_{12}(s) \\ P_{21}(s) & P_{22}(s) \end{array} \right]$$

From the lower linear fractional transformation (LFT) technique, the output would be

$$z = [P_{11} + P_{12}K(I - P_{22}K)^{-1}P_{21}]w \tag{6.22}$$

Where,

$$\begin{bmatrix} z_1 \\ z_2 \\ r - y \end{bmatrix} = \begin{bmatrix} W_e & -W_eG \\ 0 & W_u \\ I & -G \end{bmatrix} \begin{bmatrix} w \\ u \end{bmatrix} \tag{6.23}$$

To minimise the tracking error of the sideslip and rolling angles $[\beta\ \phi]^T$, the weighting function W_e is a diagonal matrix with two low-pass filters that minimises the two reference inputs. The filter will allow signals with frequencies less than the cross over frequency to pass, but attenuate signals with frequencies higher than the cross over frequency. Basic features are listed in Table 6.2.

Table 6.2 Bode diagram specifications for W_e weighting functions

W_e	Magnitude at low frequency (dB)	Cross over frequency (rad/s)	Magnitude at high frequency (dB)
For β	13.98	0.08	-60
For ϕ	28.46	0.42	-45.5

The weighting function W_e for the rolling angle ϕ is higher in magnitude than the one for bank angle β, to give it more significance in the optimisation problem as shown in the Bode plot Fig. 6.6.

The second weighting function in the H_∞ control law design is W_u. This function is used to shape the controlling efforts of the actuators. Three main sets of controls, namely the inboard ailerons, outboard ailerons, and the rudder, are available. The rolling primary effectors are the outer ailerons. Weights given to each effector are correlated to its primary task. The Bode plot, in Fig. 6.7, shows the weighting function W_u, for the control inputs.

A Matlab algorithm is used to compute the stabilising solution that minimises the cost function in Equation 6.21. Results of the tuning and computations yields the optimal stabilising solution with γ=0.998, and H_∞ control gain in the state space from as shown in Appendix.

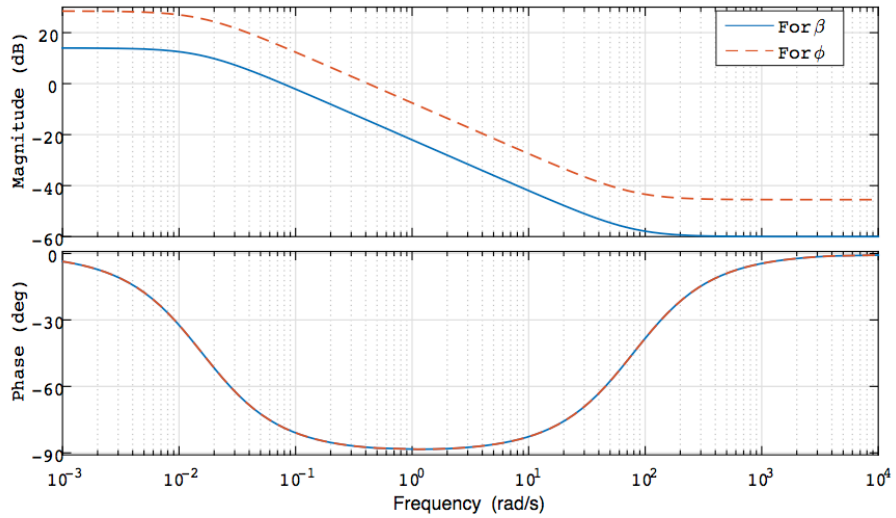

Fig. 6.6 W_e weighting functions for phi and beta.

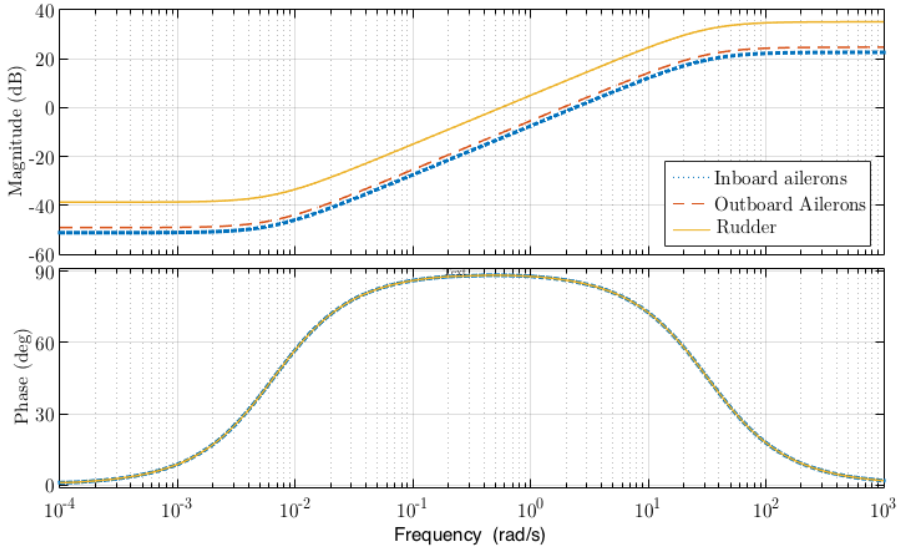

Fig. 6.7 W_u functions for aircraft's control surfaces.

6.4.2 The virtual control command

For the aircraft with 30 ft span, 6.5 ft chord, and flying at a speed of 445 ft/s, the virtual control command is computed using Equation 6.12. Aerodynamic stability and control derivatives are as follows [55]:

C_l^{β}	-0.193
C_l^{p}	-0.3
C_l^{r}	0.2
C_m^{α}	-1.15
C_m^{q}	-20
C_m^{M}	0.12
C_n^{β}	0.147
C_n^{p}	-0.06
C_n^{r}	-0.2

$C_l^{\delta_{A-ir}}$	-0.013
$C_l^{\delta_{A-il}}$	0.013
$C_l^{\delta_{A-or}}$	-0.017
$C_l^{\delta_{A-ol}}$	0.017
$C_l^{\delta_R}$	0.004
$C_m^{\delta_{A-ir}}$	0
$C_m^{\delta_{A-il}}$	0
$C_m^{\delta_{A-or}}$	0
$C_m^{\delta_{A-ol}}$	0
$C_m^{\delta_R}$	0
$C_n^{\delta_{A-ir}}$	-0.0015
$C_n^{\delta_{A-il}}$	0.0015
$C_n^{\delta_{A-or}}$	-0.0012
$C_n^{\delta_{A-ol}}$	0.0012
$C_n^{\delta_R}$	-0.108

Thus, using these parameters, the matrices in the system are as follows:

$$C_\delta = \begin{bmatrix} -0.013 & 0.013 & -0.017 & 0.017 & 0.004 \\ 0 & 0 & 0 & 0 & 0 \\ -0.0015 & 0.0015 & -0.0012 & 0.0012 & -0.108 \end{bmatrix}$$

$$C_x = \begin{bmatrix} 0 & -0.193 & -0.0101 & 0 & 0.0067 & 0 \\ -1.15 & 0 & 0 & -0.1461 & 0 & 0.12 \\ 0 & 0.147 & -0.002 & 0 & -0.0067 & 0 \end{bmatrix}$$

, and

$$x(t) = \begin{bmatrix} \alpha \\ \beta \\ p \\ q \\ r \\ M \end{bmatrix}$$

Detailed aerodynamic characteristics for the B747 are available in [146, 147]. The virtual control command, as illustrated in Fig. 6.8, is therefore computed.

The resulting computed virtual control command v(t) is composed of three vectors that represents the total required control efforts along roll, pitch, and yaw axes.

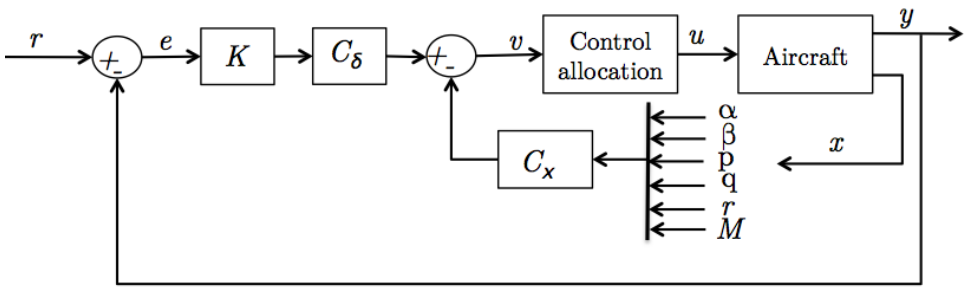

Fig. 6.8 Illustration of the computation of the virtual control command.

6.4.3 Control Allocation

Once the virtual control command v(t) is computed, it is now a task of allocating the total control efforts on the available aircraft control surfaces. At trimmed flying conditions, the desired steady state control distribution matrix that resembles the relationships between total required rolling, pitching, and yawing efforts and the corresponding control surfaces is chosen to be:

$$S = \begin{bmatrix} -5.0 & -0.05 & -0.12 \\ 5.0 & -0.05 & 0.12 \\ -10 & -0.02 & -1.0 \\ 10 & -0.02 & 1.0 \\ 0.02 & 0 & -8.0 \end{bmatrix}$$

Where the weights are $W_1 = \text{diag}\ ([2\ 2\ 2\ 2\ 2])$ and $W_2 = \ \text{diag}([8\ 8\ 10\ 10\ 10])$.

Control Allocation without saturation

The results of the computation of the control allocation filter using Matlab for the unsaturated formula yields sets of transfer functions that relate the inputs (v) to the outputs u. Hence, the transfer function of input v_{roll} to inner right aileron, neglecting the very small terms (i.e. $< 1x10^{-7}$), is:

$$\frac{\xi_{ir}}{v_{roll}} = \frac{-18.03\ s^5 + 51.7\ s^4 - 49.4\ s^3 + 15.8\ s^2}{s^5 - 2.9\ s^4 + 2.7\ s^3 - 0.86\ s^2}$$

The transfer function of input v_{roll} to inner left aileron is:

$$\frac{\xi_{il}}{v_{roll}} = \frac{18.03\ s^5 - 51.7\ s^4 + 49.4\ s^3 - 15.8\ s^2}{s^5 - 2.9\ s^4 + 2.7\ s^3 - 0.86\ s^2}$$

transfer function of input v_{roll} to outer right aileron is:

$$\frac{\xi_{or}}{v_{roll}} = \frac{-15.5\ s^5 + 44.1\ s^4 - 41.7\ s^3 + 13.17\ s^2}{s^5 - 2.9\ s^4 + 2.7\ s^3 - 0.86\ s^2}$$

transfer function of input v_{roll} to outer left aileron is:

$$\frac{\xi_{ol}}{v_{roll}} = \frac{15.5\ s^5 - 44.1\ s^4 + 41.7\ s^3 - 13.17\ s^2}{s^5 - 2.9\ s^4 + 2.7\ s^3 - 0.86\ s^2}$$

transfer function of input v_{roll} to rudder is:

$$\frac{\zeta}{v_{roll}} = \frac{0.85\ s^5 - 2.4\ s^4 + 2.3\ s^3 - 0.73\ s^2}{s^5 - 2.9\ s^4 + 2.7\ s^3 - 0.86\ s^2}$$

transfer function of input 2 (v_{pitch}) to inboard right and left ailerons:

$$\frac{\xi_i}{v_{pitch}} = \frac{-0.003\ s^5 - 0.006\ s^4 - 0.003\ s^3}{s^5 - 2.9\ s^4 + 2.7\ s^3 - 0.86\ s^2}$$

transfer function of v_{pitch} to outboard right and left ailerons:

$$\frac{\xi_o}{v_{pitch}} = \frac{-0.0008\ s^5 - 0.0015\ s^4 - 0.0007\ s^3}{s^5 - 2.9\ s^4 + 2.7\ s^3 - 0.86\ s^2}$$

transfer function of input v_{pitch} to rudder:

$$\frac{\zeta}{v_{pitch}} = \frac{-7x10^{-22}\ s^2 - 7x10^{-22}\ s}{s^5 - 2.9\ s^4 + 2.7\ s^3 - 0.86\ s^2} = 0$$

transfer functions of input 3 (v_{yaw}) to inboard right aileron

$$\frac{\xi_{ir}}{v_{yaw}} = \frac{-0.69\ s^5 + 2\ s^4 - 1.9\ s^3 + 0.62\ s^2}{s^5 - 2.9\ s^4 + 2.7\ s^3 - 0.86\ s^2}$$

transfer function of input v_{yaw} to inboard left aileron

$$\frac{\xi_{il}}{v_{yaw}} = \frac{0.69\ s^5 - 2\ s^4 + 1.9\ s^3 - 0.62\ s^2}{s^5 - 2.9\ s^4 + 2.7\ s^3 - 0.86\ s^2}$$

transfer function of input v_{yaw} to outboard right aileron

$$\frac{\xi_{or}}{v_{yaw}} = \frac{-0.56\ s^5 + 1.6\ s^4 - 1.5\ s^3 + 0.46\ s^2}{s^5 - 2.9\ s^4 + 2.7\ s^3 - 0.86\ s^2}$$

transfer function of input v_{yaw} to outboard left aileron

$$\frac{\xi_{ol}}{v_{yaw}} = \frac{0.56\ s^5 - 1.6\ s^4 + 1.5\ s^3 - 0.46\ s^2}{s^5 - 2.9\ s^4 + 2.7\ s^3 - 0.86\ s^2}$$

transfer function of input v_{yaw} to rudder

$$\frac{\zeta}{v_{yaw}} = \frac{-9.23\ s^5 + 26.3\ s^4 - 25.04\ s^3 + 7.94\ s^2}{s^5 - 2.9\ s^4 + 2.7\ s^3 - 0.86\ s^2}$$

For each actuator, the related transfer functions were added together giving the total required deflections sent to the control surface. Figure 6.9 shows the transfer functions between components of the virtual control command and each actuator. To test the control laws, the following were assumed:

$$\phi = \begin{cases} 30 & 3 \leq t \leq 30 \\ 0 & \text{otherwise} \end{cases}$$

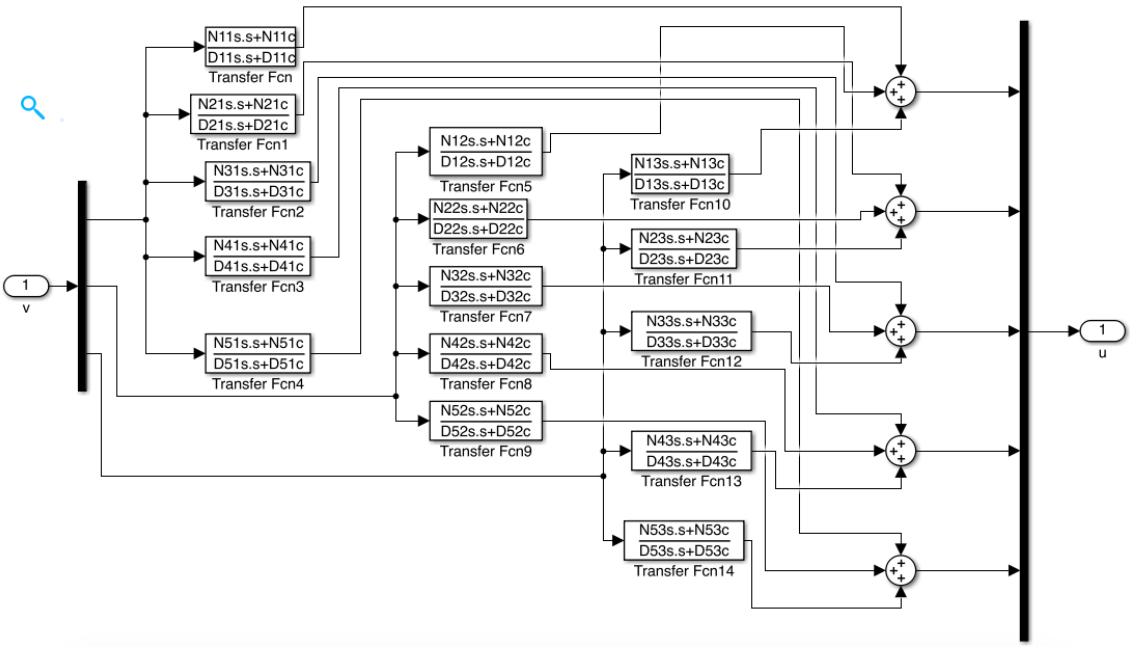

Fig. 6.9 Summation of transfer functions for each effector.

The result of using a no-saturation DCA are analysed in terms of the control deflections and the response of the aircraft, as shown in Fig. 6.10 and Fig. 6.11. Outer ailerons have identical deflections with different signs. Similarly for the inner ailerons. The rate of change of deflection was acceptable, but the outer ailerons exceeded the maximum deflection limit (±30 deg), as expected, due to the non-constraint computations.

For aircraft response, although the rise time was satisfactory, there was a 16% steady state error for the requested rolling angle, even with high actuator deflections.

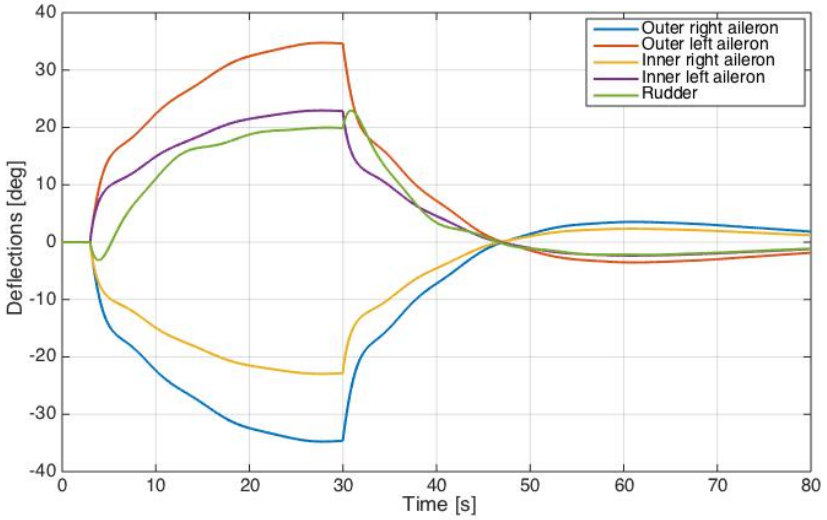

Fig. 6.10 Control surfaces' deflections using non-saturated DCA.

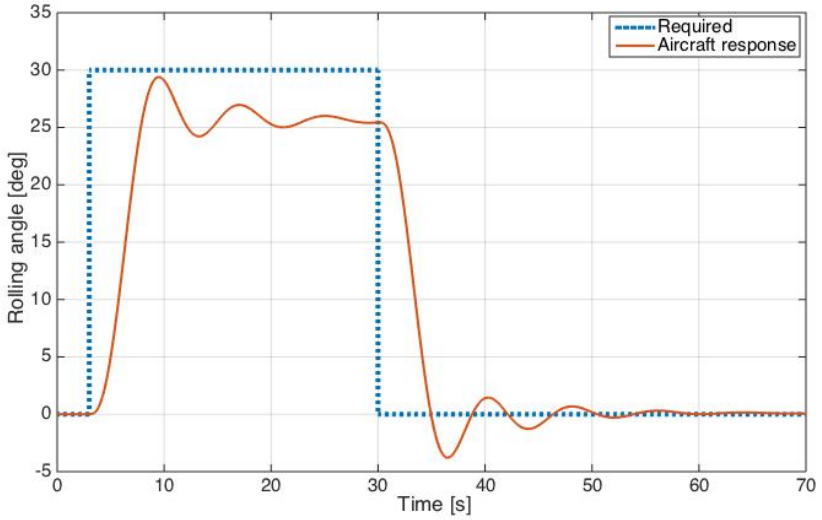

Fig. 6.11 Aircraft response using non-constrained DCA.

Constrained Dynamic Control Allocation

In this computation method, the control input u(t) is calculated based on the virtual control command optimisation function, using the weighted least-squares solver [144]. Thus, in order to give more emphasis on the virtual control command part that generates the rolling motion, the weights corresponding to the pitch and yaw motion are kept small, $Wv = \text{diag}([10\ 1\ 1])$. Results of using constrained DCA technique are shown in Fig. 6.12 for controls deflections and Fig. 6.13 for aircraft response. The deflection plot shows a higher rate of change (reaching 20 deg/s) in the controls compared to the unsaturated computation, yielded in faster aircraft

response. Moreover, the deflections were constrained by the maximum deflection position. It is shown that when one actuator saturates, the other actuators margin of deflection is exploited.

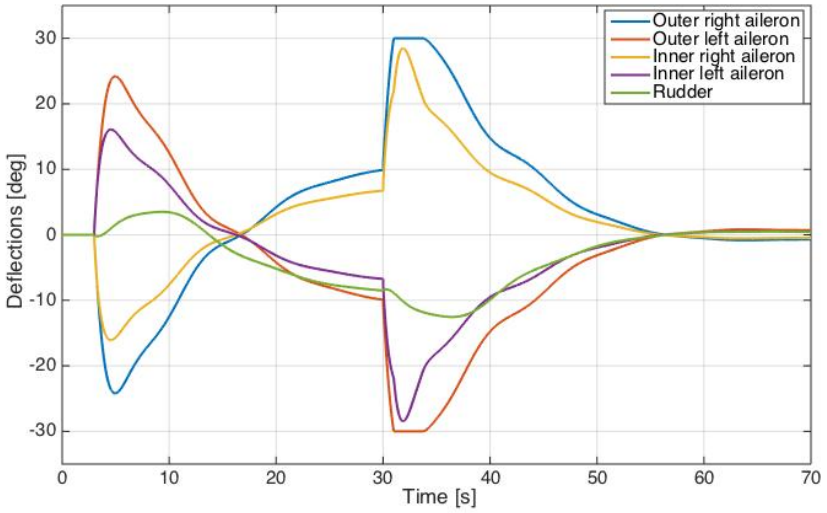

Fig. 6.12 Control surface deflections using constrained DCA.

The aircraft response is fast (rise time is 2.8 second) and well damped, resulting in a relatively small steady state error (<3%).

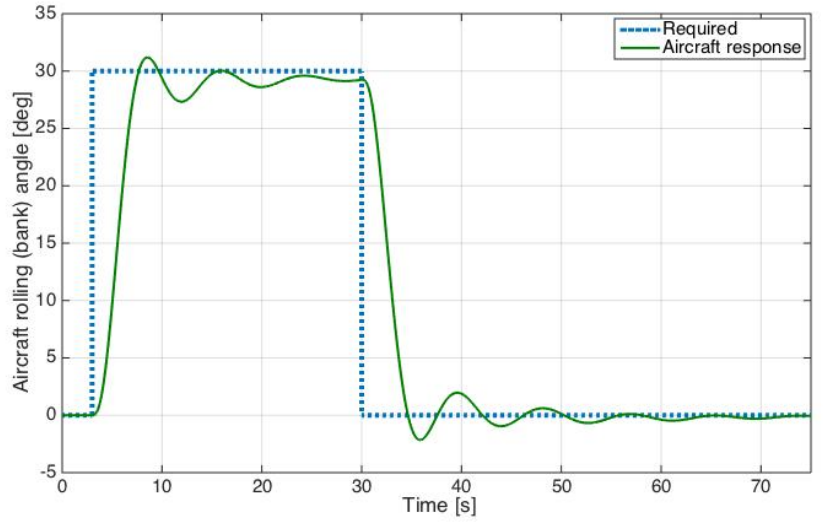

Fig. 6.13 Aircraft response using dynamic control allocation.

The constrained dynamic control allocation has the following merits over the non-saturation case. First, it has very small steady state tracking error in the aircraft response. Moreover, it takes position limits into account and utilises the optimised computation for rate limits, which produces a quicker and more accurate response.

Taking these limits into account in the design process is advisable because they will comply with actuator dynamics in real-life applications. In the next section, a fault-tolerant control allocation scheme will be developed based on the constrained control allocation approach.

6.5 Reconfigurable Fault-tolerant Control Allocation (FTCA) System

As shown in the previous section, the constrained dynamic control allocation technique led to a stable, more accurate, and faster response of the aircraft. However, how the system would respond with this control technique in the case of actuation lock in place faults. This section is devoted to addressing this problem. Faults in actuators vary from lock in place, hardover, loss of effectiveness, and float faults. For number of actuators m, the fault is expressed by:

$$u_i(t) \begin{cases} u_i(t) & \text{nominal} \\ c_i & \text{lock in place} \\ u_{i,max} & \text{hardover} \\ \rho \times u_i(t), 0 < \rho < 1 & \text{loss of effectiveness} \\ 0 & \text{float} \end{cases} \tag{6.24}$$

where i=1,. . . .,m, and c_i is a fixed constant angle that represents the jammed deflection of the corresponding actuator. In this work, lock in place and hardover faults are considered. The hardover is one type of lock in place fault but at its maximum degree. Severe rolling motions are anticipated when the aircraft is subjected to aileron hardover. The previously developed constrained control allocation system was subjected to this fault and the results are shown in Fig. 6.14. The inner right aileron of the aircraft is assumed to encounter a hardover fault 1 second after the pilot's rolling angle command. The available healthy control surfaces cooperate to accommodate the fault and deliver the required rolling angle. However, all actuators were driven to saturation when the pilot requested a rolling back to zero degree angle. This was due to the accumulative efforts passed to each control surface which results in a drastically unstable rolling of the aircraft.

The results emphasise control reconfiguration to overcome the deficiency of the available control surfaces in order to gain stable and safe flight. Since the actuators in the DCA were driven to their maximum rate of change in the design process before the fault, the reconfigurations of the weights W_1, W_2, and W_v are not appropriate.

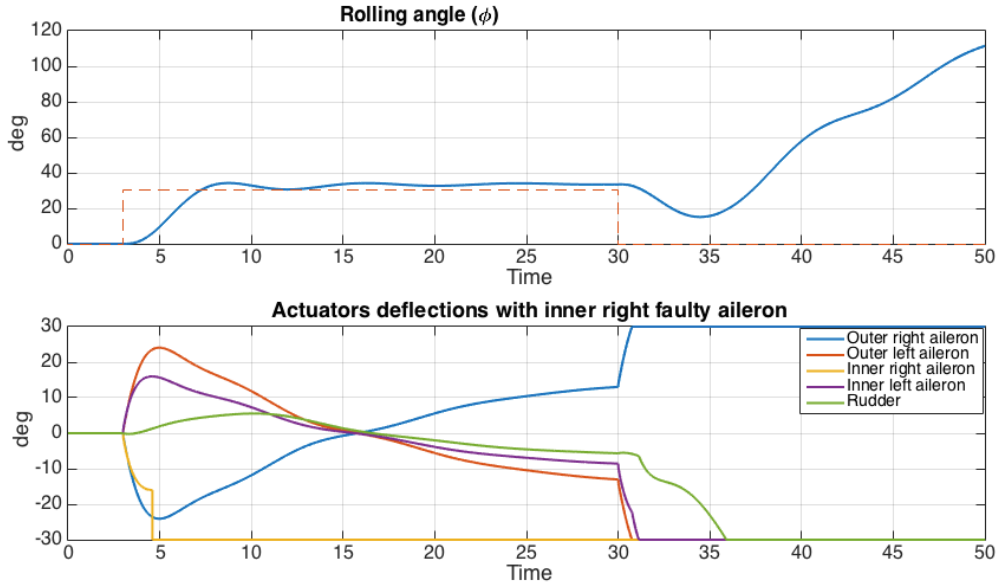

Fig. 6.14 Rolling motion and deflections effects when inner right aileron is faulty.

However, the control distribution matrix will be investigated in order to reshape the efforts directed to the available control surfaces in the presence of a fault.

6.5.1 Redistribution of the control efforts

The desired control input u_s is calculated by mapping the virtual control command $v(t)$ over the available controls using the control distribution matrix S as follows:

$$u_s(t) = S\ v(t)$$

Hence, in the case of any actuator fault, the distribution matrix S is to be updated. Since the inner ailerons are symmetric and conduct essentially the same task but with opposite directions, and similarly for the outer ailerons, faults in the inner right aileron, outer right aileron, and rudder are analysed. If any actuator is jammed, its related parameter in the S matrix will be set to zero, while other parameters will be multiplied by an updating factor (G_f). For a jammed inner right aileron, for instance, that affects the rolling motion, the control distribution matrix will be as follows:

The updating factor depends entirely on the fault type, magnitude, and location. Due to the fact that lock in place of an aileron will generate an undesirable rolling motion it will be assumed that the magnitude of the fault will start from the angle 0 degree. This corresponding to the scale of the updating gain factor G_f, that starts from 1. Thus, the table below (Table 5) summarises the requirements for updating

$$S_{updated} = \begin{bmatrix} (S_{A-ir})_{roll} \times zero & (S_{A-ir})_{pitch} & (S_{A-ir})_{yaw} \\ (S_{A-il})_{roll} \times G_f & (S_{A-il})_{pitch} & (S_{A-il})_{yaw} \\ (S_{A-or})_{roll} \times G_f & (S_{A-or})_{pitch} & (S_{A-or})_{yaw} \\ (S_{A-ol})_{roll} \times G_f & (S_{A-ol})_{pitch} & (S_{A-ol})_{yaw} \\ (S_{A-rudder})_{roll} \times G_f & (S_{A-rudder})_{pitch} & (S_{A-rudder})_{yaw} \end{bmatrix}$$

the system when lock in place fault occurs in the lateral control surfaces, ailerons, or rudder.

Table 6.3 Required updates to the system subjected to actuators lock in place faults.

Fault location	Magnitude [deg.]	Updating factor (G_f)	Max reference rate of change [deg/s]
Inner right aileron	Jam at angle $<$ 10 deg	1.1	-
	10 deg$<$ Jam $<$ 20 deg	1.25	-
	Hardover at max	1.6	-
Outer right aileron	Jam at angle $<$ 5 deg	1.55	-
	5$<$ Jam $<$ 10 deg	1.55	8.5
	10 deg $<$ Jam $<$ 20 deg	1.75	1
	Hardover at max	1.8	1
Rudder	Jam at angle $<$ 10 deg	2	-

The maximum rate of change of the reference signal was also constrained because it affects how the aircraft's actuators are excited. For instance with a step response, the sharp change in the aircraft manoeuvre demands a faster response from the controls, which yield higher magnitudes of deflections. In this FTC experiment, aircraft response was examined for two reference signals, shown in Fig. 6.15, the step and ramp inputs.

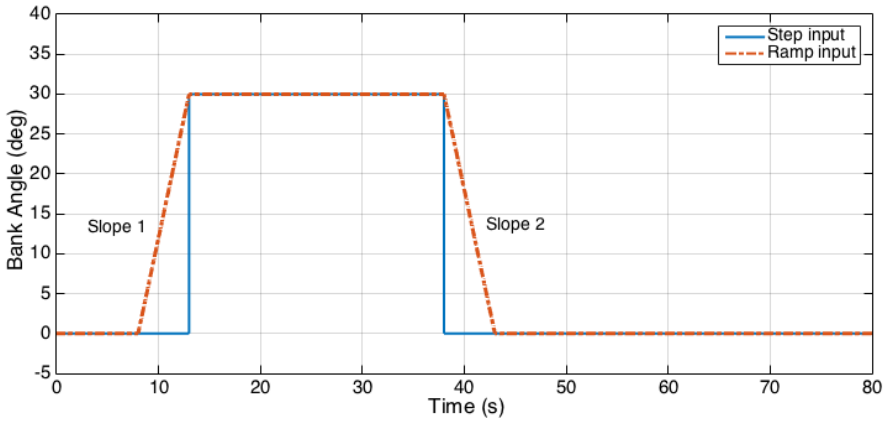

Fig. 6.15 Ramp and step reference signals.

6.5.2 Control Redistribution using Fuzzy Logic

Due to the different aspects considered in choosing the model's gain to update the control distribution matrix S, there was a need for a technique to handle these conditions. Fuzzy logic formulation is a method that can map an input space to an output space. L. Zadeh, of the University of California at Berkeley, proposed the idea of fuzzy sets [148]. Later, E. Mamdani, a professor at London University, applied fuzzy logic to the control of an automatic steam engine [149]. In recent years, the varieties of applications of fuzzy logic have been increasing significantly. The applications range from consumer products such as washing machines to industrial process control, medical instrumentation, etc. Fuzzy logic maps a range of input to a range of output, as illustrated in the following two examples. With the specification of how hot you want the water to be, a fuzzy logic system will adjust the faucet valve to the appropriate setting. Likewise, with information about how fast the car is going and also how hard the motor is working, the fuzzy logic system shifts gears. Thus, it is a prominent technique for FTC redistribution for the following features [150, 151]:

- Mapping given range of inputs (such as the faults magnitude, location, etc) to a range of outputs (such as the updating gain, or other constraining parameter, i.e. the reference signal rate of change).
- Interpolation between sets of data of the input and provision of the most relevant output.
- Moreover, fuzzy logic is cheaper to develop compared to other intelligent systems. It simplifies knowledge acquisition and representation and also accommodates complexity of rules.

To illustrate, a typical mapping of a two-input to one-output fuzzy controller is depicted in the 3-D plot shown in Fig. 6.16.

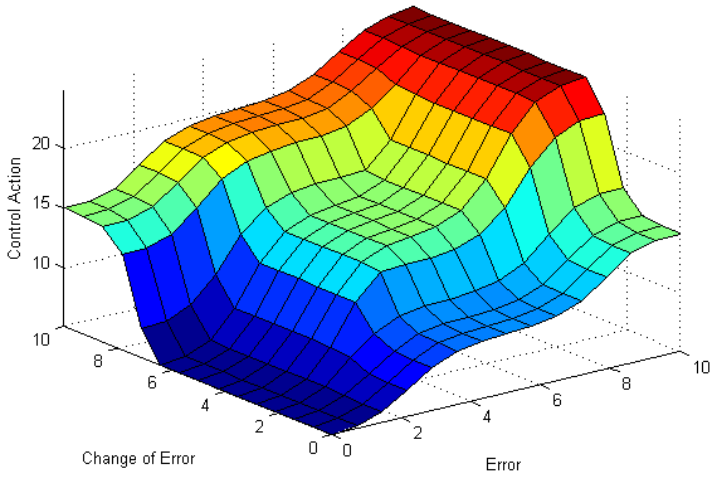

Fig. 6.16 Mapping two inputs to one output using fuzzy logic.

In this example, the fuzzy logic inputs are the signals and the change of the error, while the output is the control action inferred from the fuzzy rules. To implement a fuzzy logic technique, the following three steps are required [150]:

1. Fuzzification: convert the classical data into fuzzy data or to Membership Functions (MFs).

2. Fuzzy Inference Process: combine the membership functions with the control rules in order to get the fuzzy output.

3. Defuzzification: generate a table of the associated output. Different methods are used based on the defuzzification process.

In Matlab, fuzzy logic can be implemented using one of the following two techniques, namely, Mamdani and Sugeno fuzzy techniques. The Mamdani fuzzy inference method is among the first control systems to have been built using fuzzy theory to control a steam engine by setting linguistic control rules obtained from an experienced human operator. This type of fuzzy inference is the most commonly used method in control applications. The other type is Sugeno fuzzy inference, which was introduced by [152], and is similar to Mamdani's method in fuzzifying the inputs and applying a fuzzy operator. However, they are different in the output membership function where Sugeno's is either linear or constant.

1.Fuzzification: To categorize the inputs based on certain pre-defined degree or levels, the membership functions concept is used. For example, in the following figure, there are two plots, one is a sharp-edged signal while the other is a smoothly varying curve that passes from the not-tall to the tall data set. Both data set are tall to some extent, but one is significantly less tall than the other. Thus the curve defines the transition over the set, and determines the designation of μ, which is the output axis varying between 0 and 1 and is known as the membership value. This defines how each element in the input space is mapped to a membership value.

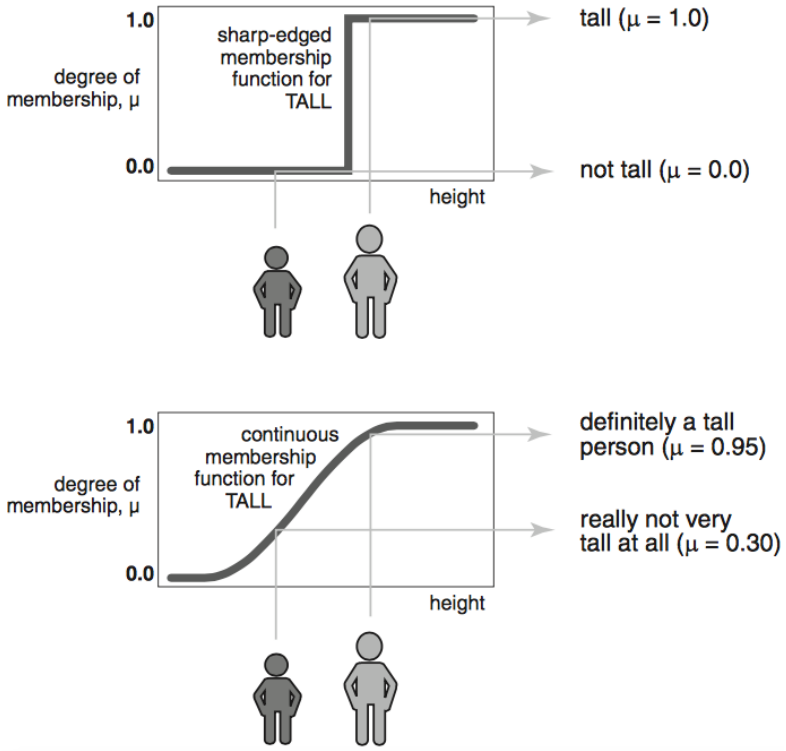

Fig. 6.17 Types of membership functions [150].

2- Fuzzy Inference Rules and Process: To generate the fuzzy inference rules between multi-input and multi-output sets, mathematical operations are used. The basic classical set of operations are the intersection, union, and complement [150], which are represented by AND, OR, and NOT operators, respectively, as follows: For two classical sets, A and B:

Intersections:

$$A \cap B = \mu_A(X) \cap \ \mu_B(X) = \min(\mu_A(X), \mu_B(X))$$

Union:

$$A \cup B = \mu_A(X) \cup \ \mu_B(X) = \max(\mu_A(X), \mu_B(X))$$

Complement:

$$A^C = X - A$$

where X is the entire set of elements and μ is the degree of membership. The complement of A is everything outside A. These operators for different membership functions are demonstrated in Fig. 6.18.

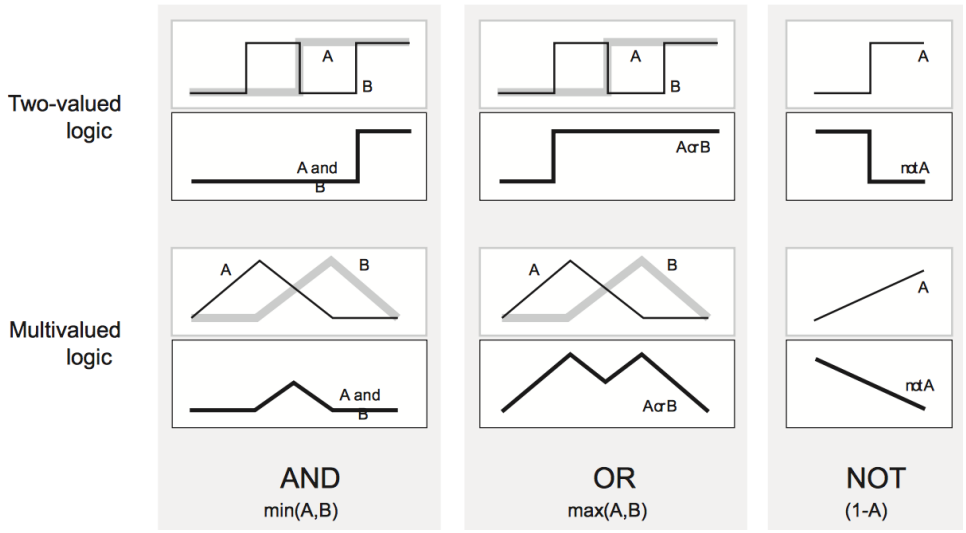

Fig. 6.18 Rules of membership functions [150].

To formulate the fuzzy rules, IF-THEN processes are used. Some examples are:

For Mamdani:

IF {conditions 1} AND/OR{conditions 2}, .. AND/OR {conditions n},

THEN {output 1}, AND/OR{output 2}, .. AND/OR {output m}.

For Sugeno:

IF {Input 1 = x} and {Input 2 = y},

THEN {Output is z = ax + by + c}

This will specify the degree to which an input data matches the condition of a rule and results in what output or action will be taken.

3- Defuzzification: Sugeno fuzzy inference results in constant or linear output, while for the Mamdani fuzzy model, the process is to convert linguistic variable fuzzy output to crisp or classical output. For this type of inference system, three defuzzification techniques are mainly used, namely, the Mean of Maximum method, the Centre of Gravity method, and the Height method. For more details see [150]. The terminal result of defuzzification in both methods is the lookup table.

6.5.3 Fuzzy logic Implementation

Fuzzy inference related calculations are performed prior to the real application. Therefore, it is not a time-consuming process when it is run online. It is implemented using Matlab/Simulink software. Sugeno's fuzzy logic method is computationally more efficient and has a more compact representation than a Mamdani system [151]. Thus, it is selected in this work. The inputs are the location and degree of the fault, while the outputs are the control distribution updating factor and the reference signals maximum rate of change. First, the membership functions are described below.

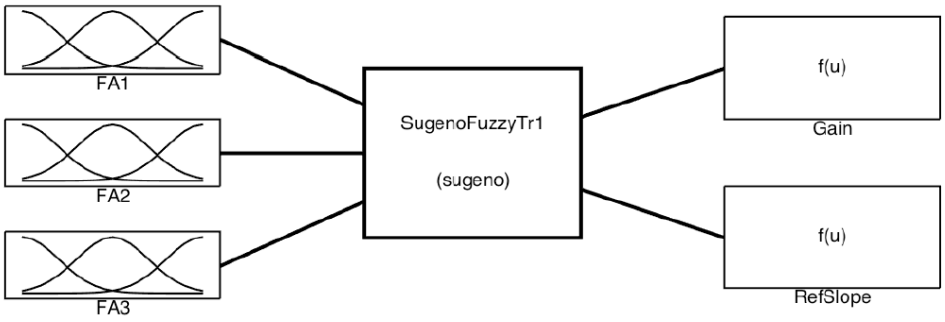

Fig. 6.19 Fuzzy logic using Sugeno's model.

As shown in Fig. 6.19, the fuzzy system comprises three inputs FA1 , FA2, and FA3 that represent the inner right aileron fault, the outer right aileron fault, and the rudder fault, respectively. For all cases, triangular membership functions have been chosen to linearly represent the faults, as shown in Fig. 6.20 for the inner right aileron fault FA1. Membership function details are listed in Table 6.4.

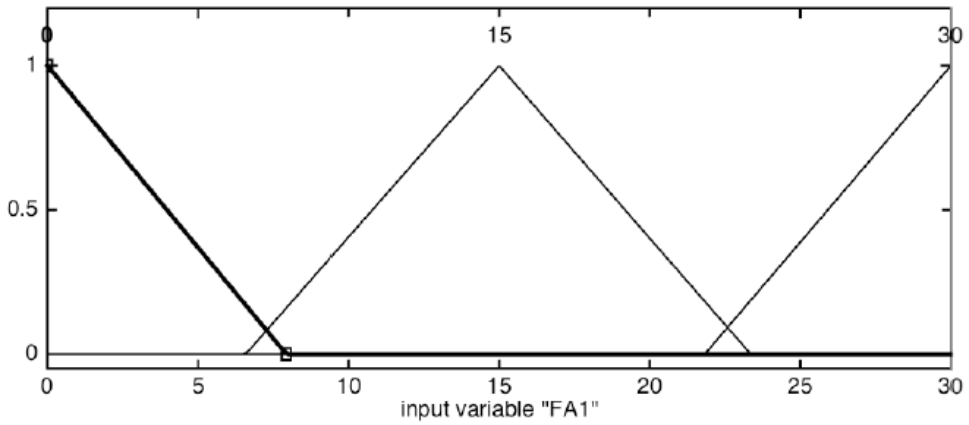

Fig. 6.20 Triangular membership functions for fault FA1.

Table 6.4 Details of membership functions characteristics

Fault location	Membership function	Centred at
Inner right aileron (FA1)	1	0
	2	15
	3	30
Outer right Aileron (FA2)	1	0
	2	2.5
	3	5
	4	10
	5	15
	6	20
	7	25
	8	30
Rudder (FA3)	1	0
	2	1
	3	10
	4	20

The next step is the implementations of the Sugeno's IF/THEN rules that set the relations between inputs and outputs, determining the shape of the required outputs.

Rules:

1. (FA1=0) $\Longrightarrow$ (Gain=1)
2. (FA1=15) $\Longrightarrow$ (Gain=1.25)
3. (FA1=30) $\Longrightarrow$ (Gain=1.75)
4. (FA2=0) $\Longrightarrow$ (Gain=1)
5. (FA2=2.5) $\Longrightarrow$ (Gain=1)
6. (FA2=5) $\Longrightarrow$ (Gain=1.5) & (RefSlope=15)
7. (FA2=10) $\Longrightarrow$ (Gain=1.5) & (RefSlope=8.5)
8. (FA2=15) $\Longrightarrow$ (Gain=1.75) & (RefSlope=1)
9. (FA2=20) $\Longrightarrow$ (Gain=1.75) & (RefSlope=1)
10. (FA2=25) $\Longrightarrow$ (Gain=1.8) & (RefSlope=1)
11. (FA2=30) $\Longrightarrow$ (Gain=1.8) & (RefSlope=1)
12. (FA3=0) $\Longrightarrow$ (Gain=1)

13. (FA3=1) $\Longrightarrow$ (Gain=1)

14. (FA2=10) $\Longrightarrow$ (Gain=2)

15. (FA3=20) $\Longrightarrow$ (Gain=2.2)

Results of the rules are illustrated by the plots for the updating gains for each fault's magnitude, as shown in Fig. 6.21 for inner aileron and rudder against the updating factor. While, Fig. 6.22 shows the plots for FA2 against the updating factor and the required maximum slope for reference angle.

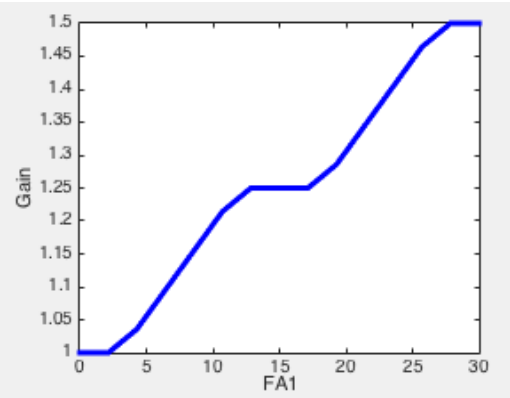

(a) FA1 vs. G_f.

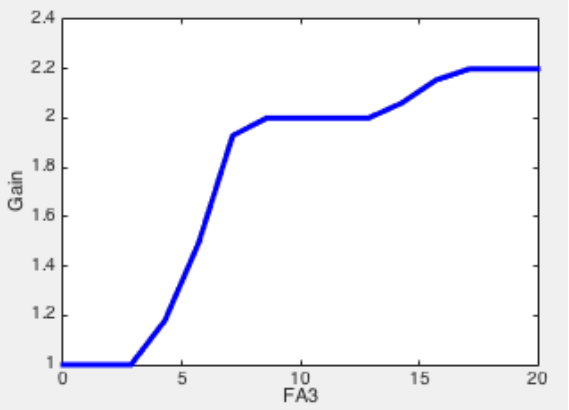

(b) FA3 vs. G_f

Fig. 6.21 Inner and outer ailerons vs. updating factor G_f

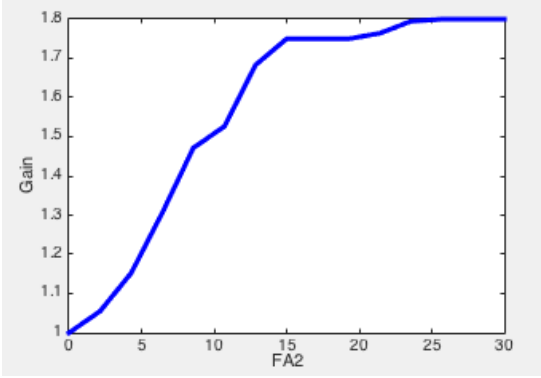

(a) FA2 vs. G_f.

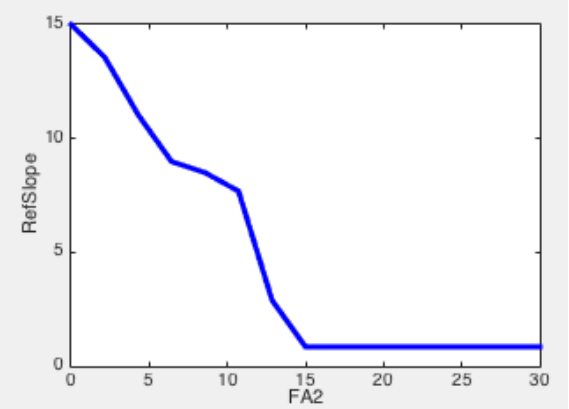

(b) FA2 vs. the slope

Fig. 6.22 Outer ailerons vs. updating factor G_f and slope

6.5.4 Process of the FTC

For this reconfigurable control allocation system in respect of lock in place faults, a summary of the development process is illustrated in Fig. 6.23. The jamming faults

were modelled using Eq.6.24. For each scenario, the control distribution matrix S is updated using fuzzy logic.

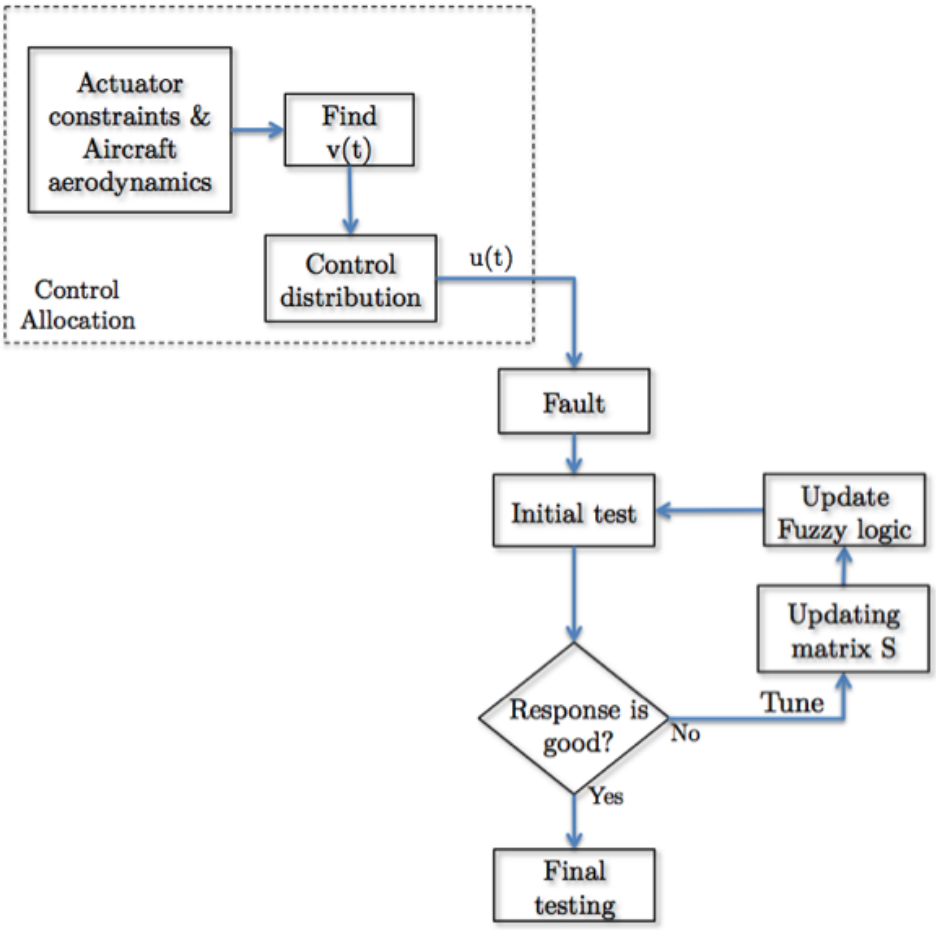

Fig. 6.23 Development process of the Fault-tolerant Control Allocation.

As the fuzzy system is created and tuned, it will be embedded as a simulation block for validation and testing. The general scheme, shown in Fig. 6.24, incorporates the control allocation system with the FTC reconfiguration, while the FDD system is assumed. Information regarding faults is provided to the pre-defined fuzzy logic block that computes the reconfiguration parameters.
Results of the experimental simulation analysis are presented in the next section.

6.6 Simulation Results

Lock in place faults and hardover scenarios have been tested. Software codes and modelling are available in Appendix D. In all scenarios, it was assumed that fault information was provided 1 second after the fault occurs, and redistribution was

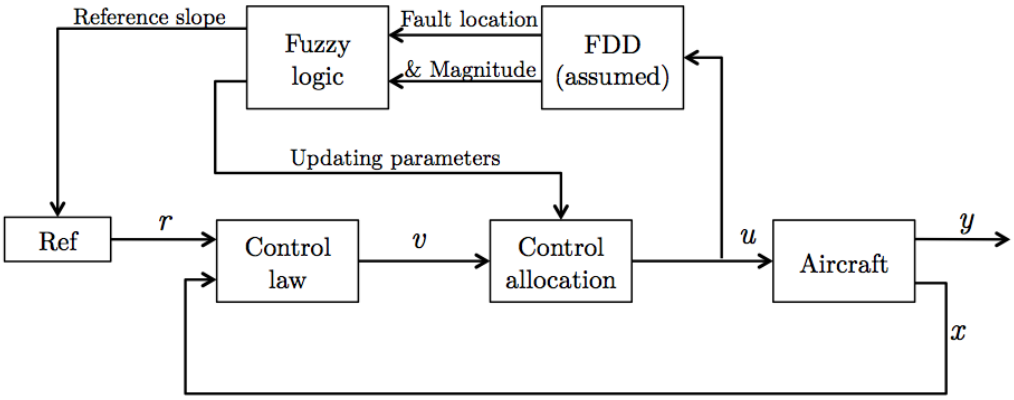

Fig. 6.24 Reconfigurable FT control allocation layout.

conducted directly afterwards. The testing was conducted for a number of fault magnitudes within the considered region.

6.6.1 Inner right aileron faults

A lock in place fault was introduced in the inner right aileron while the opposite inner left aileron was assumed to be working properly. In this experiment, the actuator stuck at a 17 degree deflection angle at time t=3 seconds. The aircraft response (in Fig. 6.25) shows how the redistributed and nominal CA dealt this situation. The difference between them was small, where both optimal computations yielded a good rise time (3 seconds) and less than 10% overshoot. The redistributed CA produced a slightly faster settling time response, and both introduced a very small settling error (<2 deg).

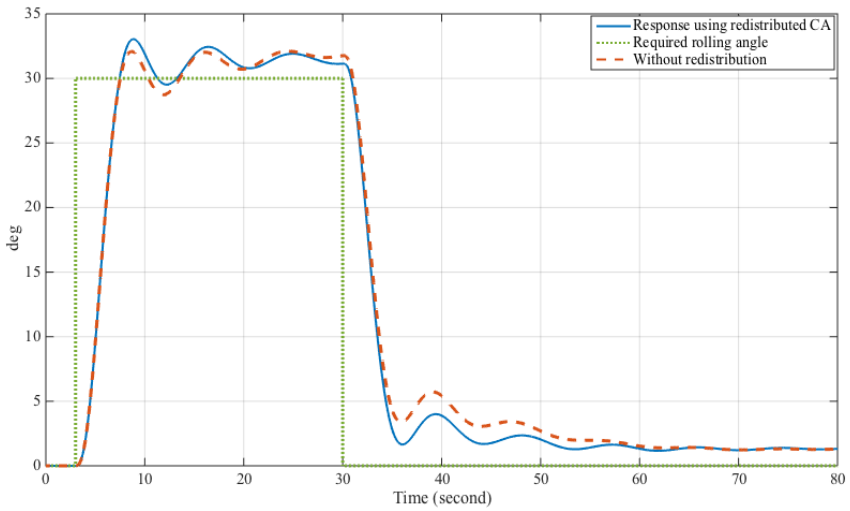

Fig. 6.25 Response with jammed inner right aileron at 17 degree.

Control deflections are shown in Fig. 6.26, where the redistributed CA had introduced a very small difference in the deflection patterns compared to the nominal ones. This was due to the small influences resulting from the secondary effects produced by the inner ailerons on the rolling motion.

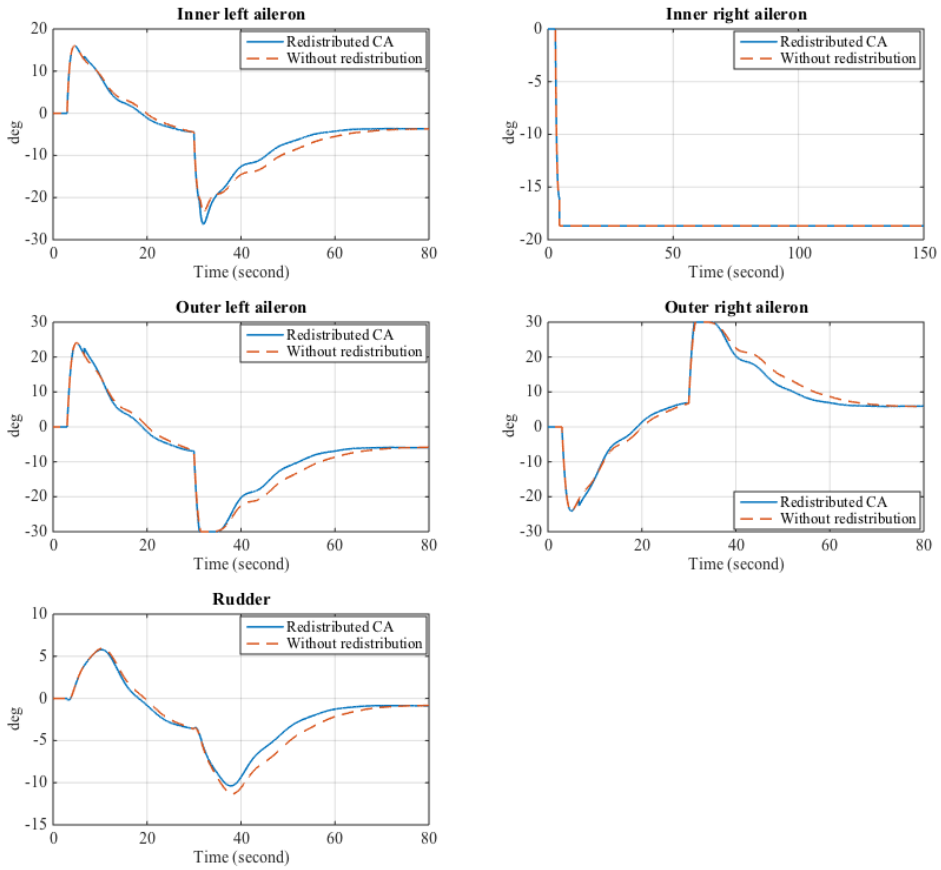

Fig. 6.26 Aircraft controls' deflections with 17deg LIP on the inner right aileron

Hardover fault:

The aircraft response against the hardover fault in the inner right aileron is shown in Fig. 6.27. The normal control allocation without redistribution was unable to maintain the stability of the aircraft, and resulted in deterioration of the stability of the aircraft. On the other hand, the redistribution of control efforts preserved the stability and leading to a great tracking response with small settling error (<3 degrees).

Deflections resulted from this situation are shown in Fig. 6.28, where in the nominal distribution case, all the available healthy actuators were driven to their

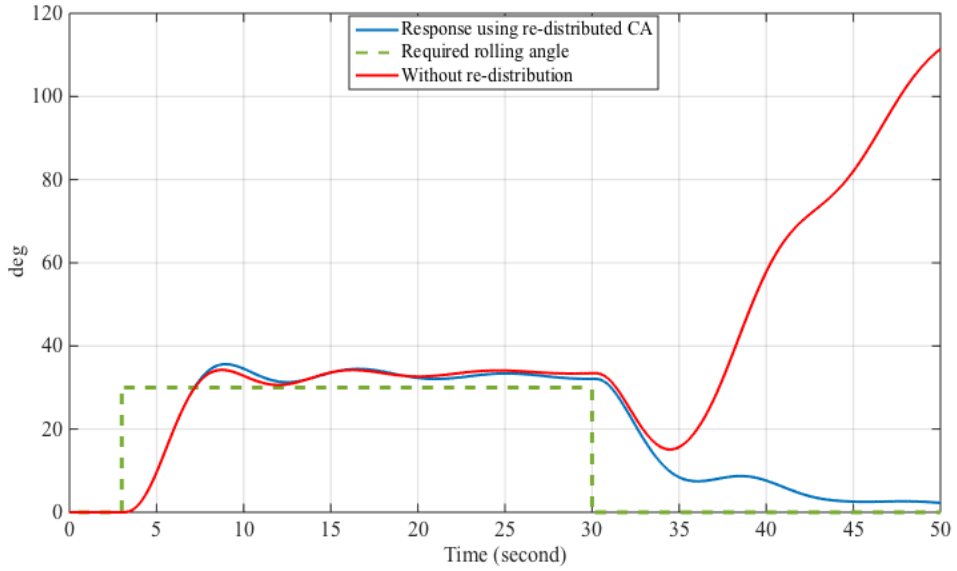

Fig. 6.27 Aircraft responses with hardover faults in the inner right aileron.

maximum deflections in order to restore the stability, but without success. However, when using the redistributed CA technique, the system accommodated the fault and the actuators were optimised for successful deflection performance against the step required reference signal.

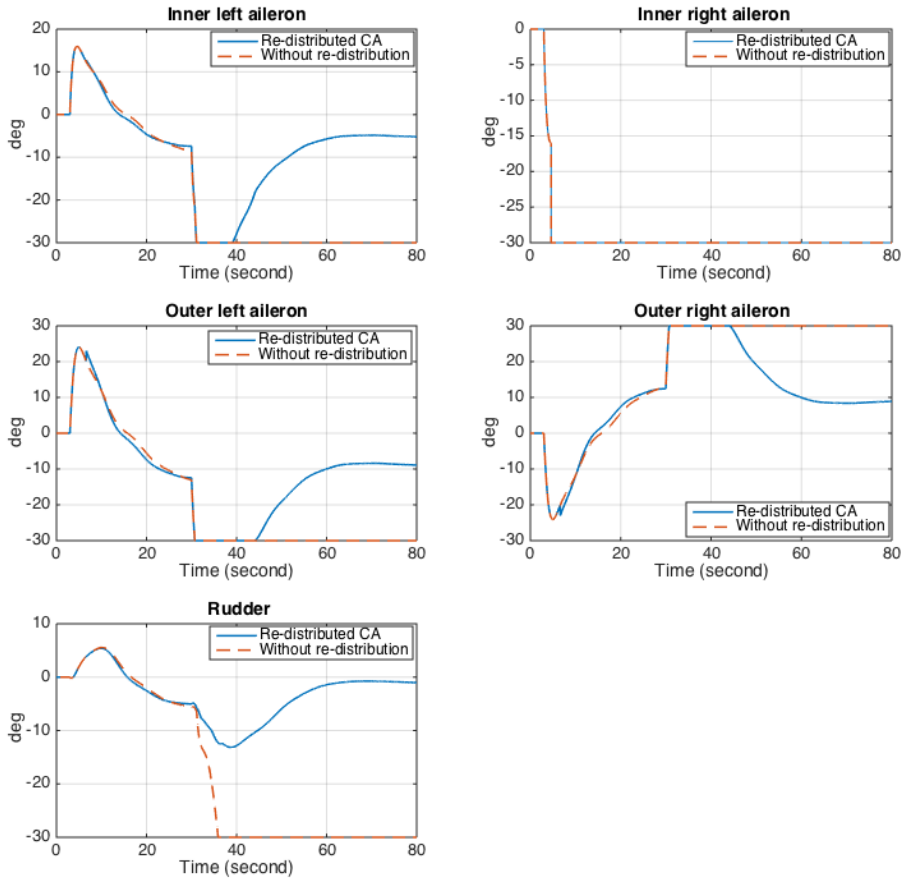

Fig. 6.28 Deflections against hardover fault in the inner right aileron

6.6.2 Outer right aileron faults

The outer ailerons are considered to be the primary effectors of rolling. Hence any lock in place fault will affect the stability and tracking performance of the aircraft. The controllability of the aircraft will be tested only using the developed FTCA approach.

10 degrees lock in place:

This fault scenario, as shown in Fig. 6.29, yielded an unstable aircraft response when the redistributed CA was subjected to a step reference input. Redistribution of control efforts achieved a stable response only when the ramp reference input was requested. This led to a substantial limitation in the rolling rate. Although this trajectory is a slow-moving pattern, the developed CA was able to guarantee the stability and automatic tracking requirements of the system.

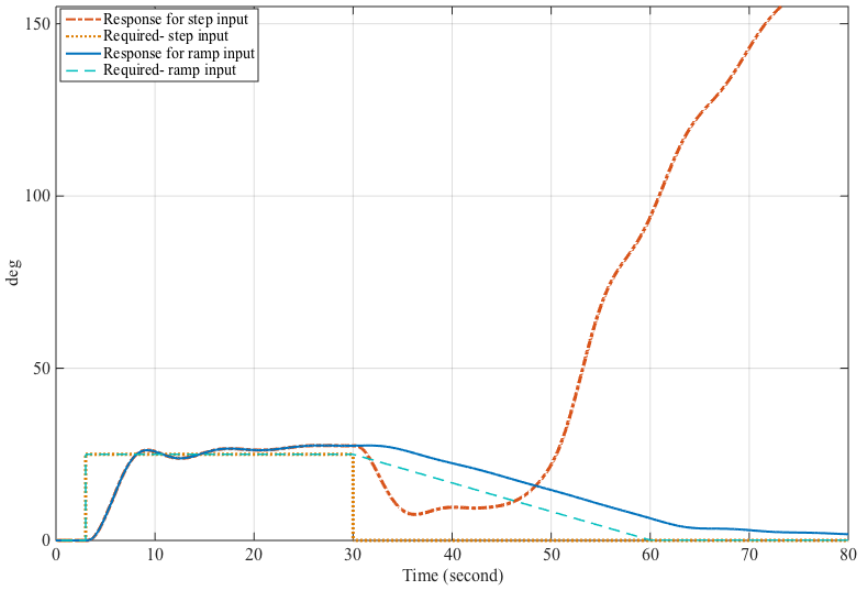

Fig. 6.29 Response for a step and ramp reference inputs, with 10deg LIP fault in outer right aileron.

Control surface deflections against the 10-deg lock in place fault in the outer right aileron are shown in Fig. 6.30, where the step reference input resulted in the saturation of all the available actuators, and hence led to the aforementioned unstable aircraft response. On the other hand, the lock in place fault in the outer right aileron was accommodated when using ramp reference input which resulted in smooth actuator deflections.

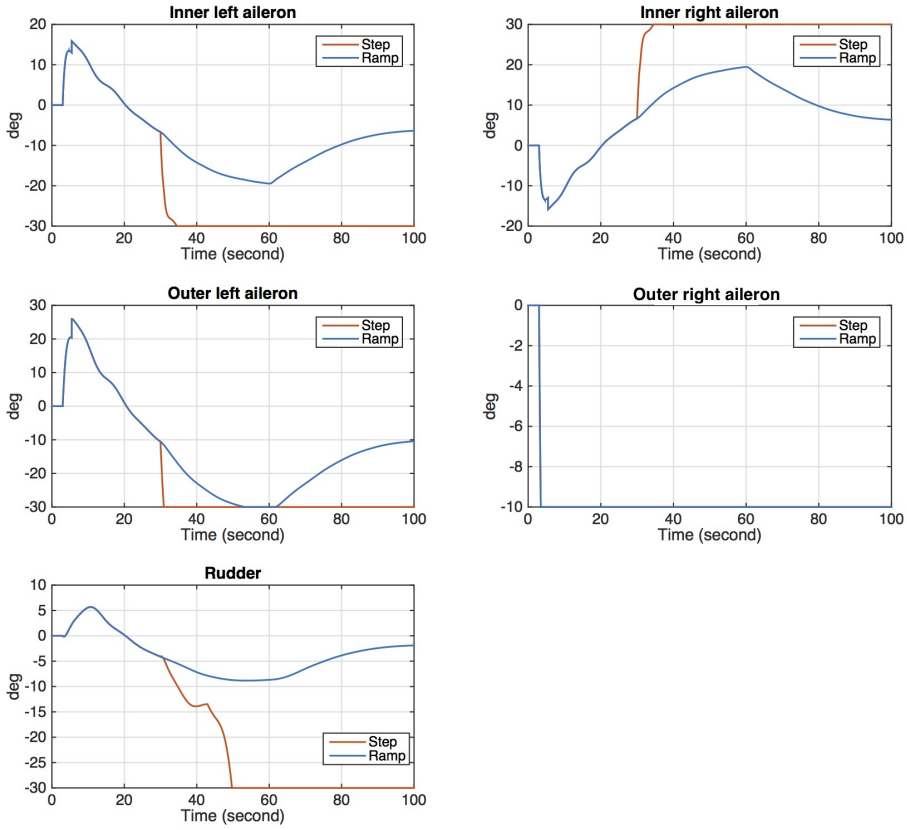

Fig. 6.30 Deflections for step vs. ramp reference inputs

16 degree lock in place:

At higher magnitude of lock in place faults occurred in the outer right aileron, the aircraft was pushed to the edge of tracking performance and stability. The 16 deg jam fault was introduced at t=5 seconds, and through the redistribution of the control efforts, the system was just able to meet the stability conditions when the constrained reference ramp input was requested, as shown in Fig. 6.31.

Control surface deflections of the redistributed CA using the constrained ramp input are shown in Fig. 6.32. As a result of the selected reference input, the deflections are smooth and maintain the actuator's limits of position and rate of change.

Magnitude of the faults of the outer right aileron was analysed to this point. Higher faults drastically affected the stability of the aircraft and led to uncontrollable aircraft manoeuvres, which are considered to be the limits of this control solution to restore the stability of the aircraft with the given conditions and optimisation.

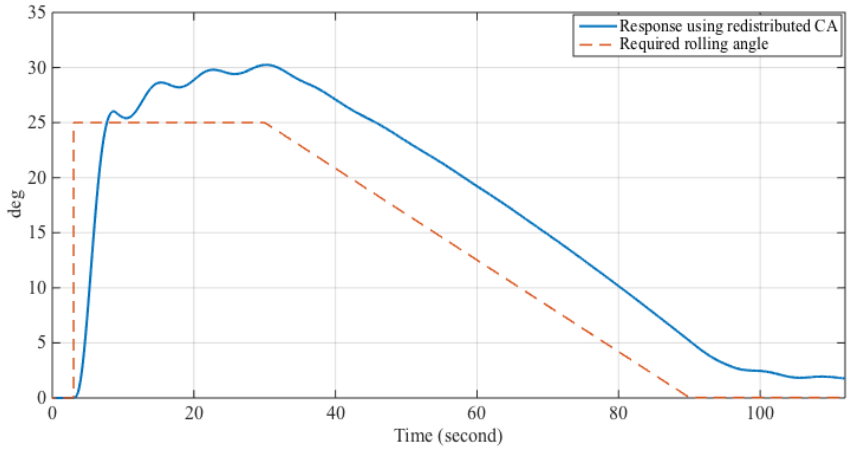

Fig. 6.31 Bank angle response for 16deg LIP fault in outer right aileron.

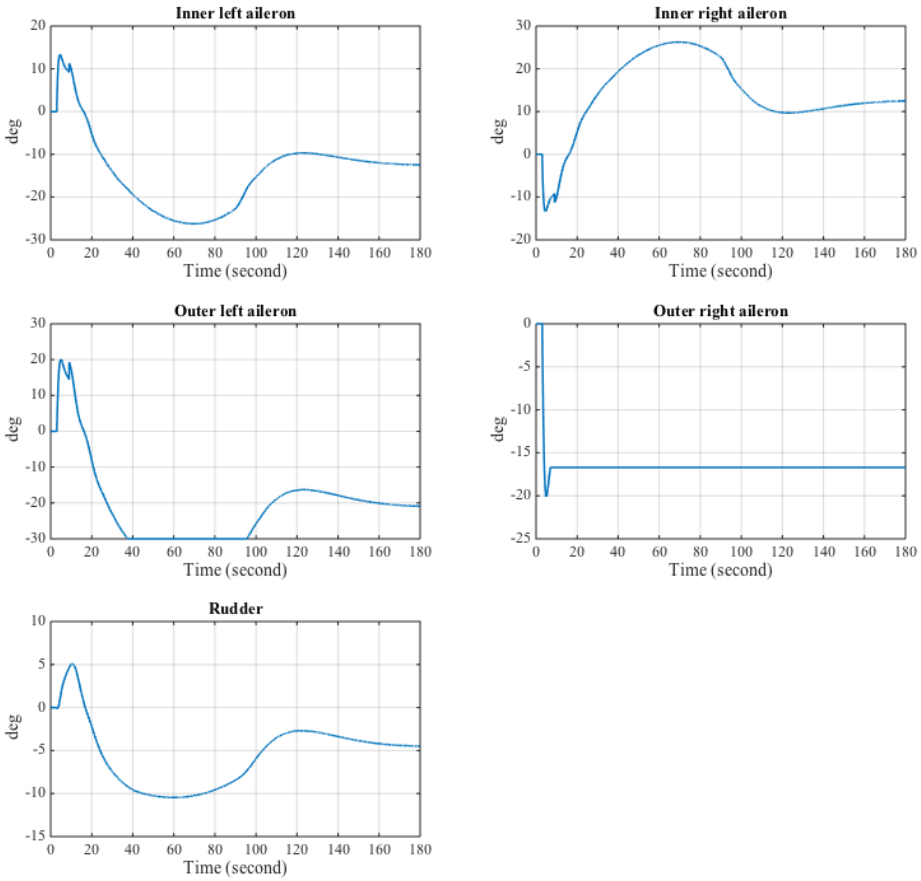

Fig. 6.32 Deflections with 16deg LIP in the outer right aileron.

6.6.3 Rudder faults

As mentioned earlier, the yawing motion is mainly controlled by the rudder. Thus, in case of lock in place faults, the available ailerons will be required to overcome this problem and maintain the stability and tracking requirements.

Lock in place at 6 degree

When the rudder jammed at 6 degrees of deflection, the aircraft in both redistributed and nominal control allocation cases had a similar stable response, as shown in Fig. 6.33. There was an overshoot and an acceptable 4 degrees steady state error in the bank angle.

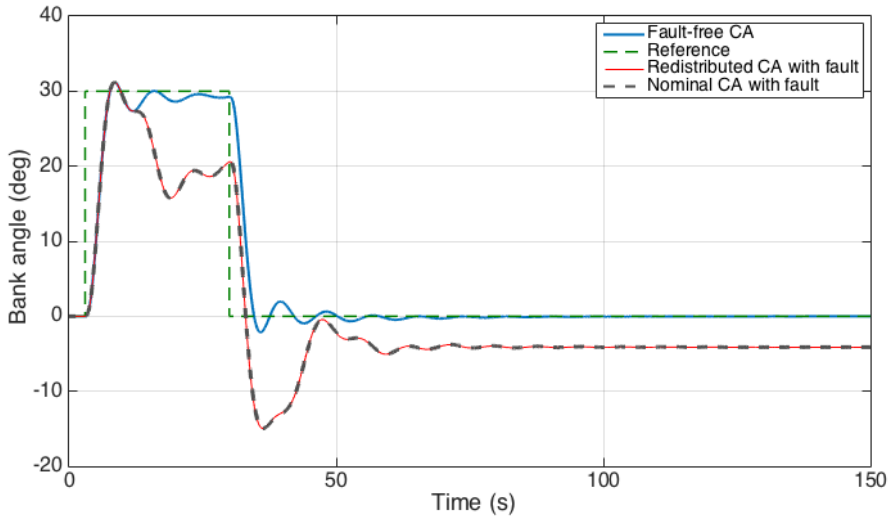

Fig. 6.33 Aircraft bank angle response against 6deg LIP fault in the rudder.

The sideslip angle (β) response in Fig. 6.34 shows that, in the free-fault case, the controller minimised the angle to zero degrees. With faults in the rudder, there was a 4-degree induced sideslip angle, with the aircraft brought back to straight flying. There was no improvement in the response due to redistribution, however, the control allocation optimal control yielded a minimum divergence of the side-slip angle.

Aircraft actuator deflections, when the aircraft was subjected to a 6-degree jammed rudder, are shown in Fig. 6.35. In the control distribution matrix S, updating the elements of the available healthy actuators, corresponding to the rolling and yawing rotation, has not yielded any improvements compared to the nominal control allocation response. This was due to the fact that the contributions from the ailerons are relatively small compared to the rudder. Yet, in general, the DCA led to a stable response.

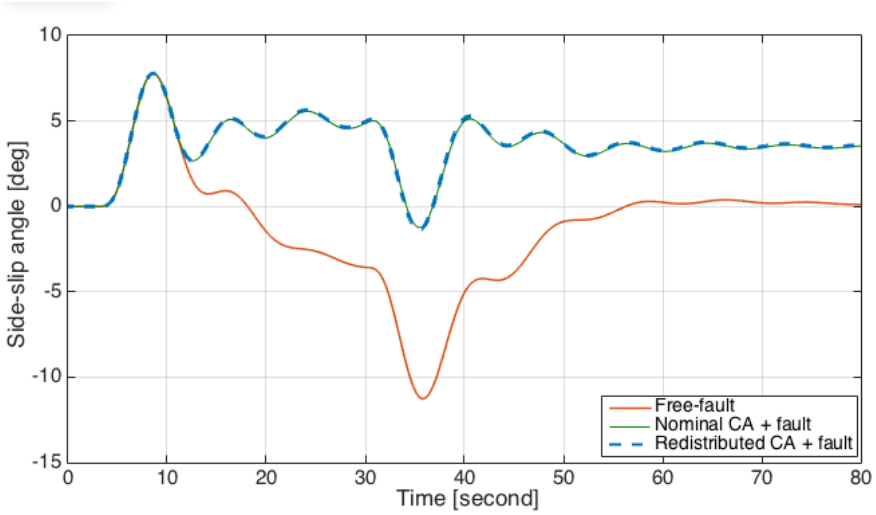

Fig. 6.34 Aircraft sideslip angle response with 6 degree LIP fault in rudder.

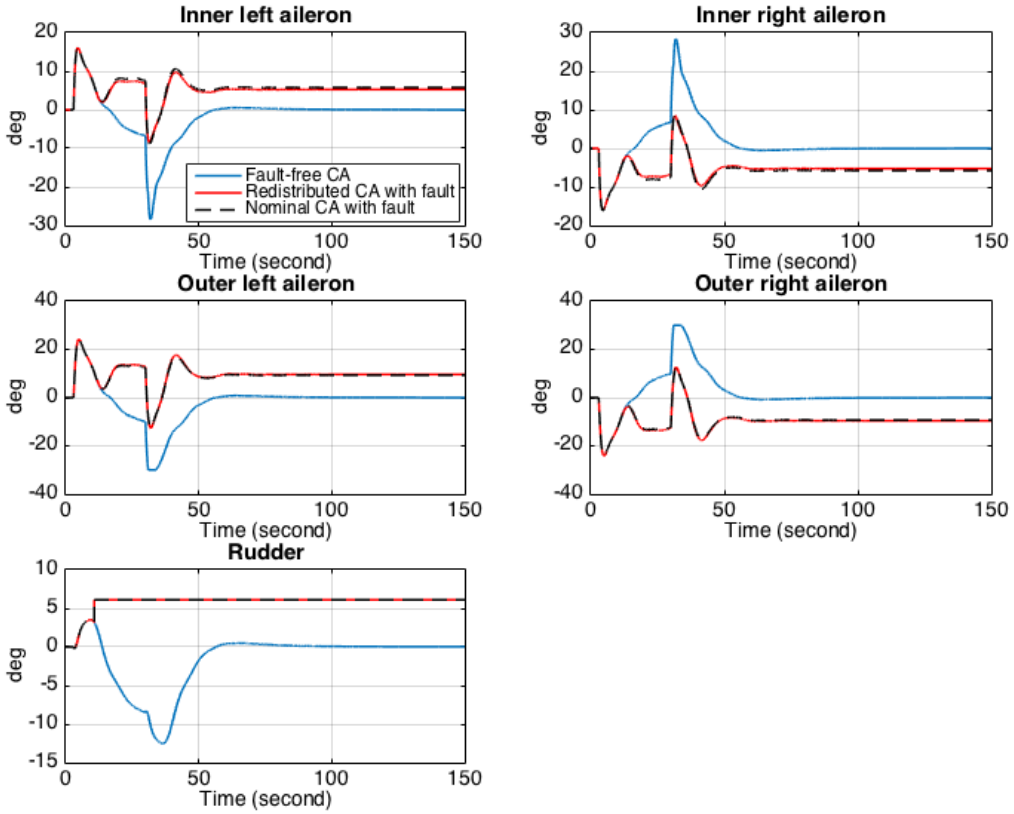

Fig. 6.35 Deflections with 6deg LIP rudder

Lock in place at 10 degree

Similarly, when applying a 10-degree lock in place at the rudder, the nominal control allocation matched the redistributed CA, as in Fig. 6.36. The optimal solution of the control allocation managed to maintain the stability of the aircraft, with an increase

in the overshoot and settling tracking error as the lock in place fault on the rudder increases.

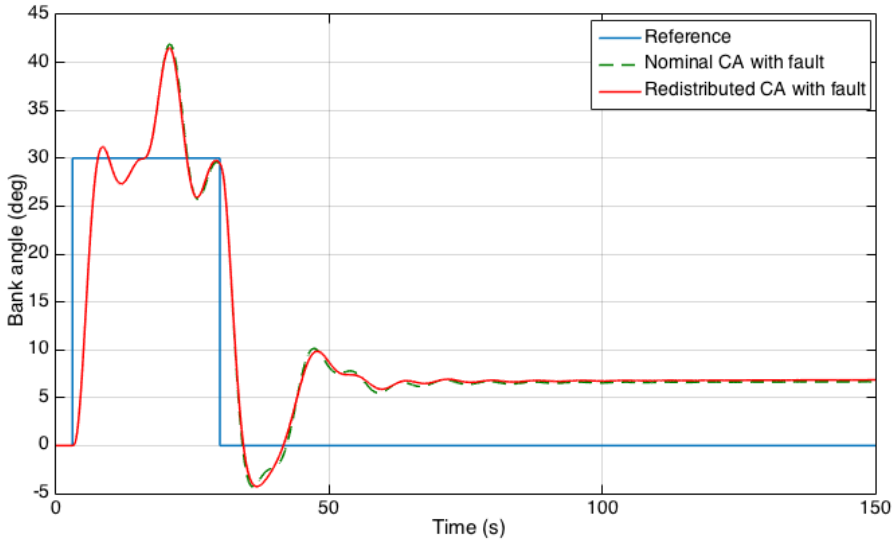

Fig. 6.36 Aircraft responses when the rudder is jammed at 10 deg.

The related deflections are shown in Fig. 6.37. Although the redistributed CA excited the available controls, there was no difference in the aircraft's response. This was due to the limited influence from the ailerons towards the compensation of rudder impairments.

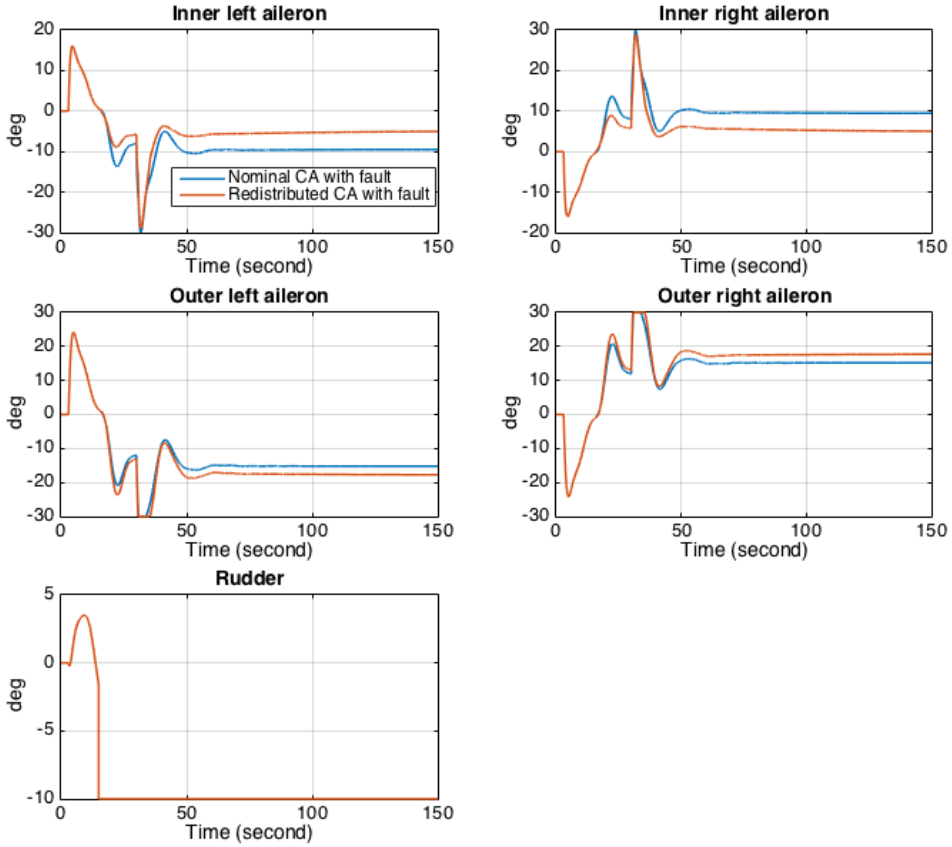

Fig. 6.37 Deflections with 10deg LIP rudder fault.

6.7 Conclusion

This chapter discusses the development of a reconfigurable fault tolerant flight control system for a multi-effector aircraft using a control allocation technique and a new efforts-distribution method among the control surfaces. The aircraft model used in the study has redundant ailerons and a rudder as the primary control inputs for the considered lateral motion. The optimal control allocation problem that handles the redundancy of the control surfaces, tracking requirements, and actuator constraints was formulated. The control input constraints included both the maximum rate of change and the saturation limits. The developed approach incorporates a new control redistribution process, which is updated at the occurrence of a fault. This approach relies on and assumes an effective on-board FDD system to provide precise fault information regarding the actuators. Fuzzy logic was implemented to correlate between the faults and the control redistribution. The fuzzy logic implementation handles a wide range of faults magnitudes online, by interpolation. The system deals with a more severe type of actuator fault, which is the lock in place fault. Due to this fault, anticipated moments are generated which need counteracting from the

available control surfaces. Both inboard and outboard ailerons and rudder faults were tested. When the inner aileron experienced a 20-degree or less lock in place fault, the system was asymptotically stabilised by both the baseline and reconfigured control allocation methods. This was due to the minor effects brought about by the inner ailerons for the rolling motion. Hardover faults on the other hand deteriorated the tracking performance as the control surfaces were driven to saturation using the baseline control allocation. Yet the system was stabilised against this fault using the redistributed control allocation, where the tracking requirements and control deflection constraints were fulfilled.

As the primary rolling effector, the testing of the system against lock in place faults in the outer aileron showed a huge influence on the aircraft response. The aircraft was only brought to stability when using the redistributed CA and the required reference signal of the bank angle took a ramp-shape, with rate of change depending on the magnitude of the fault. Higher than 16% lock in place faults in the outer aileron could not be alleviated with the proposed settings, due to the saturation limits of the available healthy actuators. Finally, in the case of rudder faults, the redistribution of control efforts to the ailerons to accommodate jammed rudder faults did not improve the response. Nevertheless, the system was stabilised with the control allocation scheme, with a slight degradation in the tracking performance. A satisfactory sideslip angle response was achieved. For further work, the linear-based controller could be tested in a nonlinear environment. Moreover, improvement of the tracking performance is suggested to overcome the problem of high outer aileron faults. Engine thrust could be integrated in the loop. Effects of the delays from the FDD could be also investigated.

Chapter 7

Conclusion and Further Work

The developments of fault tolerant controllers for fixed wing aircraft using different optimal multivariable techniques were presented in this thesis. Loss of efficiency and lock in place actuator faults were investigated. The definitions and classifications of existing fault tolerant techniques were presented in chapter 2. The required aircraft dynamics analysis and control was provided in chapter 3. This was followed by the analysis and development of the fault-tolerant control approaches as follows:

In chapter 4, the FTC scheme encompasses an optimal linear quadratic regulator control augmented with an adaptive fault-compensation-based scheme. The multivariable LQR baseline control law was formulated to handle the problem of tracking error and control energy minimisation. By an appropriate adjustment of the control weighting matrices, an optimal baseline control solution was obtained. The adaptive scheme includes fault representation and adaptive compensation terms that were added to the model. The compensation term was computed by making a faulty model as if it is the same as the free-fault one, then solving for the added term. The scheme relies on the availability of a fault detection system, which was assumed to be providing the fault information to the FTC system. In the analysis, loss of efficiency type of faults were assumed. For validation of the control practicality, a nonlinear 6-dof simulation was performed. The LQR based controller was be able to handle faults with magnitudes up to 70%, with large induced overshoot and oscillations. Yet, the rise time of the aircraft response was acceptable. When the faults increased in magnitude, the system became unstable using the LQR only control. Tracking performance also deteriorated, and the control surface deflections became unsettled. On the other hand, the FTC based control managed to handle high magnitudes of loss of efficiency faults in the actuators. The aircraft response was slightly slower in rise time, but overshoot was greatly minimised, which assured the stability of the system and eliminated the settling error. While accommodating the effects of faults

on the stability, the approach also yielded to a faster settling response and converged control surface deflections.

In chapter 5, the inherent robustness features of the H infinity and mu-synthesis techniques were utilized, where actuator loss of efficiency faults were modelled as input uncertainties to the system. This type of approach does not require any fault detection schemes. The robust computation involved the minimisation of a cost function that takes into account multiple design objectives. These objectives are tracking error minimisation, control energy minimisation, and the fault handling. The weighting functions for the optimisation objectives are selected and designed to shape the corresponding relevant requirements. When the linear-based optimised solutions were found, the system was tested in a nonlinear environment for more practical validation. Three design points were chosen within the flight envelope which are the ascending, cruise, and descending operating cases. At these selected flying scenarios, the robust optimal fault-tolerant controllers were computed and tested. Results showed that the H infinity baseline controller managed to give good tracking and control input performance for the multi-variable system. However, it could not withstand actuator faults. The system's control surface performance was deteriorated by very high frequency, rapid fluctuations and sharp deflections. On the other hand, in all flying cases, when testing the mu-synthesis-based controller, the system maintained great tracking performance and smooth rate of change of control surface deflections with 30% fault magnitudes in actuators. Results of testing the controllers at operating points near to the trimming points showed that they worked properly and maintained tracking performance, with slightly higher deflections when testing occurs at lower speed. The gain and phase margins for the system were computed in the cruising case and results showed that the system has adequate margins with the robust controller before it became unstable.

In chapter 6, a reconfigurable fault tolerant flight control system for a multi-effector aircraft is proposed using a control allocation technique and an efforts redistribution scheme among the available control surfaces. The aircraft has redundant ailerons and a rudder as the primary control inputs for the considered lateral motion. The optimal control allocation problem that handles the redundancy of the control surfaces, tracking requirements, and actuator constraints was formulated. The control input constraints included both the maximum rate of change and saturation limits. The developed approach incorporates a new control redistribution process, which is updated in the occurrence of fault. This approach relies on and assumes an effective on-board FDD system. Fuzzy logic was implemented to correlate between the faults and the control redistribution. The fuzzy logic implementation handles wide range of

fault magnitudes online, by interpolation. The system deals with a more severe type of actuator fault, which is the lock in place fault. Both inboard and outboard ailerons and rudder faults were tested. When the inner aileron experienced a 20-degree or less lock in place fault, the system was stabilised by both the baseline and reconfigured control allocation methods. This was due to the minor effects brought about by the inner ailerons for the rolling motion. Hardover faults on the other hand, deteriorated the tracking performance, where control surfaces were driven to saturation. However, the system was stabilised against this fault using the redistributed control allocation, where the tracking requirements and control deflection constraints were fulfilled. The testing of the system against lock in place faults in the outer aileron showed that the aircraft was only brought to stability when the required reference signal of the bank angle took a ramp-shape, with rate of change dependent on the magnitude of the fault. Higher than 16% lock in place faults in the outer aileron could not been alleviated using the proposed setting. Finally, in the case of rudder faults, the redistribution of control efforts to the ailerons to accommodate jammed rudder faults did not improve the response. Nevertheless, the system was stabilised with the control allocation scheme, with a slight degradation in tracking performance. A satisfactory sideslip angle response was achieved.

The proposed techniques managed to enhance the stability of the flying aircraft against different types of actuator fault. However, expansions of the work is suggested to further tackle the problem from different aspects, as follows:

- In chapter 4, further improvements of the work may include studying the effects of delays in fault information delivery on the FTC performance, and how to avoid any related deficiencies. Moreover, to cover the whole problem, a design of the FDD scheme is also suggested. Additionally, the investigations of the lock in place fault effects and accommodation would enrich the study in dealing with different kinds of fault scenarios, where a redundant-effector aircraft model could be utilised. Another important investigation would be to introduce the wind effects on the system, with a further step of testing and validation processes.
- In chapter 5, further work may include more optimisation of the mu-synthesis-based controller that may lead to an increase in the fault-tolerance degree. Another expansion is the lock in place fault accommodation problem, which may need a considerably reconfigured control law or available redundant control surfaces.
- For further work based on chapter 6, the linear-based controller could be tested in a nonlinear environment for a more realistic validation. Moreover, the investigation of the stability and tracking performance against high faults in the outer aileron, atmospheric turbulences, or delays from the FDD are particularly suggested.

References

[1] R. Nelson, *Flight stability and automatic control*. 1998.

[2] X. Yu and J. Jiang, "A survey of fault-tolerant controllers based on safety-related issues," *Annual Reviews in Control*, 2015.

[3] Y. Zhang and J. Jiang, "Bibliographical review on reconfigurable fault-tolerant control systems," *Annual Reviews in Control*, vol. 32, no. 2, pp. 229–252, 2008.

[4] M. Steinberg, "Historical overview of research in reconfigurable flight control," *Proceedings of the Institution of Mechanical*, 2005.

[5] G. Chowdhary, "Autonomous guidance and control of airplanes under actuator failures and severe structural damage," *J. Guid. Control*, 2012.

[6] J. Lunze and J. Richter, "Reconfigurable fault-tolerant control: a tutorial introduction," *European Journal of Control*, 2008.

[7] P. Goupil, "AIRBUS state of the art and practices on FDI and FTC in flight control system," *Control Engineering Practice*, 2011.

[8] J. Cieslak, D. Henry, and A. Zolghadri, "Fault tolerant flight control: from theory to piloted flight simulator experiments," *Control Theory & Applications, IET*, vol. 4, no. 8, pp. 1451–1461, 2010.

[9] Airbus, "Commercial Aviation Accidents 1958 - 2013_ a Statistical Analysis„" tech. rep., Airbus, 2013.

[10] Boeing, "Statistical Summary of Commercial Jet Airplane Accidents: Worldwide Operations 1959-2014," *Aviation Safety, Boeing Commercial Airlines, Seattle*, 2015.

[11] M. V. Cook, *Flying qualities and flight control*. Cranfield University, Lecture Notes, 2012.

[12] R. Collinson, *Introduction to avionics systems*. 2013.

[13] R. Patton, "Robustness issues in fault-tolerant control," *Fault Diagnosis and Control System Reconfiguration*, 1993.

[14] S. Osder, "Practical view of redundancy management application and theory," *Journal of Guidance, Control, and Dynamics*, 1999.

[15] H. Alwi, C. Edwards, and C. P. Tan, *Fault detection and fault-tolerant control using sliding modes*. Springer, 2011.

[16] J. Chen and R. J. Patton, *Robust model-based fault diagnosis for dynamic systems*. Kluwer academic publishers, 1999.

[17] Y. Zhang, "Active fault-tolerant control systems: Integration of fault diagnosis and reconfigurable control," *Fault Diagnosis and Fault Tolerant Control*, 2007.

[18] C. Edwards, T. Lombaerts, and H. Smaili, *Fault Tolerant Flight Control: A Benchmark Challenge*, vol. 399. Springer Verlag, 2010.

[19] J. D. Bošković and R. K. Mehra, "Failure detection, identification and reconfiguration in flight control," in *Fault Diagnosis and Fault Tolerance for Mechatronic Systems: Recent Advances*, pp. 129–167, Springer, 2003.

[20] G. Ducard, "Fault-tolerant flight control and guidance systems for a small unmanned aerial vehicle," 2007.

[21] H. Noura, D. Theilliol, J. Ponsart, and A. Chamseddine, *Fault-tolerant control systems: Design and practical applications*. 2009.

[22] R. Isermann, "Supervision, fault-detection and fault-diagnosis methods—an introduction," *Control engineering practice*, 1997.

[23] M. Blanke, M. Kinnaert, and J. Lunze, *Staroswiecki, Diagnosis and Fault-Tolerant Control*. Springer Verlag, 2003.

[24] H. Alwi, *Fault tolerant sliding mode control schemes with aerospace applications*. PhD thesis, 2008.

[25] M. Blanke and J. Schröder, *Diagnosis and fault-tolerant control*, vol. 115. Springer, 2003.

[26] Y. Yeh, "Triple-triple redundant 777 primary flight computer," *Applications Conference Proceedings*, 1996.

[27] G. Bartley, "Boeing B-777: Fly-by-wire flight controls," *Spitzer [190], chapitre*, 2001.

[28] R. J. Patton, "Fault-tolerant control systems: The 1997 situation," in *IFAC symposium on fault detection supervision and safety for technical processes*, vol. 3, pp. 1033–1054, 1997.

[29] H. Alwi, C. Edwards, and C. P. Tan, "Fault Detection and Fault-Tolerant Control Using Sliding Modes," *Advances in industrial control*, pp. 1 online resource (xxvii, 336 p.), 2011.

[30] J. Jiang and X. Yu, "Fault-tolerant control systems: A comparative study between active and passive approaches," *Annual Reviews in control*, 2012.

[31] D. McFarlane and K. Glover, "A loop-shaping design procedure using H_∞ synthesis," *Automatic Control, IEEE Transactions*, 1992.

[32] J.-F. Magni, S. Bennani, and J. Terlow, "Robust flight control (a design challenge)," *Lecture notes in control and information sciences*, 1997.

[33] A. Marcos and G. J. Balas, "A robust integrated controller/diagnosis aircraft application," *International Journal of Robust and Nonlinear Control*, vol. 15, no. 12, pp. 531–551, 2005.

[34] N. Yagiz and I. Yuksek, "Sliding mode control of active suspensions for a full vehicle model," *International Journal of Vehicle Design*, 2001.

[35] K. S. Narendra, O. A. Driollet, M. Feiler, and K. George, "Adaptive control using multiple models, switching and tuning," *International Journal of Adaptive Control and Signal Processing*, vol. 17, no. 2, pp. 87–102, 2003.

[36] J. D. Boskovic and R. K. Mehra, "A multiple model-based reconfigurable flight control system design," in *Proceedings of the 37th IEEE Conference on Decision and Control*, vol. 4, pp. 4503–4508, 1998.

[37] M. Gopinathan, J. D. Boskovic, R. K. Mehra, and C. Rago, "A multiple model predictive scheme for fault-tolerant flight control design," in *Proceedings of the 37th IEEE Conference on Decision and Control*, vol. 2, pp. 1376–1381, 1998.

[38] J. Aravena, K. Zhou, X. R. Li, and F. Chowdhury, "Fault tolerant safe flight controller bank," in *Fault Detection, Supervision and Safety of Technical Processes*, vol. 6, pp. 807–812, 2006.

[39] F. W. Burcham, J. Burken, T. A. Maine, and J. Bull, *Emergency flight control using only engine thrust and lateral center-of-gravity offset: A first look*. National Aeronautics and Space Administration, Office of Management, Scientific and Technical Information Division, 1997.

[40] F. W. Burcham, J. J. Burken, T. A. Maine, and C. G. Fullerton, *Development and flight test of an emergency flight control system using only engine thrust on an MD-11 transport airplane*. National Aeronautics and Space Administration, Dryden Flight Research Center, 1997.

[41] J. J. Burken and F. W. Burcham, "Flight-test results of propulsion-only emergency control system on MD-11 airplane," *Journal of guidance, control, and dynamics*, vol. 20, no. 5, pp. 980–987, 1997.

[42] D. Leith and W. Leithead, "Survey of gain-scheduling analysis and design," *International Journal of Control*, 2000.

[43] G. Balas, "Linear, parameter varying control and its application to a turbofan engine," *International Journal of Robust and Nonlinear Control*, 2002.

[44] S. Ganguli, A. Marcos, and G. Balas, "Reconfigurable LPV control design for Boeing 747-100/200 longitudinal axis," *American Control Conference,*, 2002.

[45] F. Wu, "A generalized LPV system analysis and control synthesis framework," *International Journal of Control*, 2001.

[46] M. Rodrigues and D. Theilliol, "Fault tolerant control design for polytopic LPV systems," *J. of Applied Mathematics*, 2007.

[47] J. Shin, N. Wu, and C. Belcastro, "Adaptive linear parameter varying control synthesis for actuator failure," *J. of Guidance, Control, and Dynamics*, 2004.

[48] J. M. Maciejowski, *Predictive Control: With Constraint*. Pearson education, 2002.

[49] J. M. Maciejowski and C. N. Jones, "MPC fault-tolerant flight control case study: Flight 1862," in *IFAC safeprocess conference*, pp. 121–126, 2003.

[50] H. Seguchi and T. Ohtsuka, "Nonlinear receding horizon control of an underactuated hovercraft," *International Journal of robust and nonlinear control*, vol. 13, no. 3-4, pp. 381–398, 2003.

[51] T. Keviczky and G. J. Balas, "Software-enabled receding horizon control for autonomous unmanned aerial vehicle guidance," *Journal of guidance, control, and dynamics*, vol. 29, no. 3, pp. 680–694, 2006.

[52] J.-J. E. Slotine and W. Li, *Applied nonlinear control*, vol. 1. Prentice hall New Jersey, 1991.

[53] K. J. AAström and B. Wittenmark, *Adaptive control, 1989*. Addison-Wesley, 1989.

[54] J. Buffington, P. Chandler, and M. Pachter, "On-line system identification for aircraft with distributed control effectors," *International Journal of Robust and Nonlinear Control*, vol. 9, no. 14, pp. 1033–1049, 1999.

[55] D. Caughey, "Introduction to Aircraft Stability and Control Course Notes for M&AE 5070," *Sibley School of Mechanical & Aerospace*, 2011.

[56] B. Kulakowski, J. Gardner, and J. Shearer, *Dynamic modeling and control of engineering systems*. 2007.

[57] R. C. Nelson, *"Flight Stability and Automatic Control ", 2-nd Ed.* McGraw-Hill, New York, 1996.

[58] R. Stengel, *Flight dynamics*. Princeton University Press, 2015.

[59] ESDU, "The equations of motion of a rigid aircraft," no. 67003, 2003.

[60] M. V. Cook, *Flight dynamics principles: a linear systems approach to aircraft stability and control*. Butterworth-Heinemann, 2012.

[61] K. Koenig, "Fundamentals of Airplane Flight Mechanics (David G. Hull)," *SIAM REVIEW*, 2007.

[62] B. L. Stevens and F. L. Lewis, *Aircraft control and simulation*, vol. 2. Wiley New York, 2003.

[63] R. Pratt, *Flight control systems: practical issues in design and implementation*. Institution of Engineering and Technology, 2000.

[64] J. F. Whidborne, *Air Vehicle Modelling and Simulation*. Cranfield University, Lecture Notes, 2012.

[65] B. Stevens and F. Lewis, *Aircraft control and simulation*. Wiley New York, 2003.

[66] J. Doyle, B. Francis, and A. Tannenbaum, *Feedback control theory*. 2013.

[67] D. Allerton, *Principles of flight simulation*. John Wiley and Sons, INC, 2009.

[68] A. Andry, E. Shapiro, and J. Chung, "Eigenstructure assignment for linear systems," *IEEE transactions on aerospace*, 1983.

[69] A. Balestrino, G. D. Maria, and A. Zinober, "Nonlinear adaptive model-following control," *Automatica*, 1984.

[70] J. Reiner, G. Balas, and W. Garrard, "Robust dynamic inversion for control of highly maneuverable aircraft," *J. of Guidance, Control, and Dynamics*, 1995.

[71] H. Kwakernaak and R. Sivan, *Linear optimal control systems*. 1972.

[72] B. Yu, Y. Zhang, J. Yan, Y. Qu, and Z. Liu, "Fault tolerant control using linear quadratic technique against actuator faults in a UAV," *Chinese Control Conference (CCC)*, 2013.

[73] Z. Zhang and Z. Long, "Linear quadratic state feedback optimal control against actuator failures," *Control and Automation*, 2007.

[74] S. an Kanev and M. Verhaegen, "Reconfigurable robust fault-tolerant control and state estimation," 2002.

[75] O. Rehman, "Robust minimax optimal control of nonlinear uncertain systems using feedback linearization with application to hypersonic flight vehicles," *Decision and Control*, 2009.

[76] B. Yu, Y. Zhang, I. Minchala, and Y. Qu, "Fault-tolerant control with linear quadratic and model predictive control techniques against actuator faults in a quadrotor UAV," *Control and Fault-Tolerant*, 2013.

[77] M. Staroswiecki, "Robust fault tolerant linear quadratic control based on admissible model matching," *45th IEEE Decision and Control,*, 2006.

[78] R. M. Murray, "Linear Quadratic Regulator Control," *Control and Dynamical Systems*, pp. 1–14, 2006.

[79] J. Hespanha, "LQG/LQR controller design," *Lecture Notes, University of California, Santa*, 2007.

[80] D.-W. Gu, P. H. Petkov, and M. M. Konstantinov, *Robust Control Design with MATLAB*. Springer, 2nd ed., 2013.

[81] D. Ye and G.-H. Yang, "Adaptive fault-tolerant tracking control against actuator faults with application to flight control," *IEEE Transactions on Control Systems Technology,*, vol. 14, no. 6, pp. 1088–1096, 2006.

[82] G.-H. Yang and D. Ye, "Adaptive Fault-tolerant H_∞ Control via State Feedback for Linear Systems against Actuator Faults," in *the 45th IEEE Conference on Decision and Control, 2006*, pp. 3530–3535, 2006.

[83] X.-J. Li and G.-H. Yang, "Robust adaptive fault-tolerant control for uncertain linear systems with actuator failures," *Control Theory & Applications, IET*, vol. 6, no. 10, pp. 1544–1551, 2012.

[84] S. Skogestad and I. Postlethwaite, *Multivariable feedback control: analysis and design*, vol. 2. Wiley New York, 2007.

[85] R. K. Yedavalli, "Robust Control of Uncertain Dynamic Systems," *AMC*, vol. 10, p. 12, 2014.

[86] S. Guo and Y. Li, "Reliability-based robust H_∞ control of linear systems with uncertain parameters," *Control and Automation, ICCA'05,*, 2005.

[87] P. Gahinet and P. Apkarian, "Structured H_∞ synthesis in MATLAB," in *Proc. IFAC, Milan, Italy*, 2011.

[88] M. Mirzaei, H. H. Niemann, and N. K. Poulsen, "A μ-synthesis approach to robust control of a wind turbine," in *the 50th IEEE Conference on Decision and Control and European Control Conference (CDC-ECC)*, pp. 645–650, IEEE, 2011.

[89] J. Doyle, K. Lenz, and A. Packard, "Design examples using μ-synthesis: Space shuttle lateral axis FCS during reentry," in *Modelling, Robustness and Sensitivity Reduction in Control Systems*, pp. 127–154, Springer, 1987.

[90] G. J. Balas, J. C. Doyle, K. Glover, A. Packard, and R. Smith, "μ-analysis and synthesis toolbox for use with Matlab: user guide," in *MathWorks, Inc., 1998.*, 2011.

[91] A. Lanzon and P. Tsiotras, "A Combined Application of H_∞ Loop Shaping and μ-synthesis to Control High-speed Flywheels," *IEEE Transactions on Control Systems Technology,*, vol. 13, no. 5, pp. 766–777, 2005.

[92] K. M. Son and J. K. Park, "On the robust LQG control of TCSC for damping power system oscillations," *IEEE Transactions on Power Systems,*, vol. 15, no. 4, pp. 1306–1312, 2000.

[93] L. Chrif and Z. M. Kadda, "Aircraft Control System Using LQG and LQR Controller with Optimal Estimation-Kalman Filter Design," *Procedia Engineering*, vol. 80, pp. 245–257, 2014.

[94] P. M. Gahinet, A. Nemirovskii, A. J. Laub, and M. Chilali, "The LMI control toolbox," in *the IEEE Conference on Decision and Control, 1994*, vol. 2, pp. 2038–2038, 1994.

[95] O. Sename, P. Gaspar, and J. Bokor, *Robust Control and Linear Parameter Varying Approaches: Application to Vehicle Dynamics*. Springer, 2013.

[96] M. Katebi, M. Grimble, and Y. Zhang, "H robust control design for dynamic ship positioning," *Control Theory and Applications*, 1997.

[97] D. Ankelhed, "On design of low order H-infinity controllers," 2011.

[98] H. Ali and S. Noor, "Design of H_∞ controller with tuning of weights using particle swarm optimization method," *International Journal of Computer Science*, vol. 38, no. 2, pp. 103–112, 2011.

[99] S. Nair, "Automatic weight selection algorithm for designing H_∞ controller for active magnetic bearing," *International Journal of Engineering Science and Technology*, vol. 3, no. 1, pp. 122–138, 2011.

[100] H. Yueming and L. Zhiyuan, "An H 2/H inf robust control approach to electric vehicle constant speed cruise," *30th Control Conference (CCC)*, 2011.

[101] Y. Min, B. Zhifeng, and C. Binggang, "Robust H2/H infinity Control for Regenerative Braking of Electric Vehicles," *Control and Automation*, 2007.

[102] L. Xie and C. de Souza, "Robust H inf control for linear systems with norm-bounded time-varying uncertainty," *Automatic Control, IEEE Transactions on*, 1992.

[103] X. Chen and F. Wang, "Application of H_∞ robust fault-tolerant control in satellite attitude control system," *2nd IEEE Conference on Industrial Electronics and applications*, 2007.

[104] S. Ye and Y. Zhang, "An LMI approach to mixed H $1/H_\infty$ robust fault-tolerant control design with uncertainties," *American Control Conference, ACC '09.*, 2009.

[105] M. Boukhnifer, "Experimental H_∞ robust control of aerial vehicle flight," in *the 19th Mediterranean Conference on Control & Automation (MED)*, pp. 242–247, 2011.

[106] G. Cai, B. Chen, and T. Lee, "Design and implementation of robust flight control system for a small-scale UAV helicopter," in *Asian Control Conference*, 2009.

[107] S. Guo and Y. Li, "Reliability-based robust H_∞ control of linear systems with uncertain parameters," in *the International Conference on Control & Automation (ICCA)*, pp. 176–180, 2005.

[108] A. Piłat and P. Włodarczyk, "The μ-synthesis and analysis of the robust controller for the active magnetic levitation system," *Automatyka*, vol. 15, no. 1, pp. 85–98, 2011.

[109] K. Natesan and M. Bhat, "Design and flight testing of H_∞ lateral flight control for an unmanned air vehicle," in *the IEEE International Conference on Control and Automation*, pp. 892–897, 2007.

[110] E. Christopher, L. Thomas, and S. Hafid, "Fault tolerant flight control–a benchmark challenge," *Lecture Notes in Control and Information Sciences*, 2010.

[111] O. Härkegard, "Dynamic Control Allocation Using Constrained Quadratic Programming," *Journal of Guidance, Control, and Dynamics*, vol. 27, no. 6, pp. 1028–1034, 2004.

[112] T. A. Johansen and T. I. Fossen, "Control allocation—a survey," *Automatica*, vol. 49, no. 5, pp. 1087–1103, 2013.

[113] G. J. Ducard in *Fault-tolerant Flight Control and Guidance Systems. Advances in Industrial Control*, pp. 89–106, Springer-Verlag London, 2009.

[114] O. Harkegard, "Resolving Actuator Redundancy Control Allocation vs. Linear Quadratic Control," *Automatica*, vol. 41, no. 1, pp. 137–144, 2005.

[115] T. A. Johansen and T. I. Fossen, "Control allocation—a survey," *Automatica*, vol. 49, no. 5, pp. 1087–1103, 2013.

[116] J. Petersen and M. Bodson, "Constrained quadratic programming techniques for control allocation," *IEEE Transactions on Control Systems Technology*, vol. 14, no. 1, pp. 91–98, 2006.

[117] H.-d. Wang, J.-q. Yi, and G.-l. Fan, "Autonomous reconfigurable flight control system design using control allocation," in *2008 2nd International Symposium on Systems and Control in Aerospace and Astronautics*, pp. 1–6, IEEE, Dec. 2008.

[118] G. Golub, "Van Loan., Matrix computations, North Oxford Academic," 1983.

[119] R. Horn, "Johnson., CR: Matrix Analysis," 1985.

[120] K. Bordingnon and W. Durham, "Closed-form solutions to constrained control allocation problem," *J. of Guidance, Control, and Dynamics*, 1995.

[121] W. S. Levine, *The Control Handbook, Second Edition: Control System Applications, Second Edition*. CRC Press, 2010.

[122] J. Shi, W. Zhang, G. Li, and X. Liu, "Research on allocation efficiency of the redistributed pseudo inverse algorithm," *Science China Information Sciences*, 2010.

[123] J. Virnig and D. Bodden, "Multivariable control allocation and control law conditioning when control effectors limit(STOVL aircraft)," *AIAA Guidance, Navigation and Control Conference,*, 1994.

[124] M. Bodson, "Evaluation of optimization methods for control allocation," *Journal of Guidance, Control, and Dynamics*, 2002.

[125] M. Oppenheimer, "Control allocation for over-actuated systems," *14th Mediterranean Conference on Control and Automation MED '06*, 2006.

[126] R. Adams, J. Buffington, A. Sparks, and S. Banda, *Robust multivariable flight control*. 2012.

[127] J. Buffington and D. Enns, "Lyapunov stability analysis of daisy chain control allocation," *Journal of Guidance, Control, and Dynamics*, 1996.

[128] W. Durham, "Constrained control allocation," *Journal of Guidance, Control, and Dynamics*, 1993.

[129] J. M. Petersen and M. Bodson, "Fast implementation of direct allocation with extension to coplanar controls," *J of Guidance, Control, and Dynamics*, 2002.

[130] A. K. Naskar, S. Patra, and S. Sen, "Reconfigurable Direct Allocation for Multiple Actuator Failures," vol. 23, no. 1, pp. 397–405, 2015.

[131] J. Paradiso, "Adaptable method of managing jets and aerosurfaces for aerospace vehicle control," *Journal of Guidance, Control, and Dynamics*, 1991.

[132] M. Bodson and S. Frost, "Load balancing in control allocation," *Journal of Guidance, Control, and Dynamics*, 2011.

[133] S. Wright and J. Nocedal, *Numerical optimization*. 1999.

[134] W. Gai and H. Wang, "Closed-loop dynamic control allocation for aircraft with multiple actuators," *Chinese Journal of Aeronautics*, 2013.

[135] H.-d. Wang, J.-q. Yi, and G.-l. Fan, "Autonomous reconfigurable flight control system design using control allocation," in *2nd International Symposium on*

Systems and Control in Aerospace and Astronautics, ISSCAA, pp. 1–6, IEEE, 2008.

[136] Q. Wang, Q. Li, N. Cheng, and J. Song, "Robust Control Allocation Method in the Presence of Control Effector Failure *," no. 2001, pp. 660–664, 2014.

[137] Y. Zhong, L. Yang, H. Duan, and G. Shen, "Control capability evaluation based reconfigurable flight control for aircraft with failures," *Proceedings of the World Congress on Intelligent Control and Automation (WCICA)*, pp. 424–428, 2010.

[138] Q. L. Zhou, Y. Zhang, C. A. Rabbath, and D. Theilliol, "Design of feedback linearization control and reconfigurable control allocation with application to a quadrotor UAV," *Conference on Control and Fault-Tolerant Systems, SysTol'10 - Final Program and Book of Abstracts*, no. 514, pp. 371–376, 2010.

[139] F. Q. Elizabeth, C. Liu, X. Zhu, and B. Jiang, "Fault Tolerant Control Based on Adaptive Control Allocation with a Multiple Effectors Aircraft Application," pp. 2533–2538, 2012.

[140] M. Wang, J. Yang, G. Qin, and Y. Yan, "Adaptive Fault-tolerant Control with Control Allocation for Flight Systems with Severe Actuator Failures and Input Saturation," pp. 5134–5139, 2013.

[141] Y. Zhang, V. S. Suresh, B. Jiang, and D. Theilliol, "Reconfigurable control allocation against aircraft control effector failures," in *IEEE International Conference on Control Applications,*, pp. 1197–1202, IEEE, 2007.

[142] O. Härkegard, "Backstepping and control allocation with applications to flight control," 2003.

[143] W. Durham and K. Bordignon, "Multiple control effector rate limiting," *J. of Guidance, control, and Dynamics*, 1996.

[144] O. Härkegard, "Efficient active set algorithms for solving constrained least squares problems in aircraft control allocation," *Proceedings of the Decision and Control conference*, 2002.

[145] H. Alwi and C. Edwards, "Fault tolerant control using sliding modes with on-line control allocation," *Fault Tolerant Flight Control*, 2010.

[146] A. Filippone, "Data and performances of selected aircraft and rotorcraft," *Progress in Aerospace Sciences*, 2000.

[147] R. Heffley and W. Jewell, "Aircraft handling qualities data," 1972.

[148] L. Zadeh, "Fuzzy sets," *Information and control*, 1965.

[149] E. Mamdani and S. Assilian, "An experiment in linguistic synthesis with a fuzzy logic controller," *International journal of man-machine studies*, 1975.

[150] Y. Bai and D. Wang, "Fundamentals of Fuzzy Logic Control—Fuzzy Sets, Fuzzy Rules and Defuzzifications," *Advanced Fuzzy Logic Technologies in Industrial Applications*, 2006.

[151] MathWorks, Inc, and W. Wang, "Fuzzy Logic Toolbox: for Use with MATLAB: User's Guide," 1998.

[152] M. Sugeno, "Industrial applications of fuzzy control," *Elsevier Science Inc.*, 1985.

Appendix A

Linear models for Business Jet Aircraft

A.1 Linearised models

Table A.1 Aircraft control input and states for the selected trimming conditions.

Symbol	Condition	Ascending	Cruise	Descending
ξ	Aileron deflection, deg	0	0	0
τ	Engine throttle, %	52.2	20.3	10
α	AoA, deg	4.08	3.64	10.8
θ	Pitch angle, deg	19.08	3.64	0.8

The ascending linear model is given by

$$\begin{bmatrix} \dot{p} \\ \dot{r} \\ \dot{\psi} \\ \dot{\phi} \\ \dot{\beta} \end{bmatrix} = \begin{bmatrix} -2.6 & 0.85 & 0 & 0 & -4.4 \\ -0.32 & -0.174 & 0 & 0 & 1.4 \\ 0 & 1 & 0 & 0 & 0 \\ 1 & 0.35 & 0 & 0 & 0 \\ 0.069 & -0.99 & 0 & 0.137 & -0.23 \end{bmatrix} \begin{bmatrix} p \\ r \\ \psi \\ \phi \\ \beta \end{bmatrix} + \begin{bmatrix} -0.0785 & 0.024 \\ -0.006 & -0.018 \\ 0 & 0 \\ 0 & 0 \\ 0 & 0.001 \end{bmatrix} \begin{bmatrix} \xi \\ \zeta \end{bmatrix} \quad \text{(A.1)}$$

The descending linear model is given by

$$\begin{bmatrix} \dot{p} \\ \dot{r} \\ \dot{\psi} \\ \dot{\phi} \\ \dot{\beta} \end{bmatrix} = \begin{bmatrix} -2.75 & 1.023 & 0 & 0 & -5.9 \\ -0.51 & -0.19 & 0 & 0 & 1.42 \\ 0 & 1 & 0 & 0 & 0 \\ 1 & 0.015 & 0 & 0 & 0 \\ 0.19 & -0.97 & 0 & 0.145 & -0.26 \end{bmatrix} \begin{bmatrix} p \\ r \\ \psi \\ \phi \\ \beta \end{bmatrix} + \begin{bmatrix} -0.082 & 0.023 \\ -0.008 & -0.02 \\ 0 & 0 \\ 0 & 0 \\ 0.0001 & 0.0009 \end{bmatrix} \begin{bmatrix} \xi \\ \zeta \end{bmatrix} \quad \text{(A.2)}$$

Appendix B

Control computation

B.0.1 Mu-synthesis generalised plant (used in Ch. 5)

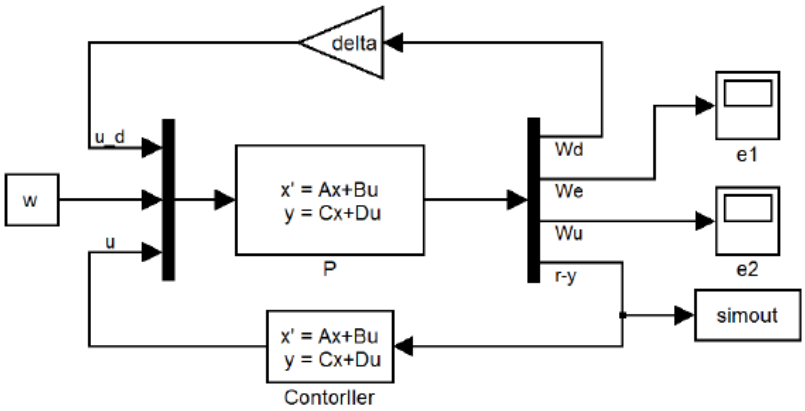

With the following relationship

$$\begin{bmatrix} W_d \\ z_1 \\ z_2 \\ r-y \end{bmatrix} = \begin{bmatrix} 0 & 0 & I \\ 0 & W_e & -W_e\, G \\ W_u & 0 & W_u \\ -G & I & -G \end{bmatrix} \begin{bmatrix} u_d \\ w \\ u \end{bmatrix}$$

B.0.2 State space model for H_∞ control for the Control Allocation

A=

$$\begin{bmatrix}
-5.245 & -7.964 & 6.102 & -7.64 & -0.1896 & 3.292 & 1.282 & -1.282 & 2.466 & -2.466 & 0.4922 \\
-0.5266 & -1.004 & 1.032 & -0.747 & -0.01895 & 0.3208 & 0.09929 & -0.09929 & 0.2694 & -0.2694 & -0.1726 \\
0.1066 & -0.9782 & -0.1096 & 0.1151 & 0.000268 & -0.004131 & -0.002044 & 0.002044 & -0.003951 & 0.003951 & 0.01431 \\
1 & 0.0893 & 2.87e-42 & 0 & -1.985e-24 & 0 & 0 & 0 & 0 & 0 & -2.753e-37 \\
0 & 0 & 2.22e-16 & 0 & -0.0158 & 0 & 0 & 0 & 0 & 0 & -3.96e-30 \\
0 & 0 & 0 & -1.11e-16 & 6.971e-39 & -0.0158 & 0 & 0 & 0 & 0 & 9.671e-52 \\
42.68 & 83.02 & -78.99 & 77.89 & 1.944 & -33.55 & -16.18 & 16.18 & -31.81 & 31.81 & -4.051 \\
-42.68 & -83.02 & 78.99 & -77.89 & -1.944 & 33.55 & 16.18 & -16.18 & 31.81 & -31.81 & 4.051 \\
83.72 & 162.7 & -155 & 152.8 & 3.792 & -65.82 & -31.69 & 31.69 & -62.38 & 62.37 & -7.791 \\
-83.72 & -162.7 & 155 & -152.8 & -3.792 & 65.82 & 31.69 & -31.69 & 62.37 & -62.38 & 7.791 \\
11.2 & 22.36 & -20.75 & 20.51 & 0.5716 & -8.813 & -4.361 & 4.361 & -8.429 & 8.429 & -1.502
\end{bmatrix}$$

B=

$$\begin{bmatrix}
-8.112e-27 & 0 \\
-1.86e-26 & 0 \\
0 & 0 \\
-1.765e-25 & 0 \\
7.025 & 0 \\
6.2e-40 & 7.025 \\
0 & 0 \\
0 & 0 \\
0 & 0 \\
0 & 0 \\
0 & 0
\end{bmatrix}$$

C=

$$\begin{bmatrix}
0.6903 & 1.343 & -1.278 & 1.26 & 0.03144 & -0.5428 & 0.2565 & 0.2617 & -0.5145 & 0.5145 & -0.06554 \\
-0.6903 & -1.343 & 1.278 & -1.26 & -0.03144 & 0.5428 & 0.2617 & 0.2565 & 0.5145 - 0.5145 & 0.06554 & \\
1.064 & 2.067 & -1.969 & 1.942 & 0.04819 & -0.8366 & -0.4028 & 0.4028 & -0.3856 & 0.7927 & -0.09902 \\
-1.064 & -2.067 & 1.969 & -1.942 & -0.04819 & 0.8366 & 0.4028 & -0.4028 & 0.7927 & -0.3856 & 0.09902 \\
0.04294 & 0.08573 & -0.07959 & 0.07866 & 0.002192 & -0.03379 & -0.01672 & 0.01672 & -0.03232 & 0.03232 & 0.1171
\end{bmatrix}$$

D=

$$\begin{bmatrix}
0 & 0 \\
0 & 0 \\
0 & 0 \\
0 & 0 \\
0 & 0
\end{bmatrix}$$

B.0.3 Matlab Codes for control gains computation

1. Baseline LQR Control

```
%1. defining A,B,C,D for model
%2. defining Q and R weights
%3. Solution for controller using: lqr command
%4. Arrangements based on primary and secondary variables
%5. Solution 2 for gains for the new arrangements
X0=[0 0 0 0 250 0 5000 0 0]'
U0 = [0.724 -2.55 0 0]' % Throttle Elevator Aileron Rudder
Y0 = [250 5000 0 0]'
A=[-0.0079    3.9198   -9.8066    0.0216    0.0000    0.0000         0
0         0;
-0.0003   -0.9972   -0.0000    1.0037    0.0000         0         0
0         0;
0         0         0    1.0000         0         0         0   -0.0000
0;
0.0001   -3.5165    0.0000   -2.1528   -0.0000         0         0
0         0;
0 -250.0000  250.0000         0         0         0         0         0
0;
-0.0000         0   -0.0000         0    0.0000   -0.2990    0.0431   -0.9991
0.0392;
0.0000   -0.0000         0         0   -0.0000   -9.2887   -2.4478    0.5494
0;
0.0000   -0.0000         0         0   -0.0000    4.7892   -0.1025   -0.5415
0;
0         0         0    0.0000         0         0    1.0000    0.0432
0]
%Deflections [de dpe dae dre] Throttle, elevator, aileron, rudder
B=[1.3625   -0.5088         0         0;
-0.0003   -0.0867         0         0;
0         0         0         0;
0.0170   -5.8916         0         0;
0         0         0         0;
0         0    0.0100    0.0598;
0         0   -2.3527    1.7970;
0         0    0.3459   -2.7287;
0         0         0         0];
C=[0 0 0 0 1 0 0 0 0;
0 0 0 0 0 0 1 0 0;
0 0 0 0 0 0 0 0 1;
0 0 0 0 0 0 0 1 0]
```

```
Cp=C(:,1:4)
Cs=C(:,5:9)
D=zeros(4,4)
% Q and R weights
Qs=[1 1 1 1 1 1 1 1 1 1 1 1 1];
Qa=diag(Qs)
Rs=[700 0.001 0.5 0.5]; %Throttle Elevator Aileron Rudder
Ra=diag(Rs);
% solve for Controller gains
%                      FAULT MODELLING, and Adaptation
p1=2;p2=4;p3=7;p4=8;
s1=1;s2=3;s3=5;s4=6;s5=9;
Acomp=[
A(p1,p1) A(p1,p2) A(p1,p3) A(p1,p4) A(p1,s1) A(p1,s2) A(p1,s3) A(p1,s4) A(p1,s5);
A(p2,p1) A(p2,p2) A(p2,p3) A(p2,p4) A(p2,s1) A(p2,s2) A(p2,s3) A(p2,s4) A(p2,s5);
A(p3,p1) A(p3,p2) A(p3,p3) A(p3,p4) A(p3,s1) A(p3,s2) A(p3,s3) A(p3,s4) A(p3,s5);
A(p4,p1) A(p4,p2) A(p4,p3) A(p4,p4) A(p4,s1) A(p4,s2) A(p4,s3) A(p4,s4) A(p4,s5);
A(s1,p1) A(s1,p2) A(s1,p3) A(s1,p4) A(s1,s1) A(s1,s2) A(s1,s3) A(s1,s4) A(s1,s5);
A(s2,p1) A(s2,p2) A(s2,p3) A(s2,p4) A(s2,s1) A(s2,s2) A(s2,s3) A(s2,s4) A(s2,s5);
A(s3,p1) A(s3,p2) A(s3,p3) A(s3,p4) A(s3,s1) A(s3,s2) A(s3,s3) A(s3,s4) A(s3,s5);
A(s4,p1) A(s4,p2) A(s4,p3) A(s4,p4) A(s4,s1) A(s4,s2) A(s4,s3) A(s4,s4) A(s4,s5);
A(s5,p1) A(s5,p2) A(s5,p3) A(s5,p4) A(s5,s1) A(s5,s2) A(s5,s3) A(s5,s4) A(s5,s5);];
App=Acomp(1:4,1:4);
Aps=Acomp(1:4,5:9);
Asp=Acomp(5:9,1:4);
Ass=Acomp(5:9,5:9);
A4lqr=Acomp;
B;
Bp=[B(p1,:);
B(p2,:);
B(p3,:);
B(p4,:)]
Bs=[B(s1,:);
B(s2,:);
B(s3,:);
B(s4,:);
B(s5,:)]
invBp=inv(Bp);
B4lqr=[Bp
Bs];
sA=size(A4lqr)
rA=sA(1)
cA=sA(2)
sB=size(B4lqr)
rB=sB(1)
```

```
cB=sB(2)
sC=size(C)
rC=sC(1)
cC=sC(2)
Aa=[A4lqr zeros(rA,rC)
−C zeros(rC,rC)];
Ba=[B4lqr
zeros(rC,cB)];
ka=lqr(Aa,Ba,Qa,Ra);
KX=[ka(:,1) ka(:,2) ka(:,3) ka(:,4) ka(:,5) ka(:,6) ka(:,7) ka(:,8) ka(:,9)];
KI=[ka(:,10) ka(:,11) ka(:,12) ka(:,13)];
KX;
KXp=[KX(:,1) KX(:,2) KX(:,3) KX(:,4)];
KXs=[KX(:,5) KX(:,6) KX(:,7) KX(:,8) KX(:,9)];
%Multiplicative actuator fault, 1=no fault and 0=full fault
gamma=diag([1 1 1 1]);
unity=diag([1 1 1 1]);
%Additive actuator fault, 0=no fault     and        not zero=there is fault
uf0=[0 0 0 0]';
%% Calculating f_a and u_add
alpha1=1; %throttle
alpha2=0.3; %elevator
alpha3=1; %aileron
alpha4=1; %rudder
n=4;%xp
k=5;%xs
p=4;%z
m=4;%u
q=4;%y
l=4;%f
Ts=0.1
Fa=B4lqr
Fap=Fa(1:4,:)
Fas=Fa(5:9,:)
```

2. Baseline Robust Control

```
% Units: 1.angles: radian    2.length: ft    3.time: second
%% Dynamical sys
Alat =[−0.1008 0 −468.2 32.2;
−.00579 −1.232 0.397 0;
0.00278 −0.0346 −0.257 0;
0 1 0 0];
Blat = [0 13.484;
```

```
−1.62 0.392;
−0.01875 −0.864;
0            0];
Clat=[0 0  0 1]; %v p r phi
Dlat=[0 0];
%Plant G
G=ss(Alat,Blat,Clat,Dlat); % plant is G
%%  Tracking performance: where 1/We is upper bound of S sensitivity function
% 1
Ms=20;wb=0.01;epsi=3;
Wetf=tf([1/Ms wb],[1 wb*epsi]);
% 2
We = tf(.3*[1 100],[1 30]);
%  3
Wedist=.055*tf([.5 10e0],[1 1e−1]); %increasing the constant will
%increase gamma/bnd and
%4
We4=tf(.5*[1 100],[1 30]);
% 5
We5=.1*tf([1 10e0],[2 1e−2]); %increasing the constant will
% increase gamma/bnd but quicker response
% select
We=We5; %bode(We);grid
%%  Controlling Efforts
% 1
MuA=1.6;wbcA=1.0;epsi1A=0.01 ;%OR only a constant
MuR=1.6;wbcR=1.0;epsi1R=0.01 ;   %OR only a constant
Wutf1=tf([1 wbcA/MuA],[epsi1A wbcA]) ;% for aileron
Wutf2=tf([1 wbcR/MuR],[epsi1R wbcR]); % for rudder
% bodemag(Wutf1,'−',Wutf2,'−−');
%Wu=append(Wutf1,Wutf2);
%Wu=ss([cWu1 0;0 cWu2]);
% 2
Wu40 = diag([1/(100*pi/180),1/(100*pi/180)]); % to capture the deflections limits
% as 40 deg in aileron and rudder
Wu30 = diag([1/(30*pi/180),1/(30*pi/180)]); % to capture the deflections limits
%as 30 deg in aileron and rudder
Wu25 = diag([1/(25*pi/180),1/(25*pi/180)]); % to capture the deflections limits
%as 25 deg in aileron and rudder
Wu20 = diag([1/(20*pi/180),1/(20*pi/180)]); % to capture the deflections limits
%as 20 deg in aileron and rudder
Wu=Wu30
%% uncertainty model
% Normalized error dynamics
Delta_G = ultidyn('Delta_G',[2 2],'Bound',1.0);
```

```
% Frequency shaping of error dynamics
% 1
w_1 = 0.5*tf([1/10 1],[1/100 1]);
w_2 = 0.5*tf([1/10 1],[1/100 1]);
Wd1 = append(w_1,w_2);
% 2
Wd2=[0.5,0;0,0.5];
% 3
Wd3=[1,0;0,1];
Wd=Wd3
% bodemag(w_1,'-',w_2,'--');
% title('Relative error on nominal model as a function of frequency')
% legend('stabilizer','rudder','Location','NorthWest');
%% Generalized plant P is found with function sysic%
systemnames ='G We Wu Wd';
inputvar ='[u_d(2); r(1); u(2)]';
outputvar ='[Wd; We; Wu; r-G]';
input_to_G ='[u+u_d]';
input_to_We ='[r-G]';
input_to_Wd ='[u]';
input_to_Wu ='[u+u_d]';
sysoutname ='P';
cleanupsysic ='yes';
sysic;
[Ap,Bp,Cp,Dp]=ssdata(P);
%% Finding H-infinity optimal controller%
nmeas=1; ncon=2;
[Khinf,CL,GAM,INFO]=hinfsyn(P,nmeas,ncon,'DISPLAY','on');
% [gopt,Khinf]=hinflmi(P,[nmeas,ncon])
[Ach,Bch,Cch,Dch]=ssdata(Khinf);
%% Mu synthesis controller
nmeas=1; ncon=2;
% [Kmu,clp,bnd]=dksyn(P,nmeas,ncon)
fmu = logspace(-2,2,60);
Delta=[ultidyn('D_1',[1 1],'Bound',0.3) 0;0 ultidyn('D_2',[1 1],'Bound',0.3)]
% Diagonal uncertainty
Punc=lft(Delta,P);
opt = dkitopt('FrequencyVector',fmu,'NumberofAutoIterations',5);
[kmu,clpmu,bnd] = dksyn(Punc,nmeas,ncon,opt);
bnd
[Acm,Bcm,Ccm,Dcm]=ssdata(kmu);
```

3. Baseline Control Law for Control Allocation

```
% Units: 1.angles: radian    2.Length: ft    3.time: second
%% Dynamical sys
%               Only bank and beta control using ailerons and rudder
U0=[0 0 0 0 0 0 0 0 0 0 0 0 0]';
% dA_ir dA_il dA_or dA_ol dsp1?4 dsp5 dsp8 dsp9?12 dR e1lat e2lat e3lat e4lat
X0=[0 0 0 0]'; %     p r beta phi
Y0=[0 0 0 0 0]'; %   p r beta phi
%states : p r beta phi
Alat=[-1.0579 0.1718 -1.6478 0.0004;
-0.1186 -0.2066 0.2767 -0.0019
0.1014 -0.9887 -0.0999 0.1055
1.0000 0.0893 0 0];
% Control input ?A_ir ?A_il ?A_or ?A_ol ?sp1?4 ?sp5 ?sp8 ?sp9?12 ?R   PLUS
e1lat e2lat e3lat e4lat
B_full_lat=[-0.0832 0.0832 -0.2285 0.2285 -0.2625 -0.0678 0.0678 0.2625 0.1187;
% 0.0246 0.0140 -0.0140 -0.0246;
-0.0154 0.0154 -0.0123 0.0123 -0.0180 -0.0052 0.0052 0.0180 -0.2478;
% 0.1269 0.0724 -0.0724 -0.1269;
0 0 0 0 0.0017 0.0006 -0.0006 -0.0017 0.0174;
% 0.0005 0.0005 -0.0005 -0.0005;
0 0 0 0 0 0 0 0 0];
% 0 0 0 0];
% control inputs are: A_ir A_il A_or A_ol rudder
Blat=[B_full_lat(:,1) B_full_lat(:,2) B_full_lat(:,3) B_full_lat(:,4) B_full_lat(:,9)]
%states : p r beta phi
Clat=[0 0 1 0; 0 0 0 1];
Dlat=zeros(2,5);
noX=4;
noI=5;
noO=2;
dtr=pi/180;
rtd=180/pi;
% : p r beta phi
%Plant G
G=ss(Alat,Blat,Clat,Dlat); % plant is G
%%  Tracking performance: where 1/We is upper bound of S sensitivity function
% 1
% Ms=20;wb=0.01;epsi=3;
% Wetf=tf([1/Ms wb],[1 wb*epsi]);
%Well established, More accurate Tunning:
lfm=50;% specify the ratio in/out:
cat=.79;
%rad/s when increase: gamma increase || deflection
hfm=.01;% specify the ratio in/out
We6=makeweight(lfm,cat,hfm);
```

```
% select
ratioInc=.53;
%when increase you require better track,
%and you got in reality ... response
ratioDec=0.1;
WeBeta=ratioDec*We6;
WePhi=ratioInc*We6;
We=[WeBeta 0;
0  WePhi]; %bode(We);grid
%%  Controlling Efforts
% Group
lfm=.01;% specify the ratio in/out (the exact ratio not the dB):
cat=.65;
%rad/s this controls the steep of deflection (rise time)

% when increase gamma decrease, deflection
hfm=49.3;% specify the ratio in/out
Wu1=makeweight(lfm,cat,hfm);
AilronR=1.1;
RudAilR=2.90;
Wu2=AilronR*Wu1;
Wu3=RudAilR*Wu1;
A_i=Wu1*1.1*.25;
A_o=Wu1*.35;
Rudd=Wu1*2.9*.4;
% choose
Wu4=[A_i 0 0 0 0;
0 A_i 0 0 0;
0 0 A_o 0 0;
0 0 0 A_o 0;
0 0 0 0 Rudd];
%CHOOSE
Wu=Wu4;
%% Generalized plant P is found with function sysic%
systemnames ='G We Wu';
inputvar ='[ r(2); u(5)]';
outputvar ='[We; Wu; r-G]';
input_to_G ='[u]';
input_to_We ='[r-G]';
input_to_Wu ='[u]';
sysoutname ='P';
cleanupsysic ='yes';
sysic;
[Ap,Bp,Cp,Dp]=ssdata(P);
%% Finding H-infinity optimal controller%
```

```
nmeas=2; ncon=5;
[Khinf,CL,GAM,INFO]=hinfsyn(P,nmeas,ncon,'DISPLAY','on');
% [gopt,Khinf]=hinflmi(P,[nmeas,ncon])
[Ach,Bch,Cch,Dch]=ssdata(Khinf);
%%
%uvirtual=1; % first kick for uvirtual
%Finding u from the virtual control
% define: B, v, plim,rlim,T,Wv,W1,W2,S
clA_ir=-0.013 ; clA_il=0.013 ;clA_or=-.017 ; clA_ol=.017 ; clR=.004;
cmA_ir=0 ; cmA_il=0 ;cmA_or=0 ; cmA_ol=0 ; cmR=0 ;
cnA_ir=-.0015 ; cnA_il=.0015 ;cnA_or=-.0012 ; cnA_ol=.0012 ;cnR=-.108 ;
B=[clA_ir clA_il clA_or clA_ol clR;
cmA_ir cmA_il cmA_or cmA_ol cmR;
cnA_ir cnA_il cnA_or cnA_ol cnR];
%for fixed alpha, Mach,
M=0.8;
alpha=2.5*dtr;
cm_alpa=-1.15          ;  cl_beta=-0.193;            cn_beta=0.147;
span= 30;             Va=445; %ft/s
cl_p=-0.3  ;             cn_p=-0.06;               chord=6.5 ;
cm_q=-20;           cl_r=0.2;
cn_r=-0.2;               cm_M=0.12;
c4moments=[0        cl_beta    (span/(2*Va))*cl_p   0
(span/(2*Va))*cl_r  0;
cm_alpa  0          0                    (chord/(2*Va))*cm_q 0
cm_M;
0        cn_beta    (span/(2*Va))*cn_p   0                   (span/(2*Va))*cn_r
0];
C4moments=[c4moments(:,2) c4moments(:,3) c4moments(:,5)];
S_old=[-5 -.05 -.12;
5 -.05 .12;
-7 -.02 -1;
7 -.02 1;
.02 0 -8];
S_basic=[-5 -.05 -.12;
5 -.05 .12;
-10 -.02 -1;
10 -.02 1;
.02 0 -8];
% Jam and saturation in First Actuator: Inner right Aileron
GainsUpdate2=1.6; % 1.6 when hardover in inner right
GainsUpdate2=1.23; % 1.23 when jam in inner right
GainsUpdate2=1.75; % 1.75 when jam at -16.7 deg in outer right
GainsUpdate2=1.55; % 1.75 when jam at -10 deg in outer right
GainsUpdate2=2; % 2 when jam at -4.22 deg in rudder
```

```
S_a1j=[0 0 0;
6 -.05 .12;
-11 -.02 -1;
11 -.02 1;
.02 0 -8];
%
S_a1Jam=S_basic;
%AcAdapt4A_ir=GainsUpdate(1,1);      %Lookup tables
AcAdapt4A_ir=GainsUpdate2;      %Fuzzy logic
S_a1Jam(1,:)=0;
S_a1Jam(2,1)=AcAdapt4A_ir*S_basic(2,1);
S_a1Jam(3,1)=AcAdapt4A_ir*S_basic(3,1);
S_a1Jam(4,1)=AcAdapt4A_ir*S_basic(4,1);
S_a1Jam;
%
S_a1s=[0     0          0;
9    -.05        .12;
-12  -.02        -1;
12   -.02        1;
.02  0           -8];
%%%%% Jam and saturation in third Actuator: outer right Aileron
S_a3Jam=S_basic;
%AcAdapt4A_or=GainsUpdate(1,1);      %lookup tables updates
AcAdapt4A_or=GainsUpdate2;          %Fuzzy logic updates
S_a3Jam(3,:)=0;
S_a3Jam(2,1)=AcAdapt4A_or*S_basic(2,1);
S_a3Jam(1,1)=AcAdapt4A_or*S_basic(1,1);
S_a3Jam(4,1)=AcAdapt4A_or*S_basic(4,1);
%%%%% Jam and saturation in fifth Actuator: rudder
S_a5Jam=S_basic;
%AcAdapt4Rudder=GainsUpdate(1,1);        %lookup tables updates
AcAdapt4Rudder=GainsUpdate2;            % Fuzzy logic
S_a5Jam(5,:)=0;
S_a5Jam(2,1)=AcAdapt4Rudder*S_basic(2,1);
S_a5Jam(1,1)=AcAdapt4Rudder*S_basic(1,1);
S_a5Jam(4,1)=AcAdapt4Rudder*S_basic(4,1);
S_a5Jam(3,1)=AcAdapt4Rudder*S_basic(3,1);
S_a5Jam(1,3)=AcAdapt4Rudder*S_basic(1,3);
S_a5Jam(2,3)=AcAdapt4Rudder*S_basic(2,3);
S_a5Jam(3,3)=AcAdapt4Rudder*S_basic(3,3);
S_a5Jam(4,3)=AcAdapt4Rudder*S_basic(4,3);
%%%%        %%%%%       %%%%%
S= S_basic;            % Selection of S for nominal intact system.
S_reAlloc=S_a5Jam ;
% Select which S for reAllocation depends on the fualt scenario
```

```
175 plim=dtr*[-30 30;
176 -30 30;
177 -30 30;
178 -30 30;
179 -30 30];
180 rlim1=dtr*[150;
181 150 ;
182 150 ;
183 150 ;
184 100];
185 rlim=[-rlim1 rlim1]; %
186 %v=virtual;
187 T=.02;
188 W1=diag([2 2 2 2 2]);       % for no of inputs: to penalize position
189 W2=diag([8 8 10 10 10]);    % for no of inputs: to penalize rates
190 Wv=diag([10 1 1]); % for penalizing moments: cl, cm, cn
```